TRINITY COLLEGE DUBLIN

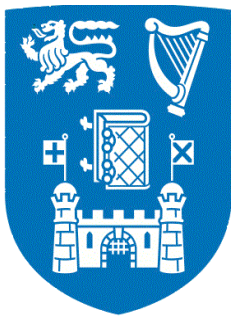

Doctor of Philosophy

Tension and compression stress-strain asymmetry in passive skeletal muscle

Author:
Melika Mohammadkhah, M.Sc

Supervisor:
Associate Prof. Ciaran K. Simms

Co-supervisor:
Prof. Paula Murphy

External Examiner:
Dr.Patrick McGarry
(National University Of Ireland, Galway)

Internal Examiner:
Dr. Mark Ahearne
(Trinity Centre for Bioengineering)

A thesis submitted to the University of Dublin
in partial fulfilment of the requirements for the degree of PhD in the
Department of Mechanical and Manufacturing Engineering

May 2017

Declaration of Authorship

I declare that this thesis is entirely my own work and has not been submitted as an exercise for a degree at this or any other university. Due acknowledgements and references are given to the work of others where appropriate.

I agree to deposit this thesis in the University's open access institutional repository or allow the library to do so on my behalf, subject to Irish Copyright Legislation and Trinity College Library conditions of use and acknowledgement.

Signed:

ID No.: 13334413

Date: May 2017

Acknowledgement

It has been three and a half years to be in Dublin and my amazing adventure in Dublin only comes to an end. This project was supported by Trinity College Dublin Postgraduate Research Scholarship. I would like to first thank Trinity College Dublin to provide me the opportunity to work on this project over the last three years.

I truly would love to thank all who have been by my side, helped and supported me through conducting this research. First and foremost, I would love to express my gratitude to my supervisor Associate Professor. Ciaran Simms of the Department of Mechanical engineering at Trinity College Dublin for his useful guidance, great feedback and ideas about the work, encouragements in the most depressed times, and continuous support. The door to his office was always open whenever I ran into a trouble spot. He steered me in the right direction whenever he thought I needed it. I am very honoured to have the opportunity to spend three years of my professional studies with him and I am so eager and interested in continuing this professional bond in the future.

I also would like to sincerely thank my co-supervisor Professor. Paula Murphy of the Department of Zoology at Trinity College Dublin for her valuable and priceless help throughout this journey. I am gratefully indebted to her for her absolutely valuable comments on this thesis and technical writing which is much appreciated. My weakness in Biology would have never been improved without her.

I would like to thank all of the staff in the Department of Mechanical and Manufacturing Engineering especially Ms. Judith Lee, the staff in the Department of Zoology, everyone who shared the office with me over this course of study in the two departments and finally all my friends in Trinity College Dublin; Gerard Cooney, Guibing Lee, Richard Blythman, Michael Gibbons, Shi Shang, Greg Tierney, Diarmuid Jackson, Mathew Lyons, Rudi O'Reilly, Claire Shea, Anurati Saha, Eoin Mac Réamoinn, Rebecca Rolfe, Dinorath Olvera, Fatemeh Golpayegani, Abdollah Malekjafarian, Ramisa Hamed, Ali Hosseinzade Vahid, Milad Ghasemi, and Nima Afraz. Being away from home was not always easy but they managed to make me feel at home in Ireland and a lot of them have become really good friends now. I cannot mention all names but I am sure they will recognise themselves.

I would like to acknowledge the assistance of Peter Stafford (the retired Chief Technical Officer of the Zoology building at Trinity College Dublin), Peter O'Reilly (the Senior Experimental Officer of the Department of Mechanical and Manufacturing Engineering at Trinity College Dublin), Annyalla Chicks Ltd to provide access to chickens. Without their passionate assistance, the current thesis could not been successfully conducted.

I also would like to thank my lovely family: my beautiful mom who has played the role of a mother as well as the role of a father for me since childhood, my gorgeous sisters, my funny brother, my thoughtful brother in law, my cute nephew, and my sister in law who has recently joined our family for their continuous emotional and mental support and encouragement from a long distance. I cannot find any word to describe how lucky I have felt to have them as the best people around myself.

Last but not least, I must express my very profound gratitude to my fiancé, Ehsan Soodmand, for providing me with unfailing support and continuous encouragement throughout the last year of my PhD. I truly appreciate his company, concerns, support and everything he has done for me. It has been many times I was very unbearable but he has been always by my side, giving me faith and motivation to do the job. I would also like to thank him for organising his/my life between Ireland and Germany. I hope he realises how much of this achievement is due to him.

A special mention goes to my father, Ataollah, who paved the path before me. I sadly lost him when I was 8 years old. I find it the best time now to thank him for choosing my adorable mom and believing in her. Dad, you must be proud of her and all she has done for us.

Table of contents

Acknowledgement ..... **I**

Table of Figures ..... **VII**

List of Tables ..... **XIII**

Publications ..... **XIV**

Glossary ..... **XV**

Abstract ..... **XVII**

Chapter 1-Introduction **1**

1.1. Background 1

1.2. Objectives 4

Chapter 2-Literature Review **7**

2.1. Skeletal muscle anatomy and microstructure 8

2.1.1. Muscle fibre 10

2.1.2. Connective tissue in skeletal muscle 11

2.2. Mechanical properties of skeletal muscle 26

2.2.1. Compressive behaviour of skeletal muscle 27

2.2.2. Tensile behaviour of skeletal muscle 30

2.2.3. Micromechanical response of connective tissue (ECM) under deformation 31

2.3. Collagen detection and visualisation 34

2.4. Mathematical models 36

2.4.1. Linear elastic 37

2.4.2. Nonlinear elastic 38

2.4.3. Linear viscoelastic 38

2.4.4. Nonlinear viscoelastic 40

2.5. Modelling of skeletal muscle 40

2.5.1. One-dimensional models 41

2.5.2. Three-dimensional nonlinear transversly isotropic modelling 44

2.5.3. Viscoelastic modelling 45

2.5.4. Micromechanical modelling 47

2.6. Concluding remarks and aims of thesis 48

Chapter 3-The *in vitro* passive elastic response of chicken pectoralis muscle to applied tensile and compressive deformation..... 51

3.1. Introduction 51
3.2. Methods 53
3.2.1. Sample preparation 53
3.2.2. Experimental set-up 55
3.2.3. Statistical Analysis 56
3.3. Data Analysis 56
3.4. Results 58
3.4.1. Passive mechanical behaviour 58
3.4.2. Rigor Mortis effects 59
3.4.3. Poisson's ratios 60
3.4.4. Fluid Exudation in compression 61
3.5. Discussion 61
3.5.1. Stress-stretch and Poisson's ratios results 61
3.5.2. Chicken versus Porcine comparison 64
3.5.3. Experimental aspects 66
3.6. Conclusions 69

Chapter 4-Visualisation of collagen in fixed skeletal muscle tissue using fluorescently tagged collagen binding protein CNA35 71

4.1. Introduction 71
4.2. Methods 74
4.2.1. Sample preparation 74
4.2.2. Wax embedding of tissue sample 74
4.2.3. Cryopreservation and preparation of frozen tissue sections 75
4.2.4. Purification of collagen binding protein 76
4.2.5. Antigen retrieval treatment 76
4.2.6. Blocking of non-specific binding and incubation with binding protein 77
4.2.7. Fluorescence visualisation 77
4.3. Results 78
4.4. Discussion 83
4.5. Conclusion 86

Chapter 5-Collagen fibril organisation in skeletal muscle perimysium under tension and compression 87

5.1. Introduction 87
5.2. Methods 90
5.2.1. Sample preparation 90
5.2.2. Analysis criteria 93
5.3. Results 96
5.3.1. Overview of visualisation of collagen fibre organisation within perimysium in different species, muscles and section planes 96
5.3.2. Perimysium collagen structure under different deformation conditions 98
5.4. Discussion 104
5.4.1. Relationship between perimysium orientation under deformation and the stress-strain response in skeletal muscle 105
5.4.2. Cross-species mechanical differences based on perimysium collagen fibre microstructure 106
5.4.3. The prospect of three-dimensional imaging 108
5.4.4. Limitations 109
5.5. Conclusion 109
Chapter 6-A microstructural-geometrical muscle model to assess tension/compression asymmetry 111
6.1. Introduction 111
6.2. Methods 114
6.2.1. Contribution of muscle fibres in stress response 115
6.2.2. Contribution of perimysium in stress response 116
6.2.3. Model parameters 126
6.3. Results 127
6.3.1. General findings 127
6.3.2. Sensitivity analysis 129
6.4. Discussion 133
6.4.1. Muscle fibres and perimysium contributions to stress response 134
6.4.2. Tension/compression asymmetry 135
6.4.3. Limitations 138
6.5. Conclusion 139
Chapter 7- General discussion and future work 141
7.1. The main contributions of the thesis 141
7.2. Guidelines for future work 149

Bibliography 153

Appendix A-The Poisson's ratio versus stretch ratio in tension and compression deformations for chicken pectoralis muscle 167

Appendix B-Purification of fusion protein from bacteria 169

Appendix C- Making LB broth/agar 173

Appendix D-The capability of the microstructural-geometrical model in predicting the porcine compressive and tensile stress response reported in Takaza et al. (2013) and Van Loocke et al. (2006) 175

Table of Figures

Figure 1. 1-Comparison of passive elastic passive behaviour of porcine skeletal muscle for deformations applied at different angles (α) with respect to the muscle fibre direction: (A) compression, and (B) tension. Yellow and red circles highlight the stress observed in tension and compression at maximum stretch ratio (adapted from Takaza et al. (2014)). 3

Figure 2. 1-Schematic representation of ECM structure of skeletal muscle (adapted from www.anatomyofthefoot.com). 9
Figure 2. 2-Skeletal muscle fibre and filaments structure (adapted from www.pinterest.com). 10
Figure 2. 3-Mechanical role of the ECM in muscle modulus on a mouse extensor digitorum longus (EDL) muscle. (a) Individual fibres show linear behaviour, whereas muscle bundles including ECM show a nonlinear relationship. (b) Fibre groups excluding ECM (made of only muscle fibres) have a modulus similar in value to single fibres, but fibre bundles containing ECM have a significantly higher modulus, indicating that ECM is responsible for the increased modulus in the muscle tissue (adapted from Meyer and Lieber (2011)). 12
Figure 2. 4-Mechanical behaviour of intact and decellularised mouse tibialis anterior muscle bundles. Comparable Stress-strain behaviour between decellularised muscle and intact muscle (adapted from Gillies et al. (2011)). 13
Figure 2. 5-The honeycomb structure of endomysium collagen fibres. Scale bar indicates 1 mm (adapted from Purslow and Trotter (1994)). 13
Figure 2. 6-SEM image of mouse extensor digitorum longus muscle. (a) Patch of ECM separated from muscle fibres during sample preparation. Each white rectangle is enlarged in other parts of the figure. (b) A longitudinal organisation of ECM on the fibre surface and its periodicity is shown with white lines. (c) Central segment of the ECM patch separated from muscle fibre surface showing the wavy and random Collagen fibre organisation. (d) The connection between the ECM patch separated and the muscle fibre surface. Scale bar indicate 10 µm in A and 2 µm in others (adapted from Gillies and Lieber (2011)). 14
Figure 2. 7-SEM image of endomysium collagen architecture in chicken pectoralis muscle for (a) a 21-day old chick, (b) a 80 day old broiler. (c) Endomysium wall in a 21-day old chick, and (d) Endomysium wall in a 80 day old broilers. Scale bar indicates 5 mm in a, 10 mm in b, and 2 mm in c & d (adapted from Das et al. (2010)). 15

Figure 2. 8-The distributions of endomysial collagen fibre orientation (in degrees) at (a) muscle rest length, (b) highly shortened muscle, and (c) highly lengthened muscle. Muscle fibre is along the horizontal axis of this Figure (adapted from Purslow and Trotter (1994)). 16
Figure 2. 9-SEM image of the perimysium collagen network of bovine flexor carpi radilais: (a) the overall structure of collagen interwoven fibres in the longitudinal direction, (b) the distribution of plexi at the surface of myofibre (p), (c) plexi attaching to the surface of adjacent myofibres (note the collagen fibres make an angle of approximately 60° with respect to the myofibres), (d) the attachment of perimysium plexi to myofibres at the level of a particular structure (the perimysial junctional plate (PJP)), and (e) high magnification image showing the merging of the perimysium with the endomysium (e) at the extremities of two branches of the same plexus (adapted from Passerieux et al. (2006)). . 19
Figure 2. 10-SEM image showing the fundamental collagen architecture of chicken pectorais muscle (80 day old broilers). (a) Secondary perimysium. S; stack of thin plate-like collagen fibres with longitudinal striation, R; reticulum of cord-like collagen fibres with transverse striation. Scale bar indicates 50 mm, (b) perimysium collagen fibres in the stack. Scale bar indicates 50 mm in (a) and 5 mm in (b) (adapted from Das et al. (2010)). 20
Figure 2. 11-SEM image of perimysium. (a) Thick perimysium in White Leghorn (WL) cock (iliotibialis lateralispars postacetabularis (ITL) muscle (scale bar=5 mm), (b) Thin perimysium in Silkie cock (scale bar=5 mm), (c & d) Thin perimysium in WL cock (scale bar=1 mm). CB; circumferential collagen fibre bundles and LB; longitudinal Collagen fibre bundles (adapted from Iwamoto et al. (2001)). 21
Figure 2. 12-SEM image of mouse EDL muscle stretched about 30% beyond resting length showing longitudinally aligned perimysium collagen cables. (a) Two muscle fibres separated by stretched collagen cables, (b) a collagen cable becomes frayed as it traverses across collagen cables (adapted from Gillies and Lieber (2011)). 22
Figure 2. 13-Light micrograph of epimysium from bovine sternomandibularis muscle, showing arrangement of collagen fibres in crossed-plies. The fibres are in two parallel layers lying at +55° and -55° to the muscle fibre axis (adapted from Purslow (2005)). 25
Figure 2. 14-SEM micrographs of epimysium of a mouse EDL muscle. (a) The muscle view where a region can be observed with sarcomere repetitions through the connective tissue layer. An individual muscle fibre is noted (dashed line), (b) A closer view of the epimysium reveals longitudinal periodicities (lines) (adapted from Gillies and Lieber (2011)). 26
Figure 2. 15-Nonlinear viscoelastic response of porcine muscle (adapted from Grieve and Armstrong (1988)). 27
Figure 2. 16-Comparison of compressive stress – strain response for skeletal muscle from previous studies. 29

Figure 2. 17-Comparison of tensile stress – stretch response for skeletal muscle from previous studies. 30
Figure 2. 18-Schematic illustration a best-fit ellipse and its components for one of the muscle fibres .The major axis is the longer diameter of the best fitted ellipse and the shorter diameter is the minor axis. The angle that the major axis makes with the horizontal edge of the image is called the major axis angle of the muscle fibre (adapted from Takaza et al. (2014)). 33
Figure 2. 19-Major axis orientation angle (degrees) of muscle fibre cross-sectional areas: (A) control samples, (B) 30% tension in the fibre direction, (C) 30% tension in the cross-fibre direction, (D) 30% compression in the fibre direction and (E) 30% compression in the cross-fibre direction (adapted from Takaza et al. (2014)). 34
Figure 2. 20-Stress-strain curve for a linear elastic material (adapted from www.pt.ntu.edu.tw). 37
Figure 2. 21-(a) Voigt model, (b) Kelvin model or standard linear solid model, (c) general Kelvin-Voigt model (adapted from www.rehab.research.va.gov). 40
Figure 2. 22- Force-velocity curve of muscle at eccentric, isometric and concentric contraction (adapted from http://www.pt.ntu.edu.tw). 41
Figure 2. 23-Hill's muscle model; parallel elastic element (PE), contractile element (CE), series elastic element (SE). 42
Figure 2. 24-Muscle twitch force verses length relative to the resting length for active, passive and total characterization of muscle behaviour (adapted from www.wikipedia.org). 43
Figure 2. 25-(a) Compression tests on aged porcine samples fitted with Humphrey's model, (b) Compression tests on aged porcine samples fitted with strain dependent Young's moduli (SYM), (c) Compression test on fresh porcine samples fitted with the SYM model, (d) comparison between experimental data and theoretical predictions using SYM model. F (compression in the fibre direction), XF (compression in the cross-fibre direction), and 30, 45, and 60° are compression in within angles (a & b adapted from Van Loocke et al. (2006) , and c & d adapted from Van Loocke (2007)). 46

Figure 3. 1-Schematic of prepared specimens: L is the longitudinal direction, T & T' are the transverse directions. 54
Figure 3. 2-Zwick machine set up used for mechanical testing (a) a sample between platens for a compression test (b) a sample between grater clamps for a tensile test(c). Scale bars indicate 10 mm. 56
Figure 3. 3-Schematic illustration of the markers on the samples before and after deformation. 58
Figure 3. 4-Cauchy stress-stretch relations for chicken pectoralis muscle tissue in fibre, cross-fibre and 45 ° orientations (mean value± one standard): (a) Applied Compression; (b) Applied Tension. 59

Figure 3. 5-The effect of time after death on the stress response of fresh chicken muscle samples; (a) Cauchy stresses in compression were calculated at λ=0.7 for all samples (b) Cauchy stresses in tension were calculated at λ=1.2 in the fibre and cross-fibre directions, and λ=1.12 in 45 ° direction (c) all compression samples combined (d) all tension samples combined (λ=1.12). 60
Figure 3. 6-The fluid exudation during quasi-static compression test for fresh chicken samples in fibre, cross-fibre and 45° orientations. 61
Figure 3. 7-Comparison of compressive stress – strain response for skeletal muscle from previous studies. 63
Figure 3. 8-Comparison of tensile stress – stretch response for skeletal muscle from previous studies. 64
Figure 3. 9-Comparison of passive elastic behaviour of porcine and chicken skeletal muscle in (a) compression, and (b) tension. 65

Figure 4. 1-The effect of tissue preparation on collagen detection using CNA35-EGFP 79
Figure 4. 2- The effect of blocking agent and preservation type on collagen detection using CNA35-EGFP. 80
Figure 4. 3-Binding protein exposure variables on collagen detection 82
Figure 4. 4-Application of fluorescent binding protein detection of collagen to a) carry out double staining of Collagen (CNA35-tdTomato (red)) and muscle by immunodetection of myosin (green) (nuclei are visible through autofluoresence in yellow) and b) use high resolution confocal microscopy to visualize collagen fibril organisation (3D image made by Imaris software from a confocal stack). (a&b) chicken pectoralis muscle. Scale bars indicate (a) 50 μm, (b) 10 μm. Section thickness: 15 μm. 83
Figure 4. 5-The flowchart shows a summary of preferred conditions to detect collagen fibres in skeletal muscle following sensitivity studies..... 84

Figure 5. 1- Proposed organization of perimysium collagen fibres in mucle ECM: (a) schematic illustration of muscle tissue showing a fascicle (outlined in blue) in cross-section; each fascicle contains a group of muscle fibres, (b) collagen fibre organization in undeformed (control) tissue; w1 and w2 (dark green) represent the perimysium visible in the cross-sectional plane and longitudinal direction respectively, while w3 is individual collagen fibril waviness (crimp) within each perimysium sheet (light green), θ: the angle of collagen fibrils within the perimysium sheet with respect to muscle fibres. L is the longitudinal muscle fibre direction, T & T’ are the transverse directions. 90

Figure 5. 2-Compressive vice (a) and tensile rig (b) used for controlled muscle deformation. Samples loaded in the tension rig for deformed(c). 93
Figure 5. 3-Exclusion of regions where perimysium became detached from adjacent muscle fascicles. 94
Figure 5. 4-Definition of collagen fibre “waviness” within perimysium requires high magnification to view individual fibrils. 95
Figure 5. 5-Visualisation of fluorescently tagged collagen fibres revealing perimysium organisation. 97
Figure 5. 6-Visualisation of w1 in collagen fibrils of perimysium in transverse sections for undeformed, and externally applied compression and tensile deformations in chicken pectoralis (i), porcine biceps femoris (ii), and porcine longissimus dorsi (iii) muscles. 100
Figure 5. 7-Visualisation of w2 in collagen fibrils of perimysium in longitudinal sections for undeformed, and externally applied compression and tensile deformations in chicken pectoralis muscle. 101
Figure 5. 8-The three-dimensional reorganisation/reorientation of perimysium collagen fibrils when the tissue is exposed to externally applied deformations in chicken pectoralis (i), porcine biceps femoris (ii), and porcine longissimus dorsi (iii) muscles. 103

Figure 6. 1-Schematic representation of muscle fascicle surrounded by its connective tissue called perimysium. 115
Figure 6. 2-Schematic representation of a muscle fascicle surrounded by perimysium under tension in the fibre direction (Tension-Fibre) deformation. 118
Figure 6. 3-Schematic representation of a muscle fascicle surrounded by perimysium under tension in the cross-fibre direction (Tension-XFibre) deformation. 121
Figure 6. 4-Schematic representation of a muscle fascicle surrounded by perimysium under compression in the fibre direction (Compression-Fibre) deformation 123
Figure 6. 5-Schematic representation of a muscle fascicle surrounded by perimysium under compression in the cross-fibre direction (Compression-XFibre) deformation. 125
Figure 6. 6-Stress response of the muscle fascicle excluding its connective tissue (perimysium) versus the applied stretch in the fibre direction. 128
Figure 6. 7-Model-predicted stress response in tension and compression in both the fibre and cross-fibre directions for the whole muscle as well as perimysium; (a) the stress-stretch response in perimysium, (b) the stress-stretch response in the whole muscle (fascicle+perimysium) in comparison with the chicken experimental data. This base model is based on the middle values for the variables ($w = 1.18$, $Esheet = 500\ MPa$ and $pc = 1.75\%$). 129

Figure 6. 8-The comparison between the stress-stretch response of the whole muscle predicted by the model and the experimental results for chicken tissue at fixed waviness of 1.18 and 1.75% connective tissue for different Elastic modulus ranging from 200-800 MPa. 130
Figure 6. 9-The comparison between stress-stretch response of the whole muscle predicted by the model and the experimental results for chicken tissue at fixed waviness of 1.18 and Elastic modulus of 500 MPa for different percentage of connective tissue existed in the muscle ranging from 0.5-3%. 131
Figure 6. 10-The comparison between stress-stretch response of the whole muscle predicted by the model and the experimental results for chicken tissue at fixed 1.75% of connective tissue and Elastic modulus of 500 MPa for different waviness ranging from 1.05-1.3. 133
Figure 6. 11-Relative contribution of the muscle fibres and perimysium to total stress observed in the muscle in Tension-Fibre and Compression-XFibre deformations using the optimum model parameters; connective tissue percentage of $pc = 1.75$, Elast modulus of $Ec = 300\ MPa$, and the waviness of $w = 1.25$. 134
Figure 6. 12-The best predication of the model for tensile and compressive response of chicken muscle tissue. (a) The stress-stretch response of the muscle predicted by the model using the optimum model parameters; connective tissue percentage of $pc = 1.75$, Elast modulus of $Ec = 300\ MPa$, and waviness of $w = 1.25$. (b) The stress response of the muscle in limited range of stretch ratios (from 0.9-1.1) to show the capability of the model to predict the experimental data. 136
Figure 6. 13-The model predication for tensile and compressive response of chicken muscle tissue by changing the waviness observed in the transverse direction($w1$)using the optimum model parameters; connective tissue percentage of $pc = 1.75$, Elast modulus of $Ec = 300\ MPa$, and waviness of $w2 = 1.25$. (a) The stress-stretch response of the muscle predicted by the model using $w1 = 1.05$. (b) The stress-stretch response of the muscle predicted by the model using $w1 = 1.15$. 137
Figure 6. 14- Comparison between Gindre et al. (2013) micromechanical model and the current model predication for the response of chicken muscle in tensile and compressive deformations applied in the muscle fibre direction. 138

Figure 7. 1-Schematic illustration of the different steps conducted in the current thesis as an effort to explore the microstructural reason for tension /compression asymmetry observed in skeletal muscle of different species. 142

List of Tables

Table 2. 1-Poisson's ratio comparison between chicken and porcine tissue in compression and tensile tests. 31

Table 3. 1-The sample size and the average specimen dimensions at different orientations for compression tests. 54
Table 3. 2-The sample size and the average specimen dimensions at different orientations for tensile test. 55
Table 3. 3-The Poisson's ratios of pectoralis chicken skeletal muscle in compression and tension 61
Table 3. 4-Poisson's ratio comparison between chicken and porcine tissue in compression and tensile tests. 66

Table 4. 1-The steps and timing for dehydration and clearing of muscle samples for wax embedding. 75
Table 4. 2- The steps and timing for dewaxing sections. 75

Table 5. 1- Overview of species, muscle type, section orientation and deformation parameters used to assess and compare collagen organisation. 92
Table 5. 2-Summary of perimysium behaviour (straightness/waviness) at transverse plane and longitudinal direction. 104
Table 5. 3-The collagen content of chicken pectoralis and porcine longissimus dorsi muscles derived from the literature. 108

Table 6. 1-Summary of model equations in different deformation applied in different directions... 126
Table 6. 2-Literature range and model range of values used for model parameters. 127

Publications

Mohammadkhah, M., Murphy, P., Simms, CK., "**The *in vitro* passive elastic response of chicken pectoralis muscle to applied tensile and compressive deformation",** J. The Mechanical Behaviour of Biomedical Materials (JMBBM) 62, 2016,pp 468-480.

Mohammadkhah, M., Simms, CK., Murphy, P., "**Visualisation of collagen in fixed skeletal muscle tissue using fluorescently tagged Collagen binding protein CNA35",** J. The Mechanical Behaviour of Biomedical Materials (JMBBM), 66, 2017, pp 37-44.

Submitted manuscripts

Mohammadkhah, M., Murphy, P., Simms, C.K., "**Collagen fibril organization in chicken and porcine skeletal muscle perimysium under tension and compression"**- submitted to J. The Mechanical Behaviour of Biomedical Materials (JMBBM).

Latorre, M., Mohammadkhah, M., Simms,C.K., Montans, F.J., **"A continuum model for tension-compression asymmetry in skeletal muscle"**- submitted to J. The Mechanical Behaviour of Biomedical Materials (JMBBM).

Conference abstracts

Mohammadkhah, M., Murphy, M., Simms, C.K. **"The relationship between skeletal muscle stress-strain response and microstructure through a microstructural-geometrical muscle model",** Accepted abstract for podium presentation in 23rd Congress of the European Society of Biomechanics (ESB 2017), Seville, Spain, July 2017.

Mohammadkhah, M., Murphy, M., Simms, C.K. **"Collagen fibril organisation in skeletal muscle perimysium under tension and compression",** Oral presentation, Bioengineering in Ireland, Belfast, Northern Ireland, January 2017.

Mohammadkhah, M., Murphy, M., Simms, C.K. **"On the relationship between stress-strain response and tissue microstructure in skeletal muscle",** podium presentation in 22nd Congress of the European Society of Biomechanics (ESB 2016), Lyon, France, July 2016.

Mohammadkhah, M., Murphy, M., Simms, C.K. **"Investigating tension/compression asymmetry in skeletal muscle",** Oral presentation, Bioengineering in Ireland, Galway, Ireland, January 2016.

Mohammadkhah, M., Murphy, M., Simms, C.K. **"Microstructure and mechanical behaviour in passive skeletal muscle",** Poster presentation in 21st Congress of the European Society of Biomechanics (ESB 2015), Prague, Czech Republic, July 2015.

Mohammadkhah, M., Murphy, M., Simms, C.K. "**The relationship between elastic passive macro mechanical behaviour and microstructure of chicken skeletal muscle**", Oral presentation, Bioengineering in Ireland, Maynooth, Ireland, January 2015.

Mohammadkhah, M., Murphy, M., Simms, C.K. "**Passive skeletal muscle form and function: Engineering insights from zoology**", Poster & oral presentation, Bioengineering in Ireland, Limerick, Ireland, January 2014.

Glossary

Term	Description	Unit
a_0	Initial edge of perimysium cross section	m
a_1	Width of perimysium cross section after applied deformation	m
a_2	Length of perimysium cross section after applied deformation	m
A_{c0}	Initial cross sectional area of perimysium	m^2
A_c	True cross-sectional area of perimysium after deformation	m^2
A_{muscle_fibre}	Cross sectional area of one muscle fibre	m^2
$A_{musclefascicle}$	Cross sectional area of muscle fascicle	m^2
E_{sheet}	Young's (Elastic) modulus of Collagen	Pa
f_{titin}	Force developed in one single titin molecule	N
F_{titin}	Force developed in one single muscle fibre	N
$F_{muscle\ fasicle}$	Force developed in muscle fascicle	N
F_{sheet_tenf}	Direct longitudinal force in perimysium in Tension-Fibre deformation	N
F_{sheet_tenxf}	Pressure-induced longitudinal force in perimysium in Tension-XFibre deformation	N
F_{sheet_compf}	Pressure-induced longitudinal force in perimysium in Compression-Fibre deformation	N
F_{sheet_compxf}	Direct longitudinal force in perimysium in Compression-XFibre deformation	N
k_b	Boltzman constant	JK^{-1}
L_p	Titin persistence length	m
L_c	Titin contour length	m
L	Longitudinal muscle fibre direction	-
n_1	Number of titin molecules per units of cross-sectional area of muscle fibre	m^{-2}
n_2	Number of titin molecules per units of length along the muscle fibre	m^{-1}
n_f	Number of muscle fibres existed in one fascicle	-
p_c	Percentage of connective tissue	%
P	Internal pressure generated by circumferentially developed force in muscle	Pa
t	Perimysium thickness	m
T	Absolute temperature	K
T & T'	Transverse directions	-
$w1$	Waviness of perimysium sheet in the transverse direction	-
$w2$	Waviness of perimysium sheet in the longitudinal direction	-
λ_{sheet}^{app}	Apparent perimysium stretch	-
λ_{sheet}^{true}	Effective (true) perimysium stretch	-

λ_L	Longitudinal stretch ratio (in L direction)	-
λ_T	Transverse stretch ratio (in T direction)	-
$\lambda_{T'}$	Transverse stretch ratio (in T' direction)	-
ε_L	Longitudinal strain (in L direction)	-
ε_T	Transverse strain (in T direction)	-
$\varepsilon_{T'}$	Transverse strain (in T' direction)	-
$\nu_{LT} = \nu_{LT'}$	Poisson's ratio (Induced deformation in the transverse directions when the tissue is deformed longitudinally)	-
υ_{TL}	Poisson's ratio (Induced deformation in the longitudinal (L) direction when the tissue is deformed in T direction)	-
$\upsilon_{TT'}$	Poisson's ratio (Induced deformation in the transverse (T') direction when the tissue is deformed in T direction)	-
σ_{sheet}	Stress developed in perimysium	Pa
Δz	Stretch in one titin molecule	-
tenf	Tension applied in the muscle fibre direction	-
tenxf	Tension applied in the cross muscle fibre direction	-
compf	Compression applied in the muscle fibre direction	-
compxf	Compression applied in the cross muscle fibre direction	-

Abstract

The general aim of this study is to advance the knowledge of the relationship between the skeletal muscle passive compressive and tensile behaviour, and the microstructure of the muscle through combined experimental, microstructural and theoretical approaches.

The mechanics of passive skeletal muscle are important in many biomechanical applications. Existing data from porcine tissue has shown a significant tension/compression asymmetry, which is not captured by current constitutive modelling approaches using a single set of material parameters, and an adequate explanation for this effect remains elusive. In this thesis, the passive elastic deformation properties of chicken pectoralis muscle are assessed for the first time, to provide deformation data on a skeletal muscle which is very different to porcine tissue. Uniaxial, quasi-static compression and tensile tests were performed on fresh chicken pectoralis muscle in the fibre and cross-fibre directions, and at 45° to the fibre direction.

Results show that chicken muscle elastic behaviour is nonlinear and anisotropic. The tensile stress–stretch response is two orders of magnitude larger than in compression for all directions tested, which reflects the tension/compression asymmetry previously observed in porcine tissue. In compression the tissue is stiffest in the cross-fibre direction. However, tensile deformation applied at 45° gives the stiffest response, and this is different to previous findings relating to porcine tissue. Chicken muscle tissue is most compliant in the fibre direction for both tensile and compressive applied deformation. Generally, a small percentage of fluid exudation was observed in the compressive samples.

Since collagen is the main structural protein in animal connective tissues, it is believed to be primarily responsible for their passive load-bearing properties. The direct detection and visualisation of collagen using fluorescently tagged CNA35 binding protein (fused to EGFP or tdTomato) is also reported for the first time on fixed skeletal muscle tissue. A working protocol is then established by examining tissue preparation, dilution factor, exposure time etc. for sensitivity and specificity. Penetration of the binding protein into intact mature skeletal muscle was found to be very limited, but detection works well on tissue sections with higher sensitivity on wax embedded sections compared to frozen sections. CNA35 fused to tdTomato has a higher sensitivity than CNA35 fused to EGFP but both show specific detection. Best results were obtained with 15 µm wax embedded sections, with blocking of non-specific binding in 1% BSA and antigen retrieval in Sodium Citrate. There was a play-off between dilution of the binding protein and time of incubation but both CNA35-tdTomato and CNA35-EGFP worked well with approximately 100 µg/ml of purified protein with overnight incubation, while CNA35- tdTomato could be utilized at 5 fold less concentration.

The tension/compression asymmetry observed in the stress-strain response of skeletal muscle is not well understood. The optimised protocol is then applied to report qualitatively on skeletal muscle ECM reorganization during applied deformation using a combination of CNA35 binding protein and confocal imaging of tensile and compressive deformation of porcine and chicken muscle samples applied in both the fibre and cross-fibre directions. Results show the overall three-dimensional structure of collagen in perimysium visible in planes perpendicular (w1) and parallel (w2) to the muscle fibres in both porcine and chicken skeletal muscle. Furthermore, there is clear evidence of the reorganization of these structures under compression and tension applied in both the muscle fibre and cross-fibre directions, which generally explains anisotropy observed in the stress-strain response of skeletal muscle both in tension and compression for chicken and porcine tissues. These observations improve our understanding of how perimysium responds to three-dimensional deformations.

The proposed three-dimensional illustration of perimysium structure is then used as a basis to create a microstructural-geometrical model to predict the passive mechanical stress-strain response observed in skeletal muscle. The current model represents the whole muscle response as a combination of both a group of muscle fibres (fascicle) response and the perimysium (ECM) response. It shows that although perimysium was believed to be a key element in the muscle stress response, the muscle fibres (in Tension-Fibre and Compression-XFibre deformations) also contribute to stress-stretch response since the order of magnitude for the stress in muscle fibres is similar to that of perimysium.

The model shows more asymmetric response than previously published micromechanical model (Gindre et al., 2013). The model yields a good prediction of the whole muscle behaviour in Tension-Fibre and Compression-Fibre deformations using the optimum values for the model parameters obtained from the conducted sensitivity studies; connective tissue percentage of $p_c = 1.75$, Elast modulus of $E_c = 300\,MPa$, and perimysium sheet waviness of $w = 1.25$. However, the model overestimates the Compression-XFibre deformation and underestimates the Tension-XFibre deformations even by using the optimum parameters.

The current model attempts to relate the mechanical stress-stretch response observed in muscle to the collagen reorganization in the muscle microstructure under load application, which further help develop better constitutive models for finite element modelling purposes.

Chapter 1-Introduction

Conquer yourself rather than the world.

RENE DESCARTES.

1.1. Background

Skeletal muscle accounts for 40% of total body mass (Chomentowski et al., 2011). These muscles are force-producing elements for locomotion and breathing, as well as postural support and protection of the skeleton by distributing loads and absorbing shocks (Powers and Howley, 2012). About 10% of skeletal muscle is made of collagen fibres which are actually protein molecules. These collagen fibres exist in the extra cellular matrix (ECM) and have shown strong mechanical properties (Williams et al., 1995, Dransfield, 1977, Meyer and Lieber, 2011, Martins et al., 1998).

The mechanical response of biological tissues, particularly skeletal muscle, to various loading and deformation conditions is of great interest as it provides a deep understanding into modelling and designing methods to prevent injuries.

The total stress response of muscle comes from both passive and active contributions; however only the passive properties of muscle tissue are evaluated in the current research. In impact experiments (the current research standard), the time scale of the event does not allow sufficient time for muscles to be activated; therefore the stress response is mainly due to the passive properties of the tissue. Similarly, in modelling of pressure sores, a quasi-static situation, the passive description of muscles is more relevant (Simms et al., 2012).

Clearly, a better description of soft tissues is required to enhance the accuracy of models. Some examples of compressive loading on skeletal muscle are found in the applied field of impact biomechanics to determine the body's impact response during automotive accidents, reduce physical injuries, and to improve automotive safety in order to decrease the large numbers of people who die in road accidents each year (Cai et al., 2014, Meijer et al., 2013, Takaza and Simms, 2012, Ivancic et al., 2007, Mukherjee et al., 2007, Praxl et al., 2008).

Another interesting area of muscle modelling is rehabilitation engineering to find solutions for an individual's disabilities by improving the design of orthopaedic or other supportive devices for them (Linder-Ganz et al., 2007, Linder-Ganz et al., 2009).

Pressure sores are an injury to the skin (especially where the bones are close to the skin, such as at the ankles, back, elbows, heels and hips) and underlying tissue caused by staying in one position for an extended period of time. Bedridden patients and wheelchair users are at risk of developing pressure sores that can cause serious infection, which can extend into muscle and bone and become life-threatening.

The average medical cost for the surgical treatment of pressure sores stage III or IV is € 20,957 in the Netherlands (Filius et al., 2013). Pressure sores cost the United States $11 billion annually, which place considerable financial burden on the patients and this has the potential to impact health care systems globally (Cushing and Phillips, 2013).

Consequently, pressure sores are an important area in which our understanding of the compressive behaviour of skeletal muscle is required to develop new treatments, which could be essential and beneficial for both health care systems and patients.

Some finite element (FE) modelling has been used to study pressure sore formation and to improve custom designs for wheelchair users, and surgical simulation (Linder-Ganz and Gefen, 2008, Oomens et al., 2003). Xiao et al. (2014) constructed a FE model of a human buttock based on damage accumulation and repair theory for deep tissue injury (DTI) introduced previously by Mak et al. (2011). They showed that tissue healing rate, the loading–unloading pattern, and cushion stiffness are the key parameters that affect damage development. Their findings help rehabilitation engineers to consider

the importance of appropriate device design based on the parameters which influence the development of damage.

The above-mentioned applications are a few examples of studies performed to investigate skeletal muscle compressive behaviour among hundreds of conducted research studies, which show the importance of establishing skeletal muscle stress response in different loading conditions. These models require a good definition of tissue geometries, as well as material properties.

The mechanical responses of skeletal muscle in compression and tension are very different. As shown in Figure 1.1A, compression in the cross-fibre direction for porcine tissue yields the stiffest response, and also under tension (Figure 1.1B) this direction yields the stiffest response. 45° is the least stiff direction in compression, whereas under tension, the fibre direction gives the least stiff response. It may be expected since the fibre direction is the physiological working orientation for muscle. Apart from the nonlinearity, anisotropy and viscoelasticity pertinent to soft biological tissues, it has been observed that the stress response to stretching in both the fibre and cross-fibre directions is two orders of magnitude stiffer for tension than compression (Takaza et al., 2013a, Van Loocke et al., 2006), but conventional fibre-reinforced composite theory fails to capture this.

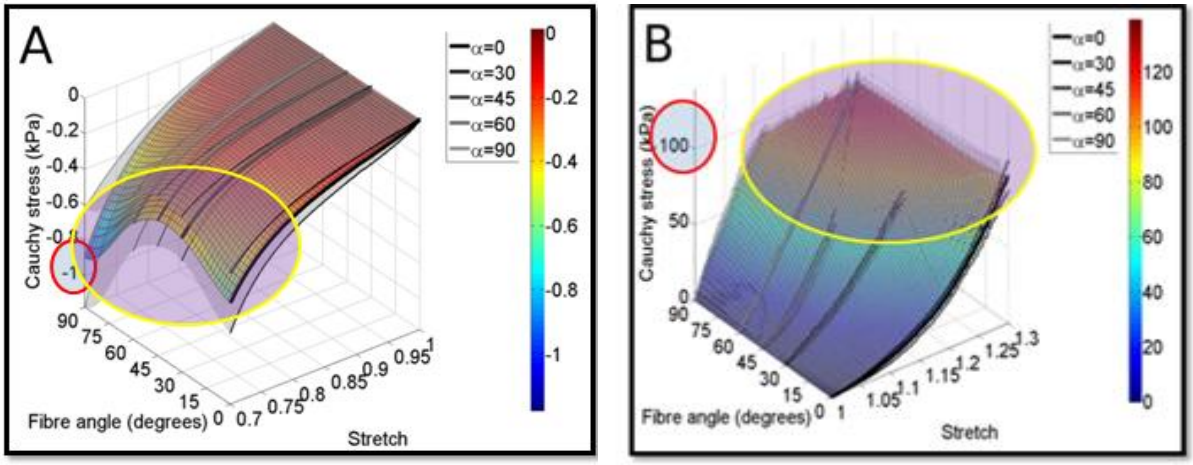

Figure 1. 1-Comparison of passive elastic passive behaviour of porcine skeletal muscle for deformations applied at different angles (α) with respect to the muscle fibre direction: (A) compression, and (B) tension. Yellow and red circles highlight the stress observed in tension and compression at maximum stretch ratio (adapted from Takaza et al. (2014)).

Skeletal muscle is different from other soft biological tissues as it is capable of active contraction. Furthermore, it has been shown that it also has a nonlinear and anisotropic behaviour due to its fibre-oriented structure and shows an asymmetrical tensional/compressive response to loading (Takaza et al., 2014, Takaza et al., 2013a, Van Loocke et al., 2006, Pietsch et al., 2014, Böl et al., 2014). However, this tension/compression asymmetry is not fully understood. Some preliminary studies have attempted to understand this asymmetrical behaviour. For instance, Takaza et al. (2014) and Pietsch et al. (2014) performed microstructural study and image analysis for porcine skeletal muscle where

the muscle was subjected to external compressive or tensile deformations. They attempted to relate the stress-strain response of muscle to the micro structural changes happening during applying deformations. Some useful informative micromechanical representations of skeletal muscle have been also conducted by the Purslow group to enhance the understanding of skeletal muscle microstructure and how it relates to the mechanical response, which will be discussed in detail in Chapter 2 (Trotter and Purslow, 1992, Purslow and Trotter, 1994, Purslow, 2010). As a result, many studies have recently focused on ECM structure as ECM influences the normal function of muscle and also alters and adapts during diseased states (Nishimura, 2010, Gillies et al., 2014, Purslow, 2010, Purslow, 2005, Purslow and Trotter, 1994, Purslow, 1989, Gillies and Lieber, 2011).

1.2. Objectives

Since skeletal muscles cover a considerable part of the body and since they play a vital role in body movement and strength, a good understanding of their response under different loading conditions, which obviously are based on their microstructure, is therefore very important to various biomechanics research areas. Therefore, the following general aims were sought to be achieved in the present project:

- To provide tensile and compressive stress-strain data on different species to gain a deeper understanding of variations in stress-strain response between species.
- To improve our knowledge/understanding of the connective tissue of skeletal muscle, particularly the perimysium, as it is believed to have a dominant role in load-bearing properties of tissue.
- To relate muscle microstructure to its stress-strain response; in particular to address the observed tension/compression asymmetry.
- To create a micromechanical-geometrical muscle model to relate the macro mechanical response to the muscle microstructure.

Chapter 2 is allocated to the literature review of published experimental and theoretical studies carried out on skeletal muscles in different scales to give insights into different aspects of the topic, which may be worthy of exploration and future research.

Chapter 3 covers the experimental investigation of passive elastic response of chicken skeletal muscle in tension and compression. Results from a uniaxial quasi-static compression and tensile tests along with Poisson's ratio measurement on chicken pectoralis muscle at different orientation of muscle fibres are presented.

Chapter 4 focuses on the visualisation of collagen in fixed chicken skeletal muscle tissue using fluorescently tagged Collagen binding protein CNA35, which helps us understand the structure of connective tissue in muscle specially perimysium to try to address tension/compression asymmetry.

In Chapter 5 the microscopic image analysis on the porcine and chicken tissues will be presented to demonstrate how muscle microstructure responds to different applied deformations at the micro level.

In Chapter 6, a microstructural-geometrical model of skeletal muscle is proposed in an effort to relate the muscle microstructure and the stress-stretch response observed in mechanical testing. This can be later used to develop better constitutive models for finite element analysis.

In Chapter 7, the main contributions of the thesis including the strengths and limitations of the work, as well as the potential future areas are discussed.

Chapter 2-Literature Review

This sky where we live is no place to lose your wings, so love, love, love.

HAFEZ, 14th CENTURY, PERSAIN POET.

The study of muscle structure and function is not a new topic as it has been an area of research for many years (Benninghoff and Rollhäuser, 1952, Gans and Bock, 1965).

Nevertheless, in the last few years, different components of the human skeletal system (bone, muscle, tendon, ligaments etc.) have been the focus of modelling to investigate their different responses to different loading conditions (e.g. tension or compression) since the qualitative and quantitative evaluation of these tissue responses are important in both damaged and healthy states (Henak et al., 2014, Li et al., 2009, Moo et al., 2014, Wu et al., 2014, Gillies and Lieber, 2011). The mechanical response of biological tissues to various loading and deformation conditions is of great interest as it provides an understanding for designing methods to prevent injuries.

Body mass primarily comprises bones and soft tissues such as skeletal muscle. The bones provide the structure and support to the body to help it keep its shape (Abraham et al., 2013), and they

undergo small deformations when exposed to physiological loads (Valdez and Balachandran, 2013). Nerve stimulation allows muscle to function actively by developing internal tension, force application then results in movement of body parts. Muscle tissue also acts passively, providing structural support and modifying the impact between bones and external loads on body.

Muscle as a soft tissue has several features commonly observed in other soft tissues such as nonlinear anisotropic stress–strain response and viscoelasticity, which have been well studied experimentally (Van Loocke et al., 2006, Van Loocke et al., 2008, Van Loocke et al., 2009, Gras et al., 2012a, Gras et al., 2012c, Gras et al., 2012b, Takaza et al., 2013a, Böl et al., 2014, Böl et al., 2012, Pietsch et al., 2014). Muscle also has excitability and contractibility, the ability to shorten in length and develop tension, which makes its description more challenging.

In this chapter different aspects of skeletal muscle studies conducted in recent years are covered as follows:

1. The microstructure of skeletal muscle is presented first to provide an overview of the tissue, which is of interest to the current study.
2. It is then followed by briefly introducing experimental studies conducted so far to characterise the passive compressive and tensile responses of skeletal muscles in different animals and types of skeletal muscle. It also discusses the experimental micromechanical studies performed to relate the mechanical response of muscle to its microstructure.
3. Detection and visualisation methods of collagen structure in skeletal muscle are then reviewed. This helps to understand the relationship between mechanical behaviour and microstructure in skeletal muscle.
4. General mathematical models, which have been used to model biological tissue, are then reviewed as the ultimate goal of performing mechanical experiments on soft tissues is to utilise the appropriate mechanical properties in modelling applications.
5. The chapter is finished by a concluding remark and outlining the aims of the current study.

2.1. Skeletal muscle anatomy and microstructure

There are three types of muscle tissue: Smooth, cardiac, and skeletal.

1. Smooth muscle exists within organs such as the stomach, intestines, and blood vessels. Smooth muscle is an involuntary muscle, which contracts an organ to move substances through the organ.
2. Cardiac muscle is also an involuntary muscle and is found only in the heart. It is responsible for pumping blood throughout the body.

3. Skeletal muscle is the only voluntary muscle tissue in the body; it is mostly controlled consciously. The function of skeletal muscle is to contract to move parts of the body closer to the bone to which the muscle is attached. Skeletal muscle cells form when many smaller progenitor cells lump themselves together to form long, straight, multinucleated, and very strong fibres. Skeletal muscle derives its name from the fact that these muscles always connect to the skeleton in at least one place (Martini, 1989).

Skeletal muscle accounts for 40% of the total body mass (Chomentowski et al., 2011). These muscles are force producing elements for locomotion, and provide breathing as well as postural support and protection to the skeleton by distributing loads and absorbing shocks (Powers and Howley, 2012). Moreover they are responsible for metabolism in body (Zurlo et al., 1990).

Another way of distinguishing skeletal muscle is through its hierarchy of organisation. Muscle components are grouped into increasingly complex structures, bound and supported by connective tissue. As shown in Figure 2.1 the skeletal muscle is composed of two main components; (1) a series of straight parallel fibres, embedded in (2) extracellular matrix (ECM), which maintains the integrity of muscle fibre bundles (Williams et al., 1995). The passive properties of muscle mostly depend on collagenous connective tissue's physical geometries such as thicknesses or diameter and its mechanical properties (Kjaer, 2004). It is no surprise why skeletal muscles studies primarily focused on the contractile feature because the contractile elements are the main part in force production in muscle (Huxley and Reconditi, 2012, Huxley, 1977, Kress et al., 1986, Nachmias et al., 1970, Oomens et al., 2003, Siebert et al., 2008). However, many studies have recently focused on ECM structure since it is indicated that the ECM influences the normal function of muscle and also alters and adapts during diseased states (Nishimura, 2010, Gillies et al., 2014, Purslow, 2010, Purslow, 2005, Purslow and Trotter, 1994, Purslow, 1989, Gillies and Lieber, 2011).

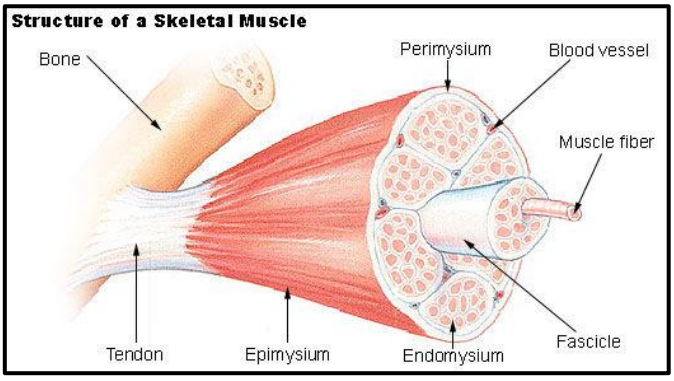

Figure 2. 1-Schematic representation of ECM structure of skeletal muscle (adapted from www.anatomyofthefoot.com).

2.1.1. Muscle fibre

The smallest contractile unit of skeletal muscle is the muscle fibre. A skeletal muscle fibre is a long, cylindrical, multinucleated cell that is filled with smaller units of filaments as shown in Figure 2.2. These filamentous structures are roughly aligned parallel to the muscle fibre itself. The largest filament is called a myofibril, composed of subunits called sarcomeres. Each sarcomere also contains filaments, known as myofilaments. There are two types of myofilaments within each sarcomere. The thicker myofilaments are composed of myosin protein, and the thinner myofilaments are composed of actin protein. Sliding of the actin myofilament along the myosin chain is the basic mechanism of muscle contraction (VanPutte and Seeley, 2014).

Approximately 20–80 muscle fibres are grouped together in a parallel arrangement called a muscle fascicle or fibre bundle (Rowe, 1974). There are two well known types of fascicle organisation: parallel and pennate fibred muscles. A pennate muscle is a muscle with fascicles obliquely attached to its tendon, and it contains more muscle fibres and as a result it generally allows for higher tension production but with a smaller range of motion (tension production is proportional to the number of contracting sarcomeres; the more muscle fibres, the more sarcomeres) (Martini, 1989, Schmalbruch, 2012). In parallel fibred muscles, the fibres are parallel to the loading direction, and sometimes muscle fibres do not cover the whole length of muscle, so the collagenous content (in other words, the ECM) plays a role in transmitting loads from muscle fibres to tendons (Archile-Contreras et al., 2010, Sharafi and Blemker, 2011).

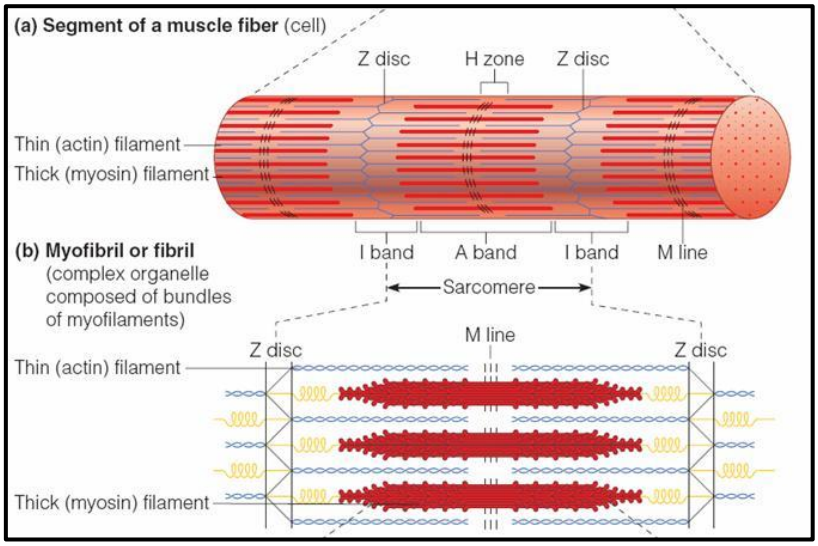

Figure 2. 2-Skeletal muscle fibre and filaments structure (adapted from www.pinterest.com).

Contraction in skeletal muscle is initiated by an electrical stimulus from the associated motor neuron causing depolarisation of the muscle fibre. As the muscle is attached to the bone at two ends, the contracting force produces a pulling force at both ends. When this force causes shortening, it is

called concentric contraction; where it results in lengthening of the muscle, it is called eccentric contraction, and where the force does not result in length change an isometric contraction happens (Herzog, 2001).

2.1.2. Connective tissue in skeletal muscle

Approximately 10% of skeletal muscles are made of collagen fibres which are essentially protein molecules arranged in a triple helix. This percentage varies from muscle to muscle between and within animal species, and the health condition of the muscle affects this ratio as well (Kjaer, 2004). These collagen fibres occupy the ECM (Williams et al., 1995, Dransfield, 1977).

Skeletal muscle contains collagen types I, III, IV, V, VI, XII and XIV (Listrat et al., 1999, Nishimura et al., 1998). The major types of collagen in skeletal muscle are type I and III (Bailey and Light, 1989, Light et al., 1985).

Collagen fibres have shown more stiffness compared to skeletal muscle fibres even though the percentage of collagen in muscles (in terms of relative mass) is not high. Single muscle fibre Young's modulus is between 6-160 kPa (Gillies and Lieber, 2011), whereas collagen has a stiffness of about 200-600 kPa (Gindre et al., 2013). The tensile strength of collagen is about 500-1000 times higher than skeletal muscle fibres (Martin et al., 1998). Skeletal muscle rich in collagen is tougher than those with low collagen content (Light et al., 1985, Nishiumi et al., 1995). However, Bailey and Light (1989) showed the pectoralis profundus muscle, with a high collagen content, has a lower stiffness than that of the gastrocnemius muscle, with low collagen content; this seems likely due to textural properties of various skeletal muscles.

There are two recently performed studies which characterised the ECM mechanical properties: 1) an indirect method which defined the ECM mechanical properties by characterising and comparing the modulus of a single muscle fibre with a muscle bundle. To calculate the ECM modulus, the load bearing areas of muscle fibre and the ECM were first defined and the rule of mixtures in composites was then used to calculate the ECM modulus. The results, as illustrated in Figure 2.3a, showed linear behaviour for a single muscle fibre and a nonlinear behaviour for a muscle bundle (Meyer and Lieber, 2011, Brown et al., 2012). However, since it was not obvious whether the ECM modulus is due to inherent nonlinearity in the ECM or if it is nonlinear because a bundle is composed of many muscle fibres with different nonlinear behaviour, some experiments were carried out to isolate many single muscle fibres to exclude the ECM and they were then grouped together into the size of the bundle. Figure 2.3b clearly shows that the group of muscle fibres without ECM also shows almost the same

range for modulus as shown in single fibres, whereas the ECM modulus is much larger (Meyer and Lieber, 2011).

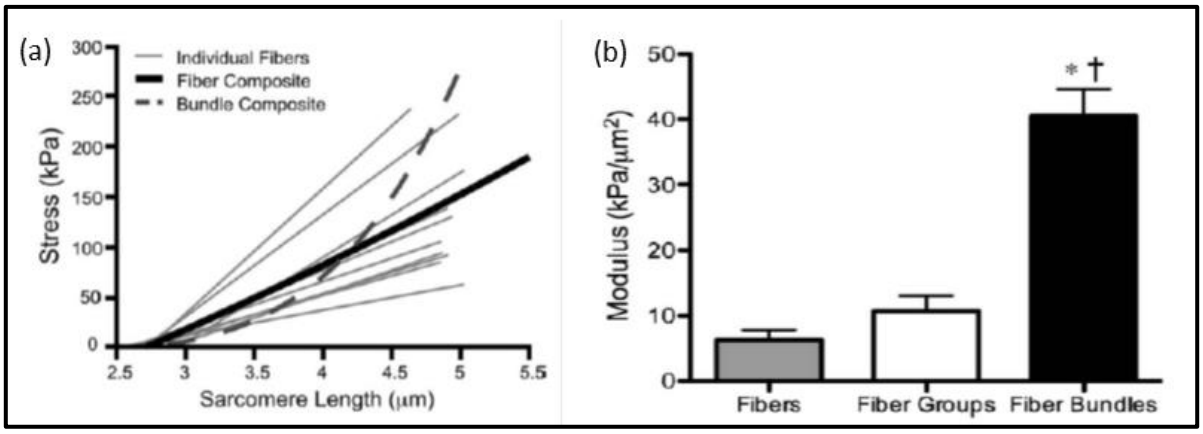

Figure 2. 3-Mechanical role of the ECM in muscle modulus on a mouse extensor digitorum longus (EDL) muscle. (a) Individual fibres show linear behaviour, whereas muscle bundles including ECM show a nonlinear relationship. (b) Fibre groups excluding ECM (made of only muscle fibres) have a modulus similar in value to single fibres, but fibre bundles containing ECM have a significantly higher modulus, indicating that ECM is responsible for the increased modulus in the muscle tissue (adapted from Meyer and Lieber (2011)).

2) In the direct method, a new approach to decellularise muscle was performed which removes muscle fibres with minimal disruption to the ECM structure (Gillies et al., 2011). In this method, 40% reduction was observed in glycosaminoglycan (GAG) which is still more efficient at retaining GAGs in muscle compared with other methods; however, opposite to other maceration methods, in this method the collagen content remains fairly constant so it is unlikely that the mechanical properties were affected (Gillies et al., 2011). This study showed that the mechanical behaviour (stress-strain relationship) of decellularised muscle was almost similar to that of intact as illustrated in Figure 2.4 This again supports the idea that the ECM is primarily the passive load bearing structure in skeletal muscle.

Evidently, the ECM plays an important role in the mechanical behaviour of skeletal muscle, which motivates further studies. In general the ECM hierarchical structure consists of the following layers: endomysium, perimysium, and epimysium.

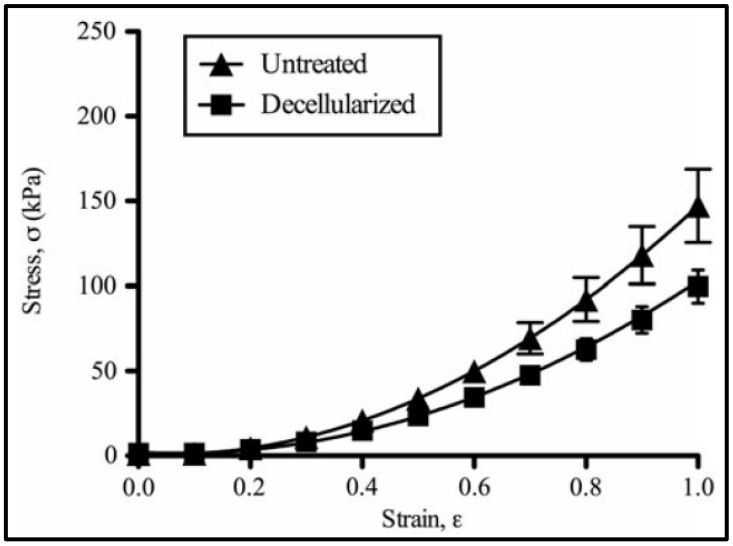

Figure 2. 4-Mechanical behaviour of intact and decellularised mouse tibialis anterior muscle bundles. Comparable Stress-strain behaviour between decellularised muscle and intact muscle (adapted from Gillies et al. (2011)).

2.1.2.1. Endomysium

A thin layer of connective tissue surrounding each individual muscle fibre is called the endomysium. Figure 2.5 shows that the endomysium in bovine muscle is like a honeycomb structure containing curvilinear collagen fibrils, which are randomly oriented (Trotter and Purslow, 1992, Purslow and Trotter, 1994, Fang et al., 1999). Endomysium consists of equal amounts of collagens type I and type III (Light and Champion, 1984). Endomysium structure seems generally similar in different skeletal muscles according to scanning electron microscopy (SEM) images taken from different animals (Purslow, 2008, Das et al., 2010, Gillies and Lieber, 2011).

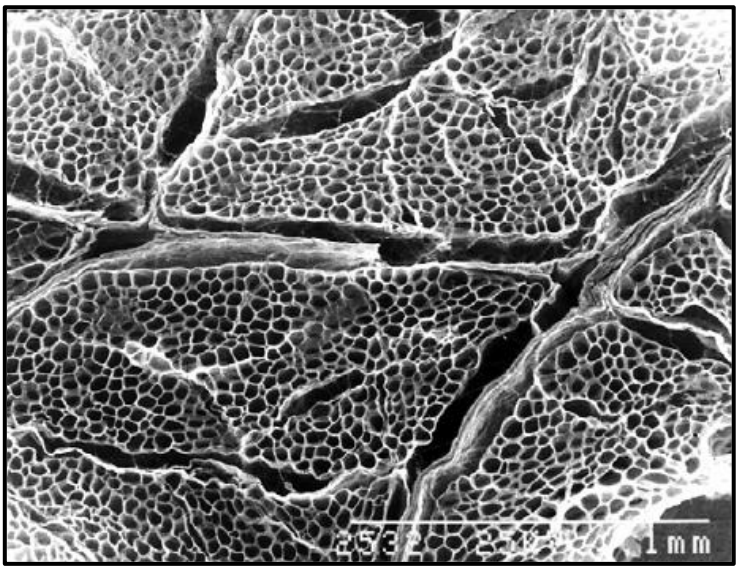

Figure 2. 5-The honeycomb structure of endomysium collagen fibres. Scale bar indicates 1 mm (adapted from Purslow and Trotter (1994)).

SEM micrographs of mouse extensor digitorum longus (EDL) revealed that where muscle fibres apparently separated during the tissue preparation process, patches of endomysium are observed (see Figure 2.6c). On the surface of muscle fibres close to the patch, the endomysium appeared to have a longitudinal orientation (see Figure 2.6b), whereas such orientation was not observed on the patch (see Figure 2.6d) (Gillies and Lieber, 2011).

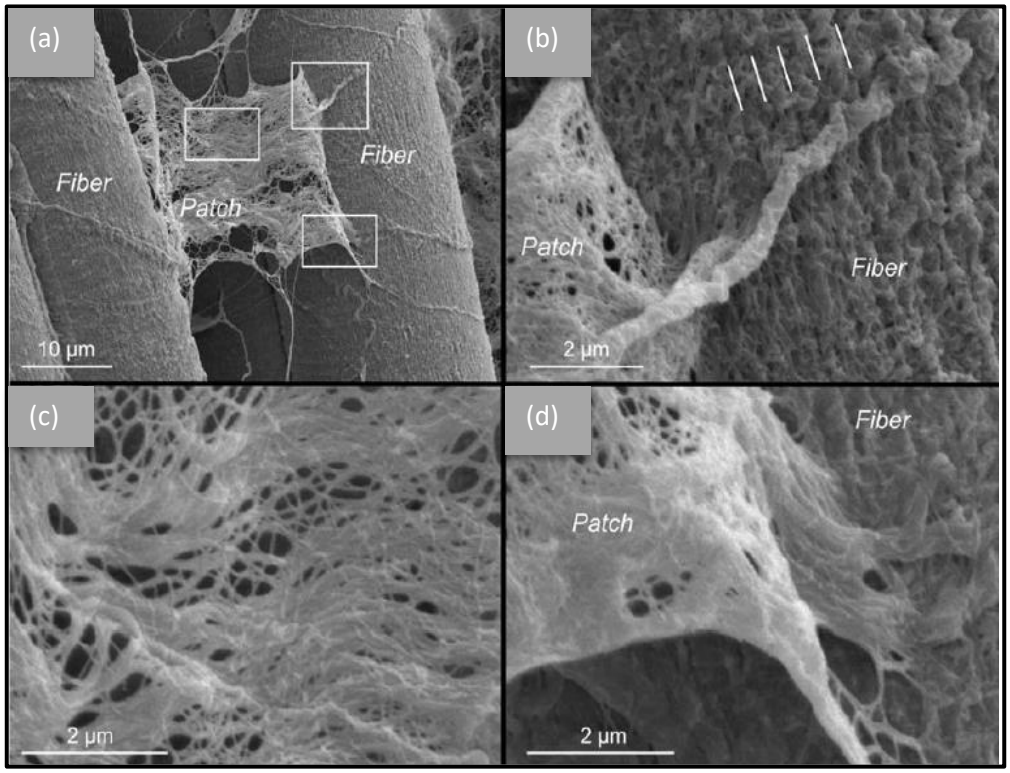

Figure 2. 6-SEM image of mouse extensor digitorum longus muscle. (a) Patch of ECM separated from muscle fibres during sample preparation. Each white rectangle is enlarged in other parts of the figure. (b) A longitudinal organisation of ECM on the fibre surface and its periodicity is shown with white lines. (c) Central segment of the ECM patch separated from muscle fibre surface showing the wavy and random Collagen fibre organisation. (d) The connection between the ECM patch separated and the muscle fibre surface. Scale bar indicate 10 µm in A and 2 µm in others (adapted from Gillies and Lieber (2011)).

Das et al. (2010) showed that in chicks of the same age (21-day old) under different nutritional diets the overall architecture of the collagen fibres are similar as shown in Figure 2.7a, whereas in broilers (adult) the endomysium was thicker consisting of thicker collagen bundles and the collagen fibrils were crossing over each other in many orientations (see Figure 2.7d). They also showed that in male chicken pectoralis muscle during growth from chick to broiler, the endomysial collagen sheet thickness increased due to collagen fibril accumulation (see Figure 2.7b) and the structure changed from an arachnoid meshwork in the chicks (see Figure 2.7c) to a felt-like fabric in the broilers (see Figure 2.7d).

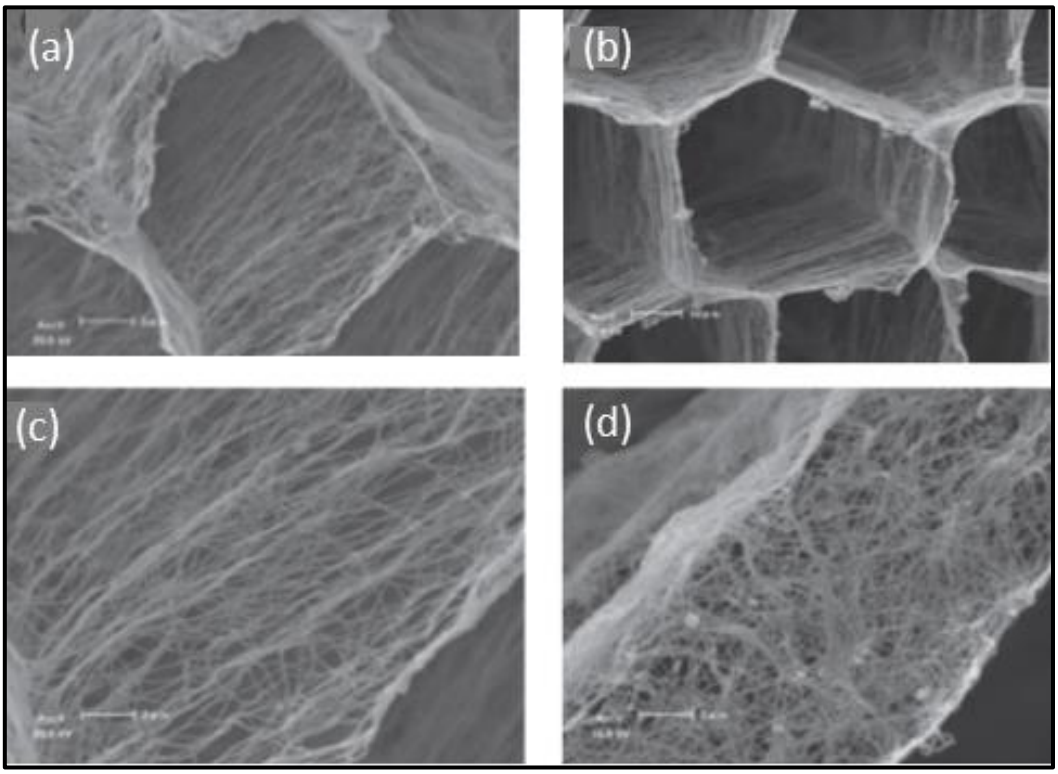

Figure 2. 7-SEM image of endomysium collagen architecture in chicken pectoralis muscle for (a) a 21-day old chick, (b) a 80 day old broiler. (c) Endomysium wall in a 21-day old chick, and (d) Endomysium wall in a 80 day old broilers. Scale bar indicates 5 mm in a, 10 mm in b, and 2 mm in c & d (adapted from Das et al. (2010)).

Morphological and mechanical properties of endomysium are important for understanding the force transmission mechanism in muscle. To study morphological changes in the endomysium network at different muscle lengths, Purslow and Trotter (1994) studied the bovine sternomandibularis muscle. The muscle was stretched and cold-shortened prior to fixation. Small pieces of fixed tissue were then used for sarcomere length determination and treated with sodium hydroxide to digest the myofibrils for SEM. As shown in Figure 2.8a, at rest, with a sarcomere muscle length of 2.05 µm, curvilinear endomysium fibres are randomly oriented at an angle of 60° with respect to the muscle fibres. This endomysium collagen fibre angle is close enough to the angle of 55°, which was found for the collagen fibre orientation in perimysium (Purslow, 1989). In a highly shortened muscle (1.1 µm), the collagen fibril orientation distribution changed in a way that the average fibril orientation is about 70° showing that they had a circumferential tendency as shown in Figure 2.8b, but at highly stretched muscles (3.89 µm), the mean fibre orientation changed to around 35°, close to longitudinal direction (see Figure 2.8c). These results agreed with the “isoareal model” proposed by Trotter and Purslow (1992). They showed that collagen fibres in the endomysium have circumferential orientation at short muscle length and longitudinal orientation at long lengths. Trotter and Purslow (1992) also showed that, in tension, the force generated in an intrafascicularly-

terminating muscles cannot be directly transmitted to tendon, and since the stress concentration at the fibre ends increase the risk of failure this force is likely to be transmitted between muscle fibres by shear through endomysium thickness (Trotter and Purslow, 1992, Turrina et al., 2013). This is in analogy with shear linkage in a fibre-reinforced composite material. Endomysium is too compliant to transfer force along the muscle fibre especially where no or small length changes happen due to applied loads (Trotter and Purslow, 1992). Instead it easily deforms to follow the length and diameter changes of muscle fibres (Meyer and Lieber, 2011) .

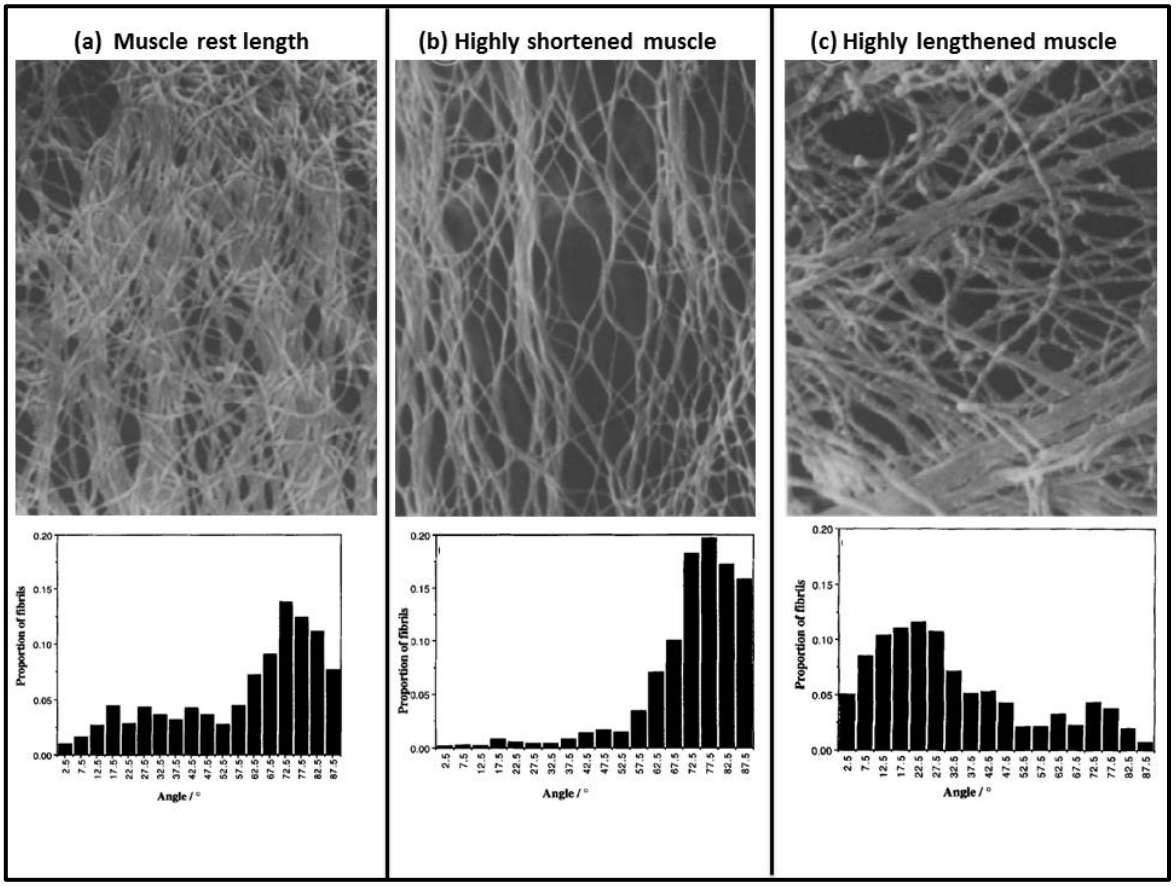

Figure 2. 8-The distributions of endomysial collagen fibre orientation (in degrees) at (a) muscle rest length, (b) highly shortened muscle, and (c) highly lengthened muscle. Muscle fibre is along the horizontal axis of this Figure (adapted from Purslow and Trotter (1994)).

Since endomysium organises a seamless connection with the muscle fibres and enables contractile force to be transferred (Huijing, 1999, Turrina et al., 2013), it is also able to transfer the tensional force generated by contraction, called trans-laminar shear, because the endomysium layer is shared between adjacent muscle fibres (Purslow and Trotter, 1994, Purslow, 2002). A uniform strain all over the tissue is then maintained due to this sideway load sharing (Passerieux et al., 2006, Sharafi and Blemker, 2010).

Detailed modelling of the tensile properties of the endomysium (Purslow and Trotter, 1994) confirmed inability of the endomysium to transmit force in tension; the model is in agreement with experimental force length measurements by Magid and Law (1985) and Podolsky (1964) who compared the tensile properties of relaxed single muscle fibres with and without the endomysium. At physiological sarcomere lengths, the difference caused by the removal of the endomysium to the passive elasticity of single fibres is very small (initial sarcomere length for intact whole muscle was 2.14±0.02 µm, while this length for skinned muscles with no endomysium was 2.16±0.02 µm), showing that the endomysium is extremely compliant in tension along the muscle fibre direction *in vivo*.

Sharafi and Blemker (2011) also showed through mechanical modelling how the parameter variation in muscle and endomysium structure or properties affects the transmitted force within the muscle. The stresses associated with shear transmission are lower than those in tensile transmission, as the total surface area of the fibre is much greater than the cross-sectional area of the endomysium. It was shown that shearing of the endomysium is more effective than tension in transmitting the force through the fibres as shear forces transmit force to the endomysium over the entire fibre surface while, tensile forces transmit force over the small cross-sectional area of the endomysium.

2.1.2.2. Perimysium

Muscle fascicle is enclosed by a continuous network of connective tissue called the perimysium, which is thicker than endomysium and was first observed by Rowe (1974). Perimysium collagen is mostly type I (Light and Champion, 1984). Over 90% of intramuscular collagen is located in the perimysium (McCormick, 1994). The perimysium does not create a distinct sheath around one fascicle, instead it is a shared structure between two fascicles (Purslow and Trotter, 1994). The perimysium is divided into secondary perimysium (a thick network) and a primary perimysium network divided by the secondary perimysium (Fang et al., 1999). The collagen fibres in a perimysium sheet are parallel to one another and it was shown that in bovine flexor carpi radialis and sternomandibularis muscles, the perimysium fibres in each ply are oriented at 55-60° with respect to the muscle fibre direction with a regular sinusoidal waviness at the resting length of muscle (Purslow, 2010, Passerieux et al., 2006, Gillies and Lieber, 2011). It was also observed that the degree of waviness increased with age in porcine semitendinosus muscle (Fang et al., 1999).

The perimysium collagen fibre angle changes by changing the muscle length, from 80° with respect to muscle fibres at a very short sarcomere length (1.1 mm) to 20° at a long length (3.9 mm) in bovine sternomandibularis muscle. These changes confirmed that the stretched fibres act as constraints to further increases in muscle length and circumference. The changes in the angles also matched with a sudden increase in the stiffness which shows the perimysium's ability to transfer tensional forces (Purslow, 1989).

Geometrical modelling of the tensile properties of perimysium using fibrous composites theory (Purslow, 1989), and direct measurements of the tensile strength and stiffness of perimysial sheets dissected from muscle (Lewis and Purslow, 1989) showed that the perimysium is easily deformed in tension until the collagen fibres become parallel to the stretching muscle fibres, to the extent that no waviness could be seen. Therefore, perimysium is highly stiff in tension and is able to carry large loads, but only at very large extensions well beyond the normal range of working lengths in living muscle, which explains why they can easily change shape. As both perimysium and endomysium have angle changes due to deformation along the muscle fibres it can be concluded that they are mechanically interlinked (Scarr, 2016).

Passerieux et al. (2006) suggested that since there have been studies investigating the perimysium organisation on different animals (bovine, ovine, rat), and also on different muscles (including the diaphragm, biceps, longissimus dorsi, and pectoralis), and yet they all presented the same description for perimysium, there may be a functionality for this connective tissue (Moore, 1983, Rowe, 1981, Borg and Caulfield, 1980, Purslow, 1989). These studies all suggested that the perimysium has three levels of organisation; (1) a loose framework of interwoven fibres (Figure 2.9a), (2) along with collagen plexi attaching to neighbouring myofibres at the muscle surface (Figure 2.9b & c), and (3) perimysial junctional plates (PJPs) which can be defined as contact regions between endomysium and perimysium, repeated at regular intervals (Figure 2.9d & e). The mechanical properties of PJPs are lower than those of the perimysium which may be due to their loose structure compared to the taut network of perimysium collagens (Lewis and Purslow, 1990).

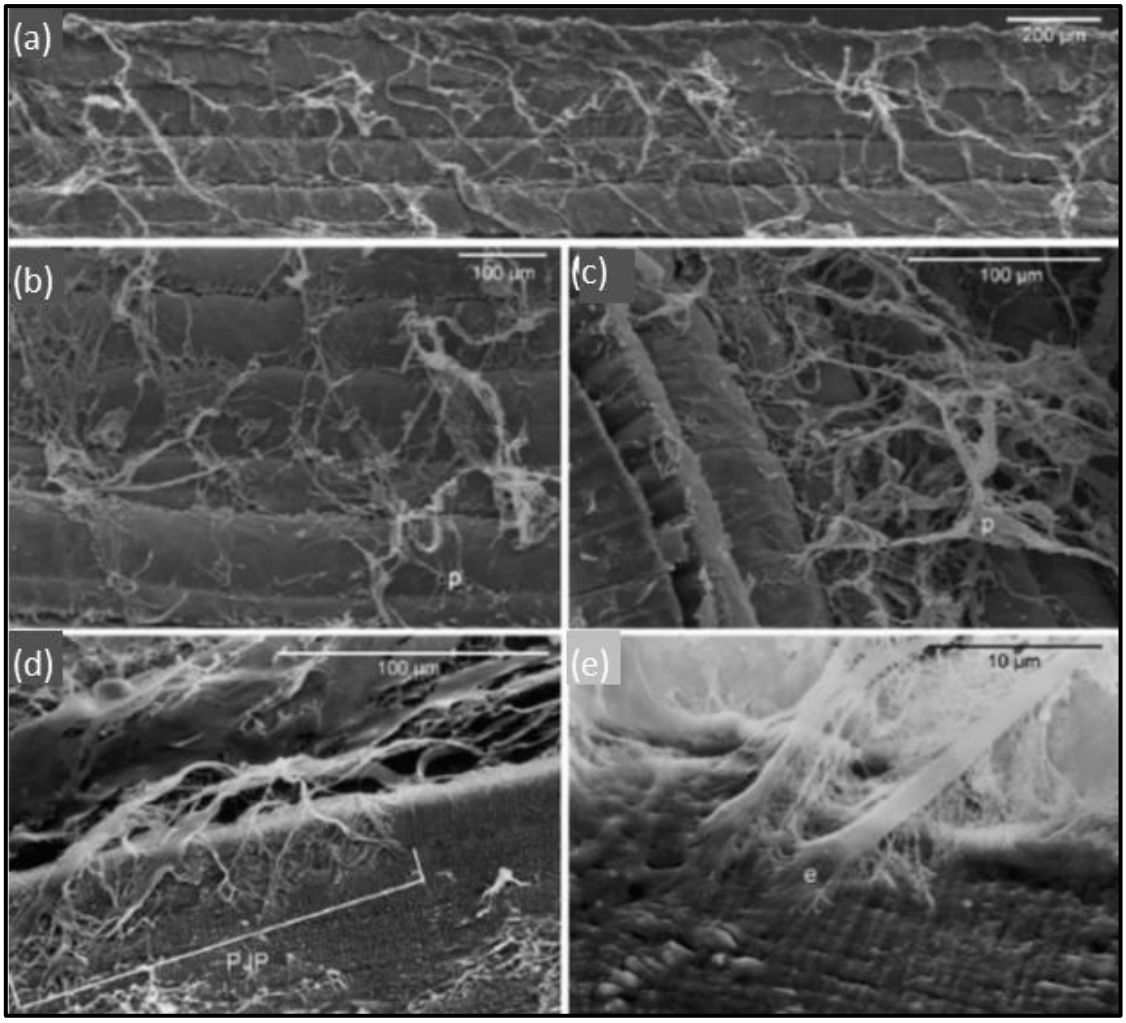

Figure 2. 9-SEM image of the perimysium collagen network of bovine flexor carpi radilais: (a) the overall structure of collagen interwoven fibres in the longitudinal direction, (b) the distribution of plexi at the surface of myofibre (p), (c) plexi attaching to the surface of adjacent myofibres (note the collagen fibres make an angle of approximately 60° with respect to the myofibres), (d) the attachment of perimysium plexi to myofibres at the level of a particular structure (the perimysial junctional plate (PJP)), and (e) high magnification image showing the merging of the perimysium with the endomysium (e) at the extremities of two branches of the same plexus (adapted from Passerieux et al. (2006)).

Das et al. (2010) showed that secondary perimysium collagen fibres were fundamentally divided into two types in chicken tissue: the plate type and cord type as shown in Figure 2.10a. The plate type collagen fibres are often observed as stack of flat cross sections and the cord type fibres show elliptical or circular cross sections (Nakamura et al., 2003, Roy et al., 2006, Oshima et al., 2007b, Oshima et al., 2007a).These plate type fibres in chick ran transversely along the surface of the myofibre fascicle (Das et al., 2010). The plate type collagen fibres in the primary perimysium were also transverse as were most of the cord type fibres in the primary and secondary perimysium. These results clarify that the existing perimysial collagen fibres in the central belly of chicken pectoralis muscle run across the myofibre fascicle and may play a major role in binding myofibres to the fascicles. In the 21-day-old chicks, the observed plate type collagen fibres were fewer than the cord type fibres in number. In the

broilers, collagen fibres were mostly plate type and were stacked to a dense layer of fibres (see Figure 2.10b). During growth from the chick to the broiler stage, the total number of the perimysial collagen fibres increased and the plate type fibres developed (Das et al., 2010).

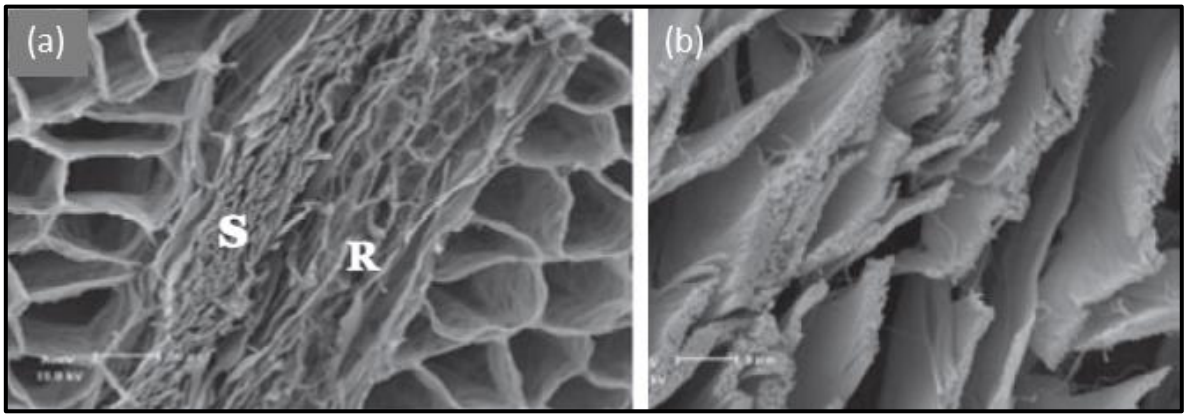

Figure 2. 10-SEM image showing the fundamental collagen architecture of chicken pectorais muscle (80 day old broilers). (a) Secondary perimysium. S; stack of thin plate-like collagen fibres with longitudinal striation, R; reticulum of cord-like collagen fibres with transverse striation. Scale bar indicates 50 mm, (b) perimysium collagen fibres in the stack. Scale bar indicates 50 mm in (a) and 5 mm in (b) (adapted from Das et al. (2010)).

Iwamoto et al. (2001) also showed that the primary and secondary perimysium in male chicken (1 to 2 years old) had different architectures of collagen fibre. The secondary perimysium in the transverse section consists of mostly large longitudinal collagen fibre bundles (LB in Figure 2.11a & b) and thin circumferential bundles (CB). Collagen fibre architecture in the primary perimysium differed based on location; the fibres grouped into a bundle (2·6 mm, Figure 2.11c) or separated from each other with main parallel striations (Figures 2.11d), which is in agreement with those of Das et al. (2010).

Collagen content is changed markedly in very young or aged animals but less in adults. Chicken iliotibialis lateralis muscle of White Leghorn (WL) and Silkie cocks (1 to 2 years old) showed no difference in total collagen content (Sakakibara et al., 2000).

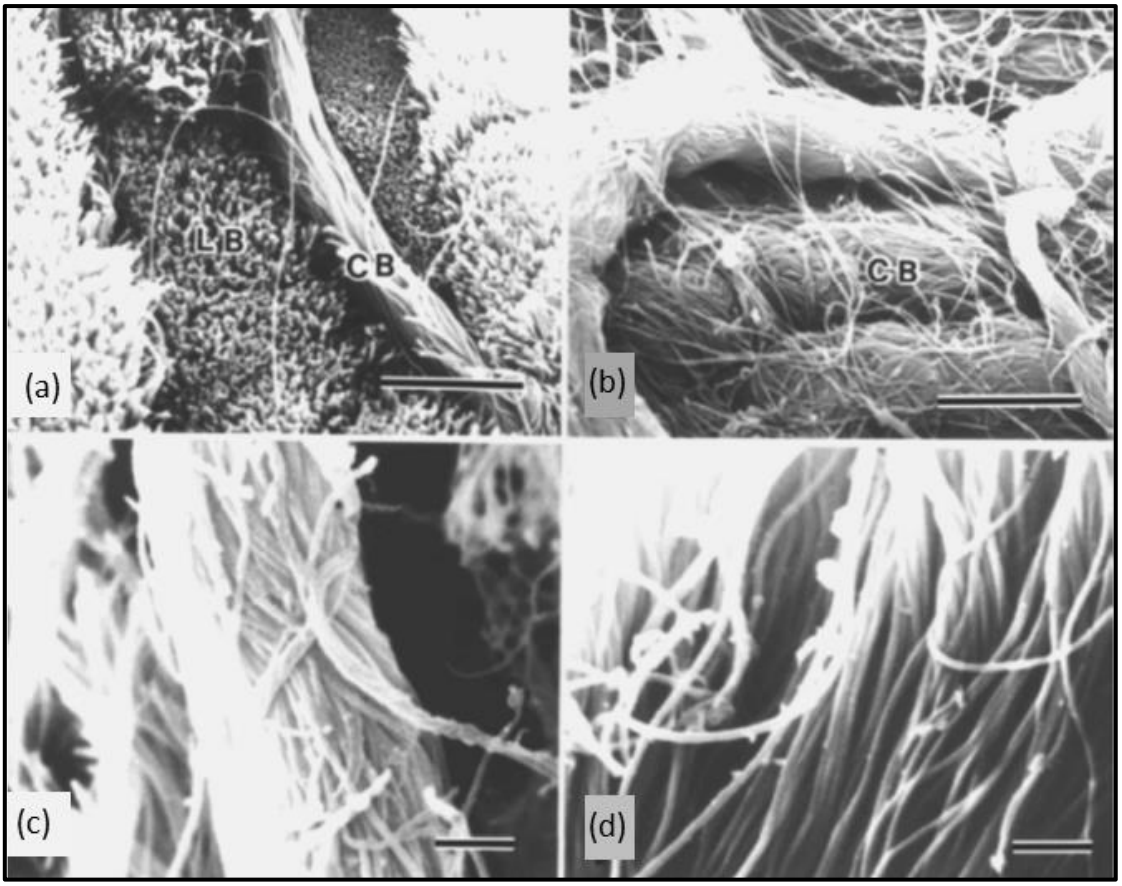

Figure 2. 11-SEM image of perimysium. (a) Thick perimysium in White Leghorn (WL) cock (iliotibialis lateralispars postacetabularis (ITL) muscle (scale bar=5 mm), (b) Thin perimysium in Silkie cock (scale bar=5 mm), (c & d) Thin perimysium in WL cock (scale bar=1 mm). CB; circumferential collagen fibre bundles and LB; longitudinal Collagen fibre bundles (adapted from Iwamoto et al. (2001)).

Fang et al. (1999) and Nishimura et al. (1999) observed in bovine and porcine muscles that wavy bundles of collagen fibres in the perimysium ran parallel without any crossing bundles. In contrast, in chicken longitudinal collagen fibre bundles with a central circumferential bundle was observed in the secondary perimysium (see Figure 2.11a). It can be concluded that in chickens, secondary perimysium can play a main role in contraction force transition and protecting the myofibre from over-extension because of a sheath of many longitudinal collagen fibres. Primary perimysium works mainly as a binding and sliding structure due to existence of the more circumferential collagen fibres. However, primary perimysium transmits its myofibre contractile force to the tendon or the secondary perimysium (Iwamoto et al., 2001).

It is reported that tenderness of muscle (muscle stiffness) is significantly directly correlated with both total collagen content and the perimysium thickness. However when the collagen concentration decreases through muscle growth, the toughness of meat increases with age, which indicates that muscle stiffness depends on the chemical and architectural changes in collagen (Nishimura et al., 1996, Fang et al., 1999).

Gillies and Lieber (2011) showed that in mouse extensor digitorum longus (EDL) muscle under 30% tension there are some long perimysium cables observed to be tightly drawn and sometimes the collagen fibres become frayed as they cross between fibres (Figure 2.12a). The cables themselves are organised as bundles of collagen fibrils (Figure 2.12b).

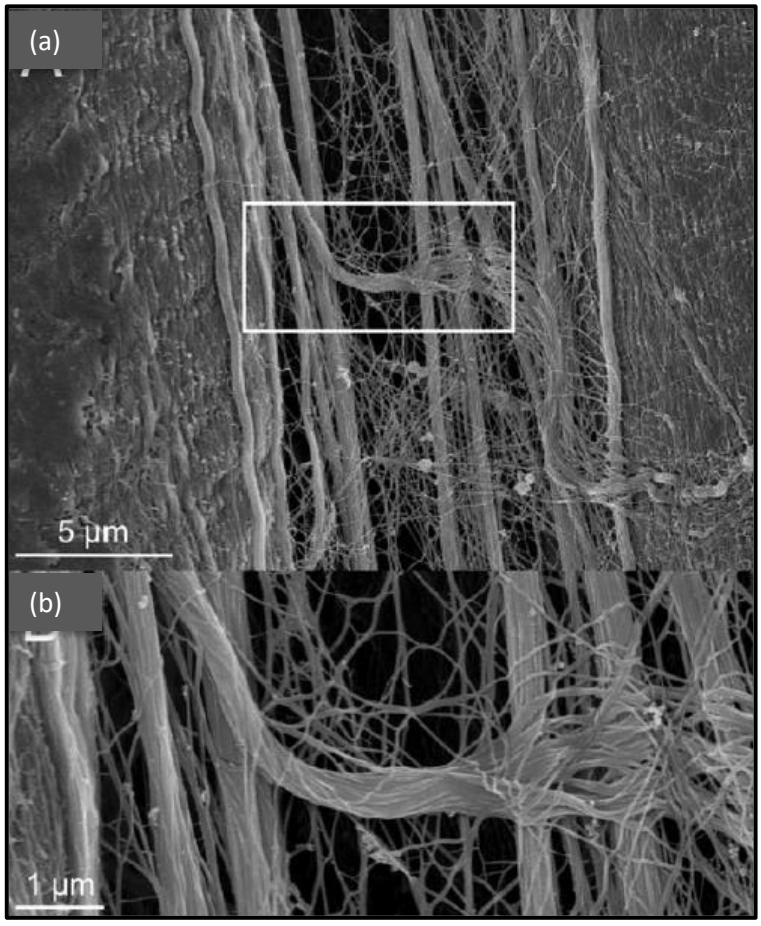

Figure 2. 12-SEM image of mouse EDL muscle stretched about 30% beyond resting length showing longitudinally aligned perimysium collagen cables. (a) Two muscle fibres separated by stretched collagen cables, (b) a collagen cable becomes frayed as it traverses across collagen cables (adapted from Gillies and Lieber (2011)).

Although studies regarding the role of connective tissues in skeletal muscle have provided valuable information about perimysium structure (Purslow, 1989, Nishimura et al., 1994, Das et al., 2010, Gillies and Lieber, 2011, Passerieux et al., 2006), its arrangement is not well understood. The list below outlines the areas in which the ECM, particularly the perimysium is not well understood; they are specifically reviewed by Gillies and Lieber (2011):

1) Generally, there is little objective information about muscle ECM compared to connective tissue such as tendon, ligament, cartilage etc.
2) The muscle ECM geometry is extremely complex. Although the studies mostly divided ECM into three hierarchical levels (endomysium, perimysium and epimysium), different methods

of microscopy reveal that it is difficult to distinguish between the different hierarchical levels, so such definitions are fairly subjective particularly for perimysium because it directly connects to the endomysium and also has a seamless connection to epimysium. Therefore, it is not very clear whether the structure observed for the perimysium is purely representative of it.

3) It is not clear whether perimysium encloses fascicles from origin to insertion or whether it is interconnected across the muscle belly like the endomysium; this needs to be addressed profoundly to help understand the normal and pathological function of muscle systematically as well as explaining the force transmission through the perimysium in the skeletal muscle.
4) Three-dimensional systematic study of muscle ECM where the proper rules of three-dimensional sampling are followed is lacking.
5) The methods of sample preparation are mostly disruptive, which may result in biased understanding of ECM structure.
6) The mechanical properties of ECM as a load-bearing structure reflect more in network geometry than the constitutive properties of the collagen fibres, meaning that the skeletal muscle behaviour may not be only dependent on the collagen fibre mechanical properties, but rather the pattern in which the collagen fibres are woven.
7) It is uncertain whether the same organisation and level of detail observed for the endomysium and perimysium are typical of all muscles across species. It is not even clear whether the ECM in the similarly-functioned muscles across species is alike. For instance, it is not known whether the collagen fibre angle within the perimysium sheet with respect to the muscle fibres (55°) reported in the literature will be also observed in other tissues (Purslow, 1989, Passerieux et al., 2006).
8) It is suggested that the perimysium is probably the main structure of the ECM responsible for load bearing in the muscle (Purslow, 2010, Nishimura, 2010, Gillies and Lieber, 2011). However, our knowledge about the perimysium is limited compared to the endomysium. Purslow (1989) for the first time performed a very valuable study on the perimysium structure and rearrangement when exposed to external deformations in the muscle fibre direction. However, it is not known how the perimysium is involved in passive load bearing in deformations applied in both the muscle fibre and cross-fibre directions. To the best knowledge of the author there is no study showing how perimysium structure differences between animals can be reflected in their mechanical response.

Since all muscles (with any fascicle shape) increase in width when contracting (Lieber and Fridén, 2000), any subsequent changes in the angle of myofibres with respect to their aponeurosis[1] at either end requires some means of sliding within the muscle to accommodate this increase in width (Purslow, 2002). Purslow (1989) found that collagen fibres lie within the perimysium sheet and do not run through the thickness of the perimysium wall, supporting the model that the perimysium membrane between adjacent fascicles can act as "neutral displacement wall" that facilitates shape changes in muscle by sliding fascicles past each other during muscle contraction (Schmalbruch, 2012).

The transverse anisotropy of perimysium suggests that muscle diameter changes will not be the same in every direction (Sharafi and Blemker, 2010), therefore it is not simple to find the exact relationship between muscle length and diameter during changes in shape, suggesting that the details of geometrical changes of this mechanism still require study.

Street (1983) conducted tensile tests on frog muscle to demonstrate that there are two ways of force transmission. The force within the fibres is transmitted either along the muscle fibres or through the ECM to the endomysium and further to the perimysium particularly in cases where skeletal muscle fibres do not cover the whole length of the muscle (Huijing, 2009, Williams et al., 1995). However, it was not shown how muscle microstructure such as reorientation of muscle and collagen fibres responds to different loading types. In recent years, many studies were performed showing that the collagenous sheaths play an important role in force transmission within the muscle, showing the importance of studying collagen fibres in parallel with skeletal muscle fibres to better understand the mechanics of skeletal muscle (Sharafi and Blemker, 2011, Sharafi and Blemker, 2010, Purslow and Trotter, 1994, Purslow, 1989, Gillies et al., 2014, Gillies et al., 2011, Meyer and Lieber, 2011, Takaza et al., 2014).

2.1.2.3. Epimysium

A distinct muscle is formed by enveloping a large number of muscle fascicles in a thick collagenous external sheath extending from the tendons that attach the muscles to the bone connective tissue layer. This external sheath is called the epimysium (Korthuis, 2011, Purslow, 2010, Gillies and Lieber, 2011).

In some long strap-like muscles the epimysium is arranged as two parallel sheets of wavy collagen fibres in crossed-ply form. As shown in Figure 2.13 at muscle resting length, the collagen fibres are placed at angle of approximately 55° with respect to muscle fibres (Purslow, 2010). In the epimysium of other muscles, particularly in pennate muscles, a thick wall of collagen fibres (1 mm thick) are

[1] A fibrous sheet or flat, expanded tendon, giving attachment to muscular fibres and serving as the means of proximal or distal attachment (origin or insertion) of a flat muscle; it sometimes also performs the functions of a fascia for other muscles.

aligned with the axis of the muscle fibres to make a dense layer that functions as an aponeurosis (Purslow, 2010, Nishimura et al., 1994). Since at the muscle surface perimysium is connected to epimysium, in some superficial layers it is difficult to distinguish perimysium from epimysium (Gillies and Lieber, 2011).

Nishimura et al. (1994) showed that in bovine semitendinosus muscle, the epimysium was composed of two distinct layers of thick sheets. The inner layer consisted of thousands of collagen fibres lying in an extremely regular wavy pattern parallel to the axis of the muscle fibre. The outer layer of epimysium was composed of several wavy sheets of collagen fibres which ran transversely to the axis of the muscle fibre. In a region of the epimysium, there was a thick wall of about 1 mm thickness, where fibre bundles of 200-300 micrometre in diameter ran longitudinally parallel to the axis of muscle fibre.

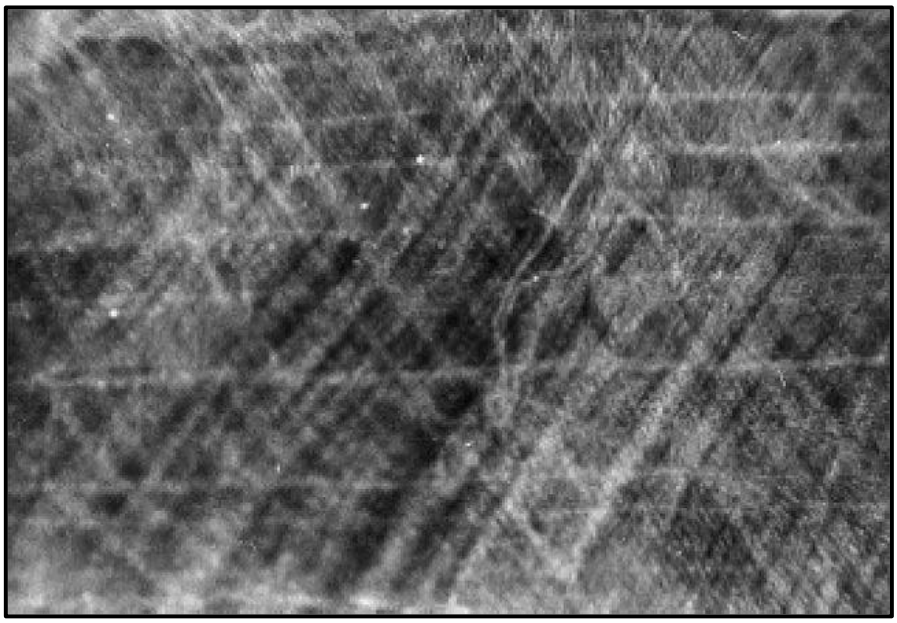

Figure 2. 13-Light micrograph of epimysium from bovine sternomandibularis muscle, showing arrangement of collagen fibres in crossed-plies. The fibres are in two parallel layers lying at +55° and -55° to the muscle fibre axis (adapted from Purslow (2005)).

The morphological shape of epimysium in mouse EDL muscle (Gillies and Lieber, 2011) shows that it is not clear whether epimysium compared with perimysium has a different structural property. Apparent repetitions of sarcomere length (Figure 2.14a, lines) as well as longitudinal ECM repetition are both observed in the epimysium (Figure 2.14b, lines). However, since tissue preparation and visualisation methods are disruptive, it is not clear if the structure shown here reflects the native ECM structure (Gillies and Lieber, 2011).

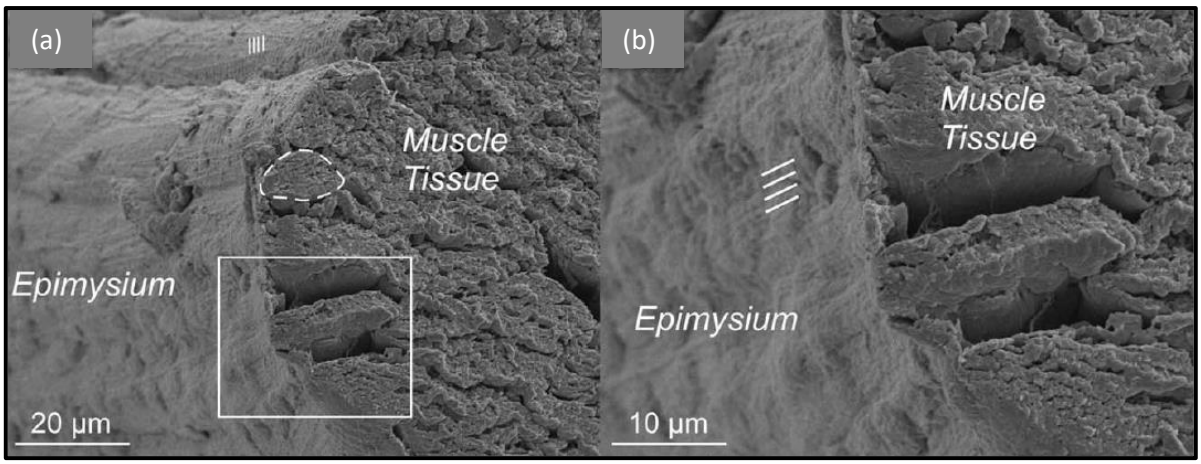

Figure 2. 14-SEM micrographs of epimysium of a mouse EDL muscle. (a) The muscle view where a region can be observed with sarcomere repetitions through the connective tissue layer. An individual muscle fibre is noted (dashed line), (b) A closer view of the epimysium reveals longitudinal periodicities (lines) (adapted from Gillies and Lieber (2011)).

2.2. Mechanical properties of skeletal muscle

Qualitative and quantitative investigation is a fundamental step in the study of mechanical properties of skeletal muscle. It is difficult to assess the skeletal muscle behaviour due to its viscoelastic, anisotropic, hierarchical nature, and its sensitivity to external parameters such as dehydration, temperature, and time after death. Aditionally, it requires *in vivo* testing to obtain data representative of the living state (Van Loocke et al., 2006). Skeletal muscle modelling also presents difficulties due to its force-producing ability; the stress response in a given muscle is the result of passive and active contributions (Herzog, 2001). Furthermore, parameters such as age, gender and species are also effective. The experiments conducted in the past focused mostly on isolated muscle fibre testing (Herzog, 2001, Huxley, 1957) until Herzog established that conducting the test at muscle level or fibre level makes no difference in the results, thus the difficult task of isolating the fibres was eliminated (Herzog, 2001). This establishment may underestimate the role of the ECM. However, micromechanical studies contradics this and emphasises on the importance of ECM (Purslow, 2010, Purslow, 1989, Purslow and Trotter, 1994).

Eshtablishing the mechanical response of muscle to externally applied deformation is of great interest for applications such as impact biomechanics (Cai et al., 2014, Meijer et al., 2013, Takaza and Simms, 2012, Ivancic et al., 2007, Mukherjee et al., 2007, Praxl et al., 2008), rehabilitation engineering (Linder-Ganz et al., 2007, Linder-Ganz et al., 2009, Turkoglu et al., 2014, Yucesoy et al., 2015, Akdeniz et al., 2015), and pressure sore prevention (Filius et al., 2013, Cushing and Phillips, 2013, Bosboom et al., 2003, Nagel et al., 2009, Mak et al., 2011, Linder-Ganz and Gefen, 2008, Oomens et al., 2003, Xiao et al., 2014). The biological tissues can be tested either *in vitro* or *in vivo*. Each method has its own

advantages and disadvantages. For instance, *in vivo* studies require clever methods to overcome the difficulties in testing within a live specimen. Bosboom et al. (2001) conducted *in vivo* experiments on rat tibialis anterior (TA) to quantify the compressive passive transverse mechanical properties of the skeletal muscle. As they noted the major disadvantage of *in vitro* testing is the separation of the muscle fibres during sample preparation and the impairment of neurovascular supply.

As muscle tissue is very soft, it makes sample preparation difficult while conducting *in vitro* studies; in addition Van Loocke et al. (2006) showed in porcine tissue that the test must be carried out within two hours after animal death in order to avoid the changes in muscular properties caused by rigor mortis because significant stiffening of muscle behaviour was observed a few hours after death of the subject. Two hours after death of the animal is a commonly used time in studies to characterise the stress-stretch behaviour of non-rigor tissue (Böl et al., 2012). Since *in vitro* studies have been mostly carried out on animals, ethical issues related to the use of animals for scientific testing is another issue that should be considered.

2.2.1. Compressive behaviour of skeletal muscle

One of the first studies on compressive behaviour of skeletal muscle was carried out by Grieve and Armstrong (1988). *In vitro* unconfined compressive measurements of porcine muscle tissue were performed at different strain rates. A viscoelastic nonlinear response was found as shown in Figure 2.15. It was also observed that the muscle shows strain-rate stiffening.

In this study, the direction of force applied with respect to muscle fibre direction was not known. Further, the samples were frozen on the day of slaughter, and thawed before testing; the athours stated this did not affect the results. However, it was shown that the time after death is an influencing factor on stress-strain response of skeletal muscle (Van Loocke et al., 2006).

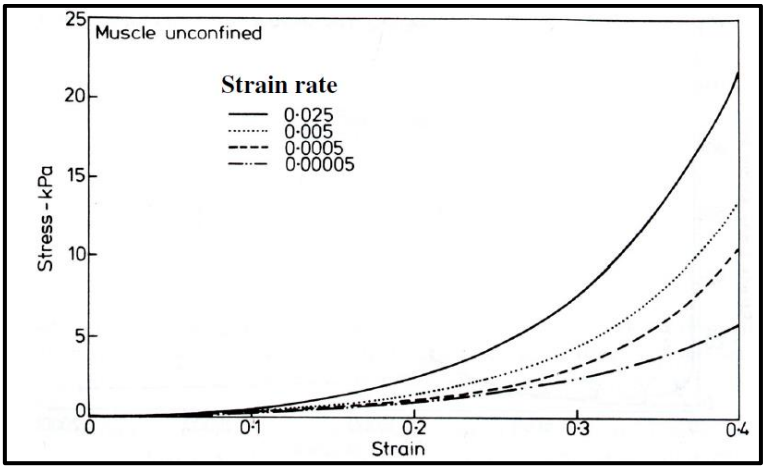

Figure 2. 15-Nonlinear viscoelastic response of porcine muscle (adapted from Grieve and Armstrong (1988)).

Figure 2.16 shows significant variation in the compressive stress-stretch response among previously published data. Direct comparison is mostly not possible, since there are some key differences in test protocols.

Van Loocke et al. (2006) performed an experimental study along with a theoretical model describing the quasi static nonlinear, compressive behaviour of skeletal muscle on aged and fresh animal muscle samples oriented at different directions at strain rate of 0.05 $\%s^{-1}$ and up to 30% deformation. An elastic nonlinear anisotropic behaviour was observed. The cross-fibre direction was found to be the stiffest, followed by fibre direction. The least stiff response is when the muscle is compressed at 45° to the muscle fibres.

Song et al. (2007) carried out compression tests with a strain rate ranging from 0.007 s^{-1} to 3700 s^{-1} on porcine tissue. A quasi static test (strain rate of 0.007 s^{-1}) showed that the muscle compressive properties are nonlinear in both fibre and cross-fibre directions. The authors found the tissue behaves more compliantly in the cross-fibre direction.

Bosboom et al. (2001) conducted compression tests on rat tibialis anterior (TA) muscles in the transverse direction. Each TA was compressed between two plates using a ramp and hold function, with a ramp speed of 0.25 mms^{-1} and a hold phase of 20 s. Due to the non-uniform geometry of the muscle tested and the fact that the TA specimens were tested *in vivo* resulted in contradiction with the studies shown in Figure 2.16.

Böl et al. (2012) also performed compression tests with a strain rate of 0.05 $\%s^{-1}$ on soleus muscles of New Zealand white rabbits with characteristic edge lengths between 3 and 6 mm. The samples were compressed up to 45%. The authors reported a similar qualitative behaviour in compression as well as considerably less stiff response in all fibre directions compared to Van Loocke et al. (2006).

Pietsch et al. (2014) carried out compressive tests in the fibre and cross-fibre directions on 8-10 month old porcine hind legs at strain rates of 0.1, 0.01 and 0.01 s^{-1}. The authors showed that deformation in the cross-fibre direction is significantly stiffer than the fibre direction at all strain rates indicating anisotropy.

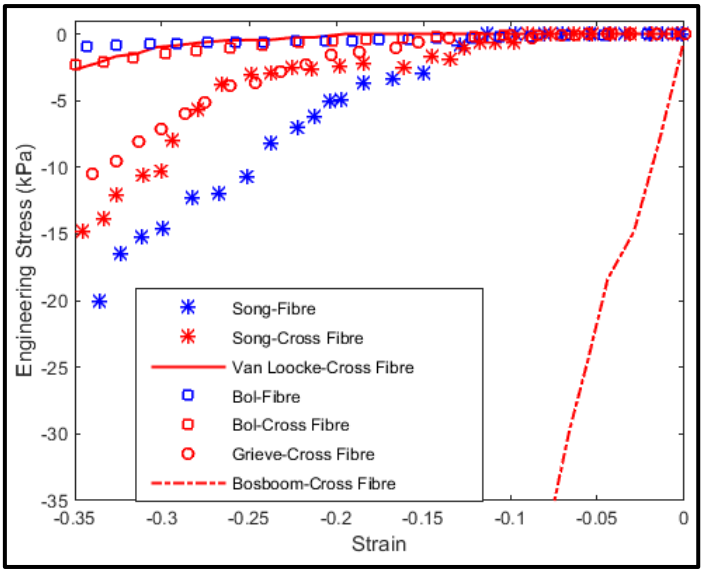

Figure 2. 16-Comparison of compressive stress – strain response for skeletal muscle from previous studies.

The interaction between the skeletal muscle components (approximately 85% water, 5% fat and 10% collagenous tissue) shows the viscoelastic nature of muscle (Duenwald et al., 2009).

Van Loocke et al. (2008) conducted a study on fresh porcine tissue at higher strain rates in different directions with respect to the muscle fibres to investigate the time-dependent properties of passive skeletal muscle using a combined experimental and theoretical approach. They displayed that muscle is a nonlinear, anisotropic and viscoelastic material and above a very small compression rate, the viscoelastic component plays a significant role in muscle mechanical properties. At low strain rates (0.05-1 $\%s^{-1}$) the loading could be considered quasi-static and the cross-fibre direction is stiffer than the fibre direction. As the strain rate was increased this relationship was inverted and the viscoelastic effect appeared resulting in greater Cauchy stresses in the fibre direction. Therefore, skeletal muscle viscoelastic behaviour is dependent on both compression rate and fibre orientation. They hypothesised that in the fibre direction and close to the fibre direction the endomysium and perimysium layers impeded the flow of fluid, thereby increasing the stress. However, these obstacles did not impede the flow in the cross-fibre direction and thus the stress was reduced (Van Loocke et al., 2008).

Van Sligtenhorst et al. (2006) applied compressive strains up to 80% at rates from 0.1 to 2300 s^{-1} on cylindrical samples of bovine muscle tissue in the fibre direction. Although the authors reported that stress-strain curves are strain rate-sensitive and concave as the typical form of muscle tissues, the curves seem linear.

Pietsch et al. (2014) also observed strain rate dependency at the higher strain rates.They showed that the stress is higher at the higher strain rates which is in agreement with the findings of Van Loocke et al. (2008). They also noted that accurate impact simulations for injuries, ligament failure, or

cartilage tear depend on the quality of model geometry as well as good constitutive relationships for each component at various stresses, strains, and strain rates (Pietsch et al., 2014).

2.2.2. Tensile behaviour of skeletal muscle

The tensile response of passive skeletal muscle is nonlinear and viscoelastic (Nie et al., 2011, Calvo et al., 2010, Martins et al., 2006, Morrow et al., 2010a, Takaza et al., 2013a, Hernández et al., 2011), anisotropic (Takaza et al., 2013a, Hernández et al., 2011), and it was particularly described transversely isotropic (Morrow et al., 2010a, Blemker and Delp, 2005).

Figure 2.17 shows the stress-stretch response of skeletal muscle to applied tensile deformation for published data on different species (porcine, rat and rabbit tissue). However, significant variation is evident even here. For instance, for the same applied strain rate (0.05 $\%s^{-1}$), Morrow et al. (2010a) showed stiffer response in the fibre direction compared to what was observed by Calvo et al. (2010) and Takaza et al. (2013a).

The strain rate applied in the tests and experimental methods are not the same; the lower strain rates in Calvo et al. (2010) likely reduced the viscoelastic effect (Van Loocke et al., 2008), and lower stiffness was observed. The stress curve of Nie et al. (2011) appears convex in shape, which is not observed in the other studies. This could be due to different experimental methods, and the higher stiffness observed could be due to defrosting the tissue which could alter the mechanical properties of the specimen. Morrow et al. (2010b) also performed the tests on whole muscle, which meant the tissue had more unimpaired fascicles that could lead to the higher stress response they reported. They also reported that the tissue behaved stiffer in the fibre direction than the cross-fibre direction, but the data of Nie et al. (2011) and Takaza et al. (2013a) demonstrate the opposite.

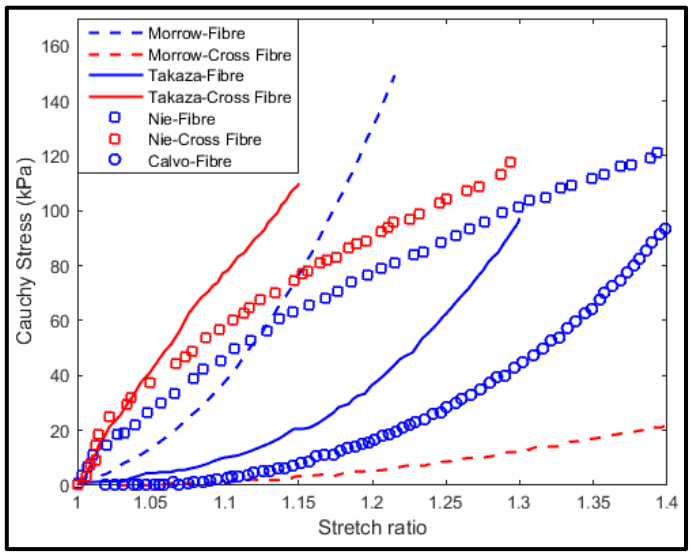

Figure 2. 17-Comparison of tensile stress – stretch response for skeletal muscle from previous studies.

Another mechanical property which enhances the understanding of skeletal muscle behaviour is Poisson's ratio which has been reported for porcine tissue (Van Loocke et al., 2006, Takaza et al., 2013a). According to Table 2.1, which displays the Poisson's ratio under various conditions, when the tissue is either compressed or stretched along the fibres, the induced deformation in the other two directions are equal (υ_{LT}=$\upsilon_{LT'}$) and about 0.50. However, when the tissue is deformed across the fibres, the induced deformation in the fibre direction (υ_{TL}) and the other transverse direction ($\upsilon_{TT'}$) were 0.36 and 0.65 in compression, and 0.74 and 0.28 in tension, which reflects tension/compression anistropy and asymmetry in porcine and chicken skeletal muscles (Van Loocke et al., 2006, Takaza et al., 2013a).

Table 2. 1-Poisson's ratio comparison between chicken and porcine tissue in compression and tensile tests.

Poisson's ratio	Compression	Tension
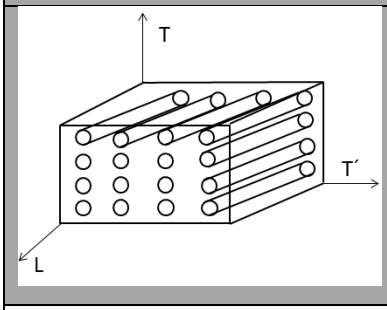	**Porcine (Van Loocke et al., 2006)**	**Porcine (Takaza et al. (2013a)**
υ_{LT}=$\upsilon_{LT'}$	0.5	0.47
$\upsilon_{TT'}$	0.65	0.28
υ_{TL}	0.36	0.74

2.2.3. Micromechanical response of connective tissue (ECM) under deformation

The ECM in skeletal muscle has two important functions: first, it is a structure that forms muscle fibres into hierarchal groups and second acts as a retaining mechanism during muscle deformation (Huijing, 2009, Rowe, 1974).

Some informative micromechanical representations of the role of connective tissues in skeletal muscle have been conducted by the Purslow group (Trotter and Purslow, 1992, Purslow and Trotter, 1994, Purslow, 2010, Lewis and Purslow, 1990, Lewis et al., 1991). They observed the collagen fibres in the connective tissue (removed from the muscle fibres) still reoriented with changes in muscle length and the perimysium was acted as a means to facilitate intramuscular sliding (Purslow, 2010). It is also reported that the intermolecular collagen cross-linking, as well as the size, orientation and organisational arrangement of the collagen fibres, affects the passive mechanical properties of

skeletal muscle (Nishimura et al., 1996, Purslow, 2010). Lewis and Purslow (1990) showed that in cooked beef the perimysial strands have higher tensile strength than junctions between the endomysium and the perimysium suggesting that the perimysium is one of the most important factors that determine the toughness of meat. However, it remained unclear how external loading relates internally to deformation of muscle fibres and the extra-cellular matrix (Takaza et al., 2014). Therefore, more analysis of the microstructure of skeletal muscle is required to explain the passive behaviour which was observed in different studies (Calvo et al., 2010, Van Loocke et al., 2006, Nie et al., 2011, Takaza et al., 2013a, Martins et al., 1998, Morrow et al., 2010a).

Microstrucural studies and image analysis were performed by several researchers to find out the geometrical changes of muscle in different deformed states (tension or compression) (Takaza et al., 2014, Pietsch et al., 2014).

Pietsch et al. (2014) conducted compression tests on porcine muscle in the fibre and cross-fibre directions. They observed that area fraction (the fraction of each image occupied by muscle fibres) increased at the tested strain rates in both directions indicating that the space normally existed between muscle fibres in the transverse plane decreases during load application on the muscle. This may be due to signifant fluid exudation from the muscle tissue (even at a quasi static strain rate of 0.001 s^{-1}). Since cryofixation of the tissues is difficult, it is not easy to avoid crystal formation, which creates holes in the sample. However, they stated the best care was taken to avoid this. The mean area of the muscle fibres in the loaded cases compared to undeformed samples showed an increase in longitudinally compressed samples, which agrees with those of Takaza et al. (2014) and a decrease in transverse loading which is in contrast with Takaza et al. (2014). Their findings supported anistropy in the muscle. They explained the increase in mean area could be due to two reasons: first, the buckling of the fibres normally associated in longitudinal compressive loading caused the muscle fibres to show a larger area in the transverse plane. Second, this was caused by aspect ratio changes. It was observed that after the cross-fibre compression, the muscle fibres and fascicles were flattened in the direction of compression. However Takaza et al. (2014) showed the opposite observation.

Takaza et al. (2014) assessed the microstructure response of fresh porcine tissue to passive external deformations in both the fibre and cross-fibre directions in compression as well as in tension. Transverse sections of the muscle were analysed visually and quantitatively using ImageJ. They introduced more parametres to explain the muscle behaviour compared to the Pietsch et al. (2014) study. The major axis angle to measure the overall orientation of the muscle fibre in the transverse plane, and the major to minor axis ratio to evaluate shape changes in the transverse plane were evaluated under different applied deformations (see Figure 2.18).

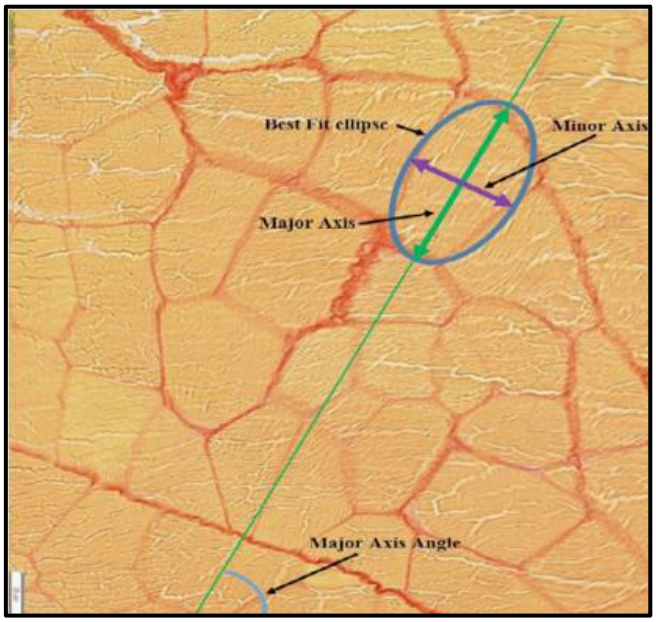

Figure 2. 18-Schematic illustration a best-fit ellipse and its components for one of the muscle fibres .The major axis is the longer diameter of the best fitted ellipse and the shorter diameter is the minor axis. The angle that the major axis makes with the horizontal edge of the image is called the major axis angle of the muscle fibre (adapted from Takaza et al. (2014)).

Takaza et al. (2014) showed that cross sectional area (CSA) decreased for tension in the fibre direction, but increased for compression in the fibre direction. For the cross-fibre tensile and compressive deformations, the CSA increased compared to the control (undeformed) sample (statistically significant difference was shown in all cases). No statistically significant difference in the major/minor axis ratio was observed between the control and the specimens either stretched or compressed in the fibre direction. This could be explained by the fact that deformation in the fibre direction the specimen experiences almost symmetric contraction/expansion in the other two orthogonal cross-fibre directions, resulting in no shape changes in the muscle fibre cross-sections. However, a statistically significant difference in the major/minor axis ratio was observed between the controls and where the tissue stretched and compressed in the cross-fibre direction.

The major axis angle measurment showed no preferred orientation for undeformed specimens; see Figure 2.19A. This indicated that even though the muscle fibre cross sectional areas are irregular in shape, no preferred major axis direction exists. A similar pattern for deformation applied in the fibre direction for tension (Figure 2.19B) or compression (Figure 2.19D) was observed. In contrast, deformations in the cross-fibre direction changed the major axis of each muscle fibre according to Figure 2.19C and E (Takaza et al., 2014), concluding that compression compacted muscle fibre cross-sections to make them perpendicular to the direction of the applied deformation, whereas tensile

deformations stretched the cross sections of muscle fibres and the fibres became parallel to the direction of applied deformation.

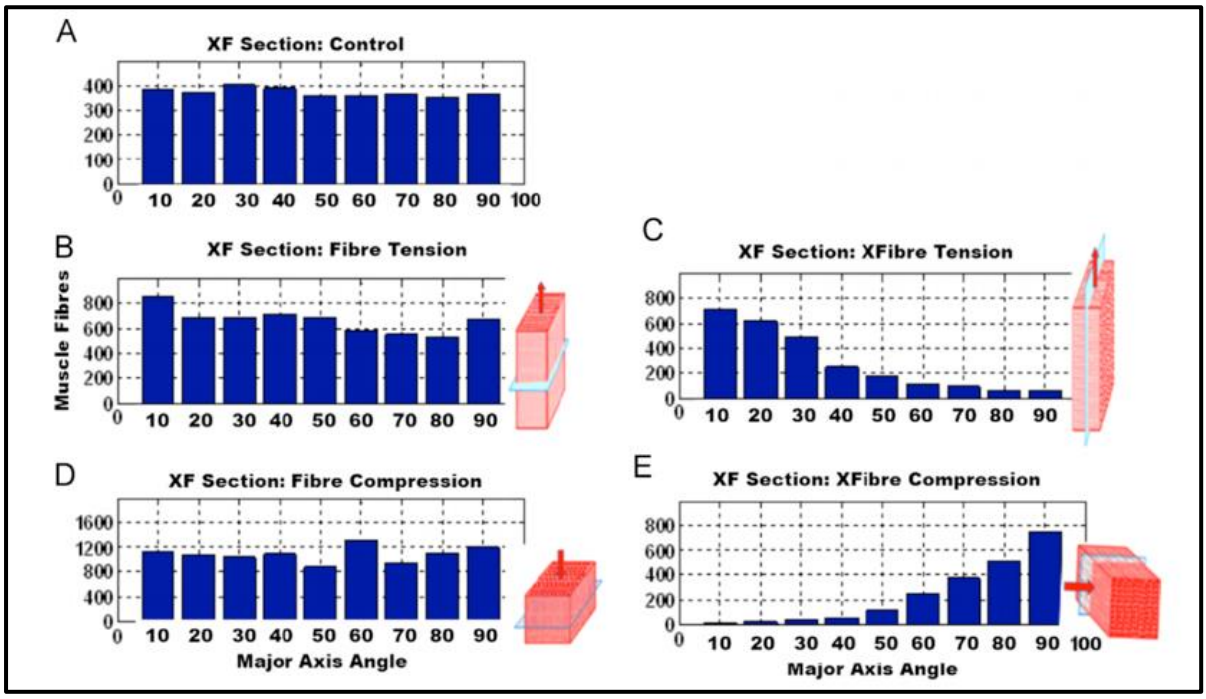

Figure 2. 19-Major axis orientation angle (degrees) of muscle fibre cross-sectional areas: (A) control samples, (B) 30% tension in the fibre direction, (C) 30% tension in the cross-fibre direction, (D) 30% compression in the fibre direction and (E) 30% compression in the cross-fibre direction (adapted from Takaza et al. (2014)).

No evidence of structural reorganisation of the endomysium collagen fibres in response to deformation was observed in SEM micrographs. However, the deformation and orientation of the muscle fibres are greatly influenced by the perimysium, meaning that the perimysium and its interaction with the surrounding muscle fibres is likely to be responsible for the tension/compression asymmetry observed in macroscopic tests of passive skeletal muscle (Takaza et al., 2014). This requires further investigations; additionally the mathematical structural models such as Gindre et al. (2013) require modifications to consider the perimysium as a predominant factor for tension/compression asymmetry.

2.3. Collagen detection and visualisation

As reviewed previously, collagen is the main structural protein in connective tissues in animals and it is primarily responsible for the passive load-bearing properties of tissues. For example collagen fibre reorientation in the muscle ECM in response to external loading has been observed by several authors (Billiar and Sacks, 2000, Purslow, 2010, Purslow and Trotter, 1994, Purslow, 1989). Thus detection and visualisation of collagen structure are important to understand the relationship between mechanical

behaviour and microstructure in skeletal muscle, which researchers have addressed principally through microscopy and mechanical modelling (Purslow, 2010, Purslow, 2002, Purslow and Trotter, 1994, Takaza et al., 2014, Krahn et al., 2006, Nishimura, 2010, Sharafi and Blemker, 2010).

The overall structure of collagen-rich tissues can be visualised by commonly used histological stains such as Hematoxylin and Eosin (H&E) (e.g. Pietsch et al. (2014)) or various forms of trichrome or von Gieson. Picrosirius red staining has been frequently used as it can differentiate collagen (red) from muscle (yellow) and it can be coupled with polarized light birefringence to distinguish different collagen compositions (Junqueira et al., 1979, Rich and Whittaker, 2005, Vidal et al., 1982, Takaza et al., 2014), however, histological stains do not specifically detect collagen or allow visualisation of collagen fibril structure. Other visualisation methods based on intrinsic collagen properties such as autofluoresence (Voytik-Harbin et al., 2001) or second harmonic generation (Cox et al., 2003) also suffer from low intensity signal and limited contrast, resolution and specificity since other tissues can also produce signal. Methods based on specific collagen binding, especially coupled with strong fluorescent probe detection, allow higher resolution analysis of collagen fibril organisation, for example using confocal microscopy.

Detection of collagen by specific binding can be achieved using antibodies raised against individual collagen types but with the existence of multiple collagen types, a panel of different antibodies is required to analyse complex tissue types such as skeletal muscle. Alternatively an adapted form of a natural collagen recognition protein called CNA35 can be used; the original binding protein is produced on the cell surface of the bacterium *Staphylococcus aureus*, isolated from patients with bacterial arthritis (Patti et al., 1994, Xu et al., 2004). Two soluble domains of the protein recognize the collagen triple helix (Patti et al., 1994, Zong et al., 2005, Rich et al., 1999) and have been developed as a collagen detection tool, first rendered fluorescent by labelling with Oregon Green 488 (CNA35-OG488) (Krahn et al., 2006). The fluorescent CNA35 “probe” has advantages over other methods for collagen detection including its ability to act as a highly specific, pan-collagen probe for skeletal muscle: Krahn et al. (2006) showed specific binding to a variety of fibril forming collagens including I, III and IV with very little cross reactivity with non-collagenous extracellular matrix proteins. Thus, CNA35 has the advantage of being a pan detector for all collagens with one tool, it does not require expensive antibodies specific for each collagen type, and it avoids the need for fluorescently labelled secondary antibodies. It also allows for using confocal microscopy to visualise collagen fibrils at high resolution. This makes CNA35 particularly valuable in examining fibril organisation. CNA35-OG488 has been used in a number of applications (reviewed in Aper et al. (2014)) including examining the effect of mechanical and biochemical cues on extracellular matrix organisation *in vivo* and in tissue engineering constructs (e.g. (de Jonge et al., 2013, Foolen et al., 2008)). Moreover, fluorescently

labelled CNA35 can be used to visualise the collagen from very small fibrils to mature collagen fibres (Boerboom et al., 2007, Krahn et al., 2006, Aper et al., 2014).

The CNA35 probe offers a number of other advantages over antibody detection of collagen. Collagen has a high density of CNA35 binding sites, so sensitivity is high, in comparison to antibody detection. Fluorescent antibodies are costly, require a two-step process and have a limited penetration capability in dense tissues, and their high affinity binding to collagen may affect tissue function in live tissues (Kumar and Rudbeck, 2009, Krahn et al., 2006). CNA35 is five times smaller than antibodies facilitating tissue penetration, it does not affect collagen properties and, when directly fluorescently labelled, it can bind and be detected in one step (Krahn et al., 2006, Aper et al., 2014, Boerboom et al., 2007, Foolen et al., 2008). For applications where the overall collagen organisation is of interest, the broad specificity to multiple fibril forming collagens is an advantage (Krahn et al., 2006). To further expand the usefulness and accessibility of CNA35 collagen probes, Aper et al. (2014) described the production of an array of further genetically engineered versions fused to six commonly used fluorescent proteins including EGFP (Enhanced Green Fluorescent Protein), tdTomato and mCherry. Because the fluorescent tag is genetically encoded and fused to the probe, it can be easily produced in high amounts through expression in *Eschericia coli* bacteria, purified using an added His tag, and can be widely shared with the research community as DNA constructs. These fluorescent fusions of CNA35 promise to be powerful tools for collagen detection in a wide variety of applications, particularly for studying the biomechanics of collagen rich tissues and the bioengineering of constructs.

Aper et al. (2014) demonstrated the use of fluorescently fused CNA35 probes to visualise collagen in live tissues, using two-photon confocal imaging of human skin and engineered cardiac cells. While CNA35 shows clear advantages for use on live or unfixed tissues, some experimental situations necessitate the use of fixed tissue. For example, current visualisation methods do not permit the observation of collagen reorientation in muscle ECM under externally applied deformation without tissue fixation to “hold” the deformation effect. Also, due to limited stain or probe penetration in mature muscle tissue which may require fixation and sectioning, further reducing visualisation capability (Takaza et al., 2014).

2.4. Mathematical models

The mechanical properties of any soft biolological tissue obtained from mechanical experiments provide data necessary to constitutive models. The purpose of constitutive equations is to relate the stress response to strain and strain rate into a mathematical form. From a constitutive point of view,

the materials can be categorised into four different types: linear elastic, nonlinear elastic, linear viscoelastic and nonlinear viscoelastic.

2.4.1. Linear elastic

Only under small deformations (infinitesimal strains), a material represents linear properties, meaning instantaneous deformation due to stress, and the material recovers immediately when stress is removed. In addition linear elasticity is valid only stress states which do not produce yielding (see Figure 2.20).

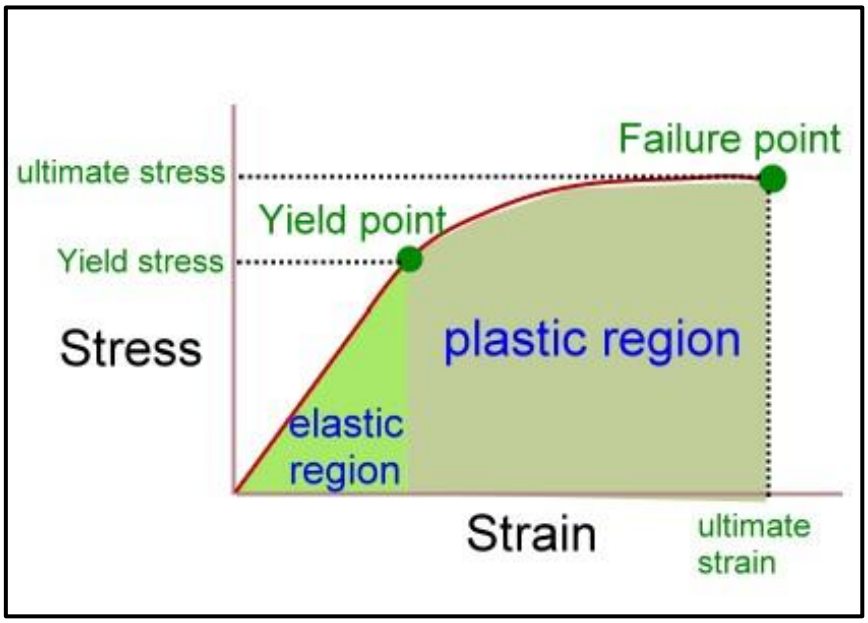

Figure 2. 20-Stress-strain curve for a linear elastic material (adapted from www.pt.ntu.edu.tw).

The relationship between stress and strain may be expressed in terms of the generalised Hooke's law for homogeneous isotropic linear elastic material:

$$\begin{bmatrix}\sigma_{11}\\ \sigma_{22}\\ \sigma_{33}\\ \sigma_{23}\\ \sigma_{13}\\ \sigma_{12}\end{bmatrix} = \frac{E}{(1+\nu)(1-2\nu)}\begin{bmatrix} 1-\nu & \nu & \nu & 0 & 0 & 0\\ \nu & 1-\nu & \nu & 0 & 0 & 0\\ \nu & \nu & 1-\nu & 0 & 0 & 0\\ 0 & 0 & 0 & \frac{(1-2\nu)}{2} & 0 & 0\\ 0 & 0 & 0 & 0 & \frac{(1-2\nu)}{2} & 0\\ 0 & 0 & 0 & 0 & 0 & \frac{(1-2\nu}{2} \end{bmatrix}\begin{bmatrix}\varepsilon_{11}\\ \varepsilon_{22}\\ \varepsilon_{33}\\ 2\varepsilon_{23}\\ 2\varepsilon_{13}\\ 2\varepsilon_{12}\end{bmatrix} \quad (2.1)$$

Where E is the Young's modulus showing the material stiffness, and ν represents Poisson's ratio. Linear elasticity is extensively used in structural analysis of most engineered materials, whereas some materials such as rubbers and soft tissues behave nonlinearly, so introducing the other types of material models is then required (Fung, 1993).

2.4.2. Nonlinear elastic

Mechanical properties of soft biological tissues have received a significant attention from continuum mechanical perspective in the last few years (Holzapfel, 2000, Holzapfel and Gasser, 2001, Holzapfel et al., 2004, Humphrey et al., 1990a, Humphrey et al., 1990b, Fung, 1970). To-date several studies have been conducted to quantify the nonlinear behaviour of biological soft tissues in form of constitutive equations. For instance, Fung (1979) firstly described the behaviour of arteries as pseudoelastic, where different elastic laws applied for loading and unloading paths. A pseudoelastic model was useful in modelling of arteries, however it was difficult to capture the viscoelastic response of arterial walls using this mode (Gasser et al., 2006, Holzapfel and Gasser, 2001). Therefore, the mechanical behaviour of biological tissues is most commonly described using a hyperelastic anisotropic material model (Holzapfel, 2000, Ogden, 1986). For nonlinear elastic materials, the constitutive laws are derived from a strain-energy density function (W). Various forms of W have been proposed to account for specific materials behaviour such as Neo-Hookean, Mooney-Rivlin etc. (Weiss et al., 1996, Holzapfel, 2008, Holzapfel and Gasser, 2001, Holzapfel, 2000), but the most commonly used model is the Ogden model (Ogden, 1978a, Ogden and Sternberg, 1985, Ogden et al., 2004). The Ogden hyperelastic formulation has been employed for rubber-like incompressible materials to numerous degrees (Ogden, 1986, Marckmann and Verron, 2006). For rubber-like materials parameter fitting of the Ogden formula involves 3–4 terms (see Marckmann and Verron (2006); Ogden et al. (2004)). However, as mechanical experimentation of biological tissues is more challenging than engineering materials (data obtained from biological samples are often sparser), models with reduced order are used with fewer parameters to be identified (Moerman et al., 2016).

2.4.3. Linear viscoelastic

Viscoelasticity is the property of materials which exhibit both viscous and elastic characteristics when undergoing deformation. In viscoelastic materials the stress depends on both deformation and the history of deformation.

When considering a viscoelastic material, there are three observed responses to applied loading:

- Stress relaxation: If a deformation is applied to a viscoelastic material, the material is deformed instantly, and where the strain is held constant, the stress in the material will decay with time (Fung, 1993).
- Creep: If the stress applied to the material is kept constant, viscoelastic material undergoes a time-dependent change (Fung, 1993).
- Hysteresis: If the viscoelastic material is loaded cyclically, different loading–unloading changes will occur (Fung, 1993).

Spring and dashpots comprise the building blocks of models describing viscoelasticity. Springs are used to account for the elastic solid behaviour and dashpots are used to describe the viscous fluid behaviour. It is assumed that a constantly applied force results in a constant deformation in a spring (deformation in spring is recoverable after force relase), and a constant deformation rate in a dashpot (the deformation that dashpot undergoes is permanent) (Gould, 1994).

A simple spring–dashpot system, where the elements are in parallel is called the Voigt model (Figure 2.21a). Spring and dashpot exhibit deformation and strain rate dependent response respectively. The total stress assuming the constant strain is obtained by addition of the elastic stress of spring to the viscous stress of dashpot as follows:

$$\sigma = \sigma_{spring} + \sigma_{dashpot} = E\varepsilon + \eta\dot{\varepsilon} \tag{2.2}$$

Where, E is system stiffness (spring coefficient), ε is srain, $\dot{\varepsilon}$ is strain rate, and η is the coefficient of viscosity of the fluid.

As shown in Figure 2.21b, a series configuration of a spring and a dashpot is called the Maxwell model. The stress here is eqaully applied to both spring and dashpot. Therefore, the resulting strain is superposition of strains in dashpot and spring as follows:

$$\dot{\varepsilon} = \dot{\varepsilon}_{spring} + \dot{\varepsilon}_{dashpot} = E\sigma + \eta\dot{\sigma} \tag{2.3}$$

In the Maxwell model, the deformation of the spring is finite, while the dashpot will keep deforming as long as the force is maintained. Therefore, the overal behaviour of the Maxwell model is more similar to a fluid than a solid. In contrast, the dashpot in the Voigt model cannot undergo continuous deformation, so the Voigt model represents a viscoelastic solid behaviour (Gould, 1994). The Maxwell model cannot account for a retarded elastic response, and the Voigt model also does not describe stress relaxation. Both models are characterised by single relaxation times, however, a spectrum of relaxation time would provide a better description (Dill, 2007). Therefore, a general model of a linear

viscoelastic material can be obtained by assembling multiple dashpots and springs (see Figure 2.21c) to be capable of modelling a continuous spectrum of relaxation (Kelvin model) (Fung, 1993).

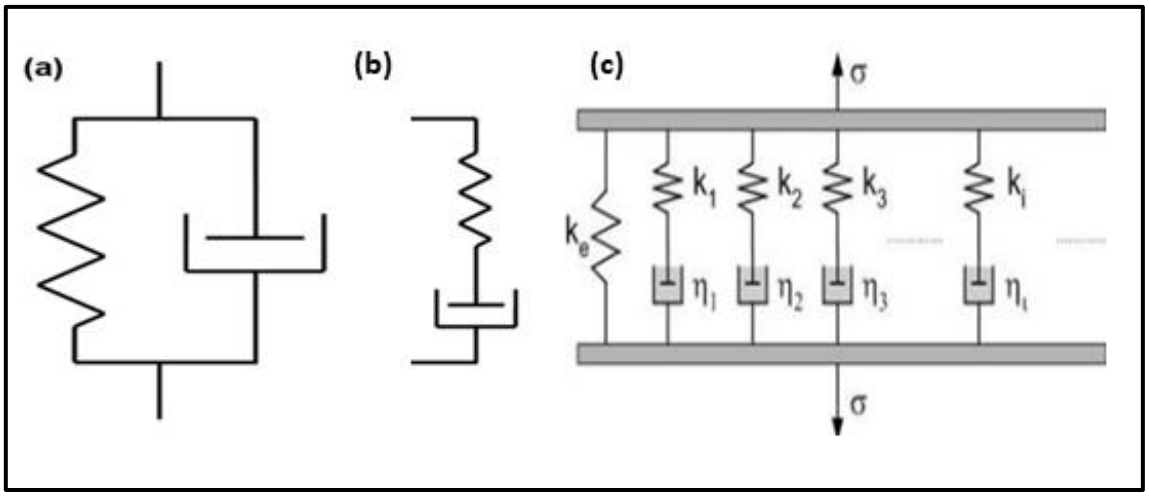

Figure 2. 21-(a) Voigt model, (b) Kelvin model or standard linear solid model, (c) general Kelvin-Voigt model (adapted from www.rehab.research.va.gov).

2.4.4. Nonlinear viscoelastic

Where the nonlinear springs or dashpots are selected for the models explained in the previous section, nonlinear viscoelatic models can be obtained. Several nonlinear viscoelastic models have been derived (Drapaca et al., 2007) thus far. However, the mostly implemented nonlinear viscoelastic model used in finite element (FE) software packages is the quasi-linear theory of viscoelastity explained by Fung (1993).

2.5. Modelling of skeletal muscle

Attempts in skeletal muscle modelling began with the simple unidirectional Hill-type model introduced in 1938 (Hill, 1938) continuing to three-dimensional continuum-based muscle models (Blemker and Delp, 2005, Blemker et al., 2005, Sharafi and Blemker, 2010, Sharafi and Blemker, 2011, Rehorn and Blemker, 2010, Yucesoy et al., 2002, Yucesoy and Huijing, 2009, Moerman et al., 2016). These models, regardless of the level of complexity, are dependent on the material properties. The large differences due to the use of different animals, different muscles, different experimental protocols, etc. illustrate the difficulty in obtaining a uniform set of data characterising muscle properties.

2.5.1. One-dimensional models

One-dimensional models have been developed to reproduce the global muscle mechanical behaviour observed in the experiments. One-dimensional model has been extensively used in modelling of muscle mechanics (Hof and Van den Berg, 1981, Brown et al., 1996, Best, 1994, Cole et al., 1996). The Hill muscle model is widely used in one-dimensional musculoskeletal modelling (e.g. (Delp et al., 2007, Lee et al., 2013, Lai et al., 2014, Biewener et al., 2014). This model today is also used as an actuator in musculoskeletal modelling software packages such as SIMM, OpenSim, LifeMOD.

Hill's equation is an empirical equation describing the force-velocity relationship of Tetanic contraction of a muscle upon an immediate release from an isometric contraction as shown in Figure 2.22.

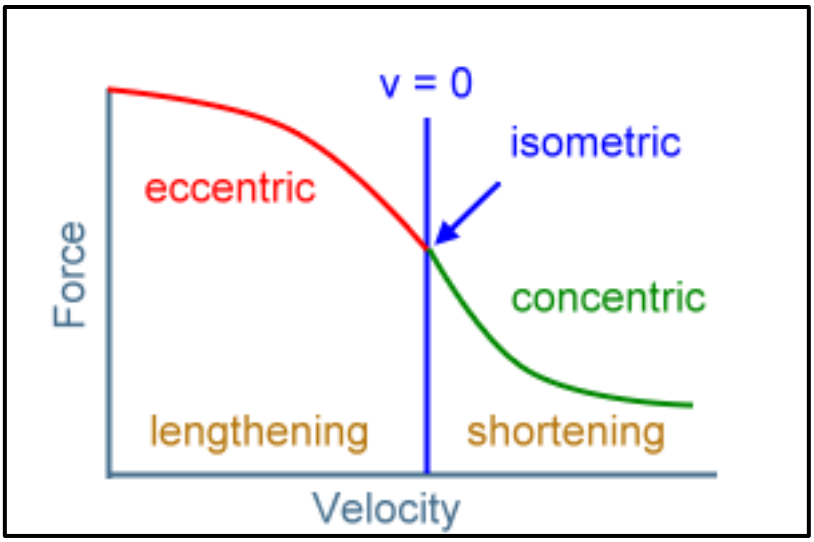

Figure 2. 22- Force-velocity curve of muscle at eccentric, isometric and concentric contraction (adapted from http://www.pt.ntu.edu.tw).

This is the most famous equation in muscle mechanics, which relates tension to velocity with respect to the internal thermodynamics as follows:

$$(v + b)(F + a) = b(F_0 + a) \tag{2.4}$$

Where, F is the tension in the muscle, v is the velocity of contraction, F_0 is the maximum isometric tension (or load) generated in the muscle, a is coefficient of shortening heat, $b = a.\frac{v_0}{F_0}$ that v_0 is the maximum velocity when the load is zero. Hill's equation illustrates that F and v has a hyperbolic relationship, therefore, the higher the load applied to the muscle, the lower the contraction velocity and vice versa. This hyperbolic form has been found to fit the empirical constant only during isotonic contractions near resting length (Fung, 1993).

Hill demonstrated that the muscle actuator is composed of three elements (Figure 2.23):

- A contractile element (CE) models the active component of the muscle.
- A series elastic element (SE), a nonlinear spring in series with the contractile element which allows for a rapid change in the muscle from inactive to active and provides an energy storing mechanism.
- A parallel elastic element (PE), a nonlinear spring in parallel with the aforementioned two elements, which is responsible for the passive muscle behaviour, even at deactivation of the contractile element.

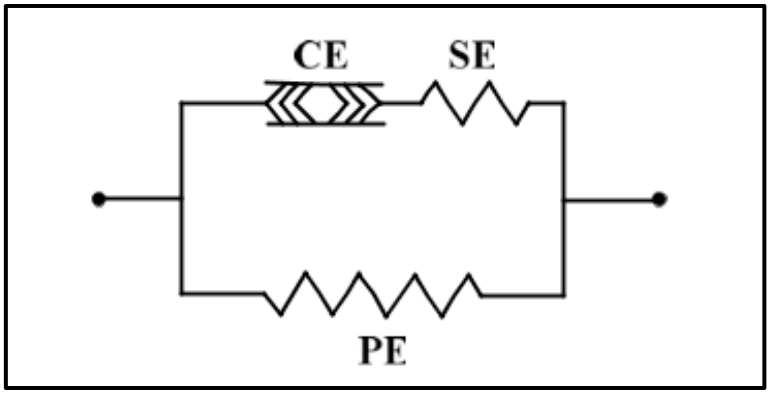

Figure 2. 23-Hill's muscle model; parallel elastic element (PE), contractile element (CE), series elastic element (SE).

The three-element Hill muscle model represents the muscle mechanical response. The active contractile element force (CE) arises from the force generated by the actin and myosin cross-bridges at the sarcomere level. It is fully extensible when inactive but capable of shortening when activated. The ECM influences the muscle's force-length curve. The parallel element (PE) represents the passive force of the connective tissues. The series element (SE) represents the tendon and the intrinsic elasticity of the myofilaments (Fung, 1993).

The total force-length characteristics of a muscle (see Figure 2.24) is a combination of the force-length response of both active and passive elements as follows:

$$F_t = F_{CE} + F_{PE}, \qquad F_{SE} = F_{CE} \tag{2.5}$$

Where, F_{CE}, F_{SE} and F_{PE} are the forces in the contractile element, in the series element and in the parallel element respectively. On the other hand the muscle length is $L_t = L_{CE} + L_{SE} = L_{PE}$. During isometric contractions the series elastic element (SE) is under tension and therefore is stretched a finite amount. Since the overall length of the muscle is held constant, the stretching of the series element (SE) can only occur if there is an equal shortening of the contractile element (CE) itself.

Since muscles present viscoelasticity, therefore a viscous damper may be included in the model (Fung, 1993).

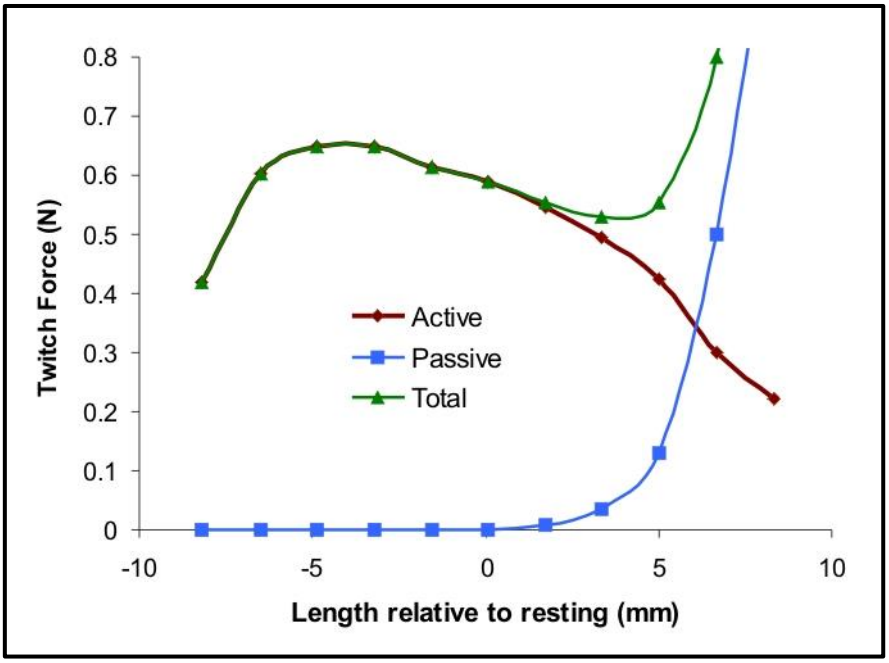

Figure 2. 24-Muscle twitch force verses length relative to the resting length for active, passive and total characterization of muscle behaviour (adapted from www.wikipedia.org).

On the basis of theory of sliding elements proposed by Hill (1938), Fung (1970) proposed a mathematical formulation of the mechanical properties of the heart muscle to represent the tensile stress in parallel and series elements. Stålhand et al. (2008) used a free energy potential function-based model to demonstrate the behaviour of smooth muscle cells. This approach analyses the behaviour of smooth muscle cells in combination with hyperelastic model in a more complex environment.

In practice, for using the Hill model, several parameter values are required to be specified such as the maximum isometric force, the optimal contractile elemnet length (CE), and the unloaded in series elastic element (SE) length. For either simulating the actions of one specific muscle or a whole-body motion actuated by many muscles, it is important to define these parameter on an appropriate basis (Caldwell, 1995, Scovil and Ronsky, 2006, De Groote et al., 2010, Carbone et al., 2016). Therefore, the most limiting aspect of the Hill models is parameter estimation since the model parameters were obtained using passive and active force–length, force–activation, force–velocity curves, which show a species variation. As reviewed earlier, the mechanical properties obtained from the literature are sparse which makes modelling very challenging.

Musculoskeletal models using the Hill model have been successfully applied to study mechanical behaviour, but without consideration of metabolic behaviour. An alternative to the Hill muscle model is the Huxley model (Huxley, 1957), in which the dynamics of cross-bridge mechanism was modelled and as such, involves a relationship between metabolic and mechanical behaviour. The original Huxley model have been widely studied, but mainly to address fast-time scale events on the single fibre level, which could not be explained by the Hill model (Huxley and Simmons, 1971, Tözeren, 1985, Campbell, 2009).

2.5.2. Three-dimensional nonlinear transversly isotropic modelling

Since skeletal muscle has a fibre-oriented structure, it is often considered as a fibre-reinforced composite consisting of parallel fibres embedded in a matrix. Unidirectional composites are transversely isotropic. However, applying engineered material insight to biological material is difficult due to the complex nature of biological structures.

The most popular models characterised nonlinear transverse isotropy behaviour of muscle using the fibre-reinforced composites theory of Spencer (Spencer and Hashin, 1986). Spencer developed a constitutive hyperelastic model in which the strain energy function and the preferred direction of material are related. Others developed Spencer's theory to govern other forms of the strain energy function for other fibre-oriented soft tissues with transversely isotropic properties to model the tensile behaviour (Weiss et al., 1996, Limbert and Middleton, 2004, Humphrey et al., 1990a, Humphrey et al., 1990b, Blemker et al., 2005, Hodgson et al., 2012).

Weiss et al. (1996) and Holzapfel et al. (2004) assumed that the fibres do not bear any load under compression, resulting in an isotropic behaviour in compression. This limits their model applicability to represent skeletal muscle compressive behaviour, since Van Loocke et al. (2006) showed that the muscle cross-fibre direction is stiffer than the fibre direction in compression (anisotropic behaviour) and the stiffness is not equal to zero in the fibre direction. Van Loocke et al. (2006) and Van Loocke et al. (2008) represented a model for skeletal muscle compressive behaviour consisting of a unidirectional composite with nonlinear, transversely isotropic properties.

The hyperelastic models have also been successfully used by different authors to model cardiac muscle behaviour in tension (Novak, 1994, Martins et al., 1998, Martins et al., 2006), skeletal muscle tissue (Bosboom et al., 2001) and skin (Groves et al., 2012).

In conventional Ogden hyperelastic models when the parameters relating to control nonlinearity in materials are regulated, the asymmetry is also affected. Therefore, nonlinearity and asymmetry in tension and compression cannot be controlled independently. However, Moerman et al. (2016) argued on tension/compression asymmetry in Ogden hyperelastic formulations for isotropic materials

using Seth–Hill strains (Seth, 1961, Hill, 1968) and they showed how the properties of the Seth–Hill strains are reflected in the model behaviour. They also presented separate control over the nonlinearity and tension/compression asymmetry proposing a novel set of generalised strain tensors, which shows a better-established model so far.

There are some Neo-Hookean models or first order Ogden models that use all positive Ogden parameters to routinely model ground matrix (Chagnon et al., 2015). The models employing all negative values are commonly used for modelling of nonlinear isotropic behaviour (e.g. skeletal muscle tissue (Bosboom et al., 2001)). Moerman et al. (2016) showed how the use of only positive or only negative Ogden parameters may lead to a model in which all behaviour is dictated by either tension or compression respectively. This also affects both nonlinearity and tension/compression asymmetry. In terms of skeletal muscle modelling, Moerman et al. (2016) formulations may help to identify the role of either the ECM, or the muscle fibres, in generating tension/compression asymmetry. The model proposed by them was implemented to show the nonlinear elastic and transversely isotropic behaviour of skeletal muscle tissue in compression.

Another approach to model nonlinear transverse isotropy was used in porcine aortic heart valves (Li et al., 2001). They used the general theory of linear elasticity for transversely isotropic materials and introduced nonlinearity by defining strain dependent Young's moduli.

2.5.3. Viscoelastic modelling

The presence of water within soft tissues accounts for their viscoelastic mechanical behaviour. The quasi-linear theory of viscoelasticity (QLV) model is probably the most extensively used model to represent soft tissue viscoelasticity which was developed by Fung in 1973 (Fung, 1993). Modelling of tendons and ligaments (Woo et al., 1981, Puso and Weiss, 1998, Abramowitch and Woo, 2004), cartilage (Mow et al., 1980), porcine aortic valve tissues (Rousseau et al., 1983, Doehring et al., 2004), and the tensile and compressive viscoelastic behaviour of skeletal muscle (Best, 1994, Van Loocke et al., 2006, Van Loocke et al., 2008) are some examples of using the QLV model.

A discretised form of the QLV theory, using a Prony series formulation for the relaxation function has been adopted by some authors to represent soft tissue behaviour: modelling of brain tissue in tension and compression (Miller and Chinzei, 1997, Miller, 1999, Miller and Chinzei, 2002), modelling of kidney in compression (Snedeker et al., 2005), and modelling of skeletal muscle in compression and tension (Van Loocke et al., 2006, Van Loocke et al., 2008, Bosboom et al., 2001, Rehorn et al., 2014).

Bosboom et al. (2001) experimentally showed a highly nonlinear viscoelastic nature for rat tibialis anterior (TA). A viscoelastic hyperelastic model (the incompressible Ogden model) was then fitted on their data showing a successful prediction of the *in vivo* forces within the rat TA.

Van Loocke et al. (2006) used a transversely isotropic hyperelastic model as well as a model using the theory of transverse isotropy and strain dependent Young's moduli (SYM) to the experimental data to model the passive compressive mechanical beviour of porcine skeletal muscle. Overall, despite the fact that the hyperelastic model does not adequately fit the data in all directions of testing, it was shown that the SYM gives a good fit to the experimental data in both the fibre and cross-fibre direction, up to 30% strain for aged samples. The model also showed good prediction of muscle behaviour at 45°. Fresh samples showed a different behaviour than aged tissues at 45°. However, the SYM was able to capture this difference and gives a good fit to the fresh experimental data in the fibre, the cross-fibre and at 45° (see Figure 2.25) (Van Loocke et al., 2006, Van Loocke, 2007).

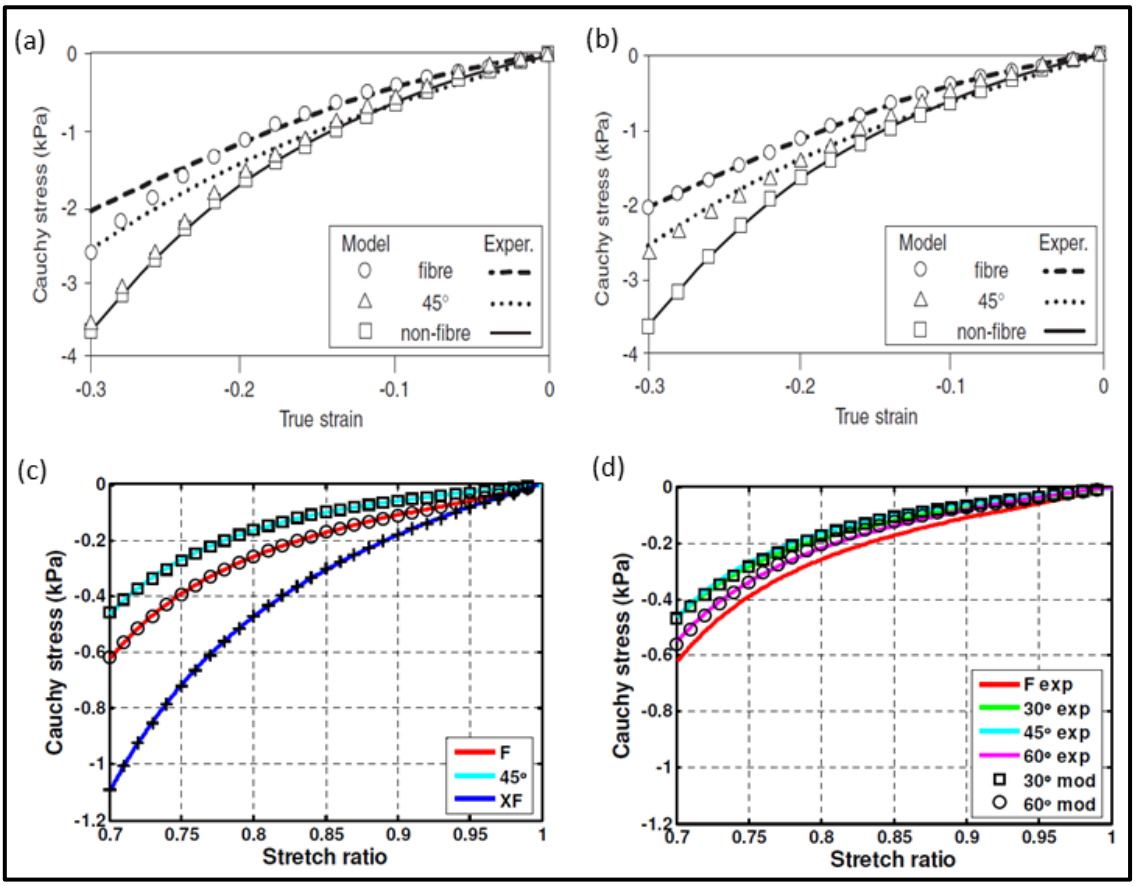

Figure 2. 25-(a) Compression tests on aged porcine samples fitted with Humphrey's model, (b) Compression tests on aged porcine samples fitted with strain dependent Young's moduli (SYM), (c) Compression test on fresh porcine samples fitted with the SYM model, (d) comparison between experimental data and theoretical predictions using SYM model. F (compression in the fibre direction), XF (compression in the cross-fibre direction), and 30, 45, and 60° are compression in within angles (a & b adapted from Van Loocke et al. (2006) , and c & d adapted from Van Loocke (2007)).

The pattern of many constitutive models, when modelling the anisotropy in soft tissues, is that the stress response can be decomposed into an isotropic part relating to the ECM and an anisotropic part related to muscle fibres, so that the contribution of the fibre part can be neglected under compression.

However Böl et al. (2014), Van Loocke et al. (2006), Takaza et al. (2013a), and Pietsch et al. (2014) provided experimental data on the anisotropic compressive response of muscle tissue showing that skeletal muscle has an anisotropic response under compression. The fibre direction provides a principal direction of transverse isotropy both under tension and compression. So, the results showed that muscle fibres surrounded by ECM are able to resist compression and contribute to the stress response. They showed that this assumption in constitutive models of skeletal muscle may not be valid.

2.5.4. Micromechanical modelling

Blemker and Delp (2005) attempted to create a 3D computational model of the psoas, iliacus, gluteus maximus and gluteus medius muscles by capturing accurate description of complex geometries using magnetic resonance imaging (MRI). The method suggested by them was effective in capturing complex geometries, however it did not consider the many muscle fibres that terminate intrafascicularly since the forces from these fibres are transmitted via shear in the surrounding endomysium layer or via tension in the endomysium connecting the muscle to the tendon. Understanding these mechanism is vital in our knowledge of compressive passive skeletal muscle behaviour. When considering the mechanical response of a sample, the efficacy of the endomysium layer in force transmision between neighbouring fibres by shear is especially important, as tendons do not exist at either end of the fibres.

Sharafi and Blemker (2010) developed a micromechanical model to assess the effect of changes in muscle geometry on the macroscopic behaviour by focusing on along-fibre shear modulus of muscle that had not been taken into account in previous works. In fact, the model proposed in their study was made by receiving geometry and properties of the microstructure in order to derive the constitutive muscle model on a macro scale. The rabbit rectus femoris (RF) and soleus muscles were studied at fibre and fascicle level. Similar shear moduli at the macroscopic fibre level were found as the fibres are alike for both muscle types. However, considerable transverse anisotropy was observed at the fascicle-level, which indicates that the transverse isotropy assumption assumed in most FE constitutive models is not completely true at least at fascicle level (Blemker and Delp, 2005, Oomens et al., 2003). Sharafi and Blemker (2010) conducted the simulation for the full activation of healthy muscle, so the passive behaviour of skeletal muscle was not considered.

The asymmetrical behaviour in passive tensile and compressive stress-strain relationship was experimentally obtained in many studies (Van Loocke et al., 2006, Bosboom et al., 2001, Morrow et al., 2010a, Calvo et al., 2010, Takaza et al., 2013a, Pietsch et al., 2014, Böl et al., 2014). There are a few studies trying to address tension/compression assymetry through microstructure studies since

there remains a lack of understanding of how external tension or compression applied in the fibre or cross-fibre direction relates to the deformation of muscle fibres and the ECM (Takaza et al., 2014, Gindre et al., 2013).

Gindre et al. (2013) developed a simplified structural model to show that the mechanical response of skeletal muscle is dominated by the interaction between the soft but incompressible muscle fibres and stiff but initially slack collagen tissue, using maximum, minimum and average values for each parameter needed according to the literature. The model consisted of a single incompressible muscle fibre surrounded by endomysium. Although it was assumed that the individual collagen fibres wrap around only a single muscle fibre, not a fascicle, the model could demonstrate the interaction between individual muscle fibres and surrounding connective tissue. Generally, the experimental data clearly show more tensile/compresive asymmetry than the Gindre et al. (2013) model does. The model showed that the collagen networks contributes to muscle stiffness through two resisting mechanisms: a longitudinal force resisting tension and a pressure force on the muscle fibre resisting compression, which partially reflected tension/compression asymmetry (Gindre et al., 2013).

In future, mathematical structural models of whole muscle including fascicles and perimysium is required to further develop the Gindre et al. (2013) model, and to understand the role of perimysium collagen fibres in tension/compression asymmetry.

2.6. Concluding remarks and aims of thesis

The primary reason that the ECM has not been thoroughly studied is that for many years the contractile element behaviour (force producing capabilities) of skeletal muscle was only of interest to researchers. However the recent advancements in pressure sore modelling, impact biomechanics, rehabilitation engineering, etc. has caused passive compressive behaviour to be considered as well.

The literature on skeletal muscle compressive and tensile properties shows different behaviours as a result of different experimental protocols (variation in species, samples, strain rates, etc.) being used, giving large variations in the published data. It was also observed that the models generally captured the incompressibility and nonlinear tensile elasticity of passive muscle tissue. However asymmetric stress-strain response in compression/tension requires further investigation.

There have been many studies which here investigated the collagenous network structure in skeletal muscle tissue in different animals. They mostly showed high quality images of endomysium and perimysium structures taken by SEM at very small length scales, and tried to describe how the connective tissue network appears. It has also been very difficult to unravel different layers of connective tissue as definition of each layer is very subjective and depends on the tissue and the animal selected for the research (Gillies and Lieber, 2011, Nishimura et al., 1994, Passerieux et al.,

2006, Purslow, 1989, Purslow and Trotter, 1994, Das et al., 2010). However, there are few studies to show how this collagenous network reorients to externally applied deformation or loading mostly focused on the deformation applied along the muscle fibres (Trotter and Purslow, 1992, Lewis and Purslow, 1989, Takaza et al., 2014). Among those only one study (Takaza et al., 2014) tried to address tension/compression asymmetry in both tension and compression applied along and also across the muscle fibres.

Although some differences in the composition of ECM appear to be pre-programmed in embryogenesis, there are some variations in the amounts of collagens as muscle grows (Listrat et al., 1999). There are also the differences in the collagen contents between muscles of different functions within animals (Nakamura et al., 2003, Sakakibara et al., 2000) or even the same muscle type in different animal group (avian versus mammalian) (Das et al., 2010, Nishimura et al., 1994, Passerieux et al., 2006, Nishimura et al., 2008). In a study of six bovine muscles, Light et al. (1985) showed a range of 1.4–7.0% of dry weight in perimysium but only a range of 0.1–0.5% in endomysium mass. Purslow (2010) reported the connective tissue content of 14 bovine muscles showing that the endomysial collagen content is between 0.47% and 1.2% of dry weight, but the perimysial collagen content in the same muscles ranges from 0.43% up to 4.6% of dry weight. Therefore, the amount of perimysium in muscles varies far more than the amount of endomysium. These variations, especially in the amount and organisation of the perimysium have been taken to show that the perimysium must play strong roles in the normal functioning of each muscle.

There have been many studies attempting to create three-dimensional model of skeletal muscle. However, the validity of those models strongly depends on the choice of constitutive models and material properties (Sharafi et al., 2011, Sharafi and Blemker, 2011, Blemker and Delp, 2005, Blemker et al., 2005). Some micromechanical models were also developed to consider the microstructure of the muscle to derive the constitutive muscle model (Sharafi and Blemker, 2011). However, there are a few studies which try to address tension/compression assymetry through a micromechanical model due to the preliminary understanding of the muscle microstructure (Gindre et al., 2013). Gindre et al. (2013) developed a simplified structural model to show the direct mechanical interaction between one muscle fibre and its surrounding endomysium, which contributes to muscle stiffness through two resisting mechanisms: a longitudinal force resisiting tension and a pressure force on the muscle fibre resisting compression. Their model was not fully capable of addressing the observed mechanical behaviour in the skeletal muscle.

Therefore, the current study aims to further advance the knowledge on the mechanical as well as structural properties of this fundamental tissue using chicken tissue (bird) as a very different type of tissue compared to porcine, bovine, rat etc. (mamals). The following aims are defined for this research:

- Tensile and compressive mechanical testing on chicken tissue is carried out to gain a deeper understanding of variations between species.
- To improve our knowledge on connective tissue particularly perimysium, CNA35-EGFP/tdTomato is used as a good method to detect and visualise the collagen fibres.
- Chicken and porcine microscopic slides from compressed and stretched specimens are generated for qualitative assessment of skeletal muscle microstructure (perimysium) under different deformations to understand microstructural differences within and between species, and to address observed tension/compression asymmetry.
- From the modelling point of view, a microstructural-geometrical model of skeletal muscle is proposed based on microstructural parameters to assess muscle behaviour under different loading conditions.

Chapter 3-The *in vitro* passive elastic response of chicken pectoralis muscle to applied tensile and compressive deformation

The inspiration you seek is already within you, be silent and listen.

RUMI, 13TH-CENTURY PERSIAN POET.

3.1. Introduction

Skeletal muscle accounts for about 40% of body mass (Chomentowski et al., 2011) and the mechanical response of muscle to externally applied deformation is of great interest for applications in impact biomechanics (Cai et al., 2014, Meijer et al., 2013, Takaza and Simms, 2012, Ivancic et al., 2007, Mukherjee et al., 2007, Praxl et al., 2008), rehabilitation engineering (Linder-Ganz et al., 2007, Linder-Ganz et al., 2009, Turkoglu et al., 2014, Yucesoy et al., 2015, Akdeniz et al., 2015), and pressure sore prevention (Filius et al., 2013, Cushing and Phillips, 2013, Bosboom et al., 2003, Nagel et al., 2009, Mak et al., 2011, Linder-Ganz and Gefen, 2008, Oomens et al., 2003, Xiao et al., 2014). For finite element (FE) modelling of whole body or body region responses, constitutive models of muscle are

needed and various continuum-based muscle models have been proposed, e.g. (Blemker and Delp, 2005, Blemker et al., 2005, Sharafi and Blemker, 2010, Sharafi and Blemker, 2011, Rehorn and Blemker, 2010, Yucesoy et al., 2002, Yucesoy and Huijing, 2009). Muscle has nonlinear and anisotropic elastic properties (Van Loocke et al., 2006, Song et al., 2007, Böl et al., 2012, Simms et al., 2012), and exhibits strongly viscoelastic behaviour. Some constitutive models have tried to represent all of these characteristics (Song et al., 2007, Van Loocke et al., 2009, Van Loocke et al., 2008, Van Sligtenhorst et al., 2006, Grieve and Armstrong, 1988, Takaza et al., 2013b, Takaza et al., 2013a). However, to date, none have successfully captured the 3D elastic tension/compression asymmetry observed in the stress-stretch response of passive skeletal muscle using a single set of material parameters (Takaza et al., 2014, Gindre et al., 2013). The reasons for this asymmetric response evidently lie in the microstructure, but a detailed explanation has not yet been proposed. This Chapter aims to provide new experimental data to help our understanding of this tension/compression asymmetry.

Muscle is first and foremost an active tissue, and the total muscle stress derives from a combination of active and passive components, and these are likely interdependent. Therefore, FE models of muscle tissue mostly require consideration of both active and passive properties of the tissue. However, only the passive properties of muscle tissue are studied here, since in impact experiments, the time scale of the event does not allow sufficient time for muscles to be activated and so the stress response is mainly due to the passive properties of the tissue. Note that the activation time for muscle contractility is about 10-100 ms (Oda et al., 2013). Similarly, in pressure sore modelling, which is a quasi-static situation, the passive description of muscles is more relevant (Simms et al., 2012). The main focus here is also on elastic tension and compression rather than viscoelastic muscle behaviour as a first step, but the importance of rate effects is acknowledged (Van Loocke et al., 2008).

The passive elastic compressive and tensile behaviour of skeletal muscle has been observed to be asymmetric, nonlinear and anisotropic in studies mostly on porcine tissue in a number of studies (Van Loocke et al., 2009, Van Loocke et al., 2008, Van Loocke et al., 2006, Takaza et al., 2013b, Takaza et al., 2013a, Takaza and Simms, 2012, Nie et al., 2011), but also using rabbit, e.g. (Böl et al., 2012, Hernández et al., 2011, Morrow et al., 2010b), rat tissue e.g. (Calvo et al., 2010, Bosboom et al., 2001) and bovine tissue (Van Loocke et al., 2006). However, tension and compression data under similar experimental conditions (sample origin, preparation, and strain rate) are currently only available for porcine tissue (Van Loocke et al., 2006, Takaza et al., 2013a) and these data show that the stress response to stretching in both the fibre and cross-fibre directions is two orders of magnitude stiffer for tension than compression. From a constitutive modelling perspective, this is surprising and existing fibre reinforced composite theories do not capture this response since the observed tensile response,

combined with the induced off-axis response (or Poisson's ratio effect), would imply a much stiffer compressive response than is actually observed.

Recent microstructural investigation (Takaza et al., 2014) of porcine tissue found significant shape changes in the muscle fibres for applied tensile and compressive deformation and hypothesised on the role of endomysium and perimysium in controlling the tension/compression asymmetry, but conclusive evidence was not presented. Overall, it remains unclear how the tension/compression asymmetry observed in porcine tissue is governed by its microstructure, which is known to be considerably variable (Takaza et al., 2014, Pietsch et al., 2014, Takaza et al., 2013a, Purslow, 2010, Purslow and Trotter, 1994, Trotter and Purslow, 1992), or how it relates to the response of skeletal muscle in other species.

One approach to better understanding the observed macroscopic deformation phenomena in skeletal muscle is to compare the macroscopic and microscopic responses in two very different kinds of skeletal muscle. The available literature suggests that the myofibre type composition, collagen content, perimysium thickness, (Liu et al., 1996, Das et al., 2010, Nakamura et al., 2003, Roy et al., 2006, Liu et al., 1994), and muscle fibre size (Sakakibara et al., 2000) in chicken muscle is different from those of porcine tissue (Fang et al., 1999, Nishimura et al., 1998, Archile-Contreras et al., 2010). Accordingly, since porcine tissue data are well reported, and chicken is readily available and is substantially different to porcine tissue, chicken muscle was chosen as a suitable comparison species. Therefore, in this study the passive elastic mechanical behaviour of chicken pectoralis muscle under tension and compression deformation was investigated and compared to previously published results on porcine muscle tissue.

3.2. Methods

3.2.1. Sample preparation

Pectoralis muscle samples were harvested from twelve three-month-old female Ross 508 chickens, with an average body weight of 3 Kgs (Annyalla Chicks Ltd) by trained personnel using ethically approved protocols. The pectoral muscles extend from the keel of the sternum, the clavicle and the sternocoracoclavicular membrane (origin) to insert on the medial pectoral crest of the humerus (insertion) and is the main depressor of the wing (O'Malley, 2005, McLelland, 1990). The samples were acquired and tested within two hours post-mortem from the Zoology Department at Trinity College Dublin. All non-muscle tissue (skin, fatty tissues, etc.) was removed from the excised muscle. Samples for compression and tensile testing were then cut with a scalpel. Due to the mobility of the freshly

harvested tissue, significant care was needed to prepare samples with approximately cuboid dimensions and the appropriate muscle fibre direction.

Compression: Cubic specimens with a nominal size of 10x10x10 mm were cut to produce samples suitable for compression in the muscle cross-fibre direction and at 45° to the muscle fibre direction (see Figure 3.1). Buckling was not observed as a concern for the samples deformed at 45° to the muscle fibre direction. For compression in the muscle fibre direction, samples with height/length aspect ratios of 1:2 were prepared to prevent buckling during testing. Thus the fibre direction sample nominal dimensions were 10x10x5 mm, see Table 3.1

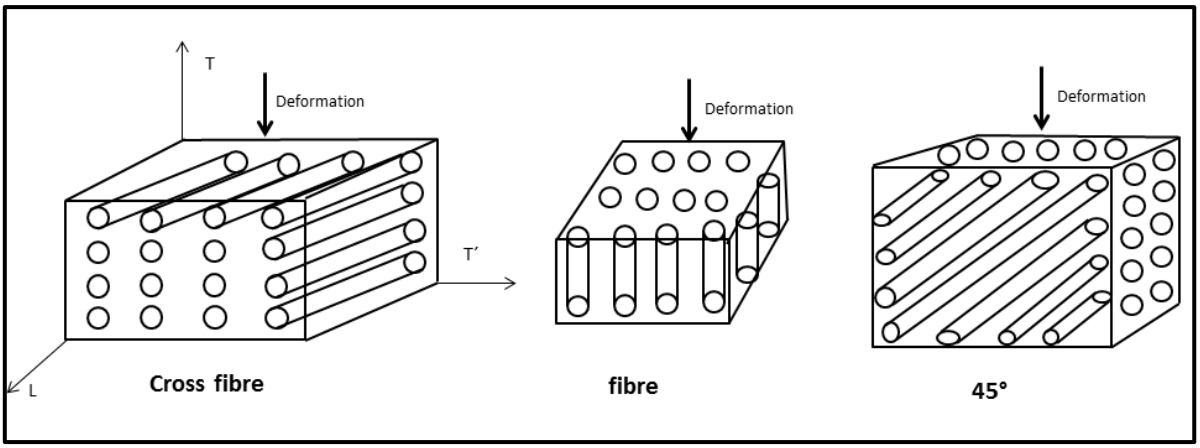

Figure 3. 1-Schematic of prepared specimens: L is the longitudinal direction, T & T' are the transverse directions.

Table 3. 1-The sample size and the average specimen dimensions at different orientations for compression tests.

orientation	Average height ±std (mm)	Average width ±std (mm)	Average thickness ±std (mm)	Sample size (N)
Fibre	5.5±0.6	10±0.5	10.5±0.7	24
Cross Fibre	9.7±0.8	10.3±0.7	10.7±0.8	23
45°	10±0.8	9.9±0.6	10.8±0.9	20

Tension: Approximately 10 mm thick and 10 mm wide samples were prepared. The sample length varied depending on the muscle bulk available but was maximised to account as much as possible for the aspect ratio guidelines in the tensile testing standard ASTM E8/E8M-15a (see Table 3.2), which are aimed at minimizing the edge effects due to tissue clamping. In general, a length to width ratio of 4 was achieved.

Both compression and tensile tests were performed at room temperature. The sample dimensions were measured when the muscle was horizontally placed on the bench to reduce the effects of gravity, and Phosphate Buffered Saline (PBS) was continuously sprayed on the sample to avoid drying and to provide more biological conditions.

Table 3. 2-The sample size and the average specimen dimensions at different orientations for tensile test.

orientation	Average height ±std (mm)	Average width ±std (mm)	Average thickness ±std (mm)	Sample size (N)
Fibre	41.6±8.5	10.6±1.6	9.5±1.2	11
Cross Fibre	39.5±6.1	10.3±1.4	10.5±1.2	11
45°	42.3±6.0	9.8±1.5	11.4±1.4	11

Rigor Mortis To assess the onset of rigor mortis in chicken, preliminary compressive and tensile quasi-static tests were conducted on chicken muscle samples at regular intervals after death of the animal, as this is not reported in the literature. The detailed results are shown later, but analysis indicated no effect of rigor mortis on stress-stretch relations within two hours of death, and all stress-stretch responses presented in this paper are thus based on tests performed within two hours of death of the animals.

3.2.2. Experimental set-up

The mechanical tests were carried out on a uniaxial test machine (Figure 3.2a), (Zwick Z005, Zwick GmbH & Co. Ulm, Germany).

Compression: The samples were compressed by 30% in the cross-fibre, fibre and 45° directions at the quasi-static strain rate of 0.05 $\%s^{-1}$ using a 5 N transducer, applying the protocol of Van Loocke et al. (2006). Samples were placed between parallel platens (Figure 3.2b), and deformation was applied via the platen attached to the moving crosshead of the machine. To reduce friction between platens and samples, silicon oil was sprayed on both platens (Böl et al., 2012). For Poisson's ratio measurements, one face of a subset of 9 or 10 of the compression samples was marked by six black dots after placing them on platens using a permanent marker. A high definition Samsung HMX-QF20 camera (Samsung Electronics Co., Gyeonggi-Do, Korea) was used to record the displacement of the markers during the test to further calculate the Poisson's ratios. To evaluate the fluid exudation during compression, the samples were patted dry with a tissue (to decrease the effect of PBS spraying) and then weighed before and after each experiment. The peak load (0.2 N) obtained from preliminary tests was considered as the maximum force and a preload of 0.01 N was chosen (1/20 maximum load) to make sure the platen touches the top surface of the tissue.

Tension: The machine was equipped with a 100 N load cell and used to stretch the samples at a rate of 0.05 $\%s^{-1}$ in the fibre, cross-fibre and 45° orientations. The samples were gripped by two grated clamps, see Figure 3.2c. The benefit of using grated clamps is to minimize over-tightening of samples,

and this matched the protocol used by Takaza et al. (2013a). The samples were stretched by 20% in the fibre and cross-fibre directions and 12% at 45 ° with respect to the fibre direction. These limits were chosen since preliminary tests showed tearing beyond these stretch ratios. The peak load (4N) obtained from preliminary tests was considered as the maximum force and a preload of 0.1 N was chosen (1/40 maximum load). This preload was sufficiently high to straighten muscle fibres in the samples without stretching them. For stretch measurement in the tensile tests, nine black dots were marked on the samples after placing them in clamps, facing the camera for displacement tracking during testing. This eliminates the error arising from clamp slippage and also allows the estimation of local strains. The test terminated when the samples reached either the chosen stretch ratio or failure (rupture of muscle specimen), whichever came first.

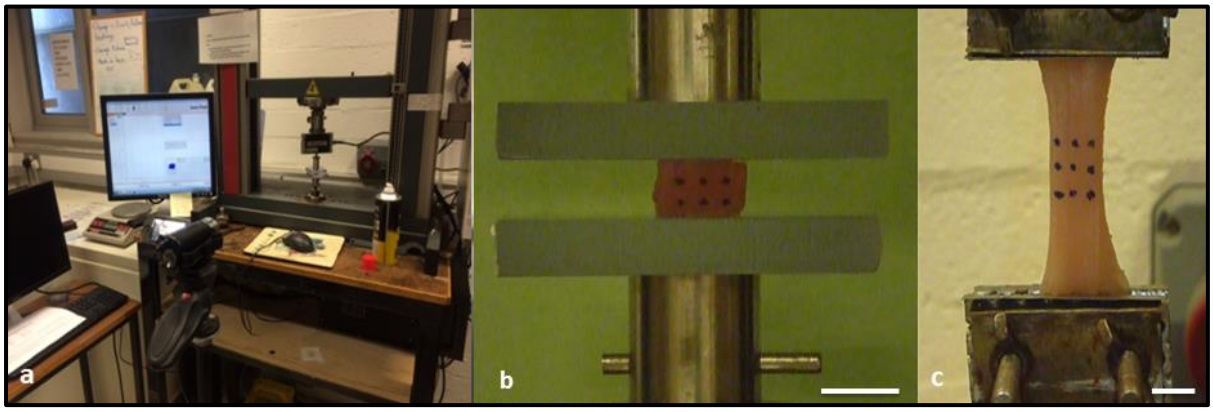

Figure 3. 2-Zwick machine set up used for mechanical testing (a) a sample between platens for a compression test (b) a sample between grater clamps for a tensile test(c). Scale bars indicate 10 mm.

3.2.3. Statistical Analysis

The data are presented as mean± standard deviation (SD). The normality of the data was checked using Excel z-value Normal Distribution Calculation. No indication for deviation from normal distribution was found. A two-way ANOVA with deformation direction and stretch ratio as the factors and t-tests (two- sample assuming unequal variances) were performed as a post hoc test (with alpha set at to 0.05) where necessary. Effect size was also calculated.

3.3. Data Analysis

The experimental force, displacement and time data from the Zwick were imported into Matlab (the Mathworks, Natick, Ma USA) to plot the relevant stress-stretch graphs. Engineering stress (σ) is the normal component of force divided by initial cross-sectional area. Cauchy Stress (σ_{Cauchy}) is the normal component of force divided by the instantaneous cross-sectional area. Assuming the material volume remains constant (Van Loocke et al., 2006, Takaza et al., 2013a):

$$\sigma_{Cauchy} = \frac{P}{A_0}(\lambda) = \sigma.\lambda, \quad (3.1)$$

where, $\lambda = \frac{A_0}{A} = \frac{L}{L_0}$ is the stretch ratio. The length after applying the preload was taken as the unstretched length.True strain is defined as:

$$\varepsilon_{true} = \int \frac{dl}{L} = ln\left(\frac{L}{L_0}\right) = ln(\lambda), \quad (3.2)$$

where, dl and L are respectively instantaneous sample length changes and current length.

For the stretch calculations derived from the matrix of applied dots on the sample faces, Matlab was used to track the displacement of the centre of the dots in the camera images. The resolution of images was 640×480 pixels (96 dpi). For a sample marked by 9 dots (see Figure 3.2c), 6 local stretch ratios in the transverse (T) and longitudinal (L) directions were obtained, see Figure 3.3. For the transverse direction:

$$\lambda_{nT} = \frac{T_n}{T_{0n}}, \quad (3.3)$$

where, *n* is a number defining the distance between 2 dots, T_n is the final deformed length and T_{0n} is the undeformed length in the T direction. The instantaneous average stretch ratio was calculated by averaging:

$$\lambda_T = \frac{1}{6}\sum_{n=1}^{6}\lambda_{nT} \quad (3.4)$$

Stretch in the longitudinal (L) direction was found similarly:

$$\lambda_{nL} = \frac{L_n}{L_{0n}} \quad (3.5)$$

$$\lambda_L = \frac{1}{6}\sum_{n=1}^{6}\lambda_{nL} \quad (3.6)$$

Poisson's ratios (υ) are the (negative) ratios of the induced true strain to the applied true strain: υ_{LT} (=$\upsilon_{LT'}$) describes induced deformation in one of the transverse directions (T or T′) when deformation is applied in the fibre direction (L). Similarly, υ_{TL} describes the longitudinal deformation resulting from deformation applied in one of the transverse directions and finally $\upsilon_{TT'}$ describes the induced deformation in the transverse direction (T') when the sample is deformed in a perpendicular transverse direction (T).

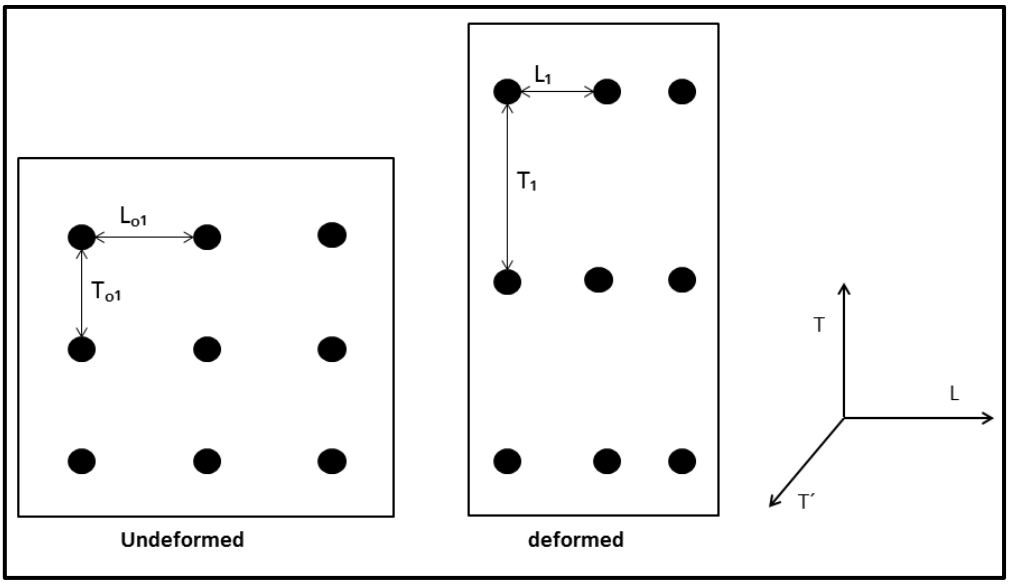

Figure 3. 3-Schematic illustration of the markers on the samples before and after deformation.

3.4. Results

3.4.1. Passive mechanical behaviour

Two-way ANOVA tests were performed to compare stress differences over the entire stress-stretch relations. It was observed that there is a significant difference for both factors (deformation direction and stretch ratio) on the stress response, and a significant interaction between the factors was also observed.

The stress-stretch response of chicken pectoralis muscle tissue in the fibre, cross-fibre and 45° directions is demonstrated for compression and tension (Figure 2.4). The colour code in the current Chapter is as follows; blue for the fibre direction, red for the cross-fibre direction and green for the 45° direction responses. Figure 3.4a shows that chicken pectoralis muscle is stiffest under compression in the cross-fibre direction and most compliant for applied deformation in the fibre direction. There is a significant difference between the mean stress response in the fibre and cross-fibre directions (p-value=$5.9 \times 10^{-7}$and effect size of 0.82) and also between the fibre and 45° directions (p-value=2.0×10^{-4} and effect size of 1.58). However, there is no statistically significant difference in mean stress response between the cross-fibre and 45° directions (p-value=0.22 and effect size of 0.93).

Figure 3.4b shows that for applied tensile deformation, chicken pectoralis muscle is stiffest when stretched at 45° to the muscle fibre direction and most compliant when stretched in the muscle fibre direction. Up to 12% stretch, only the muscle fibre and cross-fibre directions responses are not statistically significantly different (p-value=0.11 and effect size of 1.49).

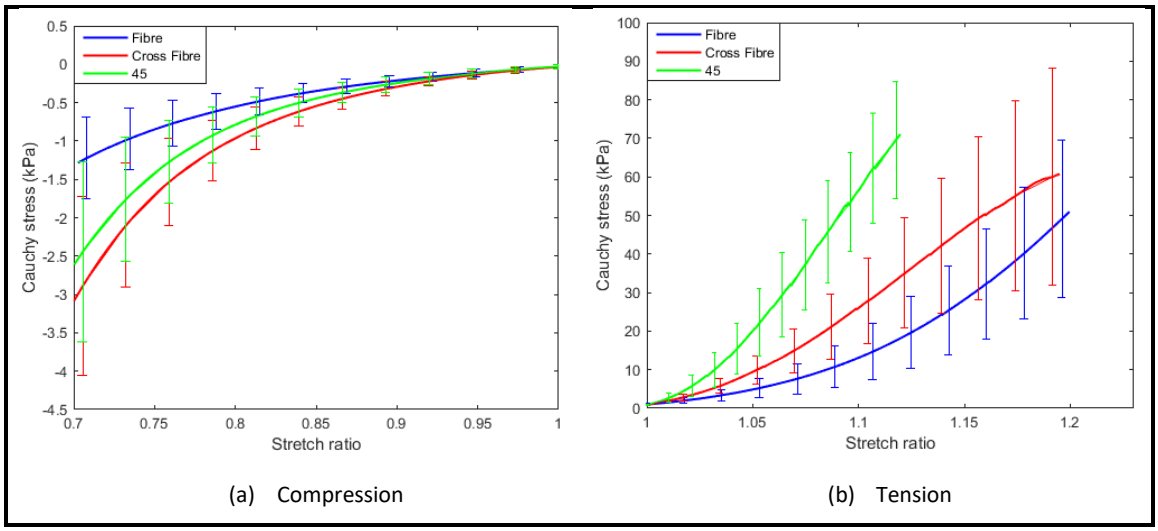

Figure 3. 4-Cauchy stress-stretch relations for chicken pectoralis muscle tissue in fibre, cross-fibre and 45 ° orientations (mean value± one standard): (a) Applied Compression; (b) Applied Tension.

For both load directions, the stress-stretch response is mostly nonlinear, as expected. The tensile response is significantly stiffer than the compressive response for all directions tested (p-values are 2.7×10^{-6} for the fibre, 4.7×10^{-5} for the cross-fibre, and 2.6×10^{-8} for the 45° directions). Scatter is reflective of standard deviations in Figure 3.4, so the variation in cross-fibre stress is considerably larger than in both other fibre directions in both compressive and tensile deformation.

3.4.2. Rigor Mortis effects

Figure 3.5a & 5c show the compressive Cauchy stress response over time while Figure 3.5b & 5d show the tensile response over time to investigate the time of rigor mortis onset for chicken tissue and its influence on chicken muscle stress response. In Figure 3.5a & 5b the different load direction data are separated, while in Figure 3.5c & 5d they are combined (λ=0.7 in Figure 3.5c, λ=1.12 in Figure 3.5d). Linear regression lines are also shown. The r^2 values are always low and there is no clearly identifiable trend observable overall.

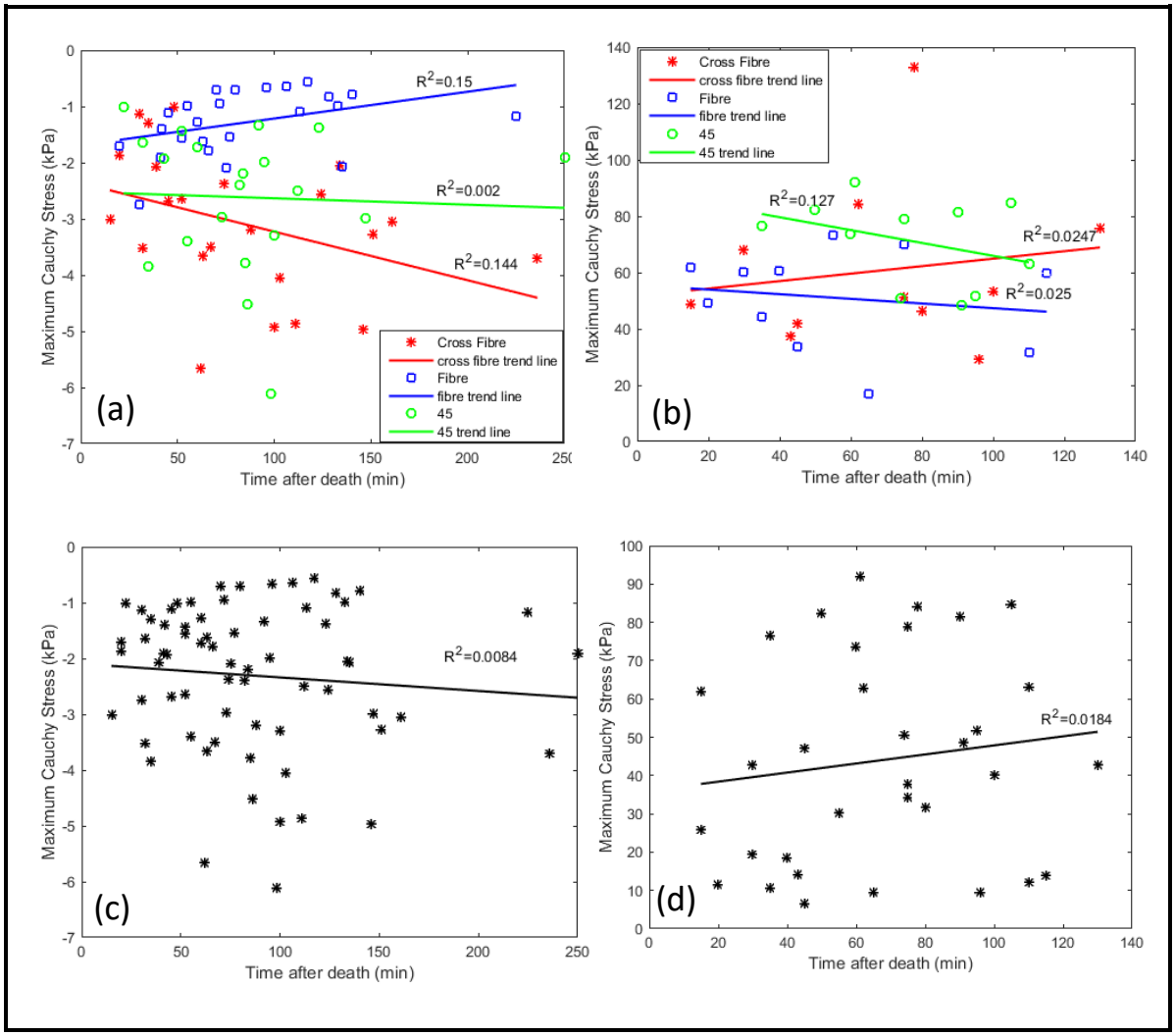

Figure 3. 5-The effect of time after death on the stress response of fresh chicken muscle samples; (a) Cauchy stresses in compression were calculated at λ=0.7 for all samples (b) Cauchy stresses in tension were calculated at λ=1.2 in the fibre and cross-fibre directions, and λ=1.12 in 45 ° direction (c) all compression samples combined (d) all tension samples combined (λ=1.12).

3.4.3. Poisson's ratios

The Poisson's ratio results for chicken muscle are shown in Table 3.3. When the tissue is either compressed or stretched along the fibres, the induced deformation in the other two directions are equal (υ_{LT}=$\upsilon_{LT'}$) and about 0.50, but when the tissue is deformed across the fibres, the induced deformation in the fibre direction (υ_{TL}) and the other transverse direction ($\upsilon_{TT'}$) was 0.34 and 0.64 in compression, while it was 0.83 and 0.17 in tension. In tension, $\upsilon_{TT'}$ was estimated based on assumed incompressibility of the tissue, so no standard deviation is available for this. The effect of the Poisson's ratio versus the stretch ratio was also investigated. It was observed that the change in stretch ratio has a minimal effect on the Poisson ratio values (see Appendix A).

Table 3. 3-The Poisson's ratios of pectoralis chicken skeletal muscle in compression and tension

orientation	Poisson ratio±std (compression)	Sample size in compression (N)	Poisson ratio±std (Tension)	Sample size in tension (N)
υ_{LT}=$\upsilon_{LT'}$	0.51±0.08	9	0. 5±0.08	11
υ_{TL}	0.34±0.06	10	0.83±0.09	11
$\upsilon_{TT'}$	0.64±0.06	9	0.17	11

3.4.4. Fluid Exudation in compression

During compression some fluid content is lost through the sample surfaces. The amount of fluid exudation is generally small in quasi-static compression (Figure 3.6). No statistically significant difference was observed in fluid exudation between any two directions.

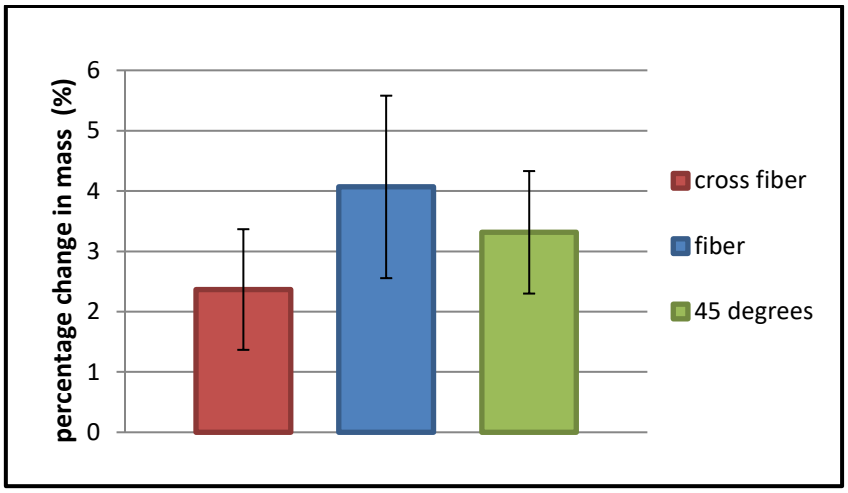

Figure 3. 6-The fluid exudation during quasi-static compression test for fresh chicken samples in fibre, cross-fibre and 45° orientations.

3.5. Discussion

3.5.1. Stress-stretch and Poisson's ratios results

General: The tension/compression asymmetry previously reported in porcine skeletal muscle has now also been observed in chicken muscle, with Figure 3.4 showing that the stress in tension is two orders of magnitude higher than in compression in all directions tested for the range of axial strain examined. As pointed out in the Introduction, this mechanical response cannot be captured by conventional fibre reinforced composite constitutive models with a single set of material parameters, since the observed tensile response, combined with the induced off-axis response (or Poisson's ratio effect) would imply a much stiffer compressive response than is actually observed. Thus the data presented here, combined in future with microstructural assessments, might help to explain this

tension/compression asymmetry which is now evident across two very different kinds of skeletal muscle (porcine and chicken tissue). It is conjectured that it is present in all skeletal muscle, including human tissue.

Compression: Figure 3.7 shows significant variation in the compressive stress-stretch responses between previously published data. Direct comparison is mostly not possible, since there are some differences in test protocol. Song et al. (2007) carried out compression tests with a strain rate of 0.007 s^{-1} on porcine tissue showing that the muscle compressive properties are nonlinear in both fibre and cross-fibre directions. However, the results are much stiffer, and also the authors found the tissue behaves more compliant in the cross-fibre direction, which contradicts the current study and those obtained by Van Loocke et al. (2006). This might be due to different strain rate and different animals used for the study.

Bosboom et al. (2001) conducted compression tests on rat tibialis anterior muscles (TAs) in the transverse direction. Each TA was compressed between two plates using a ramp and hold function, with a ramp speed of 0.25 mms^{-1} and a hold phase of 20s. Due to the non-uniform geometry of the muscle tested and the fact that TA's specimens were tested *in vivo* resulted in contradiction with the current work.

Böl et al. (2012) also performed compression tests with a strain rate of 0.05 $\%s^{-1}$ on soleus muscles of New Zealand white rabbits with characteristic edge lengths between 3 and 6 mm. The samples were compressed up to 45%. The authors reported a similar qualitative behaviour in compression as well as considerably less stiff response in all fibre directions compared to Van Loocke et al. (2006) and the current work. There is no evidence of the animal age.

(Pietsch et al., 2014) carried out compressive tests in the fibre and cross-fibre directions on 8-10 month old porcine hind legs at strain rates of 0.1, 0.01 and 0.01 s^{-1}. The authors showed that deformation in the cross-fibre direction is significantly stiffer than the fibre direction at all strain rates, which is in agreement with the current study. However, the authors showed much stiffer behaviour compared to the current study (similar to the Song et al (2007) results). As the authors reported true (Cauchy) stress, their findings were not displayed in Figure 3.7.

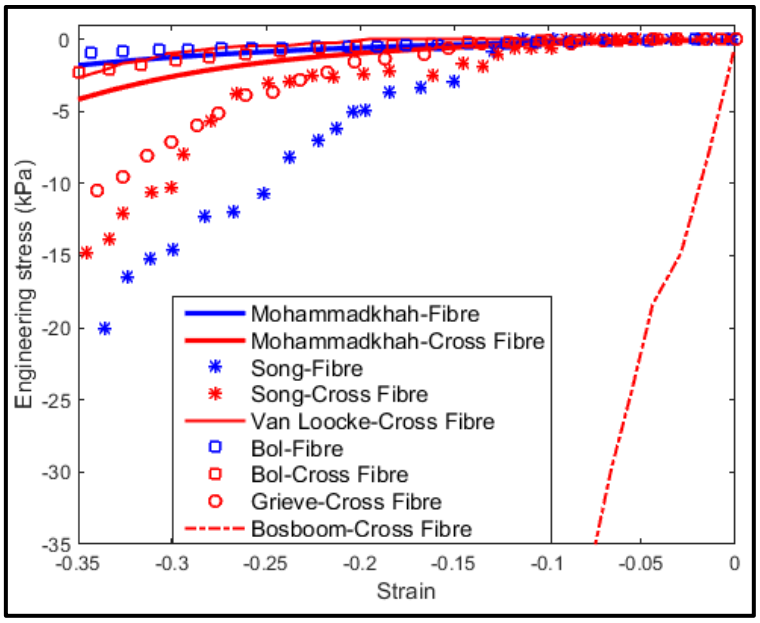

Figure 3. 7-Comparison of compressive stress – strain response for skeletal muscle from previous studies.

Tension: Figure 3.8 shows the stress-stretch response of skeletal muscle to applied tensile deformation for the current work and from published data on other species (porcine, rat and rabbit tissue).

First of all, the strain rate applied in the tests is not the same; the lower strain rates in Calvo et al. (2010) likely reduced the viscoelastic effect and the tissue exhibited more elastic behaviour (Van Loocke et al., 2008) so lower stiffness was observed. Second, a different experimental procedure was used by Morrow et al. (2010b). The stress curve of Nie et al. (2011) appears convex in shape that can be modelled using Neo-Hookean model, while in the other studies the typical concave shape for tensile stress response was observed. This could be due to different experimental methods including the sample dimensions, high preload and whether image analysis is used for the actual stretch calculation. Finally regarding the sample preparation method, the higher stiffness observed could be due to defrosting the tissue that could alter the mechanical properties of the specimen. The authors did not take into account if the thawing process affected the tissue and its stress response. Morrow et al. (2010b) also tested on whole muscle, which meant the tissue had more unimpaired fascicles that could lead to the higher stress response they reported. They also reported that the tissue exhibited higher stiffness in the fibre direction than the cross-fibre direction, but the data of Nie et al. (2011) and Takaza et al. (2013a) demonstrate the opposite. The current study has found that chicken skeletal muscle tissue is stiffer than porcine tissue in the fibre direction, and also exhibits more compliant behaviour in the cross-fibre direction compared to Takaza et al. (2013a), and similar experimental conditions were applied in both studies. One explanation is that the avian muscle performs a different

function than animal muscle. The size of the sample indicating the number of full fasicles is also important (Blackburn et al., 2014).

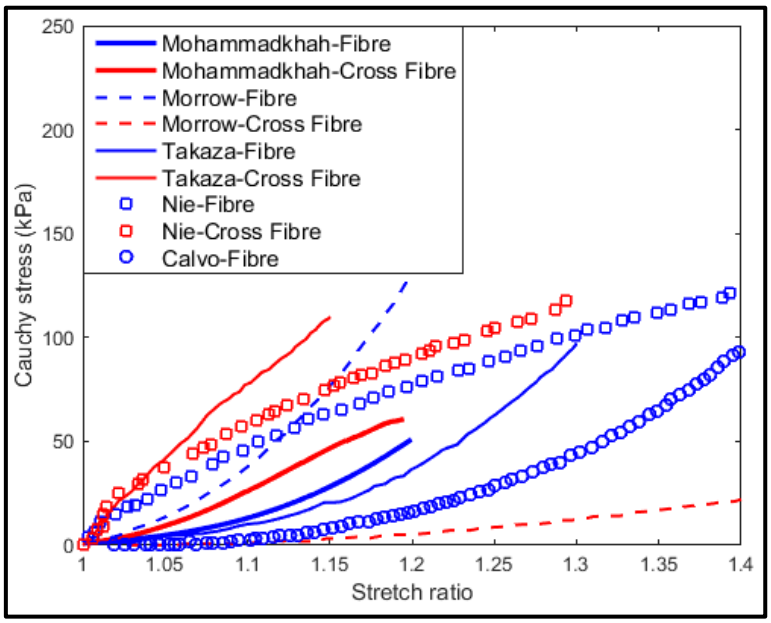

Figure 3. 8-Comparison of tensile stress – stretch response for skeletal muscle from previous studies.

3.5.2. Chicken versus Porcine comparison

3.5.2.1. Chicken versus Porcine stress-stretch comparisons

The differences within both the compressive and the tensile studies (Figures 3.7 & 3.8) are due to variation between different muscles and species with different age as well as variation in the experimental protocols, which make the interpretation difficult. However, since the current study on chicken tissue used similar protocols to the compressive and tensile tests reported by Van Loocke et al. (2006) and Takaza et al. (2013a) respectively on porcine tissue, a direct comparison of the mean responses can help assess differences in the stress-stretch responses of the different species, see Figure 3.9.

In applied compression (Figure 3.9a), deformation in the cross-fibre direction yields the stiffest response in both tissues. However, the fibre direction is the least stiff tissue in chicken while 45° is the least stiff direction in porcine tissue. The Figure also shows that chicken tissue is significantly stiffer than porcine tissue in compression. The variation in cross-fibre results is substantially larger than in any other direction, similar to the findings of Van Loocke et al. (2006).

Figure 3.9b shows that, for applied tension, the fibre direction is the least stiff response in both species, as might be expected since this is the physiological working orientation for muscle. However,

for chicken the stiffest response is the 45° direction while for the porcine tissue the stiffest is the cross-fibre direction.

The significant differences observed in stiffness of the fresh porcine and chicken tissues can be attributed to the difference in internal microstructure (Extra Cellular Matrix) between species, muscle functions and even myofibre size. The pectoralis muscle has a high collagen content (Nishimura, 2010) and collagen fibres have higher stiffness than muscle fibres (Martin et al., 1998). This might explain the generally stiffer response of chicken tissue, but it does not explain the cross-fibre tension case where the porcine tissue is much stiffer, and future microstructural assessments will be needed to investigate this further.

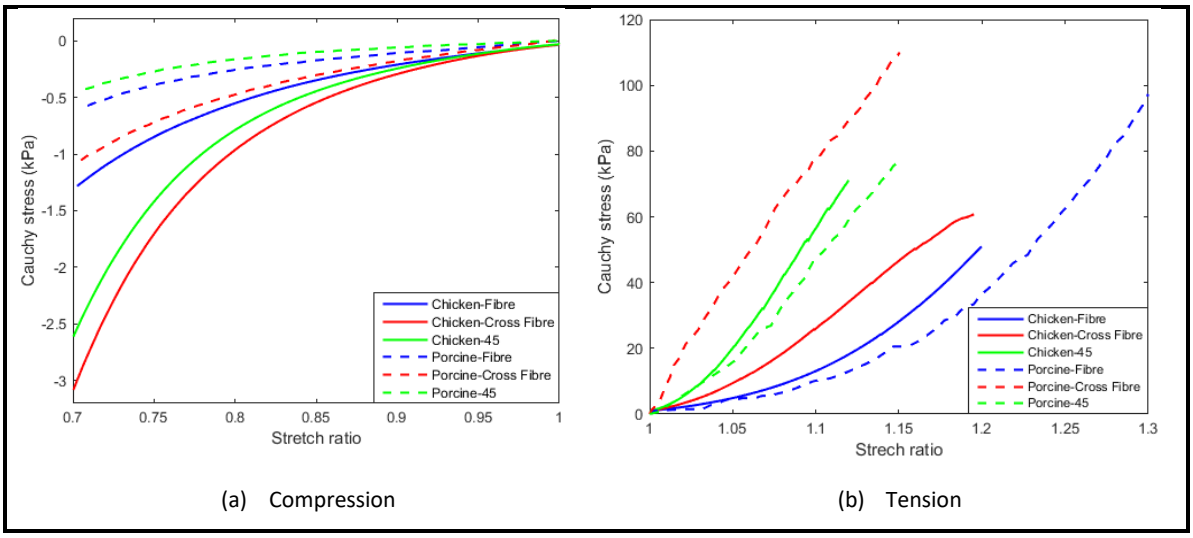

(a) Compression (b) Tension

Figure 3. 9-Comparison of passive elastic behaviour of porcine and chicken skeletal muscle in (a) compression, and (b) tension.

3.5.2.2. Chicken versus Porcine Poisson's ratio comparisons

The Poisson's ratio results for chicken and porcine tissue are compared in Table 3.4. A Poisson's ratio υ_{LT} of almost 0.5 was observed for both applied tensile and compressive deformation for both species showing both muscles behave in an approximately transversely isotropic manner in this load direction.

Chicken muscle behaves in an almost incompressible manner, which is in agreement with the findings of Takaza et al. (2013a) and Van Loocke et al. (2006) for porcine muscle. The small percentage fluid loss observed in compression (Figure 3.6) might explain why υ_{TT},+υ_{TL} is slightly less than unity for the chicken tissue in Table 3.4, but the observed fluid loss for the fibre direction compression is greatest, whereas the mean υ_{LT} is actually slightly greater than 0.5, though no statistical difference was observed.

When the tissue is deformed in the cross-fibre direction, there are two different Poisson's ratios as the induced expansion/compression is different in the fibre and other cross-fibre directions. For applied cross-fibre compression υ_{TL} = 0.34 and υ_{TL} = 0.36 were observed for chicken and porcine tissue respectively, while for applied cross-fibre tension, $\upsilon_{TL} =$ 0.83 and υ_{TL} = 0.74 were observed for chicken and porcine tissue respectively. However $\upsilon_{TT'}$ = 0.64 and $\upsilon_{TT'}$ = 0.65 were observed for compression for chicken and porcine tissue respectively, and $\upsilon_{TT'}$ = 0.17 and $\upsilon_{TT'} =$ 0.28 for tension in chicken and porcine tissue respectively. Thus the Poisson's ratio results were qualitatively similar for chicken and porcine skeletal muscle. This is surprising given the qualitative differences in the stress-stretch curves observed in Figure 3.9 and again a microstructural analysis should help providing an explanation.

For calculation of the Poisson's ratios (υ_{LT} and $\upsilon_{LT'}$), we assumed from material symmetry that υ_{LT} = $\upsilon_{LT'}$ In general, due to permanent deformation of the samples, it was not possible to retest the samples to actually measure whether υ_{LT}= $\upsilon_{LT'}$. However, for three of the nine fibre direction compression samples, permanent deformation after the first test was small and it was possible to retest the samples. The results showed very similar values for υ_{LT} and $\upsilon_{LT'}$ for these cases.

Table 3. 4-Poisson's ratio comparison between chicken and porcine tissue in compression and tensile tests.

Poisson's ratio	Compression		Tension	
	Porcine (Van Loocke et al., 2006)	Chicken Current study	Porcine (Takaza et al. (2013a)	Chicken Current study
υ_{LT}=$\upsilon_{LT'}$	0.5	0.51	0.47	0.5
$\upsilon_{TT'}$	0.65	0.64	0.28	0.17
υ_{TL}	0.36	0.34	0.74	0.83

3.5.3. Experimental aspects

Rigor mortis: To characterise the stress-stretch behaviour of fresh chicken muscle, the tests were performed in the first two hours after death of the animal to minimize the effect of rigor mortis; however the results in Figure 3.5 show that the stress response is not strongly affected within the first four hours after slaughter. *In vivo*, temperature can greatly affect the ability of muscle to contract. At cold temperatures, oxygen is more tightly bound to the haemoglobin and does not release as easily. This slower rate of release leads to a lower amount of oxygen available to muscles, making contraction

more difficult. This is observed as stiffness in muscles (Ferguson et al., 2002). Although the experiment conducted in this study was *in vitro* and performed at room temperature, the samples which were tested immediately after slaughter may show different stiffness compared to those which were tested two hours after death because they were warmer. This could be a potential reason for a large variation observed in Figure 3.5.

Sample dimensions: the sample length/width ratio is important in tensile testing to reduce the effect of clamps (see ASTM E8/E8M standard). As the chicken pectoralis muscle is not very large, it is difficult to achieve the recommended ratio of 5. However, a ratio of 4 was generally achieved, see Table 3.2. Cooney et al. (2015) recently showed in finite element analysis of tests on porcine linea alba that an aspect ratio of 4 yields quite similar results to an aspect ratio of 5 in tensile testing, so this is not likely to introduce a large error in the current data. A more precise response could be extracted using inverse finite element analysis, and Böl et al. (2012) found that this approach also substantially alters the resulting stress-stretch assessments as assumptions relating to sample geometry are not needed. However, such detail is beyond the scope of this work.

The width and thickness of samples were kept at 10 mm. It has been observed that smaller samples appear softer, probably due to the perimysium damage during sample preparation (Lewis and Purslow, 1990, Blackburn et al., 2014). However for the present data, the goal was to establish chicken skeletal muscle stress-stretch and Poisson's ratio relationships to be comparable to the Van Loocke et al and Takaza et al porcine data for compression and tension, so the samples' dimensions are consistent with the protocols in these publications.

Clamping effects: In the tensile experiments, further tightening of the clamps might have prevented sample slippage. However, this may have damaged the samples, so image analysis was instead used to calculate the stretch ratios. All stress–stretch results for tension are therefore presented with the image-based stretch measurement.

Strain rate: Strain rate is a challenge when performing quasi-static testing. It has been previously shown how rate dependent effects (viscoelastic components) play a significant role, even at very low strain rates (0.5 $\%s^{-1}$) (Van Loocke et al., 2008). The challenge for these kinds of tests is that there is a time limit to testing due to rigor mortis effects, and thus a compromise has to be made to allow a sufficient number of samples to be tested prior to rigor mortis onset while at the same time minimising viscoelastic effects. A strain rate of 0.05 $\%s^{-1}$ was adopted as a reasonable and optimal compromise between measurement of purely elastic properties (minimizing viscoelastic effects) and time elapsed between testing and death of the animal, to avoid rigor mortis effects (Van Loocke et al., 2006, Van Loocke et al., 2008). Although for the purpose of this Chapter, testing of *in vitro* tissue samples remains preferable and this strain rate is not meant to be representative of *in vivo* tests, the order of magnitude

of the *in vitro* strains to those of *in vivo* published in the literature was observed to be quite similar (Fiorentino et al., 2012, Yaman et al., 2013).

In vitro versus in vivo: It is acknowledged that *in vivo* muscle strain is an important topic as it provides information about the tissue behaviour inside the body with body temperature. Some previous works on *in vivo* muscle strain measurement have shown that interactions between muscles affect strains within a muscle (Huijing et al., 2011, Pamuk and Yucesoy, 2015, Yaman et al., 2013, Yucesoy et al., 2003). Their major results were that local strains are much higher than global strains, and also these local strains are not only limited to the specific muscle exposed to deformation, but also happen within synergistic muscles kept at constant muscle length, so that global strains do not estimate *in vivo* local strains within the muscle. However, the amplitude of the local *in vivo* strains (Fiorentino et al., 2012, Huijing et al., 2011) were of similar magnitude as the global strains applied in the current study performed at room temperature. Stress calculation and its relation to strain are absent in these *in vivo* studies.

Harvesting samples from the muscle bulk causes structural disruption in the tissue. However, due to the current limitations in non-invasive methods for *in vivo* stress and strain measurements and having better controls over experimental parameters, most studies with repeatable findings were performed *in vitro* (Van Loocke et al., 2008, Van Loocke et al., 2009, Grieve and Armstrong, 1988, Bosboom et al., 2001, Song et al., 2007, Böl et al., 2012).

In the work of Moerman et al. (2012) it was attempted to determine *in vivo* muscle strains using tagged magnetic resonance imaging. Nonetheless, the practical challenges associated with this approach (often inverse finite element optimisation or alternative approaches are required, there are challenges with global versus local strains, sample sizes tend to be rather small and the number of optimisation parameters is generally high) mean that the controlled environment possible in uniaxial mechanical testing of *in vitro* tissue samples remains preferable for the objectives of this Chapter.

To track *in vitro* muscle volume change, the samples were weighed before and after testing. Since there is a high fluid content in muscle and it is possible for fluid to be displaced from a given tissue sample, the volume could change slightly as shown in Figure 3.6 (the changes are small). This could also occur *in vivo*, and Yaman et al. (2013) observed that the *in vivo* deformation caused a drop in tissue volume, possibly due to blood expulsion from the veins resulting from muscle contraction (Valic et al., 2005, Wisnes and Kirkebo, 1976).

Active properties of muscle: Some purely passive models of skeletal muscle (Van Loocke et al., 2009, Palevski et al., 2006) successfully address some aspects of the passive behaviour. Active muscle models presented in the literature from those based on Hill-type model (Siebert et al., 2014, Best, 1994, Cole et al., 1996) to three-dimensional continuum-based muscle models (Blemker and Delp,

2005, Blemker et al., 2005, Sharafi and Blemker, 2010, Sharafi and Blemker, 2011, Rehorn and Blemker, 2010, Yucesoy et al., 2002) capture the general nonlinear viscoelastic response and force transmission in muscle tissue. However, asymmetric stress-strain response in compression/tension is not adequately addressed. Moreover, both strain rate and fibre orientation dependency of elastic and viscoelastic response of muscle (Takaza et al., 2013a, Van Loocke et al., 2006, Van Loocke et al., 2008) needs to be included in these active muscle models.

In future, one important research area in muscle modelling is the appropriate combination of passive and active muscle behaviour to enhance 3D models, where the results of the current study will be helpful.

3.6. Conclusions

The passive elastic stress-stretch and Poisson's ratio properties of chicken muscle tissue have been presented for the first time. Results show that chicken muscle elastic behaviour is nonlinear and anisotropic. The tensile stress-stretch response is two orders of magnitude larger than compression in all directions, which reflects the compression/tension asymmetry previously observed in porcine tissue. In compression the tissue is stiffest in the cross-fibre direction. However, tensile deformation applied at 45° gives the stiffest response, and this is different to previous findings relating to porcine tissue. Chicken muscle tissue is most compliant in the fibre direction for both tensile and compressive applied deformation. Generally, a small percentage of fluid exudation was observed in the compressive samples. The Poisson's ratio results show isotropic behaviour for compression or tension applied in the fibre direction, but clear anisotropy for compression or tension applied in the cross-fibre direction, so skeletal muscle is transversely isotropic as the Poisson's ratio values are symmetric about the axis of muscle fibre. The macroscopic stress-stretch differences now observable between chicken and porcine tissue should be followed by microstructural analysis of the two species to help assess the observed tension/compression asymmetry.

Chapter 4-Visualisation of collagen in fixed skeletal muscle tissue using fluorescently tagged collagen binding protein CNA35

No matter what people tell you, words and ideas can change the world.

ROBIN WILLIAMS, 1951 – 2014.

4.1. Introduction

Collagen is the main structural protein in connective tissues in animals and while collagen types I, III, IV, V, VI, XII and XIV occur in skeletal muscle extra cellular matrix (ECM) (Listrat et al., 1999, Nishimura et al., 1998), collagen types I and III are the major components (Bailey and Light, 1989, Light et al., 1985). Collagen is primarily responsible for the passive load-bearing properties of tissues, for example collagen fibre reorientation in muscle ECM in response to external loading has been observed by several authors (Billiar and Sacks, 2000, Purslow, 2010, Purslow and Trotter, 1994, Purslow, 1989). Thus detection and visualisation of collagen structure are important to understand the relationship between mechanical behaviour and microstructure in skeletal muscle, which researchers have addressed principally through microscopy and mechanical modelling (Purslow, 2010, Purslow, 2002,

Purslow and Trotter, 1994, Takaza et al., 2014, Krahn et al., 2006, Nishimura, 2010, Sharafi and Blemker, 2010).

The overall structure of collagen-rich tissues can be visualised by commonly used histological stains such as Hematoxylin and Eosin (H&E) (e.g. Pietsch et al. (2014)) or various forms of trichrome or von Gieson. Picrosirius red staining has been frequently used as it can differentiate collagen (red) from muscle (yellow) and it can be coupled with polarized light birefringence to distinguish different collagen compositions (Junqueira et al., 1979, Rich and Whittaker, 2005, Vidal et al., 1982, Takaza et al., 2014), but histological stains do not allow visualisation of collagen fibril structure. Other visualisation methods based on intrinsic collagen properties such as autofluoresence (Voytik-Harbin et al., 2001) or second harmonic generation (Cox et al., 2003) also suffer from low intensity signal and limited contrast, resolution and specificity since other tissues can also produce signal. Methods based on specific collagen binding, especially coupled with strong fluorescent probe detection, allow higher resolution analysis of collagen fibril organisation, for example using confocal microscopy.

Detection of collagen by specific binding can be achieved using antibodies raised against individual collagen types but with the existence of multiple collagen types, this requires a panel of different antibodies to analyse complex tissue types such as skeletal muscle. Alternatively an adapted form of a natural collagen recognition protein called CNA35 can be used; the original binding protein is produced on the cell surface of the bacterium Staphylococcus aureus, isolated from patients with bacterial arthritis (Patti et al., 1994, Xu et al., 2004). Two soluble domains of the protein recognize the collagen triple helix (Patti et al., 1994, Zong et al., 2005, Rich et al., 1999) and have been developed as a collagen detection tool, first rendered fluorescent by labelling with Oregon Green 488 (CNA35-OG488) (Krahn et al., 2006). The fluorescent CNA35 “probe” has advantages over other methods for collagen detection including its ability to act as a highly specific, pan-collagen probe for skeletal muscle: Krahn et al. (2006) showed specific binding to a variety of fibril forming collagens including I, III and IV with very little cross reactivity with non-collagenous extracellular matrix proteins. Thus, CNA35 has the advantage of being a pan detector for all collagens with one tool, it does not require expensive antibodies specific for each collagen type and avoids the need for 2nd fluorescently labeled antibodies. It also allows for using confocal microscopy to visualise collagen fibrils at high resolution. This makes CNA35 particularly valuable in examining fibril organisation. CNA35-OG488 has been used in a number of applications (reviewed in Aper et al. (2014)) including examining the effect of mechanical and biochemical cues on extracellular matrix organisation *in vivo* and in tissue engineering constructs (e.g. (de Jonge et al., 2013, Foolen et al., 2008)). Moreover, fluorescently labelled CNA35 can be used to visualise the collagen from very small fibrils to mature collagen fibres (Boerboom et al., 2007, Krahn et al., 2006, Aper et al., 2014).

The CNA35 probe offers a number of other advantages over antibody detection of collagen. Collagen has a high density of CNA35 binding sites, so sensitivity is high. Fluorescent antibodies are costly, require a two-step process and have a limited penetration capability in dense tissues, and their high affinity binding to collagen may affect tissue function in live tissues (Kumar and Rudbeck, 2009, Krahn et al., 2006). CNA35 is five times smaller than antibodies facilitating tissue penetration and can be used on live tissue, however neither of these characteristics are advantageous for this particular study since fixed and sliced samples were examined. CNA35 does not affect collagen properties and, when directly fluorescently labelled, it can bind and be detected in one step (Krahn et al., 2006, Aper et al., 2014, Boerboom et al., 2007, Foolen et al., 2008). For applications where the overall collagen organisation is of interest, the broad specificity to multiple fibril forming collagens is an advantage (Krahn et al., 2006). To further expand the usefulness and accessibility of CNA35 collagen probes, Aper et al. (2014) described the production of an array of further genetically engineered versions fused to six commonly used fluorescent proteins including EGFP (Enhanced Green Fluorescent Protein), tdTomato and mCherry. Because the fluorescent tag is genetically encoded and fused to the probe, it can be easily produced in high amounts through expression in *Eschericia coli* bacteria, purified using an added His tag, and can be widely shared with the research community as DNA constructs. These fluorescent fusions of CNA35 promise to be powerful tools for collagen detection in a wide variety of applications, particularly for studying the biomechanics of collagen rich tissues and bioengineering of constructs.

Aper et al. (2014) demonstrated the use of fluorescently fused CNA35 probes to visualise collagen in live tissues, using two-photon confocal imaging of human skin and engineered cardiac cells. While CNA35 shows clear advantages for use on live or unfixed tissues, some experimental situations necessitate the use of fixed tissue. For example, current visualisation methods do not permit observation of collagen reorientation in muscle ECM under externally applied deformation without tissue fixation to “hold” the deformation effect and due to limited stain/probe penetration in mature muscle tissue which therefore may require fixation and sectioning (Takaza et al., 2014). Since collagen detection by CNA35 has never been reported on fixed tissue, here specific binding following Paraformaldyhyde (PFA) treatment, which is commonly used is investigated (e.g. Briguet et al. (2004), Iwasaki et al. (2013)). This Chapter also establishes a working protocol (examining section type, determining dilution factor, exposure time etc.) for collagen detection and visualisation in fixed skeletal muscle tissue using CNA35-EGFP and CNA35-tdTomato. Confocal microscopy is then used to assess the ability to visualise collagen organisation. This approach will be valuable in future studies examining the relationship between collagen conformation and biomechanics. In particular it can be applied to study the relationship between skeletal muscle micro-structure and observed mechanical

response to applied deformation and hence constitutive modelling, tissue engineering and assessment of muscle tissue pathologies.

4.2. Methods

4.2.1. Sample preparation

Porcine and chicken skeletal muscles from 3-month old females were used. The chicken samples were harvested from pectoralis muscle of Ross 508 chickens (Annyalla Chicks Ltd. Co Kildare, Ireland) and the porcine samples were excised from the biceps femoris of an outbred pig (Perma Pigs Ltd. Co Louth, Ireland; cross between PIC line 337 and mixed breed female; 50% Large White, 25% Duroc, 25% Land Race) by trained personnel using ethically approved protocols.

4.2.2. Wax embedding of tissue sample

Immediately post mortem, cubic blocks of muscle tissue with a nominal size of 10x10x10 mm were immersed in 4% paraformaldehyde (PFA) in PBS for 48 hours as preliminary tests showed 24 hours led to incomplete fixation at the core of the block. The samples were then washed in phosphate buffer saline (PBS) for 24 hours and a further two brief washes to remove PFA. The fixed tissues were cut into 0.5 mm cubes to ensure complete dehydration and a more manageable size for sectioning (initial fixation of a larger sized block was carried out to accommodate future experiments where muscle deformation will be applied). The samples were dehydrated using the following graded alcohol series; 70% in H_2O, 90%, 100% and then immersed in Histoclear™, which clears and prepares the tissue for wax penetration in subsequent exchanges in molten paraffin at 60 °C (step details given in Table 4.1). The tissues were then placed in plastic moulds filled with molten wax and allowed to harden on a cold plate. The paraffin wax blocks were mounted on a Leica RM2255 automated microtome and 8, 15, and 20µm thick sections were cut. The sections were then floated out on a 50 °C water bath and mounted on superfrost microscope slides. They were baked for 10 mins at 60 °C and left overnight to increase adherence of sections. Prior to exposure to CNA35 probes, wax-embedded sections were dewaxed as described in Table 4.2.

Table 4. 1-The steps and timing for dehydration and clearing of muscle samples for wax embedding.

Solution	Time	Temperature
70% EtOH	1 hour	room temp
90% EtOH	1 hour	room temp
100% EtOH	1 hour	room temp
100% EtOH	1.5 hours	room temp
100% EtOH	1.5 hours	room temp
100% EtOH	2 hours	room temp
50% Histoclear™:50% EtOH	10-30 min	room temp
Histoclear™	1 hour	room temp
Histoclear™	1 hour	room temp
Histoclear™ / wax mush (1:1)	1 hour	In oven @ 60 °C
Pure fresh wax(1)	1 hour	In oven @ 60 °C
Pure fresh wax(2)	2 hours	In oven @ 60 °C

Table 4. 2- The steps and timing for dewaxing sections.

Solution	Time(min)
Dewax in Histoclear	10
Absolute alcohol	2
Absolute alcohol	2
90% alcohol	2
70%alcohol	2
50% alcohol in PBS	2
Wash in PBS (twice)	5 each

4.2.3. Cryopreservation and preparation of frozen tissue sections

Following the PFA fixation step (Section 4.2.2), the samples were equilibrated in 30% Sucrose (cryoprotectant) in PBS (24 hours) or until they sank. The blocks of tissue were then frozen on an ethanol/dry ice bath. The samples were mounted on a chuck in Optimal Cutting Temperature compound (OCT) within a Leica CM1850 cryostat, where 8 µm sections were cut, mounted on superfrost plus slides (Thermo Scientific), and stored at -80 °C.

Mouse embryos at embryonic day (E) 14.5 were fixed overnight in 4% PFA in PBS, washed in PBS and then equilibrated as above in 30% sucrose, mounted in OCT and sectioned.

Prior to CNA35-GFP probe exposure, frozen sections were removed from the freezer and left to thaw at room temperature for at least 30 mins.

4.2.4. Purification of collagen binding protein

Plasmid DNA encoding Enhanced Green Fluorescent Protein (EGFP) or tdTomato fused to CNA35 (CNA35-EGFP or CNA35-tdTomato) was provided by the laboratory of Maarten Merkx (Aper et al., 2014) and was transformed into E.coli BL21 (DE3) competent bacteria (Novagen), following manufacturer's instructions (see Appendices B and C for more detailed protocols). Single colonies were isolated from agar plates and used to inoculate 8ml Luria-Bertani (LB) medium supplemented with 30μg/ml kanamycin. The bacteria were grown overnight at 37 °C in an orbital incubator with aeration (200 rpm), then used to re-innoculate 200 ml of fresh medium and subsequent growth monitored every 15 mins until an optical density (OD) at 600nm wavelength of 0.6 was reached (approximately 2.5 hours). Expression of the plasmid encoded fusion proteins was then induced by adding 0.5mM isopropyl β-D-1-thiogalactopyranoside (IPTG, Sigma-Aldrich), during 20 hours of further growth (37 °C and 200 rpm). Bacteria were harvested by centrifugation for 10 min at 10,000 g. The pellets were re-suspended in 4 mL Bugbuster™ (Novagen) and incubated for 40 min at room temperature to lyse the cells. Next, the Bugbuster suspension was centrifuged for 20 min at 16,000 g. The resulting supernatant containing the protein fraction was purified via a Ni^{2+} affinity chromatography column (GE Healthcare) according to manufacturer's instructions, to which the fusion protein will bind due to an engineered His tag. This yielded, for example, 3.2 mg of CNA35-tdTomato and 5.7 mg of CNA35-EGFP from 200ml cultures (for more details, see Appendices B and C). The Thermo Scientific™ Pierce™ BCA Protein Assay was used for spectrophotometric protein quantification. This method combines the well-known reduction of Cu^{+2} to Cu^{+1} by protein in an alkaline medium (the biuret reaction) with the highly sensitive and selective colorimetric detection of the cuprous cation (Cu^{+1}) using a unique reagent containing bicinchoninic acid. The purple-coloured reaction product of this assay is formed by the chelation of two molecules of BCA with one cuprous ion. This water-soluble complex exhibits a strong absorbance at 562nm that is nearly linear with increasing protein concentrations over a broad working range (20-2000 μg/mL).

4.2.5. Antigen retrieval treatment

Antigen retrieval is frequently used for antibody detection of proteins in fixed tissues, particularly using formalin-based fixatives such as PFA which cross-link proteins and can mask the target protein epitope(s) from specific binding. I investigated if this would also improve CNA35-EGFP binding to PFA fixed tissues. Antigen retrieval was performed by immersing slides (tissue sections) in 0.01M sodium

citrate (1.17g sodium citrate in 400ml distilled water, pH adjusted to 8 by adding approximately 1.5mL 1MHCl) in a heated water bath as follows:

Sodium citrate buffer was placed in a plastic slide container and boiled in a microwave.
The slides were placed in the container with boiling buffer and then incubated for 3 or 20 mins in a 90 °C water bath to determine the optimal incubation time.
The slides were then cooled down to room temperature and rinsed twice in PBS for 5 mins.

4.2.6. Blocking of non-specific binding and incubation with binding protein

The following steps were conducted at room temperature in a humid chamber containing moist tissue; especially important when incubating overnight.
Detection of specific protein binding is enhanced by blocking any non-specific, off-target protein-protein adhesion. In this study the effect of blocking with 1% Bovine Serum Albumin (BSA) in PBS, and a combination of 1% BSA plus 10% goat serum using PBST as a base solution (0.1% Triton X100 in PBS) was examined. Sections were washed twice briefly in blocking solution, then each slide was covered with approximately 200 µl of blocking solution and incubated for an hour. The slides were then incubated in approximately 200 µl of CNA35-EGFP (2.4-2.8 mg/ml) or CNA35-tdTomato (1.6 mg/ml) at dilutions of 1:20, 1:50, 1:100, 1:200, and 1:500 in blocking solution for 1 hour or overnight. The slides were finally washed in PBS three times; twice for 5 mins, and the last wash for half an hour.

Negative controls were included in all experiments where sections were processed in the same manner in all other respects but without binding protein.

Aliquots of CNA35-EGFP protein stored at -80◦C for more than 2 years have been used with no obvious loss of binding or fluorescence over time.

4.2.7. Fluorescence visualisation

Slides were left to dry in the dark for 24 hours prior to assessment under a fluorescence microscope (Olympus BX 40) with appropriate filters (tdTomato: excitation wavelength: 554 nm, emission wavelength: 581 nm; EGFP: excitation wavelength: 488 nm, emission wavelength: 507 nm) using 20X and 40X magnification objectives, photographed using an Olympus DP72 camera and processed using CellSens Standard version 1.6 software using exposure times of 90 to 700 ms. Confocal microscopy was carried out on a Leica SP8 scanning confocal using 40X magnification objective and the same spectral properties of the fluorescent proteins outlined above. The confocal stack was then processed using Imaris version 7.6 software.

For contemporaneous visualisation of muscle fibres and cell nuclei, samples were co-incubated with tagged binding protein (as above) and a monoclonal antibody specific for myosin (MF20, Developmental Hybridoma Bank, 50µg/ml IgG), at 1:20 dilution. Following incubation in primary antibody, a 15 min wash in PBS was carried out. The sections were then incubated with secondary antibody (goat anti-mouse IgG, conjugated with Alexa Fluor 568 or Alexa Fluor 488 (Invitrogen) at dilution of 1:200 in fresh blocking solution for 60 mins, followed by two 15 min washes in PBS at room temperature.

Slides were then mounted under glass coverslips with Mowiol (10% Mowiol® 4-88 in 0.2 M Tris HCl (ph 8.5) with 2.5% DABCO (1,4-diazabicyclo-[2.2.2]-octane) or ProLongR Gold Anti-Fade Reagent containing DAPI counterstain (Life technologies).

4.3. Results

As a positive control, the ability of recombinant fluorescent binding protein to specifically detect collagen in fixed tissue was first assessed by examining known collagen rich sites in developing embryonic tissue (Figure 4.1 a-c). This showed highly specific detection in the forming cartilaginous skeletal rudiments of the limb (Figure 4.1a) and the vertebrae (Figure 4.1c) and in the epithelia of the forming kidney glomeruli (Figure 4.1b).

It is more challenging to detect collagen and visualise collagen organisation within the perimysium and epimysium of mature skeletal muscle. In order to investigate tissue organisation, it would be beneficial to visualise fluorescently labelled collagen in intact muscle samples, which could then be imaged and reconstructed in 3-dimensions (3D) using Optical Projection Tomography (Summerhurst et al., 2008). However, this would require good penetration of the binding protein into intact muscle samples. To test this, a 5×10×10 mm block of chicken tissue was incubated in 1:20 dilution of CNA35-GFP for 30 mins prior to fixing (only a limited time was possible prior to fixing). The block was then fixed and processed precisely as described (Sections 4.2.1 to 4.2.3). Detection under these conditions was compared to exposure of the binding protein to thin sections (8µm) of previously fixed tissue, mounted on microscopic slides. Figure 4.1d shows that the CNA35-EGFP binding protein does not penetrate intact mature muscle as only collagen at the surface of the tissue block was bound (arrow), whereas the collagen fibres around each individual muscle fibre (endomysium) and around each fascicle (perimysium) are fluorescently labelled when a thin section is prepared prior to exposure (Figure 4.1e).

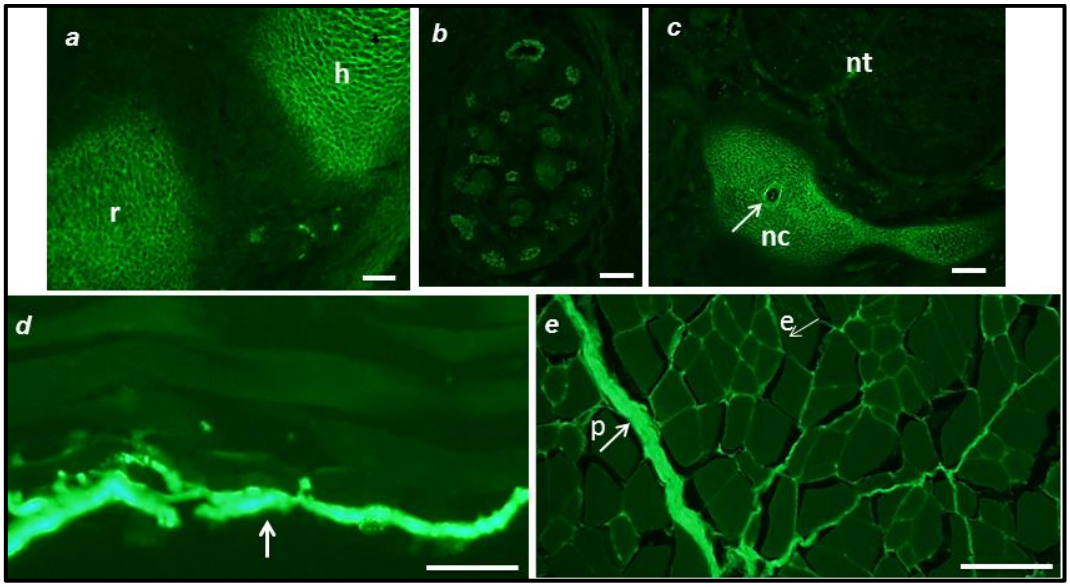

Figure 4. 1-The effect of tissue preparation on collagen detection using CNA35-EGFP

Top row: <u>Positive control;</u> PFA fixed mouse embryo (E14.5) cryo-sections through (a) sites of collagen accumulation in adjacent skeletal rudiments of the developing limb (abbreviations: h, humerus; r, radius) (b) collagen rich epithelia of the forming glomeruli in the developing kidney, and (c) the cartilage of the forming vertebral column (abbreviations: nt, neural tube; nc, notochord). Section thickness: 8 µm.

Bottom row: <u>The ability of CNA35-EGFP to detect collagen in whole muscle tissue samples or thin sections</u>; (d) whole muscle block (5x10x10 mm) exposed to binding protein, followed by fixation and sectioning (longitudinal); note that fluorescence is restricted to the surface of the tissue (arrow) (e) an 8 µm section incubated in binding protein following fixation and sectioning (transverse) (abbreviations: p, perimysium; e, endomysium).- Exposure time: 500 ms. section thickness: 15 µm. 1:20 dilution of binding protein for 24 hours incubation. (Image e: porcine biceps femoris, and d:chicken pectoralis). Scale bars indicate 100 µm (d&e) and 50 µm (a-c).

In order to enhance collagen detection, we assessed the effect of blocking non-specific binding of the collagen probe to improve the signal to noise ratio. Comparing Figure 4.2a, without blocking, with Figure 4.2b using 1% BSA, shows that clearer specific staining is obtained when non-specific binding is blocked. No extra benefit was found by blocking additionally with 10% serum (not shown).

To investigate if the extensive processing involved in paraffin wax embedding might reduce CNA35-EGFP collagen binding, wax sections were compared to frozen sections (Figure 4.1, bottom row). While collagen was detected on both section types (compare Figure 4.1d and 1e), staining was stronger on wax embedded sections. A negative control is shown in Figure 4.1c (no binding protein added) which shows auto-fluorescence from the tissue under the visualisation parameters used; the localised autofluoresence at the periphery of some muscle fibres is in the typical position of nuclei, which indeed stain positive with DAPI (not shown).

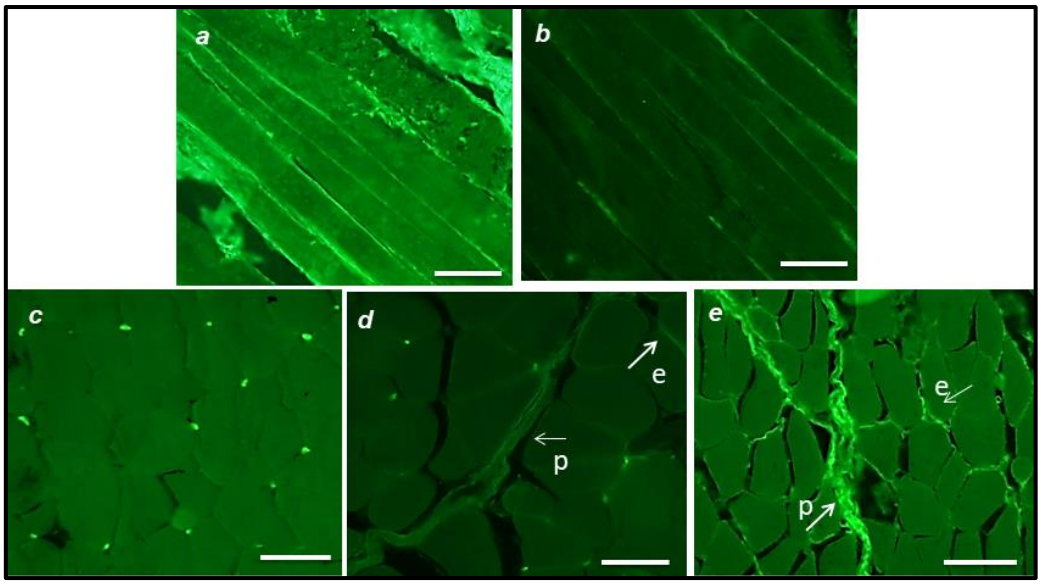

Figure 4. 2- The effect of blocking agent and preservation type on collagen detection using CNA35-EGFP.

Top row: <u>The effect of blocking non-specific binding of CNA35</u>; longitudinal sections, (a) without blocking, (b) blocked with 1% BSA. Exposure time: 90 ms. section thickness: 8 µm.

Bottom row: <u>The effect of preservation type on collagen detection</u>; (c) negative control (note autofluoresence in the typical position of nuclei (DAPI positive) (d) cryosection (e) wax-embedded section. (abbreviations: p, perimysium; e, endomysium) Exposure time: 200 ms. section thickness: 8 µm.

1:20 dilution of binding protein for one hour incubation. (Images a-e: chicken pectoralis). Scale bars indicate 50 µm.

For better detection and visualisation of collagen in fixed muscle tissue, a suitable combination of binding protein exposure variables is also required: Duration of incubation in binding protein and binding protein dilution were tested. Series of adjacent sections from the same chicken pectoralis muscle wax-embedded samples were selected, dewaxed, and blocked with 1% BSA, then incubated in either CNA35-EGFP or CNA35-tdTomato at a series of dilutions (section 4.2.6) for 1 hour or 24 hours. Purification of the binding proteins (as described in the Methods) yielded concentrations for CNA35-EGFP of 2.4 and 2.8 mg/ml and for CNA35tdTomato of 1.6 mg/ml. The negative control (Figure 4.3a) again showed only auto-fluorescence from nuclei. Both recombinant binding proteins showed specific detection at 1:20 and 1:100 dilutions (Figure 4.3 (top and middle rows) but not when more dilute. CNA35-tdTomato showed somewhat higher sensitivity where 1:100 dilution, even with only 1 hour incubation, showed reasonable detection (Figure 4.3g) at an exposure level where CNA35-EGFP shows little specific signal (Figure 4.3c). However, when the time of incubation was increased to 24 hours even 1:100 dilution of both binding proteins worked well. 1:100 and 1:20 dilutions of CNA35-tdTomato for 24 hours (Figure 4.3h & 3i) showed comparable detection levels, whereas a dilution 1:20 provided better visualisation with CNA35-EGFP (Figure 4.3d & 3e), even at the longer incubation time.

Figure 4.3d, 3e, 3h &3i together demonstrate that on the whole the longer incubation time of 24 hours is better, especially when the higher dilution was used, as the collagenous sheaths are very clearly visible around each muscle fibre (endomysium) and group of muscle fibres (perimysium).

The effect of antigen retrieval on collagen detection by recombinant protein in PFA fixed mature muscle tissue is shown in Figure 4.3j-l. Antigen retrieval through treatment with Sodium Citrate showed enormous improvement in sensitivity of detection, increasing further with prolonged heat treatment. To establish optimal conditions for binding protein detection, three sets of sections from the same chicken pectoralis muscle sample blocks were dewaxed and rehydrated as described earlier, prior to antigen retrieval treatment. The sections were immersed in Sodium Citrate buffer which had just been at boiling temperature and either left to cool (mild treatment-Figure 4.3j) or maintained at 90 °C for 3 or 20 mis respectively (Figure 4.3k and 3l). It is clear that extending the period of time at 90 °C increased sensitivity (note the exposure times of the images in Figure 4.3i-l vary from 400 to 50 ms). Although 20 min heat treatment shows higher sensitivity this is a harsh treatment and since the 3 min treatment shows excellent detection at only 200 ms exposure, this treatment regime was preferred.

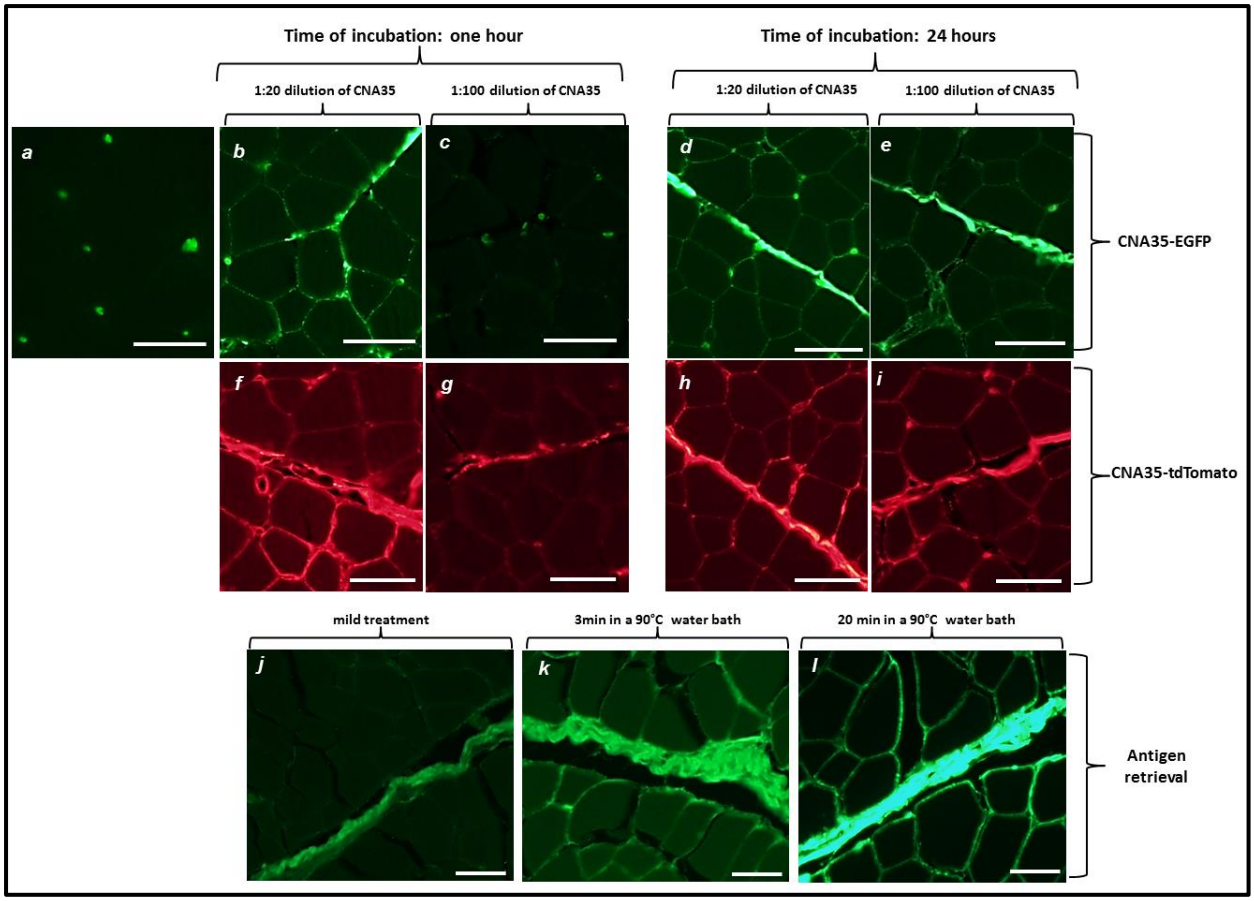

Figure 4. 3-Binding protein exposure variables on collagen detection

Top and middle row: <u>The effect of binding protein dilution factor and incubation time</u>; chicken pectoralis muscle sections blocked in 1% BSA incubated with binding protein as indicated; (a) negative control (b- e) in CNA35-EGFP at 1:20 dilution (b,d) or 1:100 dilution (c,e) for 1 hour (b,c) or 24 hours (d,e). (f- i) in CNA35-tdTomato at 1:20 (f,h) or 1:100 (g, i) for 1 hour (f, g) or 24 hours (h, i). Exposure time for all: 150 ms.

Bottom row: <u>The effect of antigen retrieval</u>; chicken pectoralis muscle sections blocked in 1% BSA and incubated with 1:20 diluted binding protein for 24 hours (j) mild treatment in boiling Sodium Citrate buffer without prolonged heating, time extended for (k) 3 mins (l) 20 mins. Exposure time: (j) 400 ms, (k) 200 ms, and (l) 50 ms. Scale bars indicate 50 µm. Section thickness: 15 µm in all cases.

Figure 4.4a shows use of the current developed protocol to detect collagen (CNA35-tdTomato; red) together with myosin (anti-myosin antibody; green) in chicken pectoralis muscle sections. Strong auto-fluoresence renders nuclei visible (yellow) at the periphery of some muscle fibres. Figure 4.4b illustrates the use of confocal microscopy to visualise collagen fibril organisation in the perimysium.

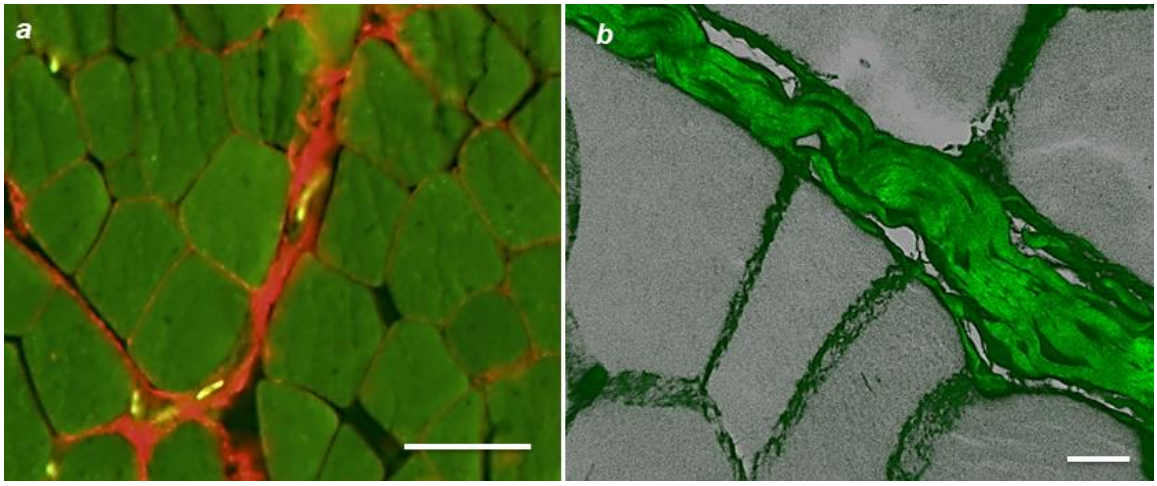

Figure 4. 4-Application of fluorescent binding protein detection of collagen to a) carry out double staining of Collagen (CNA35-tdTomato (red)) and muscle by immunodetection of myosin (green) (nuclei are visible through autofluoresence in yellow) and b) use high resolution confocal microscopy to visualize collagen fibril organisation (3D image made by Imaris software from a confocal stack). (a&b) chicken pectoralis muscle. Scale bars indicate (a) 50 µm, (b) 10 µm. Section thickness: 15 µm.

4.4. Discussion

To investigate the mechanical response of passive skeletal muscle to deformation, microscopic analysis is generally required to observe conformational/structural changes in the tissues. The first step is to detect collagen fibres within the muscle that are known as important components in load bearing (Takaza et al., 2014, Purslow, 2010). Although, the use of CNA35 to detect collagen has previously been reported in cells and live tissues (Krahn et al., 2006), the current study adapts CNA35 for detection of collagen fibres in fixed tissue for the first time. Here a method that can be used to detect collagen in a variety of fixed tissues is presented, which would be useful for many bioengineering questions such as structure-functions studies, constitutive modelling, tissue engineering and assessment of muscle tissue pathologies. Indeed detection of collagen is reported specifically and sensitively in cartilage and epithelia (kidney) as well as skeletal muscle (Figure 4.1) and we can confirm visualisation of collagen organisation also in other epithelia including vasculature (not shown). Detection in mature skeletal muscle presents particular challenges since the collagen rich perimysium and endomysium are fine and very localised within dense muscle fibres, however, it was shown that this approach can provide some of the detail and resolution required to investigate collagen fibril organisation within the perimysium.

Given that the detection of collagen and visualisation of perimysium and endomysium structure is challenging in mature skeletal muscle, a series of sensitivity studies were carried out to determine

suitable conditions and parameters for sensitive and specific detection using the CNA35-EGFP/tdTomato binding protein, and the preferred conditions are summarised in Figure 4.5.

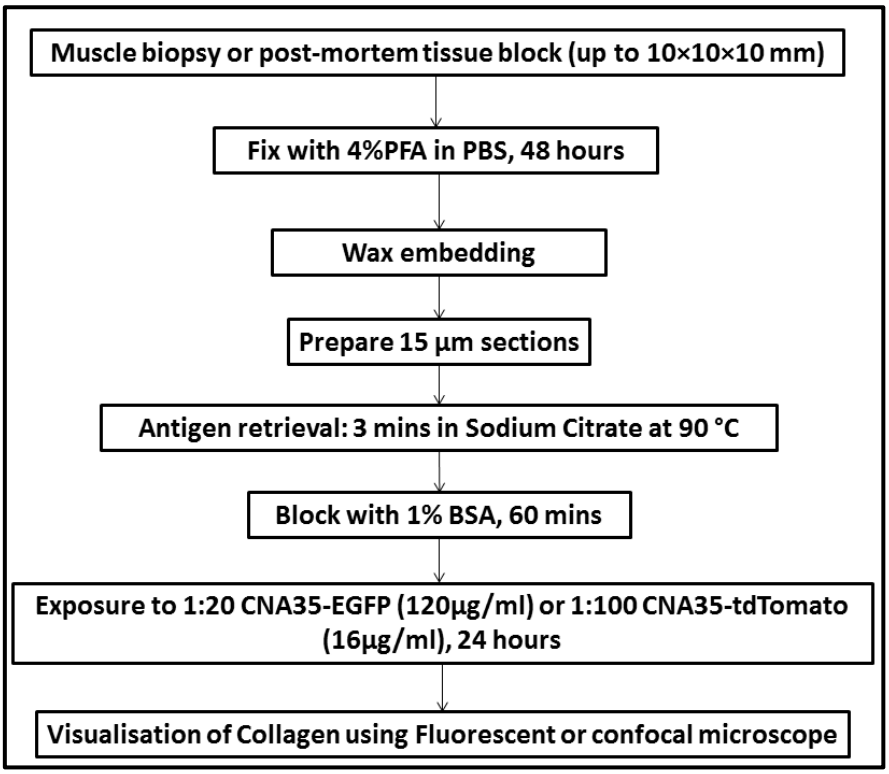

Figure 4. 5-The flowchart shows a summary of preferred conditions to detect collagen fibres in skeletal muscle following sensitivity studies.

The penetration of recombinant CNA35 into a block of skeletal muscle tissue was tested because detection within an intact piece of tissue, which potentially could then be imaged in 3D, would be ideal for examining structure, especially under various forms of physical deformation. However, it was shown that the recombinant protein binds only to the superficial face of the tissue. It is possible that penetration into the block of tissue could be improved by increasing the incubation time; however the superficial nature of the binding indicates resistance to penetration under these conditions (Figure 4.1d), and a means of permeabilising the tissue without loss of structural components would be required. Some potent permeabilising agents have recently been developed for 3D imaging (Susaki and Ueda, 2016, Chung et al., 2013), however, these may alter collagen structure and this would need to be explored. This finding emphasises the structural complexity of mature muscle tissue and the resulting requirement to cut tissue sections for collagen detection.

Frozen tissue sections can be processed in a shorter amount of time than wax-embedded sections. However, freezing is not adequate for long-term preservation of the tissues. Frozen sections can be stored at -80 °C for up to 1 year whereas wax embedding offers the best option for long-term tissue preservation. On the other hand, in many cases, frozen sections can allow better accessibility of

proteins for binding recognition (e.g. presentation of recognizable epitopes for antigen binding by antibodies) than wax sections. Unfixed tissue can also be sectioned following freezing, presenting proteins in their more 'native' form (Renshaw, 2013, Ralton and Murray, 2011, Kumar and Rudbeck, 2009), however there are many cases where fixation of tissue is required. A major advantage of fixed tissue is control over applied deformation in excised tissue samples for mechanical characterisation. A repeatable uniform compressive or tensile stretch is possible in isolated tissue blocks which can then be fixed and sectioned, whereas the very soft nature of muscle makes this kind of applied deformation very difficult in unfixed tissue. Wax embedded sections can give better structural preservation; i.e. better quality sections and in this case it was found that detection of collagen using recombinant binding protein is more sensitive on wax sections compared to frozen sections of the same thickness. Section thickness was also tested (8, 15 and 20 µm) and the best detection was observed with 15 µm sections. In particular, 20 µm sections showed reduced sensitivity although longer incubation time slightly improved detection.

For CNA35-tdTomato, a 1:100 dilution of eluted protein (approx 1.6 mg/ml) worked equally well as a 1:20 dilution of CNA35-EGFP. We also show that longer incubation generally provides better collagen detection, especially at high dilution of the binding protein. Figure 4.3d & 3b show that, even by using low dilution of the binding protein, the collagen detection (perimysium) is better when the sections are incubated for longer. Although Figure 4.3h & 3f illustrate that even at low dilution (1:20) of CNA35-tdTomato the collagen structure can be detected equally well at one hour or 24 hours of incubation, there is no harm in longer incubation and this has informed my recommendation (Figure 4.5). The increased sensitivity of the tdTomato probe is despite a slightly lower concentration of this recombinant protein as used here (1.6 vs. 2.4-2.8 mg/ml) but is in line with previous findings of higher sensitivity on fresh tissue (Aper et al., 2014).

The yield of recombinant protein following the protocol described here was in the order of 3.2-5.7 mg from 200 ml bacterial culture (1.6-2.8 mg/ml as eluted) which provides enough probe to analyse approximately 160 tissue slides (if low dilution is used) from a single round of purification (200ml bacterial culture). Given the open availability of the plasmid DNA encoding the recombinant proteins (Aper et al., 2014), this represents a widely accessible approach since it is fast, economical and not technically demanding to produce highly specific fluorescent collagen probe with relatively basic bacterial and molecular facilities. This facilitates the use of the approach in bioengineering applications.

All images shown in this study, except Figure 4.4b, were produced with a standard fluorescent microscope, and they clearly show the localisation of collagens within the overall tissue structure. However, much higher resolution can be achieved with confocal microscopy, revealing more detail

about collagen fibril organisation (Figure 4.4b) (Wolf et al., 2003). The use of two-photon microscopy (Sahai et al., 2005, Foolen et al., 2008) or stimulated emission depletion (STED) microscopy (Lauterbach et al., 2010, Mishina et al., 2015) in conjunction with these collagen binding fluorescent probes would provide further detail in the visualisation of collagen organisation including imaging of tissues to about one milimetre in depth. Alternatively, Scanning Electron Microscopy (SEM) (Takaza et al., 2014, Lu et al., 2004) and Strong forward scattered Second Harmonic Generation (SHG) (Cox et al., 2003, Williams et al., 2005) can also be used to visualise organisation in collagen rich tissues, however these approaches do not specifically detect collagen. Therefore, analysis of fluorescent CNA35 probed tissue sections, as produced here, by confocal (Figure 4.4b) and/or other high resolution fluorescent imaging techniques will provide more detailed description of collagen organisation and further our understanding of how the microstructure can explain the mechanical behaviour observed in skeletal muscle (Gindre et al., 2013). This is important because the ECM plays a significant role in muscle fibre force transmission and restoration and ECM changes are implicated in muscle pathologies such as cerebral palsy (Gillies and Lieber, 2011).

4.5. Conclusion

Some important factors were established in this Chapter:

- Collagen can be detected using CNA35-EGFP/tdTomato on fixed tissue, including cartilage, epithelia and the perimysium and endomysium of skeletal muscle.
- Penetration of the probes into intact mature muscle tissue is very limited but the probes work effectively on wax embedded sections; better than frozen sections.
- 1% BSA provides sufficient blocking of non-specific binding.
- Antigen retrieval using Sodium citrate greatly increases the efficiency of binding in PFA fixed tissue.
- A working protocol has been developed including binding protein concentration and incubation time.

Chapter 5-Collagen fibril organisation in skeletal muscle perimysium under tension and compression

To live is the rarest thing in the world. Most people exist, that is all.

OSCAR WILDE, IRISH POET.

5.1. Introduction

In skeletal muscle, the ECM has two important functions: it is a structure that organises muscle fibres into hierarchal groups and it acts as a mechanism holding the muscle in position during deformation (Rowe, 1974, Huijing, 2009). Approximately 10% of skeletal muscle volume is composed of collagen fibres and collagen is the main protein of the ECM (Williams et al., 1995, Dransfield, 1977). Skeletal muscle contains collagen types I, III, IV, V, VI, XII and XIV, but the major ones are type I and III (Nishimura, 2010). It is reported that perimysium collagen is mostly type I, whereas endomysium and epimysium consist of equal amounts of collagen type I and type III (Light and Champion, 1984). It has been suggested that the mechanical properties of passive skeletal muscle depend on the size,

orientation and organisational arrangement of collagen fibres, particularly in the perimysium (Rowe, 1974, Purslow, 2010, Nishimura et al., 1996), but the details of this are not well understood.

The literature on skeletal muscle compressive and tensile properties shows high variability, partly due to inherent biological variation but also arising from different experimental protocols (species, samples, strain rates, etc.). However, the incompressibility, anisotropy, viscoelasticity and nonlinear behaviour of passive muscle tissue are generally well described and are broadly similar to other soft tissues (Van Loocke et al., 2008, Van Loocke et al., 2006, Takaza et al., 2013a, Böl et al., 2014, Calvo et al., 2010, Nie et al., 2011). In contrast, the tension/compression asymmetry observed in the stress-stretch response of porcine and chicken skeletal muscle (Chapter 3) are not well understood, though this asymmetry has also been noted in other soft tissues (Mow et al., 1980, Huang et al., 2001, Akizuki et al., 1986, Huang et al., 2003, Fang et al., 2014, Oliveira et al., 2016). The reasons for this asymmetric response in muscle evidently lie in the microstructure, but a detailed explanation has not yet been proposed and requires more microstructural analysis.

Muscle ECM geometry is extremely complex. Although it has been categorized into three hierarchical levels as endomysium, perimysium and epimysium, distinguishing these can be subjective. Despite studies on the structure of muscle connective tissue (Purslow, 1989, Nishimura et al., 1994, Das et al., 2010, Gillies and Lieber, 2011, Passerieux et al., 2006, Purslow, 2010, Purslow and Trotter, 1994, Purslow, 2002, Purslow, 2005, Trotter and Purslow, 1992), there remains a much less clear understanding of muscle ECM, particularly perimysium, compared to connective tissues like tendon, ligament and cartilage. This was recognised by Gillies and Lieber who stated in their 2011 review paper that a three dimensional systematic study of muscle ECM organisation is lacking (Gillies and Lieber, 2011). Furthermore, it is unknown whether perimysium structural differences between species reflect differences in the mechanical response of skeletal muscle to deformation (Takaza et al., 2014, Takaza et al., 2013a, Van Loocke et al., 2006, Böl et al., 2014, Bosboom et al., 2001). It has been suggested that perimysium is the main structure of the ECM responsible for load bearing in muscle (Purslow, 2010, Nishimura, 2010, Gillies and Lieber, 2011, Takaza et al., 2014) but our knowledge of perimysium is poor compared with endomysium. Purslow (1989) reported on aspects of perimysium rearrangement during deformation in the muscle fibre direction. However, it is not known how the perimysium network responds to deformations applied in both the muscle fibre and cross-fibre directions. It is likely that the mechanical properties of ECM as a load-bearing structure are more a reflection of the network geometry than the constitutive properties of the collagen fibrils (Gillies and Lieber, 2011). However, much of the reported literature on skeletal muscle ECM is based on SEM investigation which provides very high magnification but makes interpretation of the overall ECM structure a challenge due to the multi-scale nature of ECM.

Accordingly, the aims of this Chapter are:

1. To improve our understanding of the three-dimensional structure of perimysium in skeletal muscle. The focus is to observe the perimysium structure and record differences across species (chicken and porcine) in the transverse and longitudinal planes at a scale that can show the overall network structure.
2. To subject muscle samples from different species (porcine and chicken) to tensile and compressive deformations and to qualitatively investigate how perimysium structure is altered in response to externally applied deformations.
3. To relate the observed stress-strain relationships (Takaza et al., 2013a, Van Loocke et al., 2006), and Chapter 3) to the internal structure of the muscle observed here to address the microstructural reasons for the observed tension/compression asymmetry (Takaza et al., 2014), and Chapter 3).

Therefore, to frame the results and analysis presented in this Chapter, it is proposed that a further important aspect of perimysium structure is the orientation and organization of the sheets of collagen fibrils which comprise the perimysium. Figure 5.1a shows the general arrangement of muscle fibres into groups to form fascicles and Figure 5.1b presents my proposal of levels of collagen fibre organization within perimysium. A reflection of collagen organization is the degree of "waviness" (w) of collagen: one order of collagen organization is reflected in both w1 and w2 (dark green), the waviness of perimysium sheet (made of groups of tightly-woven collagen fibres) in planes transverse (TT' plane) and longitudinal (LT) to the muscle fibres respectively, while w3 (light green) is the waviness of collagen within the perimysium sheet, as previously reported (Nishimura et al., 1994, Purslow, 1989). w3 could not be visualised in the current study. The concept of w1 and w2 are novel and are introduced here as a tool to assess the relationship between microstructure and passive stress-strain behaviour observed in muscle. It is here proposed that collagen sheets are wavy when muscle is in the un-deformed state but that stretching of these sheets under applied deformation may be largely responsible for the tension/compression asymmetry observed in the stress strain response of skeletal muscle.

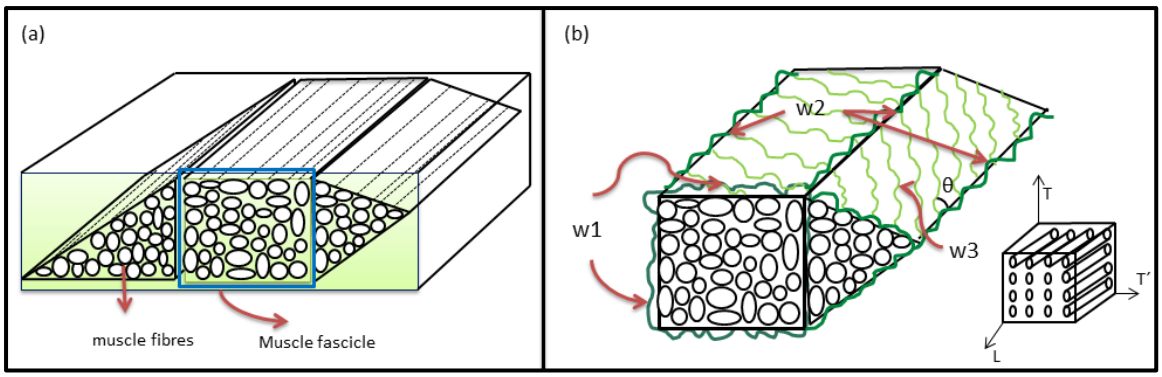

Figure 5. 1- Proposed organization of perimysium collagen fibres in mucle ECM: (a) schematic illustration of muscle tissue showing a fascicle (outlined in blue) in cross-section; each fascicle contains a group of muscle fibres, (b) collagen fibre organization in undeformed (control) tissue; w1 and w2 (dark green) represent the perimysium visible in the cross-sectional plane and longitudinal direction respectively, while w3 is individual collagen fibril waviness (crimp) within each perimysium sheet (light green), θ: the angle of collagen fibrils within the perimysium sheet with respect to muscle fibres. L is the longitudinal muscle fibre direction, T & T' are the transverse directions.

This Chapter reports on testing the proposal about the organization of perimysium through observation of collagen structure across species, viewed in skeletal muscle in both transverse and longitudinal sections, under different loading conditions. These structural observations are also used to assess the source of the tension/compression asymmetry observed in the previous stress-stretch results from tension and compression experiments on isolated porcine and chicken muscle samples applied in both the muscle fibre and cross-fibre directions (Chapter 3 together with the work of Takaza et al. (2013a) and Van Loocke et al. (2006)).

This approach provides a means to yield new insights into the internal organisation of muscle structure, with the long term aim of developing constitutive models of skeletal muscle to capture both the passive tension and compression characteristics observed. The limitation associated with not being able to study the same piece of tissue under different loading conditions using this approach is acknowledged.

5.2. Methods

5.2.1. Sample preparation

Porcine and chicken skeletal muscles from 3-month old females were used by trained personnel using ethically approved protocols (see Section 4.2.1 for more details). Table 5.1 gives an overview of the tissues and samples analysed. The sample preparation is the same as described in Section 3.2.1 of Chapter 3 and Sections 4.2.1 and 4.2.2 of Chapter 4.

Briefly, two sets of samples were prepared. Cubic and cuboid specimens (with characteristic length of 10 mm for compression in the muscle cross-fibre direction and at 45° to the muscle fibre direction and 5 mm for compression in the muscle fibre direction) were deformed by 30% compression by a custom made vice as shown in Figure 5.2a. For the fibre direction compression, the sample height was halved to avoid buckling (Van Loocke et al., 2006).

For tension, approximately 10 mm thick, 10 mm wide and 50 mm long samples were prepared. The samples were stretched by 20% for the fibre, cross-fibre and 45° to the muscle fibre directions using a custom made rig as shown in Figure 5.2b. The applied stretch was measured using a ruler. The tensile testing standard ASTM E8/E8M for sample length requirement was considered as much as was practically possible. Control samples were also prepared to which no deformation was applied. Tissue was immersed in 4% paraformaldehyde (PFA) in PBS for 48 hours while under tension and compression or control. The PFA solution chemically fixed the tissue microstructure in the deformed configuration. Immersing fresh tissue in fixative crosslinks the components of the tissue, preserving structure and molecular components. PFA is the most commonly used fixative for detection of molecular components of the tissue (e.g. (Briguet et al., 2004, Iwasaki et al., 2013)), but needs to be tested for suitability for each new detection method as it can interfere with antibody based detection of specific molecular epitopes. Sample lengths were measured before and after the chemical fixation process.

Table 5. 1- Overview of species, muscle type, section orientation and deformation parameters used to assess and compare collagen organisation.

Species	Muscle	Section types	Applied Deformation	Abbreviation	Number of specimens	Number of replicates/each specimen	Total number of prepared sections	Number of informative sections	Number with consistent pattern
Chicken	Pectoralis	Transverse (T)	Control	C	13	4	52	46	46
			Fibre compression	Comp-F	7	4	28	21	21
			Cross fibre compression	Comp-XF	4	9	36	29	29
			Fibre tension	Ten-F	20	2	40	32	32
			Cross fibre tension	Ten-XF	8	2	16	15	15
		Longitudinal (L)	Control	C	4	1	4	4	4
			Fibre compression	Comp -F	6	1	6	4	4
			Cross fibre compression	Comp -XF	5	1	5	4	4
			Fibre tension	Ten-F	3	2	6	4	4
			Cross fibre tension	Ten-XF	4	2	8	2	2
Porcine	Biceps femoris (BF)	Transverse (T)	Control	C	16	1	16	16	16
			Fibre compression	Comp -F	3	3	9	8	8
			Cross fibre compression	Comp -XF	1	4	4	3	NA
			Fibre tension	Ten-F	12	1	12	12	12
			Cross fibre tension	Ten-XF	9	2	18	14	14
		Longitudinal (L)	Control	C	3	1	3	0	NA
			Fibre compression	Comp -F	2	1	2	0	NA
			Cross fibre compression	Comp -XF	1	1	1	0	NA
			Fibre tension	Ten-F	3	2	6	0	NA
			Cross fibre tension	Ten-XF	1	--	--	--	--
	Longissimus dorsi (LD)	Transverse (T)	Control	C	13	3	39	32	32
			Fibre compression	Comp -F	3	2	6	5	5
			Cross fibre compression	Comp -XF	3	6	18	15	15
			Fibre tension	Ten-F	11	3	33	30	30
			Cross fibre tension	Ten-XF	5	4	20	14	14
		Longitudinal (L)	Control	C	2	3	6	0	NA
			Fibre compression	Comp -F	2	--	--	--	--
			Cross fibre compression	Comp -XF	1	1	1	0	NA
			Fibre tension	Ten-F	6	1	6	0	NA
			Cross fibre tension	Ten-XF	1	--	--	--	--

Sample preparation and fixing were performed within 2 hours after death of the animal to minimise the effects of Rigor Mortis (Van Loocke et al., 2006). Undeformed samples were directly placed in the fixative. Following fixation, blocks of tissue were dehydrated in different graded alcohols and infiltrated with molten paraffin wax prior to sectioning (as described in Chapter 4, Section 4.2.2). The core part of the samples was selected for analysis to minimise clamp effects.

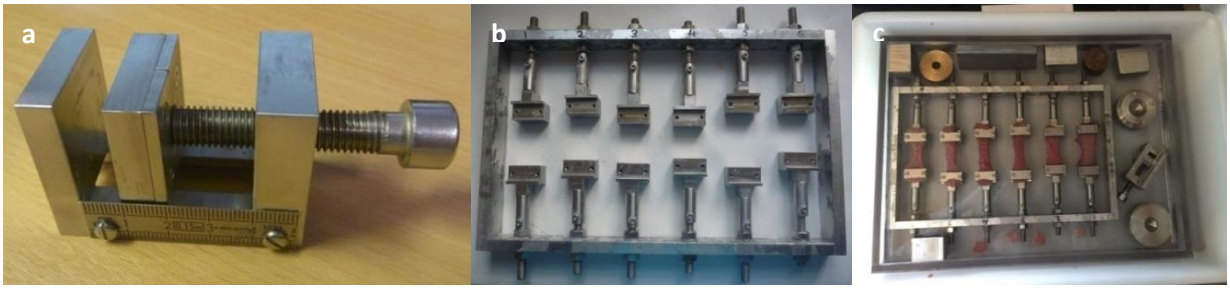

Figure 5. 2-Compressive vice (a) and tensile rig (b) used for controlled muscle deformation. Samples loaded in the tension rig for deformed(c).

15 µm thick sections were cut on a Leica RM2255 microtome in longitudinal and transverse orientations with respect to the direction of the muscle fibres. Collagen was detected and visualised with an optimised protocol described in Chapter 4, Sections 4.2.4-4.2.6, using a specific collagen binding protein, CNA35 fused to either EGFP or tdTomato. The CNA35-EGFP was used for the sections shown here, which stains the entire collagen fibre network green (including the endomysium and perimysium).

Stained sections were first viewed using a compound fluorescent microscope (Olympus BX 40) to make a first-pass analysis of collagen structure and to select the best sections for analysis by confocal microscopy (Leica SP8 scanning confocal) for clearer and more detailed visualisation and analysis of collagen fibril orientation.

Production of longitudinal sections posed particular technical challenges. In addition the difficulty of viewing continuous stretches of collagen fibres in longitudinal section meant they were less informative. Therefore, few longitudinally sectioned examples are shown in the Figures presented. Most data presented were viewed through sections cut perpendicular to the muscle fibre direction (Table 5.1).

5.2.2. Analysis criteria

5.2.2.1. Exclusion of images with detached connective tissue

To systematically investigate the structure of collagen fibrils in skeletal muscle, particularly perimysium, it is necessary to set analysis criteria. As shown in Figure 5.3 (top row) in both chicken

and porcine muscle sections, there were some cases where perimysium had separated from the adjacent fascicles. This could arise when tissue sections are stretched on a warm water bath prior to floating on slides, which could cause tissue to tear along the weakest line. This may be exacerbated by previously applied deformation of the tissue because these separations were more frequently seen in deformed samples. Since this represents an experimental artifact, such regions were excluded from analysis and only those which remained attached to fascicles, at least on one side, were considered (see Figure 5.3 (middle row)). Figure 5.3 (bottom row) shows the perimysium disconnected from fascicles at some points but it still remained connected over a continuous distance, within which it was suitable for analysis.

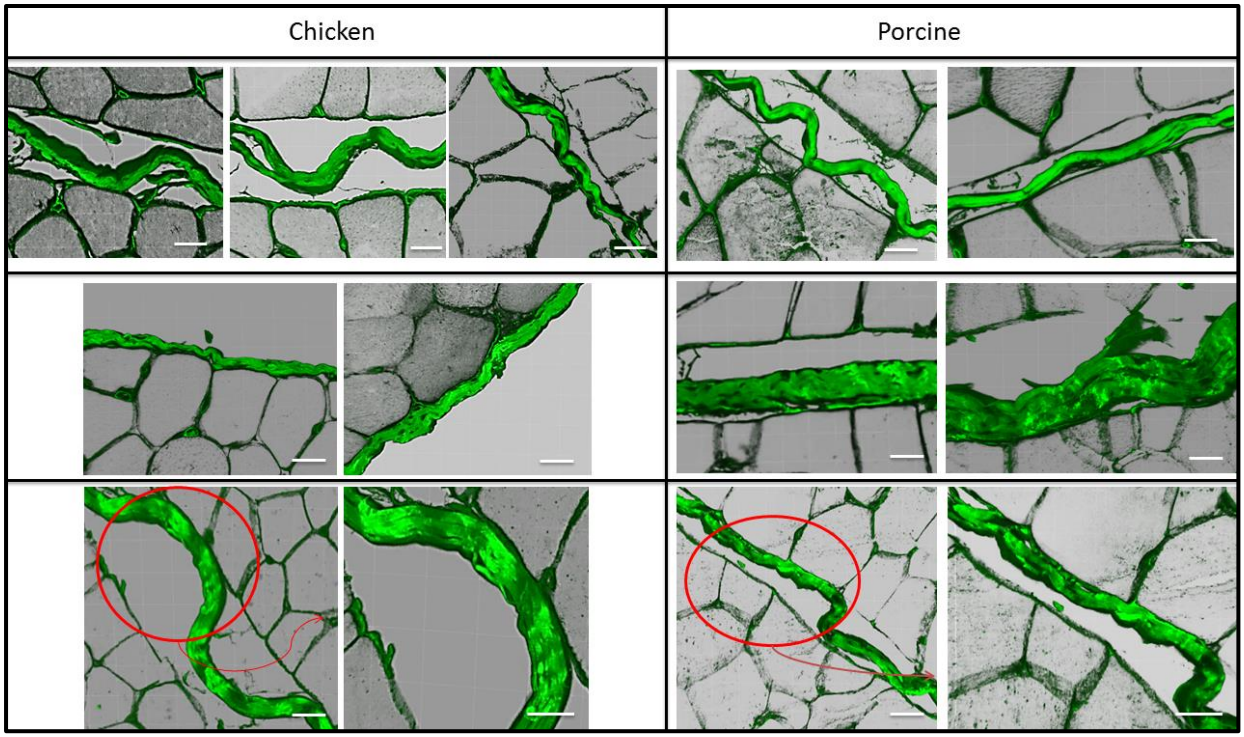

Figure 5. 3-Exclusion of regions where perimysium became detached from adjacent muscle fascicles. Top row: excluded images of chicken and porcine muscles in which perimysium was separated from the neighbouring fascicles. Middle row: sections included in analysis because a continuous piece of perimysium is attached to the underlying fascicles at least on one side. Bottom row: sections included in analysis where perimysium is attached to fascicles over a continuous stretch. Scale bars indicate 20 µm.

5.2.2.2. Definition of collagen waviness in this analysis

Figure 5.1 illustrates how the structure of the collagen fibrils in the perimysium sheet can be viewed in different planes; the degree of waviness in fibres viewed in transverse sections, is designated as w1 and viewed in longitudinal sections is designated as w2. Viewing the perimysium at different scales shows different levels of detail. Figure 5.4a shows the whole perimysium sheet which is distorted due

to partial separation from the muscle fascicle, so the condition of the whole ECM viewed at this scale is not reflective of the collagen fibril organisation within (waviness). However, higher magnification (Figure 5.4b) and confocal microscopy (Figure 5.4, bottom row) shows the orientation of individual collagen fibres as either “straight” (c), “less wavy” (d), “wavy” (e) or “more wavy” (f) pattern; this is highlighted by the manually drawn orange lines in each case. For the analysis, images with higher magnification were only considered. The waviness was visually categorised into 4 groups of “straight”, less wavy”, “wavy”, and “more wavy”. There is no quantification for the amount of waviness for this qualitative analysis.

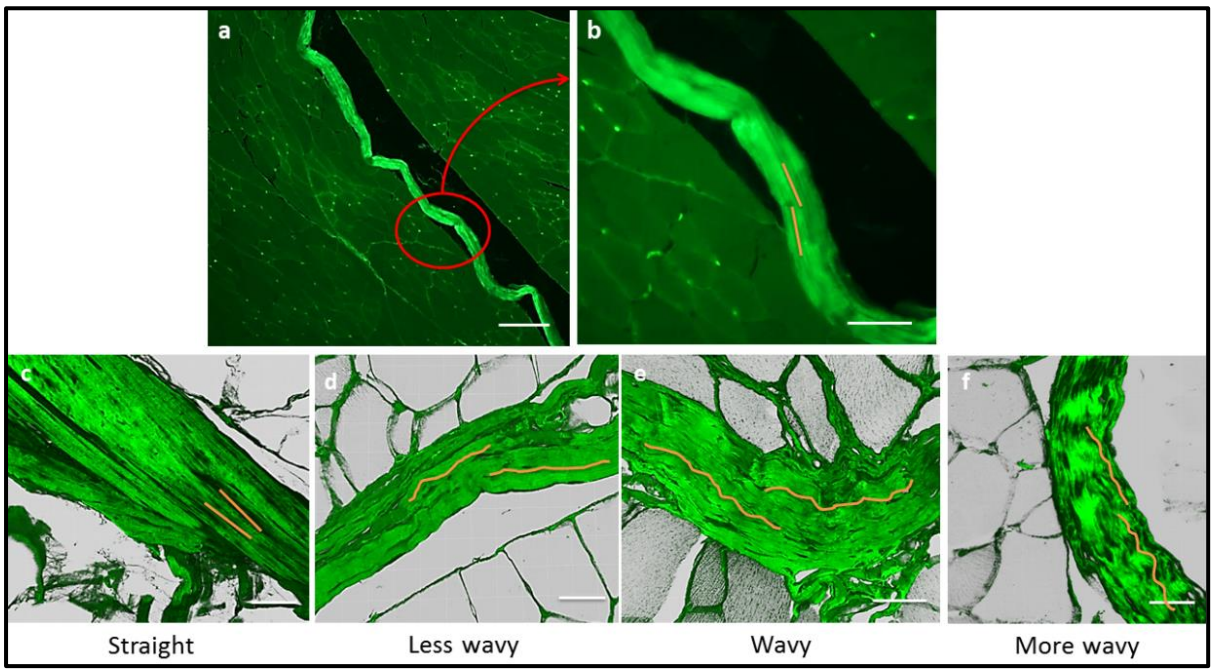

Figure 5. 4-Definition of collagen fibre “waviness” within perimysium requires high magnification to view individual fibrils.

(a) Distorted perimysium sheet due to partial separation from the muscle fascicle; the condition of the whole ECM sheet at this scale is not reflective of the collagen fibril organisation within, (b) straight collagen fibrils within the same perimysium shown in “a”, (c) “straight” pattern for collagen fibrils of perimysium, (d) “less wavy” pattern for collagen fibrils of perimysium, (c) “wavy” pattern for collagen fibrils of perimysium, (d) “more wavy” pattern for collagen fibrils of perimysium. Orange lines are hand drawn to indicate the “waviness” of the collagen fibrils within. Exposure time: 700 ms for a and 300 ms for b. The images a & b were taken using compound fluorescent microscope with 10X for lower magnification and 20X for higher magnification and the images in bottom row were taken using confocal microscope. Scale bars indicate 100 µm in a, 50 µm in b, and 30 µm in Comp-F.

5.2.2.3. Representative descriptions

To ensure that the recordings and descriptions of collagen structure under different deformation conditions are representative, a systematic approach with repetition at a number of levels was

established to account for variability. Several repeat sections (adjacent sections) were assessed from a number of repeat samples, as laid out in Table 5.1 for each set of conditions. At least 3-4 locations within each section were assessed (so replicate areas, within adjacent sections, within replicate tissue blocks were assessed).

As explained above, longitudinal sections were less informative than transverse sections so the number of sections assessed was less and for some conditions in porcine tissue it was not possible to clearly assess any longitudinally sectioned samples (see Table 5.1). Therefore, the most informative data came from transverse sections at each loading condition for both animals. In each deformation condition, as laid out in Table 5.1, all analysed samples showed the same pattern, from which it can be concluded that the behaviour seen in perimysium, as presented in the Results section, is representative of that condition. The number of specimens prepared for tension is more than those prepared for compression because according to the dimension of the tissue exposed to the applied deformation (see Section 5.2.1) it was practical to have more samples in tension than in compression. The sections in which perimysium was torn or separated from both sides were removed from analysis, therefore in most cases, the number of analysed sections were less than the prepared sections.

5.3. Results

5.3.1. Overview of visualisation of collagen fibre organisation within perimysium in different species, muscles and section planes

As shown in Figure 5.5a & e & i, the collagenous sheaths are very clearly visible around each muscle fibre (e; endomysium) and group of muscle fibres (p; perimysium) in both species. Porcine tissue maintained structure better through processing (m, Figure 5.5f), whereas chicken perimysium more often showed a zigzag pattern (z, Figure 5.5b) due to its detachment from adjacent fascicles. Furthermore, the porcine perimysium is thicker than chicken perimysium (Figure 5.5f & j).

As illustrated in Figure 5.5 for porcine tissue, there are some groups of muscle fibres within one fascicle which are surrounded by more intensely stained endomysium (encircled by red). The porcine skeletal muscle (LD and BF) have a mixture of more intensely stained and less intensely stained endomysium within the same fascicle, whereas chicken pectoralis muscle contained mostly fibres surrounded with evenly stained endomysium.

To observe three dimensional reorientation of perimysium when the muscle is exposed to external deformations, it would be ideal to be able to observe perimysium when the tissue is cut in different planes (transverse and longitudinal). Figure 5.5c & g & k represent longitudinal sections for chicken and porcine muscles, which show detection of collagen in endomysium in both tissues, but only clear

distinctive identification of perimysium (larger tracts) in chicken. It is unclear why perimysium is not clearly identifiable in porcine muscle longitudinal sections when it is clearly visible in transverse sections.

Visualisation of fluorescently tagged collagen using a compound fluorescent microscope shows the overall perimysium structure as shown in Figure 5.5. However, confocal microscopy revealed the more detailed structure of perimysium showing very small collagen fibrils in the perimysium sheet and their condition of "waviness" (see Figure 5.5d & h & l).

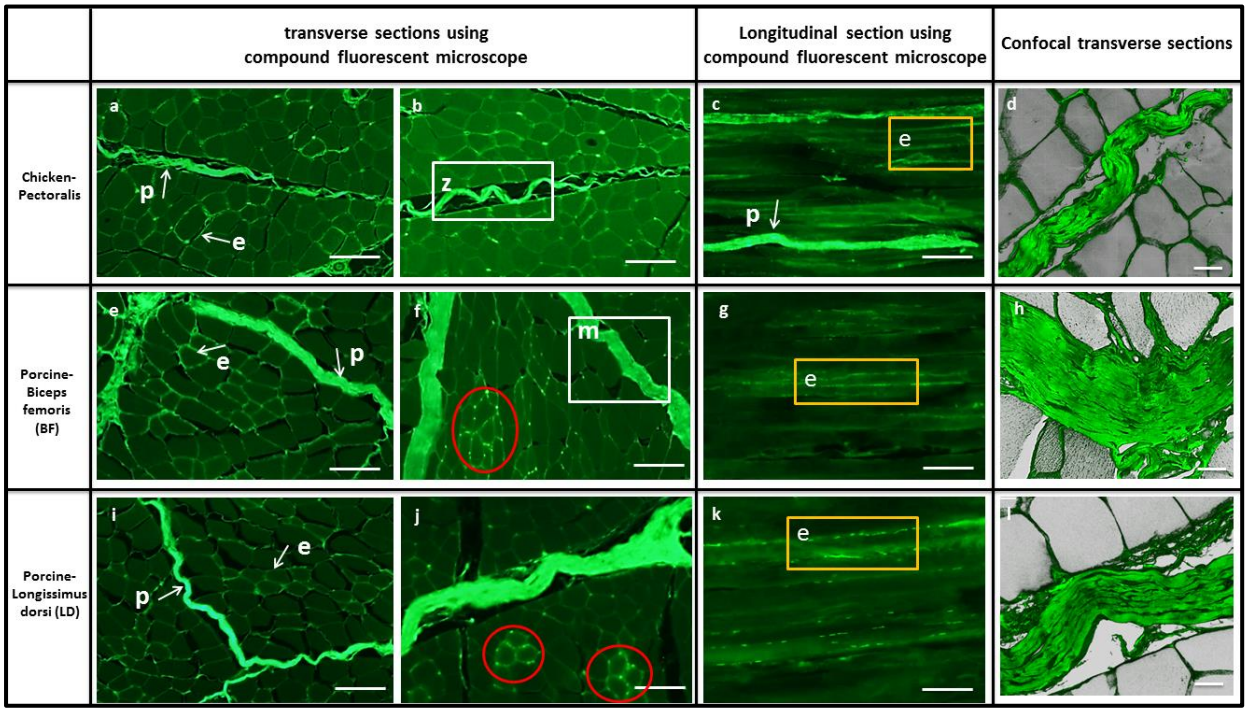

Figure 5. 5-Visualisation of fluorescently tagged collagen fibres revealing perimysium organisation.

(a) transverse section of chicken pectoralis muscle showing the overall structure of connective tissue, (b) transverse section of chicken pectoralis muscle showing detachment of fascicles due to experimental artefact, (c) longitudinal section of chicken pectoralis muscle showing both endomysium and perimysium, (d) confocal image of chicken pectoralis transverse section showing very detailed structure of collagen fibrils in perimysium, (e) transverse section of porcine biceps femoris muscle showing connective tissue structure (f) transverse section of porcine biceps femoris muscle showing groups of muscle fibres surrounded by more intensely stained endomysium (encircled by red) as well as some surrounded by less intensely stained endomysium (g) longitudinal section of porcine biceps femoris muscle showing endomysium (yellow box), (h) confocal image of porcine biceps femoris muscle transverse section, (i) transverse section of porcine longissimus dorsi muscle, (j) transverse section of porcine longissimus dorsi muscle showing groups of muscle fibres within one fascicle surrounded by more intensely stained endomysium (encircled by red), (k) longitudinal section of porcine longissimus dorsi muscle showing endomysium (yellow box), (l) confocal transverse image of porcine longissimus dorsi muscle with detailed description of collagen fibrils . (Abbreviations: p, perimysium; e, endomysium; z, zigzag pattern due to perimysium detachment from adjacent fascicles; m, perimysium maintained its attachment to adjacent fascicles) and slow-twitch muscle fibres (red circles). Exposure time: 300 ms for all cases. Scale bars indicate 100 µm for sections visualized using compound fluorescent microscope (a-c, e-g, and i-k),

and 20 µm for confocal images (d, h, and l). The tissue is in undeformed state in all cases except images c, g, k, and h, which are under tension in the fibre direction (Ten-F).

5.3.2. Perimysium collagen structure under different deformation conditions

To test the proposal presented in section 5.1 stating that skeletal muscle perimysium is hierarchical with two distinct orders of collagen fibre organisation which respond differently to applied deformation, collagen fibre orientation in transverse sections of chicken pectoralis, porcine biceps femoris, and porcine longissimus dorsi muscles under different deformation conditions were analysed and are illustrated in Figure 5.6i-iii respectively. For each condition, a series of images from different specimens are presented.

In undeformed chicken samples, as shown in Figure 5.6i(a), the perimysium in the transverse plane (w1) is wavy since there is no load on the tissue.

Where the chicken tissue was compressed along the direction of the muscle fibres (Comp-F), collagen fibre organisation in perimysium, viewed in cross section (w1) is straight, (see Figure 5.6i (b)). Comp-F causes shortening of the tissue in the direction of the muscle fibres and accordingly expansion in cross sectional plane resulting in a larger block cross section. Therefore, perimysium stretches due to the increase in cross section area of the tissue showing straighter collagen fibrils (w1) compared to the control case.

Where the tissue was compressed perpendicular to the muscle fibres (Comp-XF), the tissue expanded in the muscle fibre direction (indicated as L in Figure 5.1) and other perpendicular direction (T', Figure 5.1). Where perimysium in the transverse plane is parallel to compressive deformation (T), the collagen fibrils were wavy with dramatic change in the aspect ratio of muscle fibres (see Figure 5.6i(c), top image). Conversely, where perimysium was aligned perpendicular to the deformation direction the collagen fibrils straightened (see Figure 5.6i(c), two bottom images).

In tension in the muscle fibre direction (Ten-F), the tissue cross section becomes smaller resulting in wavy collagen fibrils (w1) in perimysium.

In tension applied perpendicular to the muscle fibres (Ten-XF), the collagen fibrils in the transverse plane aligned with the load direction became straight (see Figure 5.6i(e), three top images), because the tissue elongated in the deformation direction, but the perimysium perpendicular to the tensile deformation was relieved and showed waviness (see Figure 5.6i(e), bottom image).

Cross-species comparison shows that the same collagen reorientation (w1) was seen in both porcine tissues, i.e. wavy collagen in control but less wavy than chicken tissue; straight collagen fibrils in Com-F (see Figure 5.6ii & iii, Comp-F); less wavy collagen in Comp-XF where the perimysium is perpendicular to the direction of deformation (see Figure 5.6iii(c), the top image), and wavy

perimysium where perimysium is aligned with the direction of deformation(see Figure 5.6iii(c), bottom image); wavy structure in Ten-F (see Figure 5.6ii & iii, Ten-F); and straight collagen fibrils in Ten-XF where the perimysium aligned with the direction of deformation (see Figure 5.6ii(d) and Figure 5.6iii(e), three top images), and less wavy collagen fibrils where perimysium is perpendicular to the direction of deformation. The collagen waviness observed in Ten-F case for porcine BF muscle is greater than in the case of LD muscle.

i.	**Chicken pectoralis**	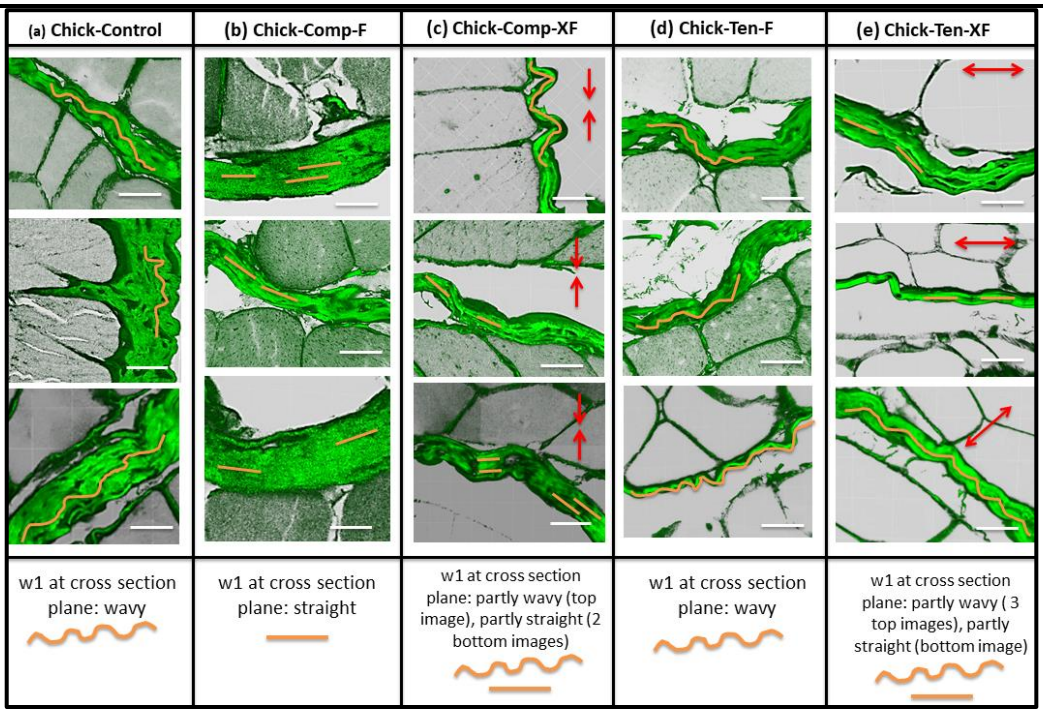			

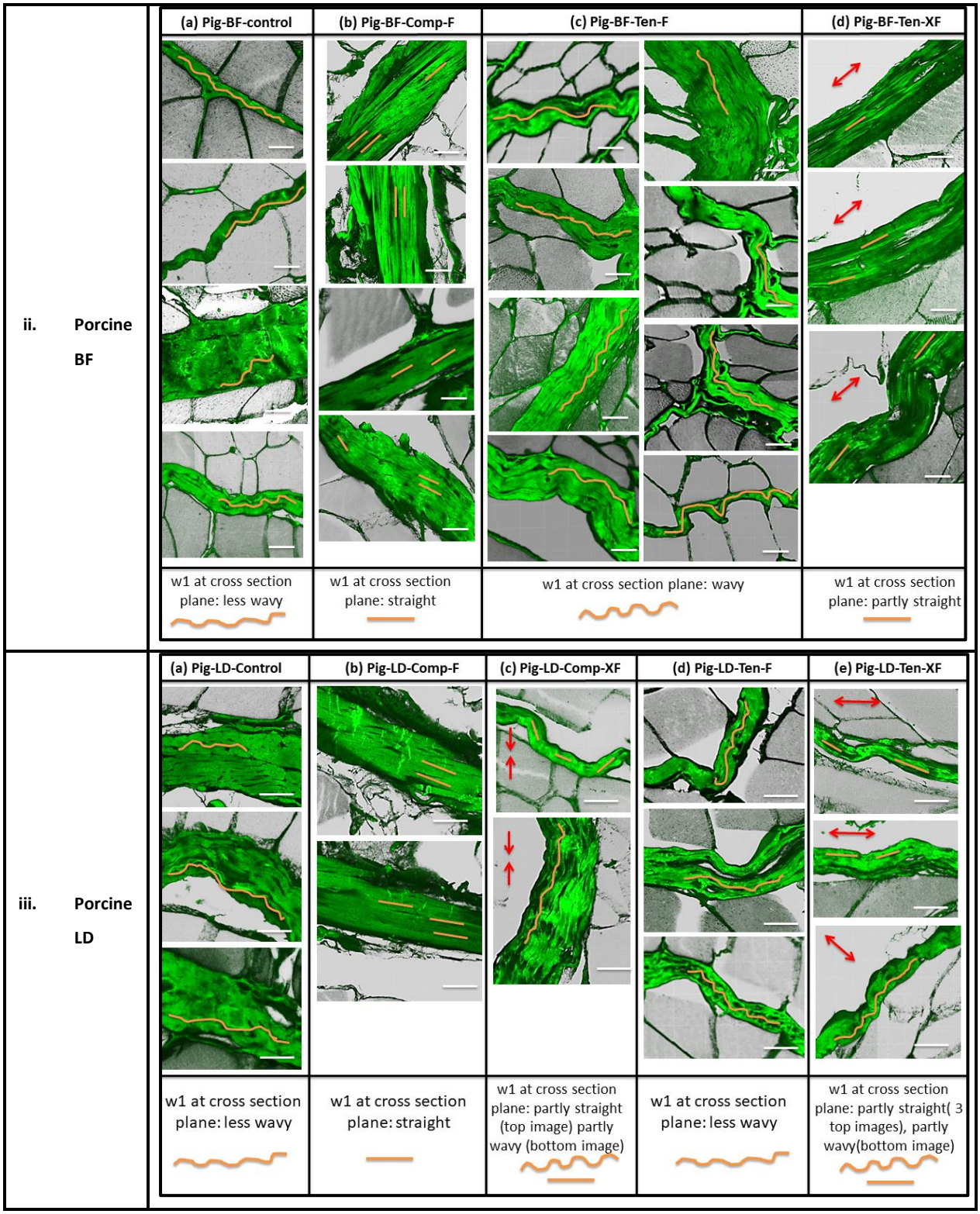

Figure 5. 6-Visualisation of w1 in collagen fibrils of perimysium in transverse sections for undeformed, and externally applied compression and tensile deformations in chicken pectoralis (i), porcine biceps femoris (ii), and porcine longissimus dorsi (iii) muscles.

Several example micrographs for control (a), Comp-F (compression in the muscle fibre direction, b), Comp-XF (compression in the muscle cross-fibre direction, c), Ten-F (tension in the muscle fibre direction, d), and Ten-XF (tension in the muscle cross-fibre direction, e) conditions, visualised by confocal microscopy in the transverse plane. Red arrows

represents the direction of applied deformations in Comp-XF and Ten-XF cases. Manually drawn curves/lines in yellow indicate the condition of collagen fibril waviness viewed in the transverse plane. Scale bars indicate 20 µm.

Changes in w2 were viewed and analysed in longitudinal sections of chicken muscle tissue under different deformation conditions, presented in Figure 5.7. Perimysium is observed to be wavy in control (a) as there is no load applied on the tissue. It is also observed that the collagen fibrils in Comp-F (b) are also wavy as the tissue shortens in the direction of muscle fibres in this deformed state. The collagen fibrils in Comp-XF (c) stretched due to the induced deformation resulting in less wavy collagen fibrils in the longitudinal direction (w2), see yellow lines. In Ten-F (d) the collagen fibrils were straight (yellow lines) because there is a direct deformation along the perimysium in the muscle fibre direction. Since in Ten-XF (e) the tissue shortening is induced in the longitudinal direction, collagen waviness was observed in this direction (w2).

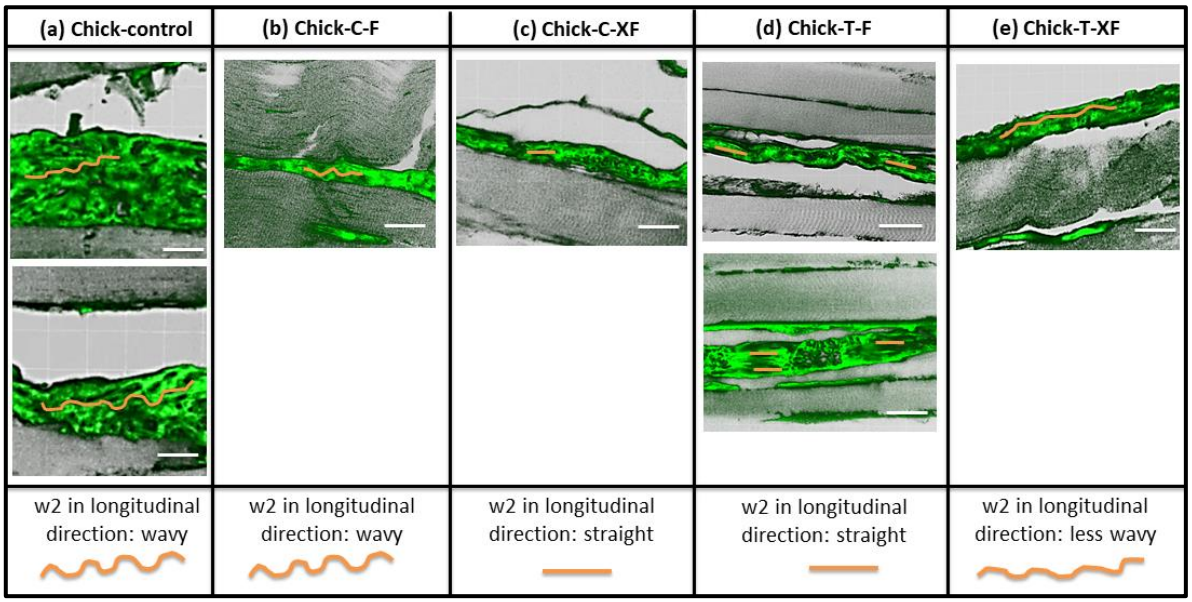

Figure 5. 7-Visualisation of w2 in collagen fibrils of perimysium in longitudinal sections for undeformed, and externally applied compression and tensile deformations in chicken pectoralis muscle.

Several example micrographs for control (a), Comp-F (compression in the muscle fibre direction, b), Comp-XF (compression in the muscle cross-fibre direction, c), Ten-F (tension in the muscle fibre direction, d), and Ten-XF (tension in the muscle cross-fibre direction, e) conditions, visualisedby confocal microscope in the longitudinal direction. Manually drawn curves/lines in yellow indicate the condition of collagen fibril waviness viewed in the lonitudinal direction. Scale bars indicate 20 µm.

The hierarchical organisation of muscle perimysium was proposed to change under deformation and contributes to the tension/compression asymmetry observed in stress-strain behaviour of skeletal muscle. This was tested through examining the confocal images of chicken and porcine tissues in different mechanical conditions. Figure 5.8 illustrates the three-dimensional

reorganisation/reorientation of perimysium collagen fibrils when the tissue is exposed to externally applied deformations showing that collagen fibrils in perimysium responds to the deformation differently in different planes; these findings supported the proposal. Therefore, the straightness in collagens represents load resistance in the structure because when no load is borne in a particular plane, the collagen is wavy in that plane.

i. **Chicken pectoralis**	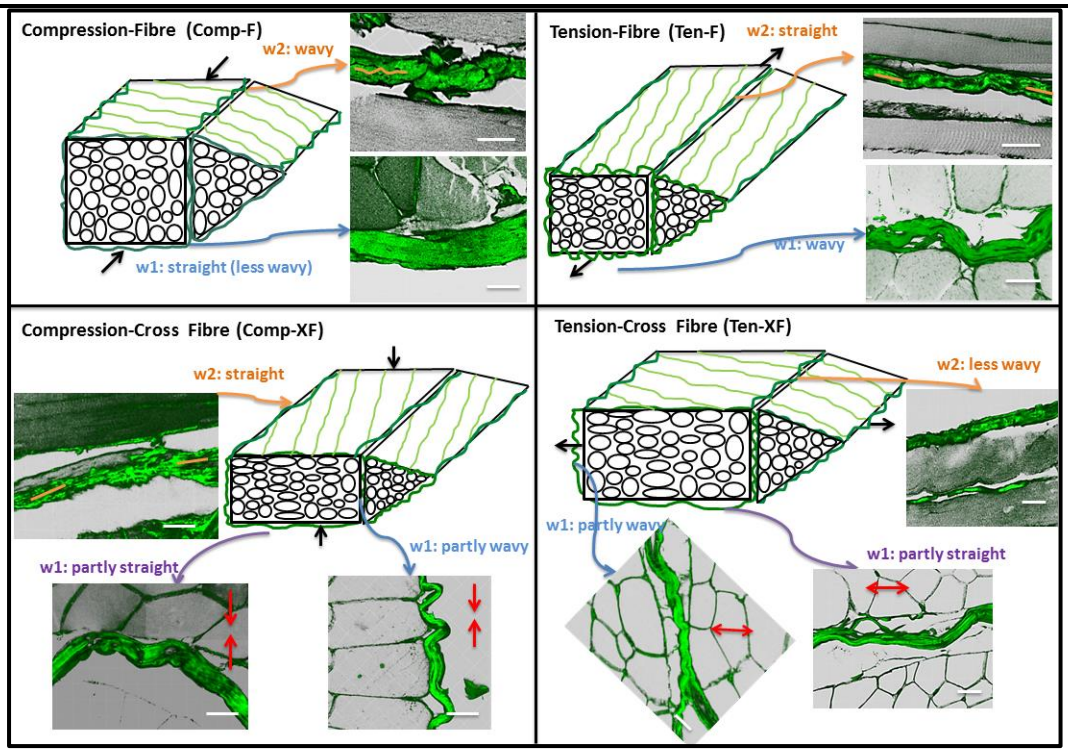
ii. **Porcine BF**	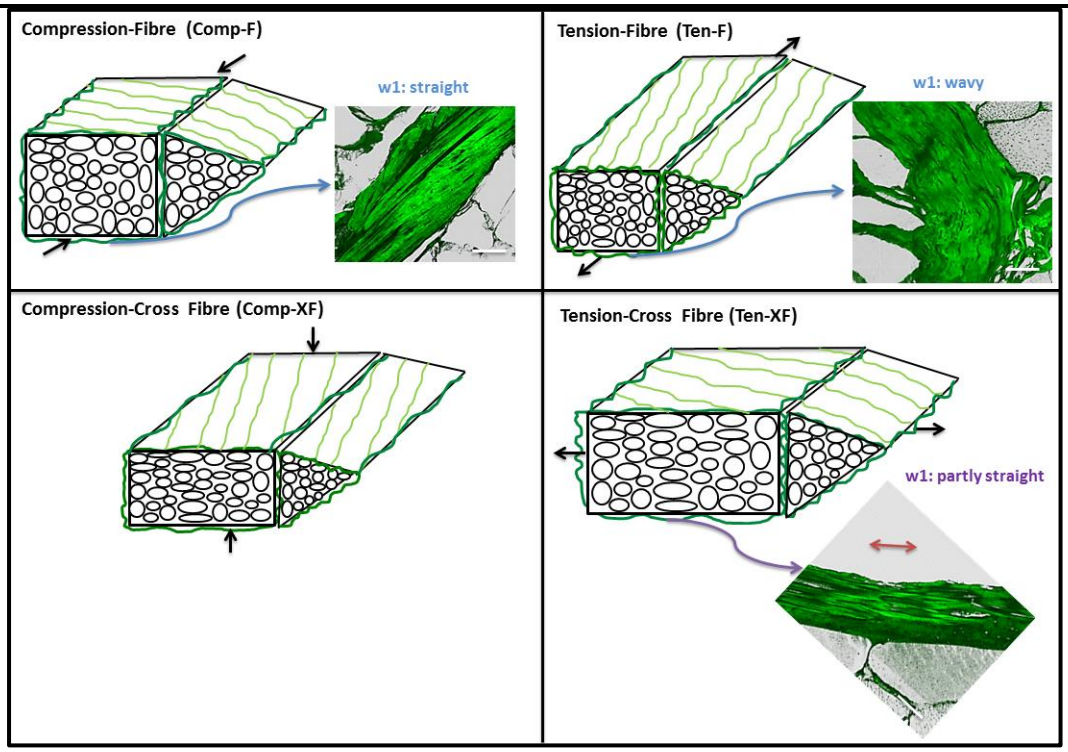

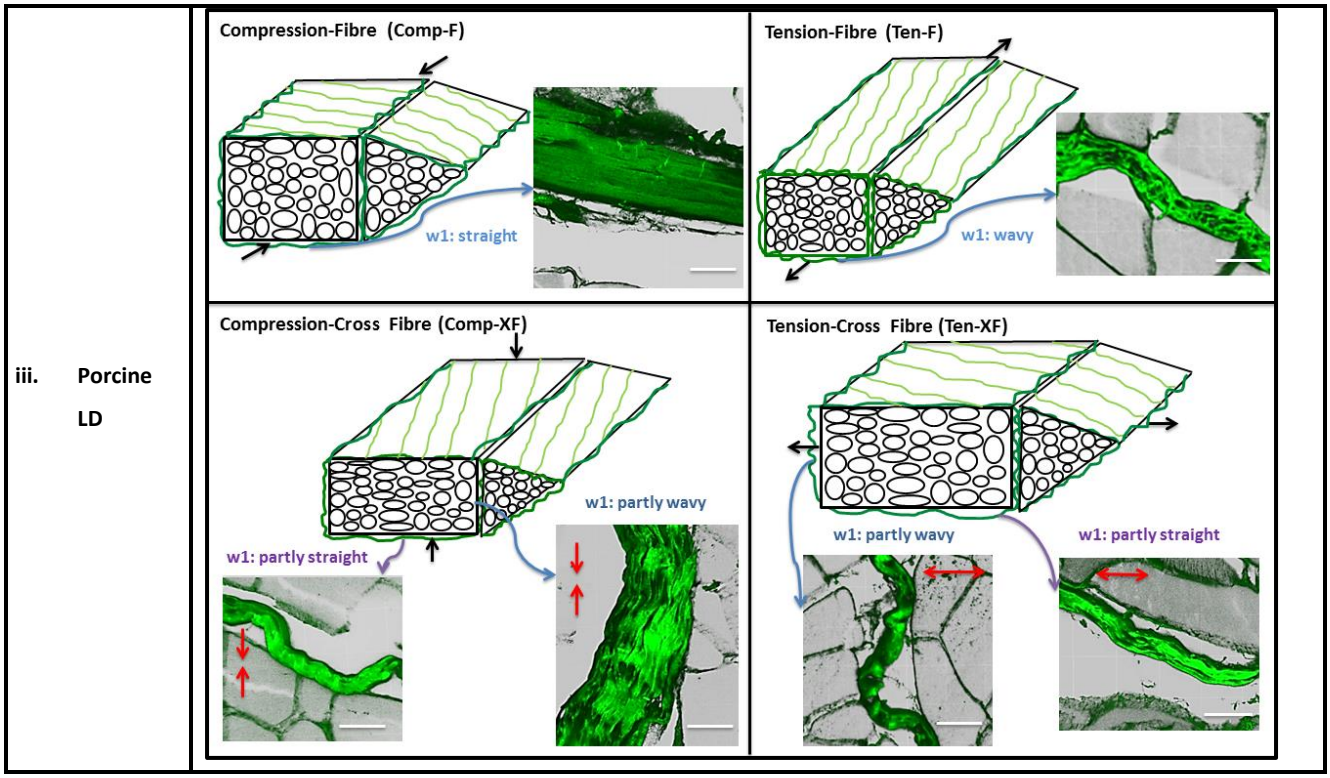

Figure 5. 8-The three-dimensional reorganisation/reorientation of perimysium collagen fibrils when the tissue is exposed to externally applied deformations in chicken pectoralis (i), porcine biceps femoris (ii), and porcine longissimus dorsi (iii) muscles.

Sample micrographs in Comp-F (compression in the muscle fibre direction), Comp-XF (compression in the muscle cross-fibre direction), Ten-F (tension in the muscle fibre direction), and Ten-XF (tension in the muscle cross-fibre direction) conditions were taken by confocal microscopy. w1 and w2 (dark green) represent the condition of the perimysium viewed in the cross sectional plane and longitudinal direction respectively. Black arrows in cartoons and red arrows in the images show the direction of applied deformation. Observed w1 (in blue for partly wavy pattern, and purple for partly straight pattern), and w2 (in orange) are shown here in the deformed conditions. Scale bars indicate 20 µm.

This approach investigates how the mechanical response relates to microstructural organisation (summarised in Table 5.2). It should be noted that the data from longitudinal sections of porcine tissue are missing due to technical issues associated with generating longitudinal sections (see Section 5.4.4, point 2).

Table 5. 2-Summary of perimysium behaviour (straightness/waviness) at transverse plane and longitudinal direction.

	w1 (at cross sectional plane)			w2 (in longitudinal direction)
Deformation condition	**Chicken**	**Porcine BF**	**Porcine LD**	**Chicken**
Control	wavy	wavy	wavy	wavy
Comp-F	straight	straight	straight	wavy
Comp-XF	partly straight/partly wavy	--	partly straight/partly wavy	less wavy
Ten-F	wavy	wavy	wavy	straight
Ten-XF	partly straight/ partly wavy	partly straight	partly straight/ partly wavy	wavy

5.4. Discussion

Given that investigating the structural changes in skeletal muscle to interpret mechanical response of passive skeletal muscle to deformation requires microscopic analysis, collagen fibril orientation in perimysium under different loading conditions was viewed in transverse and longitudinal section planes in two different species to observe the structural properties of perimysium.

Overall the organisation and pattern of perimysium and endomysium was similar between chicken and porcine samples with some notable differences. In general, perimysium in the porcine muscle examined was larger (Figure 5.5) and porcine tissues also revealed a combination of more intensely stained and less intensely stained endomysium within the same fascicle in porcine LD and BF muscles, whereas in chicken pectoralis muscle the fibres surrounded with evenly stained endomysium were observed. Two types of muscle fibre can be found in skeletal muscle; slow-twitch[2] and fast-twitch fibres. Slow-twitch fibres use primarily oxidative respiration (uses oxygen to make energy) while fast-twitch fibres use primarily anaerobic respiration (Plowman and Smith, 2013). It was previously shown that the slow tonic muscles such as pectoralis and soleus have higher amounts of collagen as they correspond to postural control rather than fast activities (Velten and Welch Jr, 2014, KOVANEN et al., 1980, Rodrigues et al., 1996). Kovanen et al. (1984) attempted to show whether the difference observed between muscle types in terms of collagen content is also observable at the level of individual muscle fibres (fast-twitch and slow-twitch). Through histochemical staining they showed that perimysium and endomysium stained more strongly in the slow twitch area of rat gastrocnemius muscle than in the fast twitch area. Therefore the more intensely stained endomysium observed in porcine tissue in the current study may represent slow-twitch muscle fibres. Indeed LD and BF are

[2] The slow-twitch fibres are usually smaller in diameter, contain more mitochondria, use aerobic respiration for ATP supply, fire slowly but take long to fatigue. They are suited for endurance type activities

mixed-type muscles, whereas chicken pectoralis muscle is reported to contain mostly slow-twitch fibres (Velten and Welch Jr, 2014).

5.4.1. Relationship between perimysium orientation under deformation and the stress-strain response in skeletal muscle

In this study it was demonstrated how perimysium organisation changes after deformation applications. In compression in the fibre direction (Comp-F), the collagen fibrils in longitudinal direction are wavy (w2) and bear no load, but since the collagen fibrils are straight in the transverse plane (w1) for both chicken and porcine tissues they are assumed to take part in load bearing in this condition (see Figure 5.8i-iii). In compression in the cross-fibre direction (Comp-XF) there is both wavy and straight perimysium in the transverse plane (w1). Takaza et al. (2014), through polarised light images, showed that 30% compressive deformation in the cross-fibre direction caused the collagen fibrils to be pushed together and showed an increase in waviness, which agrees with the findings of this study; that in Comp-XF, where the perimysium is aligned with the deformation direction, the collagen fibrils become wavy. However, the portion of perimysium which is aligned perpendicular to the applied deformation (straight fibrils) is greater than the proportion that is wavy, indicating that perimysium mostly reorients to bear the load. In their study, the colour changes of perimysium strands within the tissue were an indicator of the perimysium reorganization. However, in the current study, the waviness of perimysium collagen fibres were clearly visible in confocal images and it was shown how the perimysium responds under different deformation conditions. Takaza et al. (2014) also showed when the tissue is compressed perpendicular to the muscle fibres, the perimysium showed a preferred orientation to become perpendicular to the load direction and this preferred alignment is accompanied with more stretch in collagen fibrils. On the other hand, the collagen fibrils in the longitudinal direction under Comp-XF become straight, taking part in passive load bearing (see Figure 5.8i-iii). The compressive stress-stretch response in skeletal muscle reported in Chapter 3 showed generally that the tissue (either chicken or porcine) is stiffer in Comp-XF. It can be concluded that the stiffer response in Comp-XF than Comp-F (regardless of small difference between them) is because in Comp-XF collagen is involved in load bearing in two perpendicular planes (the less wavy collagen seen in the longitudinal direction induced by the deformation (Figure 5.7(c), w2)) as well as the stretched collagen in the transverse plane caused by direct deformation (Figure 5.6i(c), w1)). However in Comp-F only induced straightness in the transverse plane is responsible for passive load bearing.

It was also shown that in tension in the fibre direction (Ten-F), the collagen fibrils in the transverse plane (w1) are wavy, but the waviness is less than the control case indicating the collagens are partly engaged in load bearing. At the same time, the very straight collagen fibrils in the longitudinal direction

(w2) mostly bear the load. In contrast in tension in the cross-fibre direction (Ten-XF), the stretched perimysium in the transverse plane (w1) plays a key role in resisting the load in both species since the collagen acquires a wavy pattern in the longitudinal direction (see Figure 5.8i-iii). Takaza et al. (2014) also showed that application of a tensile cross-fibre deformation led to straightening of the perimysium collagen fibre networks. Stretched perimysium in the transverse plane (w1) observed in Ten-XF and those in the longitudinal direction (w2) observed in Ten-F are both caused by direct deformation in that direction. It seems the straightness is more extreme in Ten-XF (Figure 5.6i(e)) than Ten-F (Figure 5.7(d)) which may explain the stiffer response seen in Ten-XF for both animals shown in Chapter 3.

Puslow's group investigated the perimysium and endomysium collagen fibril changes in response to deformation applied in the fibre direction (Purslow and Trotter, 1994, Lewis and Purslow, 1989). They showed that in Ten-F collagen fibrils within the perimysium sheet (w3) re-orientate to become more aligned with the muscle fibres with smaller angles to the muscle fibre direction (θ), whereas in Comp-F they lie at a very large angle. However, direct comparison is not possible since w3 was not captured in this study.

Aforementioned observations do not show a strong evidence to explain why the stress response in tension is two orders of magnitude higher than in compression (as reported in Chapter 3). However, they generally explain anisotropy observed in stress-strain response of skeletal muscle both in tension and compression.

5.4.2. Cross-species mechanical differences based on perimysium collagen fibre microstructure

As observed in Figure 5.6, collagen fibrils (w1) in Comp-F are straighter in porcine than chicken tissue. However the mechanical results showed stiffer compressive response in chicken than porcine tissue (see Chapter 3). On the other hand, it should be noted that the perimysium in undeformed samples in porcine tissue showed a straighter pattern than those of chicken, which may indicate the reason why a straighter response in collagen fibrils (w1) was observed in porcine perimysium in Comp-F. The w2 comparison does not additionally inform the species difference in this condition since the tissue shortens in the longitudinal direction in Comp-F causing an increase in w2 resulting in load bearing.

In Comp-XF deformation, the collagen fibril waviness in the transverse plane (w1) showed a straighter pattern in chicken than porcine tissue (see Figure 5.6i and iii). The stiffer mechanical response observed in chicken in Comp-XF reported in Chapter 3 is explained by this pattern as it indicates that collagen fibrils in chicken are involved in load bearing more than porcine tissue. The

perimysium collagen fibrils in the longitudinal direction (w2) in chicken tissue are also straight, which emphasises the stiffer compressive response in chicken tissue than porcine in Comp-XF. However, the data in the longitudinal direction for porcine tissue is missing; if available it would help make a stronger statement.

Collagen fibril orientation in the longitudinal direction (w2) is important in Ten-F deformation because collagen fibrils are straight in the longitudinal direction (see Figure 5.7d) and bear load while w1 is wavy. However, the reduced waviness observed in the transverse plane in Ten-F deformation (w1) in chicken than porcine tissue (especially compared to those of porcine BF) can explain the stiffer tensile response in chicken. Lack of data in the longitudinal direction for porcine tissue is acknowledged, and additional information is required for porcine tissue.

In Ten-XF, although there is no image evidence for porcine in the longitudinal direction, the perimysium is wavy in this direction for this deformation condition and the collagen fibrils are not involved in load bearing. However, it cannot be stated clearly in which species waviness viewed in the transverse plane (w1) is greater, so it is difficult to address the stiffer tensile response observed for porcine tissue in the cross-fibre direction in this analysis.

Fang et al. (1999) and Nishimura et al. (1999) observed in bovine and porcine muscles that wavy bundles of collagen fibrils in perimysium ran parallel without any crossing bundle. In contrast Iwamoto et al. (2001) showed that secondary perimysium in chicken (1 to 2 years old) in transverse section consists of mostly large longitudinal collagen fibre bundles (LB in Figure 2.11a & b) and thin circumferential bundles (CB), which may explain why the chicken tissue shows a stiffer tensile response in the fibre direction. The stiffer tension response in porcine muscle, cross-fibre direction, may be due to the fact that there is no crossing bundle in porcine tissue and this allows the muscle to stretch more in the cross-fibre direction and experience more stress, whereas the crossing bundle in the chicken tissue acts as a barrier and does not allow for further stretching under the cross-fibre tension.

The collagen content reported in the literature for chicken pectoralis muscle, approximately at the same age as used in this study, is between 1.01-1.99 mg/g (Das et al., 2010, Roy et al., 2006), which is lower than a 3-month old porcine longissimus dorsi muscle (0.46-0.5 g $100g^{-1}$) (Čandek-Potokar et al., 1998), (Table 5.3). It is also reported that the muscle stiffness is directly correlated with both total collagen content and the perimysium thickness (Nishimura et al., 1996, Fang et al., 1999). Higher collagen content in porcine longissimus dorsi and also thicker perimysium observed in porcine sections (see Figure 5.5) may explain why porcine tissue shows a stiffer response in tension in the cross-fibre direction. However, collagen stiffness itself cannot explain the differences observed in the mechanical response. Therefore, understanding how collagen fibrils are woven in perimysium (architectural

shape) is also very important in investigating why perimysium responds differently in different deformation conditions, and this certainly needs further investigation.

Table 5. 3-The collagen content of chicken pectoralis and porcine longissimus dorsi muscles derived from the literature.

	Collagen content	Animal age
Chicken pectoralis muscle (Das et al., 2010)	1.01-1.88 mg/g	90 days old
Chicken pectoralis muscle (Roy et al., 2006)	1.99-1.93 mg/g	80 days old
Chicken pectoralis muscle (Nakamura et al., 2003)	2.92 mg/g	1 year old
Chicken pectoralis muscle (Sakakibara et al., 2000)	4.7-6.34 mg/g	1-2 years old
Porcine longissimus dorsi muscle (Čandek-Potokar et al., 1998)	4.6-5 mg/g	83 days

5.4.3. The prospect of three-dimensional imaging

Although the images produced with a compound fluorescent microscope shown in this study clearly show the collagenous sheaths (endomysium and perimysium) for both species, much higher resolution was achieved with confocal microscopy, revealing more detail about collagen fibril organisation and condition of “waviness” (Figure 5.5) (Wolf et al., 2003). Even greater detail could be achieved with the use of two photon microscopy (Sahai et al., 2005, Foolen et al., 2008) which, along with the collagen binding fluorescent probe, would facilitate the visualisation of collagen organisation in detail including imaging of tissues to about one milimetre in depth. However, this would require the development of a custom made mechanical device of suitable size to fit on microscope stage, and was therefore not possible in this study. Optical Projection Tomography (OPT) could in theory also be used to scan an intact muscle rather than a section to help visualise the tissue in three dimensions (Summerhurst et al., 2008). The great advantage of this would be to reduce the damaging consequences of mechanical sectioning, which was a challenging issue in the current study. However, this would require penetration of CNA35 into intact muscle tissue block. As shown in Chapter 4, the binding protein could not penetrate the complex skeletal muscle tissue and staining was purely superficial. Longer incubation with CNA35 is predicted not to help due to the extremely limited penetration of CNA35 observed in Chapter 4, so some potent permeabilising agents have recently been developed for 3D imaging to resolve the problem of limited penetration using a sizeable block of tissue (Susaki and Ueda, 2016, Chung et al., 2013), however these may alter collagen structure and this would need to be explored.

5.4.4. Limitations

In the current study, there were some limitations due to experimental issues as described below.

1. As described in Chapter 4, the Methods section, the tissue needs to go through a series of processing steps prior to sectioning. In the first round of generating the samples, the tissue was fixed overnight, but this led to incomplete fixing, as the core part of tissue remained unfixed. This required repeating the whole experiment with a longer fixation time, which could cause dryness in the tissue that makes sectioning very challenging.
   In most cases, the sections cut well. Although much effort was required to ensure good, intact sections were carried through the analysis, there were some cases where the tissue was dry and brittle causing difficulty in saving the sections while cutting. In some cases, the tissue detached from the slides in different washing steps prior to exposure to CNA35.

2. Challenges associated with sectioning of longitudinal sections led to having few slides to work with (Table 5.1). Permysium was successfully observed in only a few cases in porcine tissue. This could be due either to 1) sections not being cut precisely through the longitudinal plane, although this is unlikely as the sections viewed by compound fluorescent microscope revealed that the whole length of the fibres were observable, or 2) the perimysium detached from the whole section during the sectioning process due to brittleness of the sample. Thus, analysis of porcine longitudinal sections was so limited so that it had to be removed from the study. However, understanding the perimysim behaviour viewed through longitudinal sections is important, especially when deformation is in the fibre direction.

5.5. Conclusion

- A three dimensional schematic illustration of perimysium structure and different degrees of waviness/straightness in transverse and longitudinal planes was proposed for the first time to improve our understanding of how perimysium responds to three-dimensional deformations, which can be an important basic model to enhance constitutive models of passive behaviour of skeletal muscle.
- For the first time it was shown that perimysium, which is believed to be the main load bearing structure in skeletal muscle behaves differently under different loading conditions in fibre and cross-fibre directions and in both tension and compression, aligned with the mechanical response and potentially explaining aspects of the behaviour. However no clear reason was found for tension/compression asymmetry. For each loading condition,

collagen straightness in one of the planes, or sometimes in both planes, appear to play a role in resisting externally applied deformations.

- Some differences between perimysium structure across species was observed, which may depend on muscle function.

Chapter 6-A microstructural-geometrical muscle model to assess tension/compression asymmetry

So many books, so little time.

FRANK ZAPPA.

6.1. Introduction

The validity of finite element (FE) models which have been widely used to predict *in vivo* soft tissue responses critically depends on constitutive laws as well as material parameters employed (Taylor and Humphrey, 2009, Sharafi et al., 2011, Sharafi and Blemker, 2010, Sharafi and Blemker, 2011, Blemker et al., 2005, Blemker and Delp, 2005). Since skeletal muscle tissue accounts for a considerable part of human body weight, models predicting its mechanical response are of importance for many biomechanical applications, for instance, impact biomechanics (Meijer et al., 2013), and rehabilitation engineering (Turkoglu et al., 2014, Linder-Ganz et al., 2007).

A substantial effort has recently been made to experimentally obtain the quasi-static and dynamic passive mechanical response of skeletal muscle in both tension and compression (Takaza et al., 2013a,

Calvo et al., 2010, Morrow et al., 2010b, Nie et al., 2011, Van Loocke et al., 2006, Böl et al., 2012, Pietsch et al., 2014). Apart from the fact that skeletal muscle (like the other soft tissues) exhibits nonlinearity, anisotropy, viscoelasticity (Van Loocke et al., 2008, Van Loocke et al., 2006, Böl et al., 2012, Pietsch et al., 2014, Morrow et al., 2010b, Takaza et al., 2013a), tension/compression asymmetry was also observed. It has been shown that in porcine tissue stress-stretch response in tension is about two orders of magnitude larger than in compression in both the fibre and cross-fibre directions (Takaza et al., 2013a). Tension/compression asymmetry was also observed for chicken skeletal muscle as reported in Chapter 3. Aforementioned characteristics present complexity in FE models.

It is believed that muscle microstructure is responsible for mechanical response especially as muscle has a hierarchical connective tissue structure and collagen fibres within muscle connective tissue were observed to reorient by muscle length changes (Lewis and Purslow, 1989, Purslow, 2008, Purslow, 2002, Purslow, 1989, Purslow and Trotter, 1994). Takaza et al. (2014), experimentally assessed the microstructure response of porcine tissue to passive external deformations in both the fibre and cross-fibre directions in compression as well as in tension as an effort to address the asymmetry observed in the tension/compression response. They introduced several parametres to explain the muscle behaviour: the major axis angle to measure the overall orientation of the muscle fibre in the transverse plane,and the major to minor axis ratio to evaluate shape changes in the transverse plane. Takaza et al. (2014) showed that cross sectional area (CSA) decreased for tension in the fibre direction, but increased for compression in the fibre direction. For the cross-fibre tensile and compressive deformations, the CSA increased compared to the control (undeformed) sample. No statistically significant difference in the major/ minor axis ratio was observed between the control and the specimens either stretched or compressed in the fibre direction. However, a statistically significant difference in the major/minor axis ratio was observed between the controls and where the tissue stretched and compressed in the cross-fibre direction. They showed that although the muscle fibres' cross sectional areas are irregular in shape, no preferred major axis direction exists. A similar pattern for deformation applied in the fibre direction for tension and compression was observed. In contrast, deformations in the cross-fibre direction changed the major axis of each muscle fibre. Takaza et al. (2014) concluded that compression compacted muscle fibre cross-sections to make them perpendicular to the direction of the applied deformation, whereas tensile deformations stretched the cross-sections of muscle fibres and the fibres became parallel to the direction of applied deformation. No evidence of structural reorganisation of the endomysium collagen fibres in response to deformation was observed in SEM micrographs. However, the deformation and orientation of the muscle fibres are greatly influenced by the surrounding perimysium, which leads to the conclusion

that the perimysium is likely to be responsible for the tension/compression asymmetry observed in skeletal muscle (Takaza et al., 2014). However, no clear explanation for this behaviour has been presented. In Chapter 5, more detailed assessment of muscle microstructure through confocal images was performed to partially answer this. Simms et al. (2012) had reviewed that there were no adequate constitutive models for passive muscle to observe this asymmetric behaviour. However, Moerman et al. (2016) discussed tension/compression asymmetry in Ogden hyperelastic formulations for isotropic materials using generalised strains including Seth–Hill strains (Seth, 1961, Hill, 1968). They also presented separate control over the nonlinearity and tension/compression asymmetry proposing a novel set of generalised strain tensors, which shows a better-established model at the present. In terms of skeletal muscle modelling, Moerman et al. (2016) formulations may help to identify the role of either the ECM, or the muscle fibres in generating tension/compression asymmetry. The model proposed by them was implemented to show the nonlinear elastic and transversely isotropic behaviour of skeletal muscle tissue in compression using data from Van Loocke et al. (2006).

From a microstructural point of view, Gindre et al. (2013) developed a simplified structural model to show the interaction between one muscle fibre and surrounding connective tissue (endomysium) to explain the muscle mechanical response. For simplicity this model assumed that only a single muscle fibre was enclosed by individual collagen fibres. However, their model could demonstrate the direct interaction between individual muscle fibres and surrounding endomysium. When a muscle is loaded, two items were believed to be involved in the stress response: the connective tissue surrounding muscle fibres and the titin molecules contained inside muscle fibres (Gindre et al., 2013). Their model showed that the collagen networks contribute to muscle stiffness through (1) a longitudinal force resisiting tension and (2) a pressure-induced force on the muscle fibre resisting compression, which partially reflected tension/compression asymmetry (but less than those of experimental studies) (Gindre et al., 2013).

Although Gindre et al. (2013) presented a useful micromechanical model, their model was not capable of predicting the real mechanical response of skeletal muscle in tension and compression. This can be due to this fact that only endomysium surrounding only one muscle fibre was modelled, while perimysium has been shown to have a key role in stress response (Takaza et al., 2014, Purslow, 2010). Therefore, it would be appropriate to develop a structural model to show the role of the perimysium in load bearing. The objective of this Chapter, then, is to make a development on the Gindre et al. (2013) model to show how perimysium as muscle ECM and a group of muscle fibres (fascicle) may be responsible for the asymmetrical behaviour of muscle tissue witnessed in tension and compression experiments.

6.2. Methods

The model is composed of a muscle fascicle enclosed by perimysium (see Figure 6.1). The muscle fascicle was modelled as an incompressible prism containing groups of muscle fibres. Muscle fascicle represents the contribution of muscle fibres (containing titin molecules) in stress response. Each muscle fibre is surrounded by endomysium, however, only perimysium was assumed to play a role in muscle passive response since skeletal muscle contains much more perimysium than endomysium (Purslow, 2010). Perimysium is represented as a sheet surrounding one muscle fascicle containing many collagen fibres tightly attached to each other, all aligned in a parallel pattern and at a known angle (θ) with respect to muscle fibres (see Figure 6.1). Although, perimysium does not create a distinct sheath around one fascicle, instead it is a shared structure between two fascicles (Purslow and Trotter, 1994), in this model it was assumed that muscle fascicle is enclosed by one perimysium sheet. Tensile and compressive deformations in the fibre and cross-fibre directions are applied to the muscle. A squared cross sectional shape was assumed for muscle as per the preliminary observations of muscle cross sections in two species. Constant volume was also assumed for the muscle fascicle (Van Loocke et al., 2006, Gindre et al., 2013). The perimysium was assumed to remain attached to fascicle's surface area, therefore, it deforms with the fascicle. The aim of model is to calculate the whole muscle force which contains the longitudinal force developed by a group of muscle fibres ($F_{muscle\ fasicle}$), and the force developed by perimysium sheet (F_{sheet}). F_{sheet} is either the "longitudinal force directly developed by perimysium sheet" (F_{sheet}) in tension in the fibre direction (Tension-F) and compression in the cross-fibre direction (Compression-XFibre) deformations or the "pressure-induced longitudinal force developed by perimysium" in compression in the fibre direction (Compression-Fibre) or tension in the cross-fibre direction (Tension-XFibre) deformations.

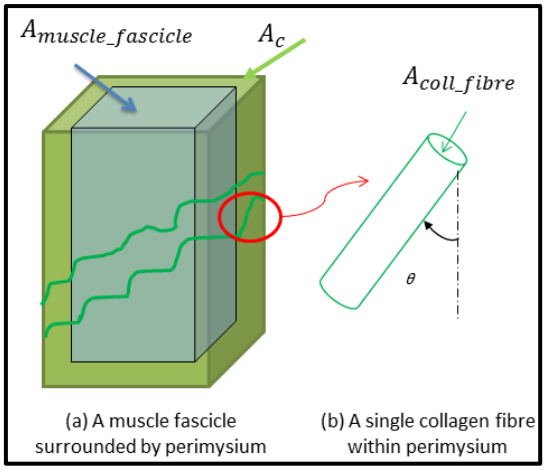

Figure 6. 1-Schematic representation of muscle fascicle surrounded by its connective tissue called perimysium. (a) A muscle fascicle with the cross sectional area of $A_{muscle_fascicle}$ surrounded by perimysium with the cross sectional are of A_c. Perimysium consists of parallel collagen fibres aligned at an angle of θ with respect to the muscle fibre direction (The Figure schematically shows the collagen fibres discrete). (b) A single collagen fibre with the cross sectional area of A_{coll_fibre}.

6.2.1. Contribution of muscle fibres in stress response

$F_{muscle\ fasicle}$ is F_{titin} developed in one single muscle fibre multiplied by the number of muscle fibres present in one fascicle (n_f) as formulated in equation (6.1):

$$F_{muscle\ fasicle} = n_f F_{titin} \tag{6.1}$$

The total titin force F_{titin} is then calculated as a function of the force developed in one single titin molecule (f_{titin}) as follow (Gindre et al., 2013):

$$F_{titin} = f_{titin} n_1 A_{muscle_fibre} \tag{6.2}$$

Where, n_1 represents the total number of titin molecules per unit area in a muscle fibre (in m^{-2}) and A_{muscle_fibre} is the cross sectional area of one muscle fibre. The muscle fibres contribute in load bearing only where stretched (Tension-Fibre and Compression-XFibre deformations). When the muscle is stretched it shows a low stiffness at low stretches and very high stiffness when approaching up to a limiting stretch. Beyond the limiting stretch (when the tissue tears), the molecule starts failing. Therefore, this behaviour is usually modelled by a wormlike chain model (Leake et al., 2004, Kellermayer et al., 2003, Gindre et al., 2013). The model expresses f_{titin} as a function of the molecule extension as follow:

$$f_{titin} = \frac{K_b T}{L_p}\left(\frac{\Delta z}{L_c} + \frac{1}{4\left(1-\frac{\Delta z}{L_c}\right)^2} - \frac{1}{4}\right) \tag{6.3}$$

Δz is the stretch in one titin molecule. L_c is the molecule's contour length (the maximal length of the molecule when completely unfolded after force application). L_p is the persistence length of the molecule. K_b and *T* are the Boltzmann constant and the absolute temperature respectively.

The extension of a single titin molecule in a muscle fibre can be written as a function of λ_{muscle_fibre} :

$$\Delta z(\lambda) = \frac{(\lambda_{muscle_fibre} - 1)}{n_2} \quad (6.4)$$

Where n_2 is the number of titin molecules by length units (in m^{-1}) at rest length along the muscle fibre. $F_{muscle\ fasicle}$ can therefore be expressed as a function of λ_{muscle_fibre} only. In compression ($\lambda_{muscle_fibre} < 1$), $F_{muscle\ fasicle}$ is zero.

$$\mathrm{F_{muscle\ fasicle}} = n_f A_{muscle_fibre} n_1 \frac{K_b T}{L_p} \left(\frac{\lambda - 1}{n_2 L_c} + \frac{1}{4\left(1 - \frac{\lambda - 1}{n_2 L_c}\right)^2} - \frac{1}{4}\right) \quad \text{if} \quad \lambda_{muscle_fibre} > 1 \quad (6.5)$$

Therefore, to calculate $F_{muscle\ fasicle}$, the parameters defining mechanical properties of one molecule (L_c and L_p), and n_1 and n_2 which are structural parameters of a muscle fibre, are required.

6.2.2. Contribution of perimysium in stress response

The force developed in perimysium depends on type of deformation (tension or compression), as well as the direction of applied deformation (in the fibre or cross-fibre direction) as explained in the next sections.

6.2.2.1. Perimysium contribution to longitudinal force in Tension-Fibre deformation

When the tissue is stretched in the muscle fibre direction (Tension-Fibre), perimysium sheet elongates in the longitudinal direction resulting in smaller cross sectional area (see Figure 6.2b), and the stress developed in perimysium $\sigma_{sheet-tenf}$ is defined as shown in equation (6.6), where λ_{sheet}^{true} is greater than one.

$$\sigma_{sheet-tenf} = E_{sheet} . \ln(\lambda_{sheet}^{true}) \quad if\ \lambda_{sheet}^{true} > 1 \quad (6.6)$$

E_{sheet} denotes the Elastic modulus of collagen, which is the building element of perimysium (Gindre et al., 2013). Perimysium contributes to stress only when stretched. The apparent perimysium stretch is the same as the stretch in muscle fibres ($\lambda_{sheet}^{app} = \lambda_{muscle_fibre} > 1$). At the resting length of the muscle, the perimysium has a certain waviness (Lepetit, 2008, Lepetit, 1991). Therefore, the stretch

in the longitudinal direction (direction of applied stretch) will produce stress in the sheet only by considering a certain amount of $w2$ (the waviness of perimysium sheets in the longitudinal direction, see Chapter 5). So, the effective (true) stretch in perimysium (λ_{sheet}^{true}) is corrected as follows:

$$\lambda_{sheet}^{true} = \frac{\lambda_{muscle_fibre}}{w2} \tag{6.7}$$

The term $\sigma_{sheet-tenf}$ results in a force acting along the perimysium sheet in the longitudinal direction in Tension-Fibre deformation.

$$F_{sheet_tenf} = \sigma_{sheet-tenf}.A_{c-tenf} \tag{6.8}$$

Where, A_{c-tenf} is the true cross-sectional area of a perimysium sheet as shown in Figure 6.2b. The muscle is stretched in the fibre direction with a stretch ratio of (λ_{L-tenf}). The stretch ratios in other transverse directions are equal due to transversely isotropic behaviour observed experimentally for this deformation (see Chapter 3). The strain in the longitudinal direction (ε_{L-tenf}) is calculated as written in equation (6.9):

$$\varepsilon_{L-tenf} = ln(\lambda_{L-tenf}) \tag{6.9}$$

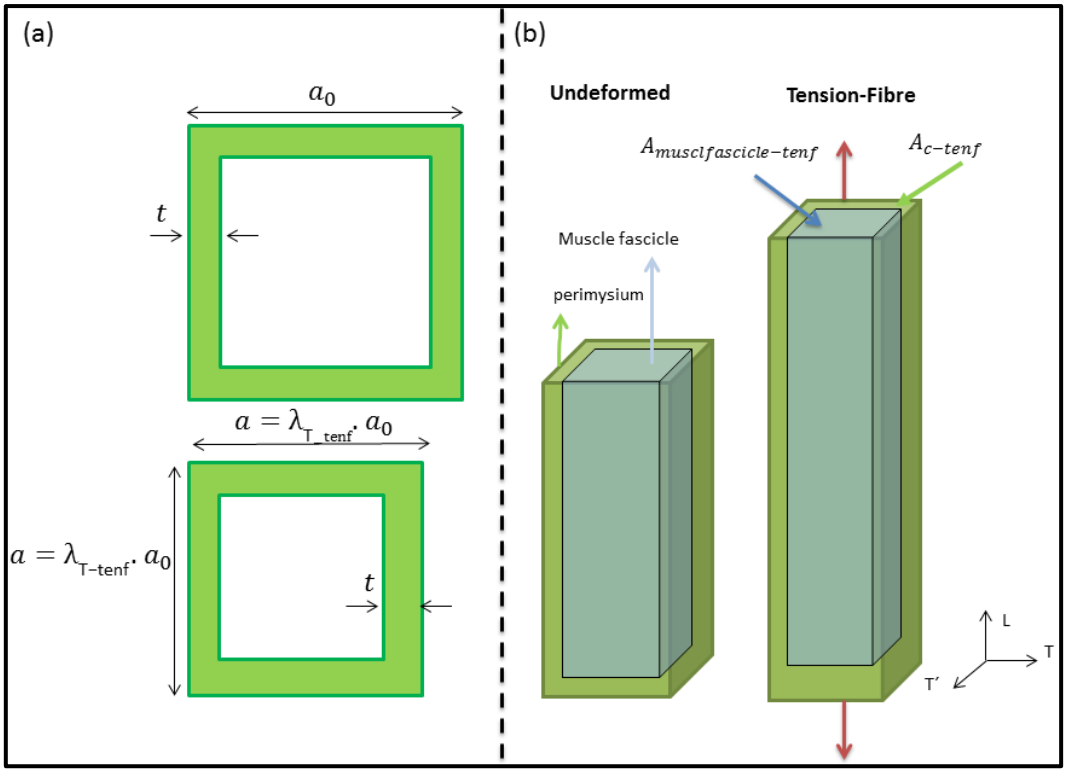

Figure 6. 2-Schematic representation of a muscle fascicle surrounded by perimysium under tension in the fibre direction (Tension-Fibre) deformation.

(a) The cross sections of the muscle fascicle and perimysium before and after applied deformation, (b) The muscle fascicle shown in "undeformed" form and after applied deformation showing $A_{musclefascicle-tenf}$ as the cross sectional of deformed muscle fascicle and A_{c-tenf} as the cross sectional area of perimysium after deformation. a_0 is the initial edge of squared cross section. a is the edge of perimysium cross section after applied deformation; t is the perimysium thickness (remains unchanged). λ_{T-tenf} is the stretch ratio in *T* direction. *L* indicate the longitudinal muscle fibre direction, *T* & *T'* are the transverse directions. Red arrows indicate the direction of applied deformation.

The transverse strains are calculated using the Poisson's ratio value of 0.5 reported in Chapter 3 (equation (6.10)), and the stretch ratios are accordingly calculated as shown in equations (6.11):

$$\varepsilon_{T-tenf} = \varepsilon_{T'-tenf} = -\nu_{LT-tenf}\, \varepsilon_{L-tenf} \tag{6.10}$$

$$\lambda_{T-tenf} = \lambda_{T'-tenf} = e^{\varepsilon_{T-tenf}} \tag{6.11}$$

Where, $\nu_{LT-tenf}$ is the Poisson's ratio for the transverse induced deformation when the tissue is stretched along the fibres. A_{c-tenf} can be calculated as $A_{c-tenf} = \lambda_{T-tenf}.A_{c0}$ (see Figure 6.2a), where A_{c0} is initial cross sectional area of perimysium. Given the experimental data reported in Chapter 3, the initial cross sectional area of a muscle sample is known so by introducing the percentage of connective tissue (p_c) in the cross sectional area of a muscle sample, A_{c0} can be found.

As a result the longitudinal force in perimysium after Tension-Fibre deformation can be found as $F_{sheet_tenf} = E_{sheet}.ln\left(\frac{\lambda_{L-tenf}}{w2}\right).\lambda_{T-tenf}.A_{c0}$.

6.2.2.2. Perimysium contribution to pressure-induced longitudinal force in Tension-XFibre deformation

As shown in Figure 6.3b, in Tension-XFibre deformation, perimysium undergoes a circumferential expansion generating hydrostatic pressure and resulting in a shorter muscle fascicle. Since the muscle is deformed across the muscle fibres, it does not show isotropy in the plane perpendicular to the applied deformation, therefore the change in the edge of the perimysium cross section is not equal in the T and T' directions. The stretch ratios in other directions are calculated using Poisson's ratio values for Tension-XFibre ($\nu_{TT'-tenxf} = 0.17$ and $\nu_{TL-tenxf} = 0.83$ as reported in Chapter 3) and applied stretch ratio ($\lambda_{\mathrm{T-tenxf}}$). The strain in the T direction (the direction of applied deformation) is calculated as $\varepsilon_{T-tenxf} = ln(\lambda_{T-tenxf})$. The strain in the L and T'directions are then calculated as follows:

$$\varepsilon_{T'-tenxf} = -\nu_{TT'-tenxf}\ \varepsilon_{T-tenxf} \tag{6.12}$$

$$\varepsilon_{L-tenxf} = -\nu_{TL-tenxf}\ \varepsilon_{T-tenxf} \tag{6.13}$$

Where, $\upsilon_{\mathrm{TL-tenxf}}$ is the Poisson's ratio for the induced deformation in the fibre (longitudinal) direction, and $\upsilon_{TT'-tenxf}$ is the Poisson's ratio for the induced deformation in the other transverse direction when the tissue is deformed across the fibres. The stretch ratios are then known using equations (6.14) and (6.15):

$$\lambda_{T'-tenxf} = e^{\varepsilon_{T'-tenxf}} \tag{6.14}$$

$$\lambda_{L-tenxf} = e^{\varepsilon_{L-tenxf}} \tag{6.15}$$

Consequently, the edges of perimysium cross sections will be $a_1 = \lambda_{T-tenxf}\ a_0$ and $a_2 = \lambda_{T\prime-tenxf}\ a_0$(see Figure 6.3a). The force developed circumferentially generates a pressure *P* inside the muscle fascicle (see Figure 6.3c). This pressure then results in a longitudinal force F_{sheet_tenxf}.

$$F_{sheet_tenxf} = A_{musclefascicle-tenxf}P \tag{6.16}$$

Equation (6.6) is then used to define the stress developed in the perimysium sheet ($\sigma_{sheet-tenxf} = E_{sheet}.ln(\lambda_{sheet}^{true})$). λ_{sheet}^{true} in this case is calculated using the transverse stretch in the T direction (direction of applied deformation), so $\lambda_{sheet}^{true} = ln\left(\frac{\lambda_{T-tenxf}}{w1}\right)$.

The force balance for the half-muscle fascicle considering one perimysium sheet can now be written as follows (see Figure 6.3c):

$$\sigma_{sheet-tenxf}\ (2tL) = P\big(\lambda_{T-tenxf}.a_0 - 2t\big)L \tag{6.17}$$

Therefore, pressure inside the muscle fascicle will be:

$$P = \frac{2t}{\lambda_{T-tenxf}.a_0 - 2t}\sigma_{sheet-tenxf} \tag{6.18}$$

Perimysium thickness is assumed to be very small and unchanged, so t^2 in the calculations can be ignored. $A_{muslcefascicle-tenxf}$ and $A_{c-tenxf}$ are then calculated as follows (see Figure 6.2a):

$$A_{musclefascicle-tenxf} = \big(\lambda_{T-tenxf}.a_0 - 2t\big)\big(\lambda_{T'-tenxf}.a_0 - 2t\big) \tag{6.19}$$

$$A_{c-tenxf} = \lambda_{T-tenxf}\lambda_{T'-tenxf}.{a_0}^2 - \big(\lambda_{T-tenxf}.a_0 - 2t\big)\big(\lambda_{T'-tenxf}.a_0 - 2t\big) = 2ta_0(\lambda_{T-tenxf} + \lambda_{T'-tenxf}) \tag{6.20}$$

By substituting equations (6.18) and (6.19) in equation (6.16), F_{sheet_tenxf} is found as shown below:

$$F_{sheet_tenxf} = \big(\lambda_{T-tenxf}.a_0 - 2t\big)\big(\lambda_{T'-tenxf}.a_0 - 2t\big).\frac{2t}{\lambda_{T-tenxf}.a_0 - 2t}\sigma_{\text{sheet-tenxf}} = 2t\lambda_{T'-tenxf}.a_0\ \sigma_{\text{sheet-tenxf}} = \frac{\lambda_{T'-tenxf}}{\lambda_{T-tenxf}+\lambda_{T'-tenxf}}A_{c-tenxf}\ \sigma_{\text{sheet-tenxf}} \tag{6.21}$$

Where, $A_{c-tenxf} = \frac{\lambda_{T-tenxf}+\lambda_{T'-tenxf}}{2}\ A_{c0}$ and $\sigma_{sheet-tenxf} = E_{sheet}.\ ln\left(\frac{\lambda_{T-tenxf}}{w1}\right)$. Therefore, the longitudinal force induced by internal pressure in muscle can be found as $F_{sheet_tenxf} = \frac{1}{2}E_{sheet}.\ln\left(\frac{\lambda_{T-tenxf}}{w1}\right)\lambda_{T'-tenxf}\ A_{c0}.\ w1$ is the perimysium sheet waviness observed in the transverse direction (see Chapter 5).

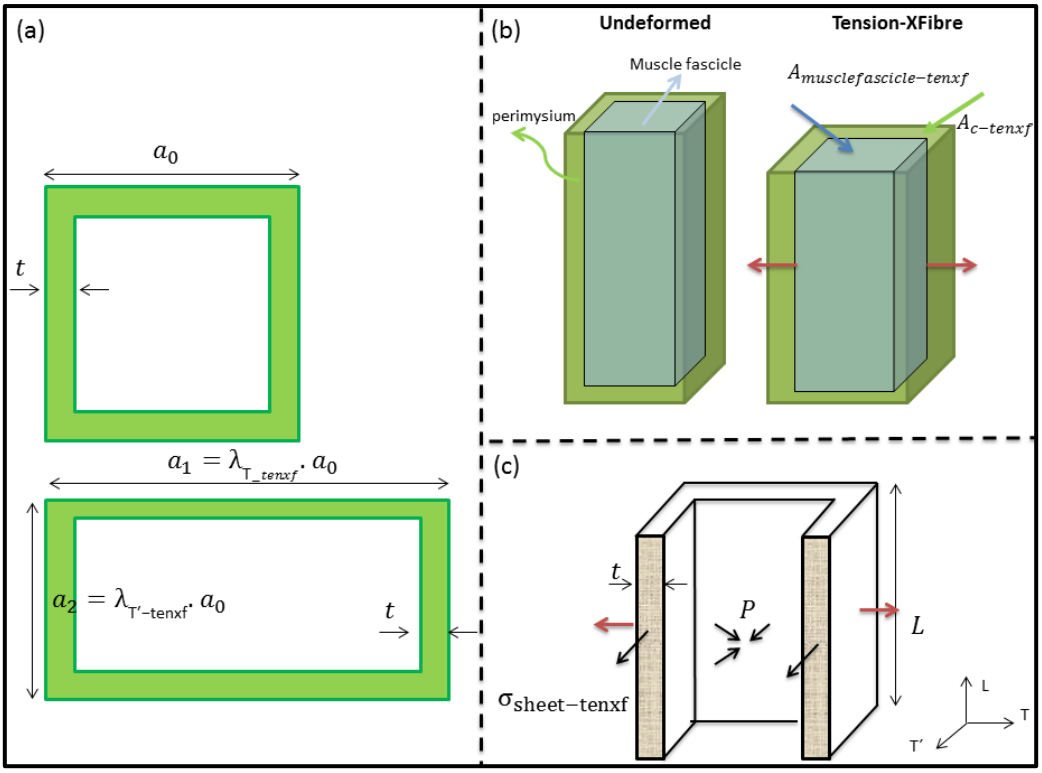

Figure 6. 3-Schematic representation of a muscle fascicle surrounded by perimysium under tension in the cross-fibre direction (Tension-XFibre) deformation.

(a) The cross sections of the muscle fascicle and perimysium before and after applied deformation, (b) The muscle fascicle shown in "undeformed" form and after applied deformation showing $A_{musclefascicle-tenxf}$ as the cross sectional area of deformed muscle fascicle and $A_{c-tenxf}$ as the cross sectional area of perimysium after deformation. a_0 is the initial edge of squared cross section. a_1 and a_2 are length and width of perimysium cross section after applied deformation; *t* is the perimysium thickness (remains unchanged), (c) Perimysium surrounding half-muscle fascicle to consider the circumferential stress developed in perimysium. L is the length of muscle fascicle, and $\sigma_{sheet-tenxf}$ indicate circumferential stress developed in perimysium due to Tension-XFibre deformation. $\lambda_{T-tenxf}$ and $\lambda_{T'-tenxf}$ are the stretch ratios in *T* and T'directions. L indicate the longitudinal muscle fibre direction, *T* & *T'* are the transverse directions. Red arrows indicate the direction of applied deformation.

6.2.2.3. Perimysium contribution to pressure-induced longitudinal force in Compression-Fibre deformation

In Compression-Fibre deformation, perimysium also undergoes a circumferential expansion generating hydrostatic pressure (see Figure 6.4c). Since the muscle is transversely isotropic (with the Poisson's ratio values of 0.5-see Chapter 3), the edges of perimysium cross section are equally expanded in both T and T' directions (the square shape is retained). For simplicity the final edge of the cross section is called a. The circumferentially developed force generates a pressure *P* the same as shown in section 6.2.2.2. This pressure then results in a longitudinal force F_{sheet_compf}.

$$F_{sheet_compf} = A_{musclefascicle-compf} P \tag{6.22}$$

As shown in equation (6.6), the stress developed in the perimysium sheet will be $\sigma_{\text{sheet}-\text{compf}} = \text{E}_{\text{sheet}}.\ln\left(\lambda_{\text{sheet}}^{\text{true}}\right).\ \lambda_{sheet}^{true}$ in this case is calculated using the transverse stretch ($\lambda_{T-compf}$).

By writing the force balance for the half-muscle fascicle considering one perimysium sheet (see Figure 6.4c):

$$\sigma_{sheet-compf}\ (2tL) = P(a-2t)L \tag{6.23}$$

Therefore the pressure inside the muscle fascicle is as follows:

$$P = \frac{2t}{a-2t}\sigma_{\text{sheet}-compf} \tag{6.24}$$

$A_{musclefascicle-compf}$ and $A_{c-compf}$ are calculated as follows (see Figure 6.4a):

$$A_{musclefascicle-compf} = (a-2t)(a-2t) = a^2 - 4at \tag{6.25}$$

$$A_{c-compf} = a^2 - (a^2 - 4at) = 4at \tag{6.26}$$

By substituting equations (6.24) and (6.25) in equation (6.22), $F_{sheet_comp\ f}$ is found as follow:

$$F_{sheet_compf} = a(a-4t).\frac{2t}{a-2t}\sigma_{sheet-compf} = 2at\sigma_{sheet-compf} = \frac{A_{c-compf}}{2}\sigma_{sheet-compf} \tag{6.27}$$

Where, $A_{c-compf} = \lambda_{T-compf}.A_{c0}$. Therefore, the longitudinal force in perimysium after Compression-Fibre deformation can be written as:

$$F_{sheet_compf} = \frac{1}{2}E_{sheet}.ln\left(\frac{\lambda_{T-compf}}{w1}\right).\lambda_{T-compf}.A_{c0}.$$

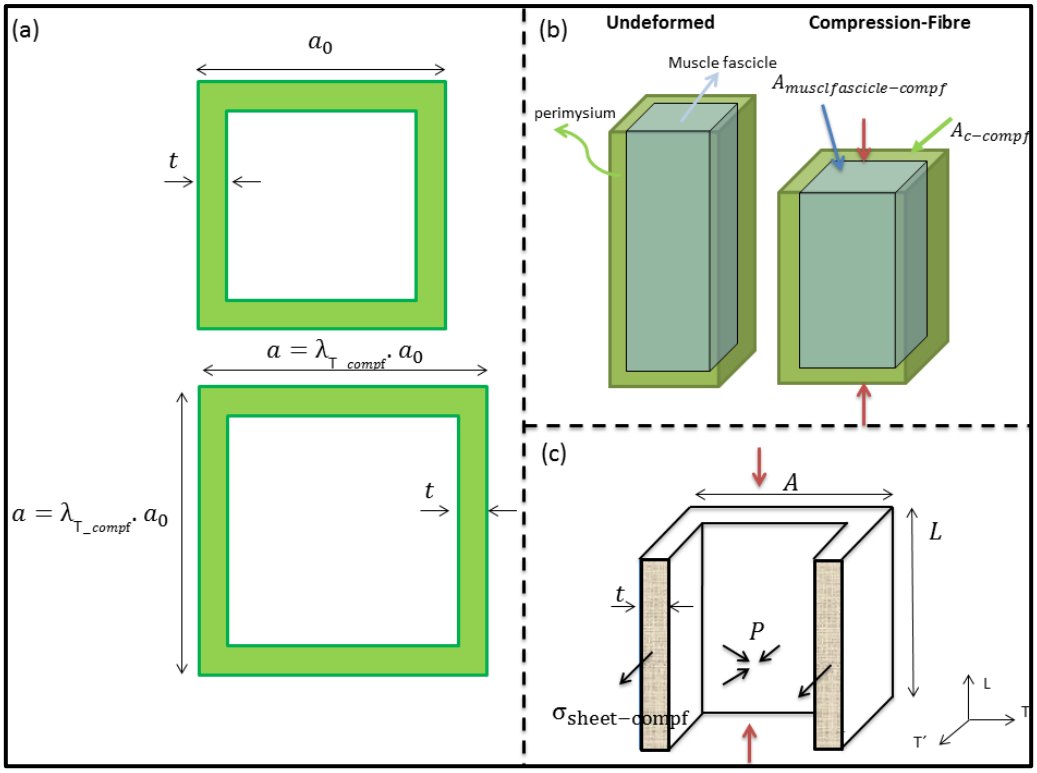

Figure 6. 4-Schematic representation of a muscle fascicle surrounded by perimysium under compression in the fibre direction (Compression-Fibre) deformation.

(a) The cross sections of the muscle fascicle and perimysium before and after applied deformation, (b) The muscle fascicle shown in "undeformed" form and after applied deformation showing $A_{musclefascicle-compf}$ as the cross sectional area of deformed muscle fascicle and $A_{c-compf}$ as the cross sectional area of perimysium after deformation. a_0 is the initial edge of squared cross section. a is the edge perimysium cross section after applied deformation; *t* is the perimysium thickness (remains unchanged), (c) Perimysium surrounding half-muscle fascicle to consider the circumferential stress developed in perimysium. L is the length of muscle fascicle, and $\sigma_{sheet-compf}$ indicate circumferential stress developed in perimysium due to Tension-XFibre deformation. $\lambda_{T-compf}$ is the stretch ratio in *T direction. L* indicate the longitudinal muscle fibre direction, *T & T'* are the transverse directions. Red arrows indicate the direction of applied deformation.

6.2.2.4. Perimysium contribution to longitudinal force in Compression-XFibre deformation

In Compression-XFibre deformation, perimysium stretches in the longitudinal direction, the force developed in perimysium ($\sigma_{sheet-compxf}$) is defined as $F_{sheet_compxf} = \sigma_{sheet-compxf}.A_{c-compxf}$.

No transverse isotropy is observed due to applied deformation across the muscle fibres, so the change in the edges of the perimysium cross section are different in the T and T' directions. The tissue is deformed with a known stretch ratio ($\lambda_{T-compxf}$), the stretch ratios in other directions are calculated using Poisson's ratio values for Compression-XFibre ($\nu_{TT'-compxf} = 0.64$ and $\nu_{TL-compxf} = 0.34$).

The strain in the direction of applied deformation (*T*) is calculated as $\varepsilon_{T-compxf} = ln(\lambda_{T-compxf})$. The strains in the L and T'directions are then calculated as follows:

$$\varepsilon_{T'-compxf} = -\nu_{TT'-compxf}\ \varepsilon_{T-compxf} \tag{6.28}$$

$$\varepsilon_{L-compxf} = -\nu_{TL-compxf}\ \varepsilon_{T-compxf} \tag{6.29}$$

Where, $\upsilon_{TL-compxf}$ is the Poisson's ratio for the induced deformation in the fibre direction, and $\upsilon_{TT'-compxf}$ is the Poisson's ratio for the induced deformation in the other transverse direction when the tissue is deformed across the fibres. The stretch ratios are then known using equations (6.30) and (6.31):

$$\lambda_{T'-compxf} = e^{\varepsilon_{T'-compxf}} \tag{6.30}$$

$$\lambda_{L-compxf} = e^{\varepsilon_{L-compxf}} \tag{6.31}$$

Consequently, the edges of perimysium cross sections will be $a_1 = \lambda_{T-compxf}\, a_0$ and $a_2 = \lambda_{\mathrm{T'-compxf}}\, a_0$ (see Figure 6.5a).

Where, $A_{c-compxf} = \frac{\lambda_{T-compxf}+\lambda_{T'-compxf}}{2}\, A_{c0}$ and $\sigma_{sheet-compxf} = E_{sheet}.\, ln\left(\frac{\lambda_{L-compxf}}{w2}\right)$. Therefore, the longitudinal force in muscle can be found as $F_{sheet_compxf} = E_{sheet}.\ln\left(\frac{\lambda_{L-compxf}}{w2}\right).\frac{\lambda_{T-compxf}+\lambda_{T'-compxf}}{2}\, A_{c0}$.

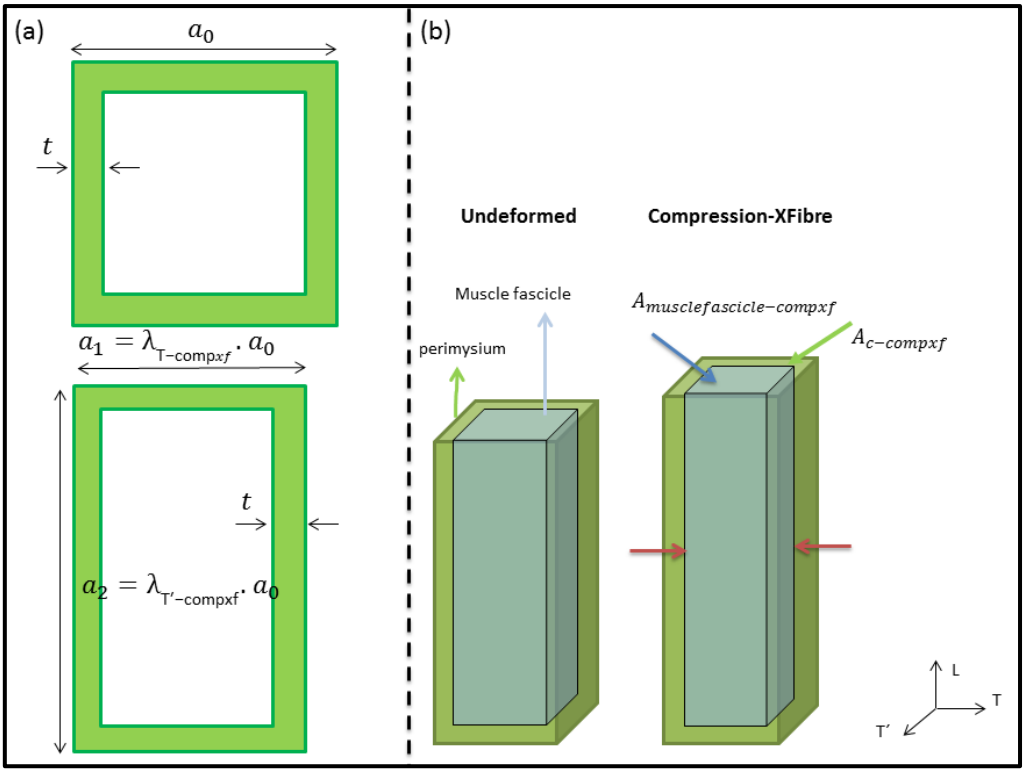

Figure 6. 5-Schematic representation of a muscle fascicle surrounded by perimysium under compression in the cross-fibre direction (Compression-XFibre) deformation.

(a) The cross sections of the muscle fascicle and perimysium before and after applied deformation, (b) The muscle fascicle shown in "undeformed" form and after applied deformation showing $A_{musclefascicle-compxf}$ as the cross sectional area of deformed muscle fascicle and $A_{c-compf}$ as the cross sectional area of perimysium after deformation. a_0 is the initial edge of squared cross section. a_1 and a_2 are width and length of perimysium cross section after applied deformation; *t* is the perimysium thickness (remains unchanged). $\lambda_{T-tenxf}$ and $\lambda_{T'-tenxf}$ are the stretch ratios in *T* and *T'* directions. *L* indicate the longitudinal muscle fibre direction, *T* & *T'* are the transverse directions. Red arrows indicate the direction of applied deformation.

Table 6.1 summarises the model equations. The equations are all independent of the length of muscle fibre. The model was implemented in Matlab (the Mathworks, Natick, Ma USA).

Table 6. 1-Summary of model equations in different deformation applied in different directions

Deformation type	Equation for modelling	
Tension-Fibre	$\mathrm{F_{tot}} = \mathrm{F_{muscle\ fasicle}} + \mathrm{F_{sheet_tenf}}$	$F_{sheet_tenf} = E_{sheet}.ln\left(\frac{\lambda_{L-tenf}}{w2}\right).\lambda_{T-tenf}.A_{c0}$
Tension-XFibre	$F_{tot} = F_{sheet_tenxf}$	$F_{sheet_tenxf} = \frac{1}{2}E_{sheet}.ln\left(\frac{\lambda_{T-tenxf}}{w1}\right)\lambda_{T'-tenxf}\,A_{c0}$
Compression-Fibre	$F_{tot} = F_{sheet_compf}$	$F_{sheet_compf} = \frac{1}{2}E_{sheet}.\ln\left(\frac{\lambda_{T-compf}}{w1}\right).\lambda_{\mathrm{T-compf}}.A_{c0}$
Compression-XFibre	$F_{tot} = F_{muscle\ fasicle} + F_{sheet_compxf}$	$F_{sheet_compxf} = E_{sheet}.\ln\left(\frac{\lambda_{L-compxf}}{w2}\right).\frac{\lambda_{T-compxf} + \lambda_{T'-compxf}}{2}\,A_{c0}$
		$\mathrm{F_{muscle\ fasicle}} = n_f A_{muscle_fibre} n_1 \frac{K_b T}{L_p}\left(\frac{\lambda-1}{n_2 L_c} + \frac{1}{4\left(1-\frac{\lambda-1}{n_2 L_c}\right)^2} - \frac{1}{4}\right)$

6.2.3. Model parameters

Table 6.2 shows the values used in the current model. The values reported for collagen Elastic modulus mostly lies between 200-570 MPa (Shen et al., 2008, Yang et al., 2008, van der Rijt et al., 2006).

As reviewed in Chapter 2, Lewis and Purslow (1989) reported that in bovine muscle perimysium collagen ranges from 0.43% to 4.6% of muscle dry weight, therefore a range of 0.5- 3% was chosen for this model as the percentage of connective tissues in muscle (Gindre et al., 2013).

Waviness in muscle connective tissues (endomysium and perimysium) was reported from 1.05 to 1.3 (Lepetit, 2008, Lepetit, 1991). Since in Chapter 5 it was stated that $w1$ and $w2$ represent one degree (level) of waviness), therefore, in the model $w1$ and $w2$ were assumed to be similar.

Approximately 20–80 muscle fibres ($\mathrm{n_f}$) are grouped together in a muscle fascicle (Rowe, 1974). So $\mathrm{n}_f = 50$ was used in the model.

The number of titin molecules were reported in some studies (Linke et al., 1998, Maruyama, 1994). A wide range of values for contour and persistence lengths for a titin molecule was reported as listed in Table 6.2 (Leake et al., 2004, Kellermayer et al., 2003). However, Gindre et al. (2013) showed their model was not very sensitive to the titin filament parameters. Therefore, in this model similar to Gindre et al. (2013) model, average values for wormlike chain parameters and number of titin molecules were used for simplicity.

Table 6. 2-Literature range and model range of values used for model parameters.

Perimysium Parameters	Description	Model value	Literature range	Unit
E_{sheet}	Collagen Elastic modulus	[200×10^6 -800×10^6]	[200×10^6 -860×10^6]	Pa
p_c	Percentage of connective tissue	[0.5-3]	[0.5-3]	%
$w1$ & $w2$	Perimysium sheet waviness	[1.05-1.3]	[1.05-1.3]	-
Muscle Parameters				
n_f	Number of muscle fibres in one fascicle	50	20-80	-
k_b	Boltzman constant	1.38.10^{-23}	1.38.10^{-23}	JK^{-1}
L_p	Titin persistence length	7.5.10^{-9}	[1.5×10^{-9} -13.5×10^{-9}]	m
L_c	Titin contour length	2100.10^{-9}	[900×10^{-9} -3400×10^{-9}]	m
n_1	Number of titin molecules per units of cross-sectional area of muscle fibre	3.10^{15}	[0.8×10^{15} -6.28×10^{15}]	m^{-2}
n_2	Number of titin molecules per units of length along the muscle fibre	10^6	[0.77×10^6 -1.25×10^6]	m^{-1}

6.3. Results

6.3.1. General findings

6.3.1.1. Muscle fascicle stress response

Figure 6.6 shows the stress-stretch response of the muscle fascicle which is made of a group of muscle fibres ($n_f = 50$) without any perimysium collagens. The Figure shows that when the muscle is under compression applied in the fibre direction, the muscle fibres bear no load. However, in tension applied in the fibre direction ($\lambda > 1$) the stress increases nonlinearly by an increase in stretch ratio.

It also should be noted when the muscle is stretched across the fibres, the fibres bear no load as they shorten, whereas in compression applied in the cross-fibre direction the muscle fibres undergo a stretch and they will then resist the load.

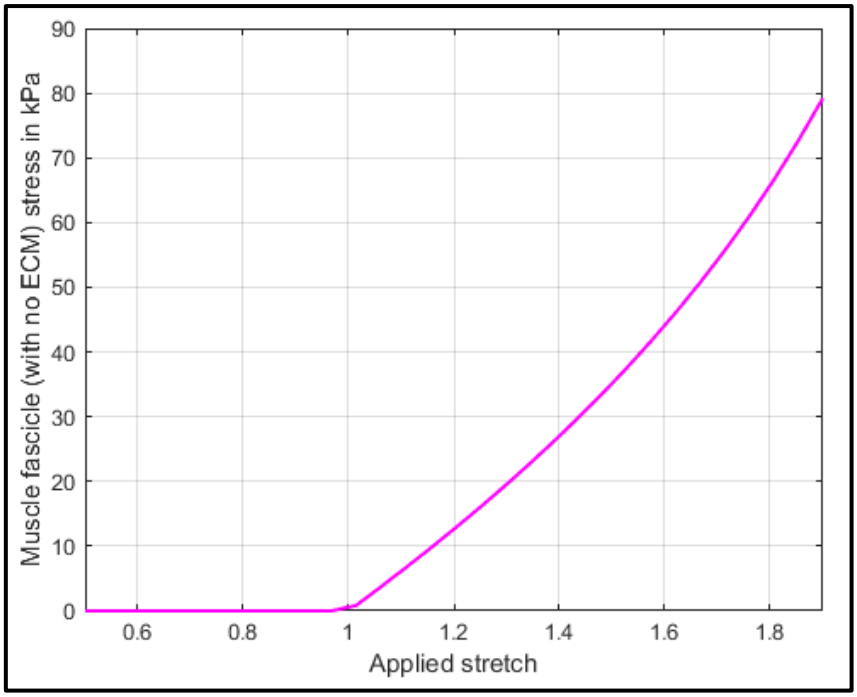

Figure 6. 6-Stress response of the muscle fascicle excluding its connective tissue (perimysium) versus the applied stretch in the fibre direction.

6.3.1.2. Perimysium sheet stress response

The nonlinear and anisotropic response of the whole muscle as well as perimysium was well obtained by the model as shown in Figure 6.7, which demonstrates the stress response of both perimysium (Figure 6.7a) and the whole muscle (Figure 6.7b) for a constant waviness of 1.18 and the Elastic modulus of 500 MPa and 1.75% connective tissue. Figure 6.7b shows the stress response of the whole muscle by combining the muscle fibres' response shown in Figure 6.6 and the perimysium response illustrated in Figure 6.7a. It also compares the capability of the model using the average values for input parameters to predict the mean compressive and tensile passive response of chicken tissue. The model could also capture asymmetry; the stress response in tension is stiffer than compression in both the fibre and cross-fibre directions. However, compared to the experimental results (see Chapter 3), it presented a stiffer response in compression applied in both directions and less stiff response in tension applied in the cross-fibre direction (Tension-XFibre), therefore, less asymmetric response was observed by the model. The model predicts that compression in the cross-fibre direction yields a stiffer response than compression in the fibre direction as do the experiments, but in tension, the response in the fibre direction is stiffer than the cross-fibre deformation, which is different to the experiments.

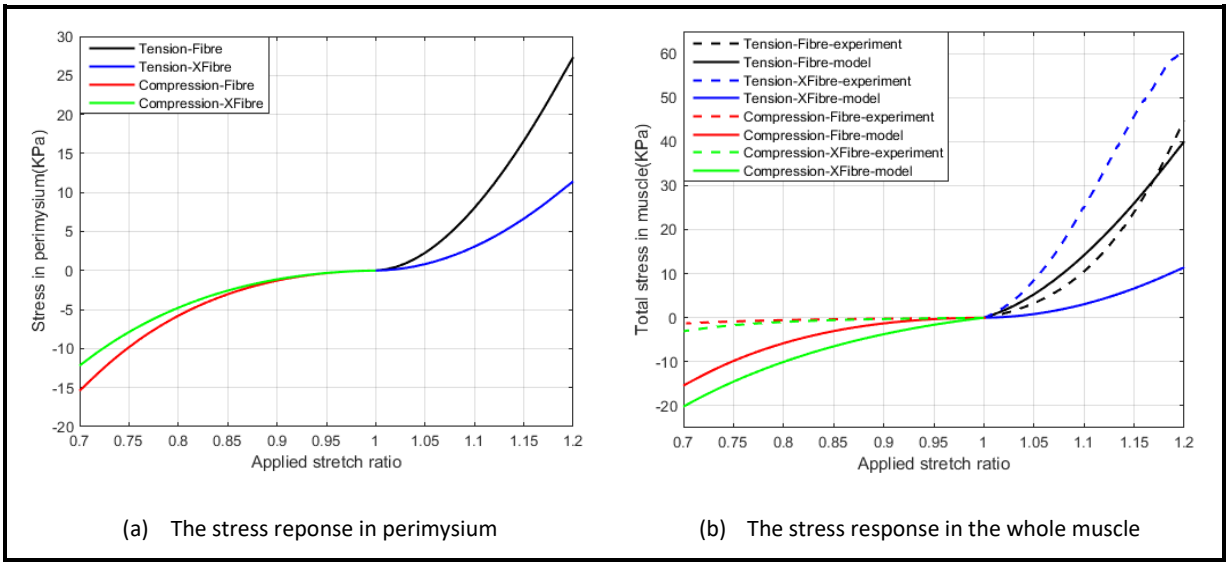

(a) The stress reponse in perimysium (b) The stress response in the whole muscle

Figure 6. 7-Model-predicted stress response in tension and compression in both the fibre and cross-fibre directions for the whole muscle as well as perimysium; (a) the stress-stretch response in perimysium, (b) the stress-stretch response in the whole muscle (fascicle+perimysium) in comparison with the chicken experimental data. This base model is based on the middle values for the variables ($w = 1.18$, $E_{sheet} = 500\ MPa$ and $pc = 1.75\%$).

6.3.2. Sensitivity analysis

6.3.2.1. Sensitivity to Elastic modulus (E_{sheet}) and percentage of connective tissue (p_c)

The model showed sensitivity to perimysium parameters; perimysium sheet stiffness (E_{sheet}) and percentage of connective tissues in muscle sample (p_c). The perimysium contribution to stress is linearly linked to these two parameters. Figure 6.8 demonstrates the response range of the model and its comparison to the chicken mechanical response for 4 values of E_{sheet} by keeping w=1.18 and $p_c = 1.75\%$ constant. As expected, perimysium in the model shows a stiffer stress response by an increase in Elastic modulus.

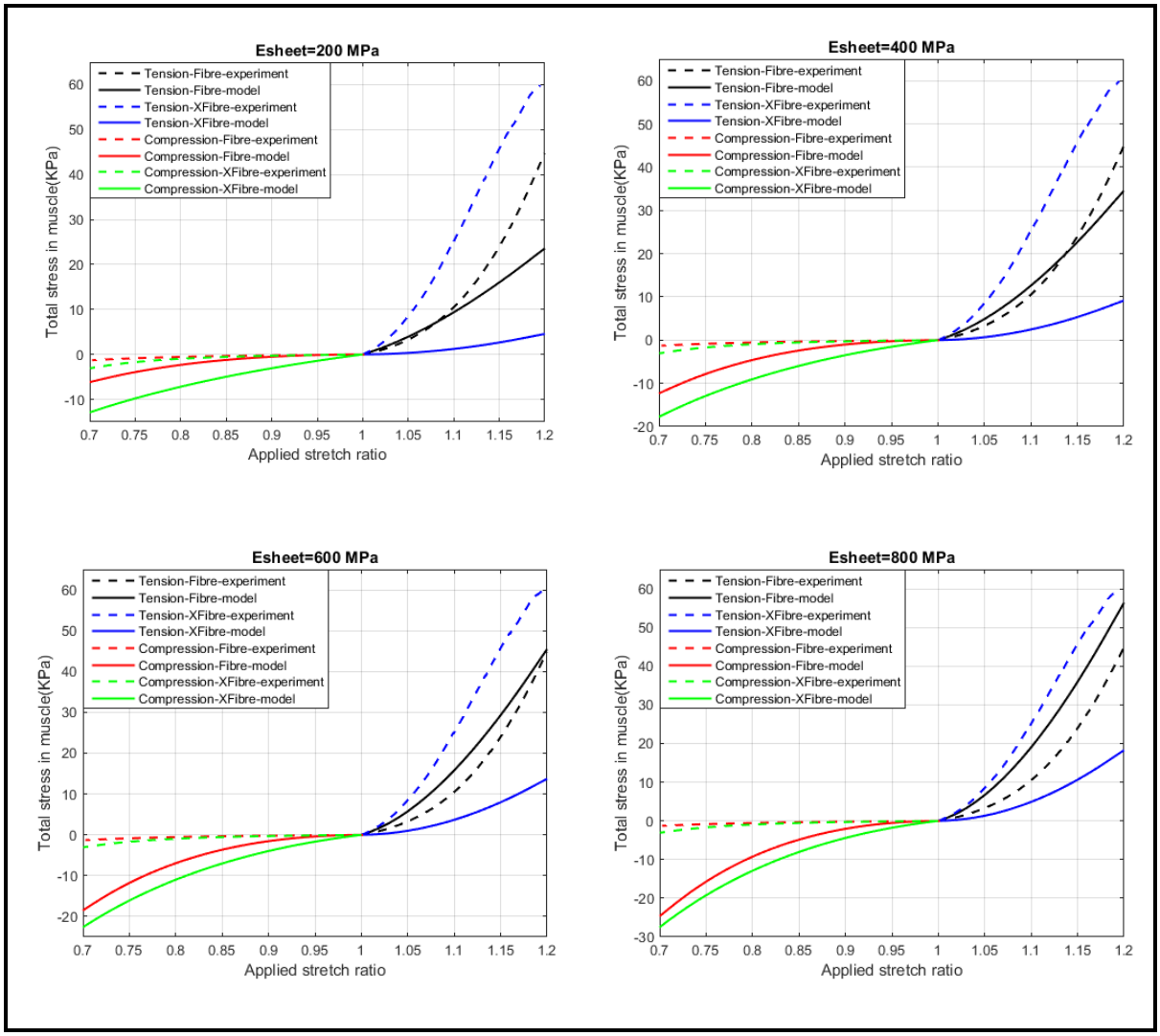

Figure 6. 8-The comparison between the stress-stretch response of the whole muscle predicted by the model and the experimental results for chicken tissue at fixed waviness of 1.18 and 1.75% connective tissue for different Elastic modulus ranging from 200-800 MPa.

Figure 6.8 demonstrates that the compressive response better matched with the model at smaller Elastic modulus, whereas the tensile response is well predicted by increasing Elastic modulus.

Figure 6.9 represents the response range of the model for the whole muscle for 4 different values of p_c and compares it with the experimental results available for the chicken tissue at a fixed Elastic modulus of 500 MPa and the waviness of 1.18. Where there are more connective tissues in the muscle, the stiffer response was observed in both deformations. At lower amounts of connective tissues the model better predicted the compressive response, whereas the tensile response could be better modelled at higher amounts of connective tissues in the muscle. The difference between the stress response in Compression-Fibre and Compression-XFibre deformations becomes less by increasing the amounts of connective tissue.

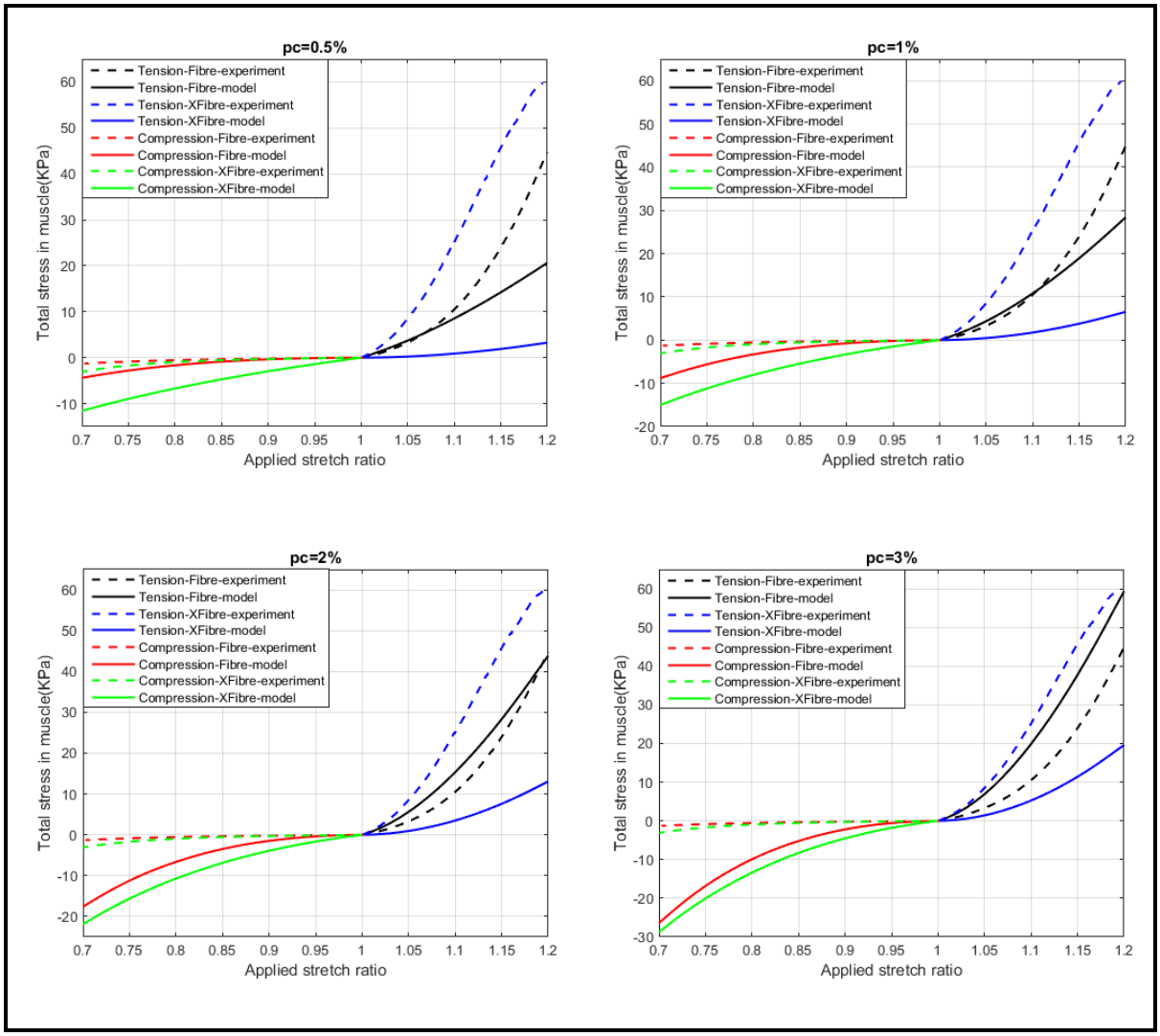

Figure 6. 9-The comparison between stress-stretch response of the whole muscle predicted by the model and the experimental results for chicken tissue at fixed waviness of 1.18 and Elastic modulus of 500 MPa for different percentage of connective tissue existed in the muscle ranging from 0.5-3%.

The model in general overestimates the compressive response of the muscle. However, it was observed that compression data are better fitted with smaller values of E_{sheet} and p_c. Tension-XFibre deformation condition is underestimated by the model and increasing E_{sheet} and p_c slightly helps the model predict the Tension-XFibre data. In general, a best fit to the experimental data is found with a mid-value proportion of collagen fibres $p_c = 1.75$ and the collagen Elastic modulus of $E_{sheet} = 300$ MPa.

6.3.2.2. Sensitivity of the model response to perimysium waviness

Figure 6.10 compares the model-predicted muscle response with the available experimental data for different waviness of perimysium sheet at a fixed Elastic modulus of 500 MPa and p_c=1.75.

As illustrated perimysium waviness is a key factor in determining the muscle response. At the lowest value of waviness (w=1.05), except the Tension-XFibre deformation condition, the model overestimates the response of the muscle in other deformations. At this waviness, the compressive response predicted by the model is more nonlinear than the tensile response predictions. However, by increasing the waviness, the tensile response shows more nonlinearity. Moreover, in both tension and compression in both directions, the muscle model showed a less stiff response by increasing waviness. The asymmetry was observed depending mainly on the chosen value for perimysium sheet waviness because increasing the waviness caused the compressive response and Tension-Fibre response to match the experiments better. However, the Tension-XFibre response becomes more different than the experimental data.

It was also observed that the model at the waviness of 1.25 captured the chicken stress response better than the other waviness levels. Furthermore, the model is capable of predicting the passive response in low stretch ratios both in tension (up to the stretch ratio of 1.1) and in compression (up to stretch ratio of 0.87).

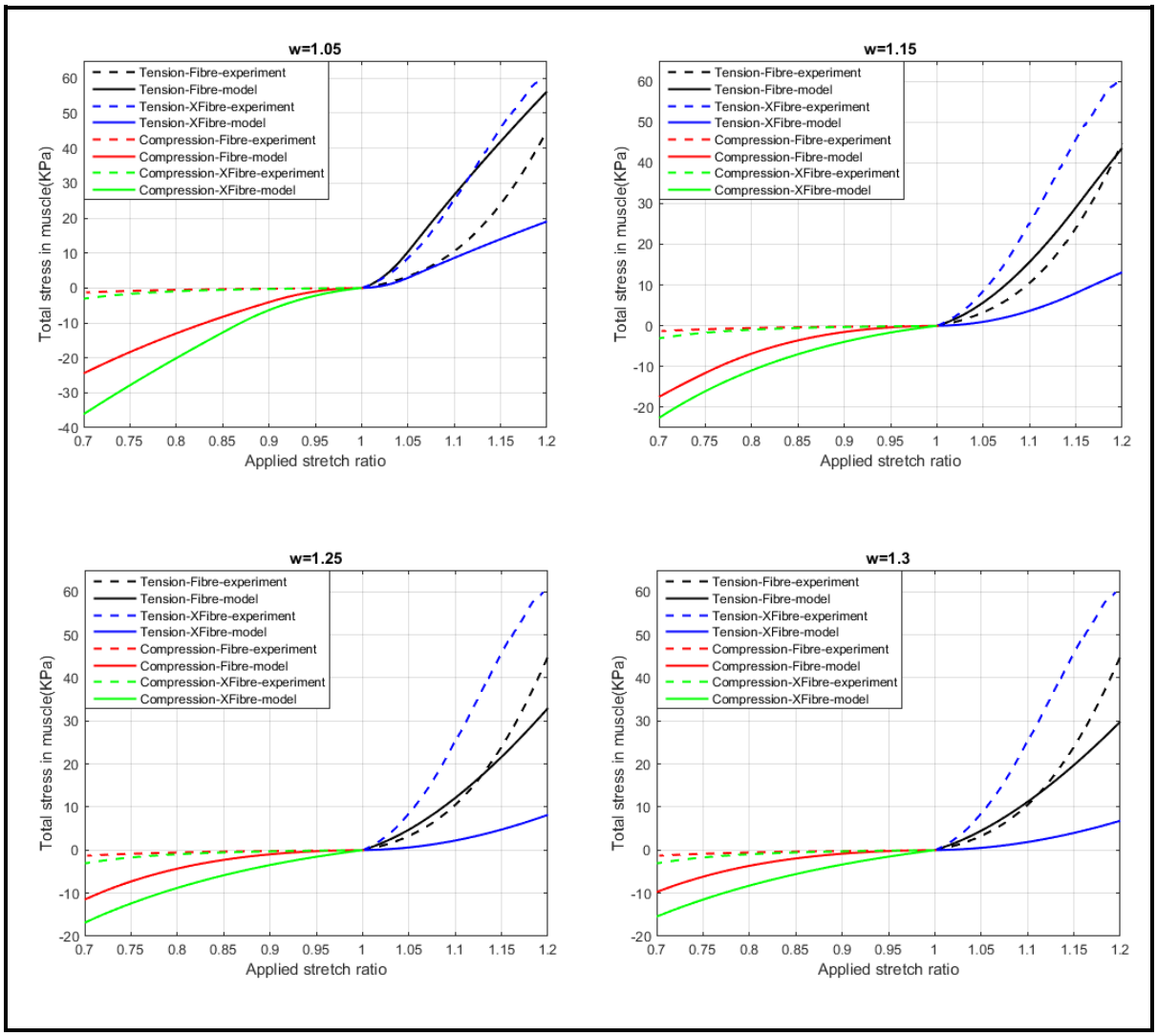

Figure 6. 10-The comparison between stress-stretch response of the whole muscle predicted by the model and the experimental results for chicken tissue at fixed 1.75% of connective tissue and Elastic modulus of 500 MPa for different waviness ranging from 1.05-1.3.

6.4. Discussion

Since the muscle tissue has a high fluid content, the model predicted muscle behaviour based on the assumption of tissue incompressibility. The model used the combination of highly stiff but initially slack perimysium and less stiff muscle fibres in predicting skeletal muscle response to deformations. The model is used to test whether it can predict the tensile and compressive response shown in Chapter 3, Takaza et al. (2013a) and Van Loocke et al. (2006), which demonstrated that stress is much larger in tension than in compression both along and across the fibres (Van Loocke et al., 2006, Takaza et al., 2013b, Calvo et al., 2010, Morrow et al., 2010b, Böl et al., 2012, Grieve and Armstrong, 1988, Nie et al., 2011).

6.4.1. Muscle fibres and perimysium contributions to stress response

To include the muscle fascicle stress contribution to the model, the wormlike chain model was used. Although the model seemed to be dependent on many parameters, Gindre et al. (2013) showed that the muscle response is not very sensitive to the model parameters so the average values were selected for simplicity. Muscle fibres provide a stress contribution only in Tension-Fibre and Compression-XFibre deformations since the muscle fibres are stretched in these two conditions (see Figure 6.6). At first glance it may be assumed that the muscle fibres are only responsible for tension/compression asymmetry. However, Figure 6.11 shows the relative contribution of muscle fascicle as well as perimysium in tension applied in the fibre direction and compression applied in the cross-fibre direction demonstrating the role of both in load bearing in the muscle. It was also observed in Tension-Fibre deformation that the muscle fibres (being made of titin molecules) contribute to the stress response from a very low stretch ratio, and after a stretch ratio of about 1.22 the contribution of the perimysium is greater than the muscle fascicle. In Compression-XFibre deformation, similar to Tension-Fibre deformation, the contribution of muscle fibres to stress becomes less during load application, but the perimysium's role in stress response becomes greater. However, over a range of stretch ratios from 1 to 0.7, muscle fibres show a dominant role in load bearing.

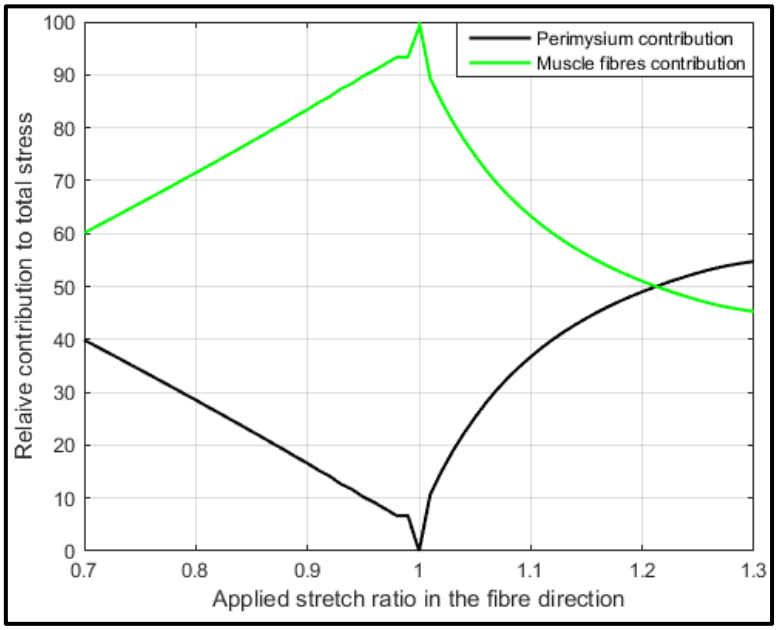

Figure 6. 11-Relative contribution of the muscle fibres and perimysium to total stress observed in the muscle in Tension-Fibre and Compression-XFibre deformations using the optimum model parameters; connective tissue percentage of $p_c = 1.75$, Elast modulus of $E_c = 300\ MPa$, and the waviness of $w = 1.25$.

In Tension-Fibre and Compression-XFibre deformations, the forces developed in the muscle fibres and perimysium work simultaneously to resist the applied stretch, whereas in Tension-XFibre and

Compression-Fibre only the perimysium takes part in resisting the applied stretch as shown by the model and summarised in Table 6.1. The mechanical response of the model is observed to be equally dominated by the collagen network surrounding the muscle fibres as well as the muscle fibres in Tension-Fibre and Compression-XFibre conditions, however, it is essentially dominated by the collagen network in the other two conditions which is in agreement with Gindre et al. (2013).

The nonlinearity of the response is due to the fact that the connective tissue network undergoes stretching of the fibres, and that stretch is a function of waviness which plays an important role (see Figure 6.10). If the collagenous-based perimysium sheet was not wavy at all, very little nonlinearity would be observed in the stress response.

6.4.2. Tension/compression asymmetry

The microstructural model presented here aimed to provide an explanation for the passive tension/compression asymmetric response observed experimentally in different muscle tissues[3] both in the fibre and the cross-fibre directions.

As shown in the Results section, the model prediction depends on the choice of perimysium parameters such as the Elastic modulus, the percentage of connective tissue, and more importantly the waviness observed in the perimysium sheet. However, a set of parameters was found which could predict the experimental data quite well (except Tension-XFibre deformation, which was underestimated by the model, and Compression-XFibre which was overestimated). Figure 6.12a shows the stress response of the muscle using the optimum parameters from the sensitivity studies as $p_c = 1.75$, $E_c = 300\ MPa$, and $w = 1.25$. This illustrates that in a limited range of stretch ratios (0.9-1.1) as shown in Figure 6.12b the model prediction agrees very well with the Compression-Fibre stress data. It was also able to acceptably predict the stress response in Tension-Fibre deformation. However, Tension-XFibre was predicted to be less stiff, which does not match the experimental result. One reason for this could be that the pressure-induced longitudinal force (as used for Tension-XFibre) is less than the direct longitudinal force (used for Tension-Fibre); this requires further investigation. Furthermore, in Tension-XFibre deformation, as the muscle fibres shorten they do not contribute to the stress response, which is another reason for a more compliant response in this condition.

[3] The capability of the microstructural-geometrical model in predicting the porcine compressive and tensile stress response is reported in Appendix D.

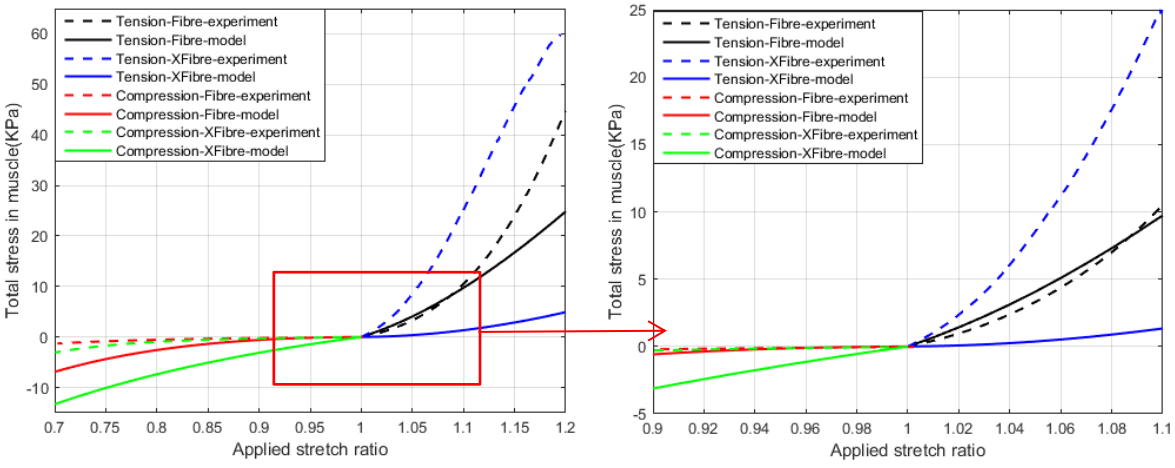

(a)The stress reponse in the muscle using the optimum parameters

(b)The stress response in the muscle from the stretch ratio of 0.9-1.1

Figure 6. 12-The best predication of the model for tensile and compressive response of chicken muscle tissue. (a) The stress-stretch response of the muscle predicted by the model using the optimum model parameters; connective tissue percentage of $p_c = 1.75$, Elast modulus of $E_c = 300\ MPa$, and waviness of $w = 1.25$. (b) The stress response of the muscle in limited range of stretch ratios (from 0.9-1.1) to show the capability of the model to predict the experimental data.

However, another influential factor is the choice of an appropriate value for perimysium sheet waviness. As explained in Chapter 5, in the proposed three-dimensional model for muscle, two degrees of waviness were defined for the perimysium. One is the waviness of the perimysium observed in either the longitudinal direction ($w2$) or the transverse direction ($w1$) and another one is $w3$ which is the waviness of the collagen fibres within the sheet of perimysium. Therefore, the same value for $w1$ and $w2$ was selected as they were both defined to be in the same level of waviness ($w3$ was not considered in the current model). To investigate the effect of this, different (individual) values of waviness were selected for $w1$ and $w2$. The model was run using the values of 1.05 and 1.15 for $w1$ while keeping the optimum value of 1.25 for $w2$, the Elastic modulus and the percentage of connective tissues from the sensitivity studies. As shown in Figure 6.13, only changing $w1$ to the minimum value causes the model to show a stiffer response in Tension-XFibre deformation, but still less than the Tension-Fibre deformation contradicting the experimental data. However, the model still underestimates the Tension-XFibre response. Changing $w1$ also led to much stiffer response in Compression-Fibre deformation so that in Figure 6.13a the Compression-Fibre response overlaps the Compression-XFibre response, which disagrees with the experimental data. Therefore, it suggests that in future, better understanding of the pressure term is required to more accurately describe the

relationship between the circumferentially developed force and internal pressure in muscle for "Tension-XFibre" and "Compression-Fibre" conditions.

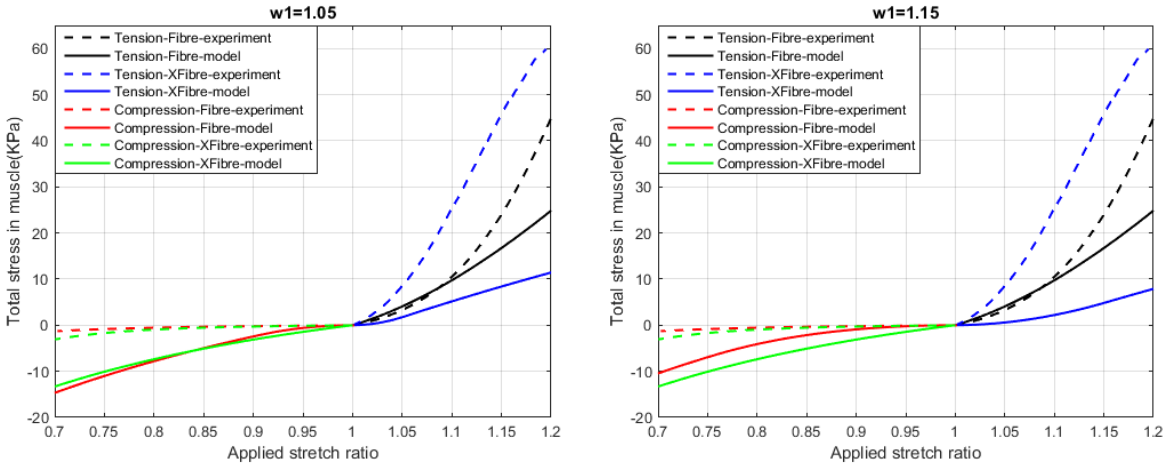

(a)The stress reponse in the muscle using the optimum parameters, but $w1 = 1.05$

(b) The stress reponse in the muscle using the optimum parameters, but $w1 = 1.15$

Figure 6. 13-The model predication for tensile and compressive response of chicken muscle tissue by changing the waviness observed in the transverse direction(w_1)using the optimum model parameters; connective tissue percentage of $p_c = 1.75$, Elast modulus of $E_c = 300\ MPa$, and waviness of $w2 = 1.25$. (a) The stress-stretch response of the muscle predicted by the model using $w1 = 1.05$. (b) The stress-stretch response of the muscle predicted by the model using $w1 = 1.15$.

This model provided an improvement on the Gindre et al. (2013) model in several aspects: Their model assessed the mechanical response of a single muscle fibre and its interaction with the endomysium, which was not a complete description of a real muscle. Although they only considered the endomysium surrounding one muscle fibre, their result in general showed a much stiffer response compared to the current model (see Figure 6.14); however, the current model predicted the muscle stress response closer to the stress response observed in the experiments. It was demonstrated that the observed asymmetry results from the contribution of the collagen network more than the muscle fibres, which agrees with the findings of Gindre et al. (2013). In general, Gindre et al. (2013) showed less tension/compression asymmetry than was shown in the current model which could a result of not considering the perimysium as the main structure in load bearing. Finally, Gindre et al. (2013) modelled the deformation applied only in the fibre direction, whereas, the current model accounts for the cross-fibre deformations as well.

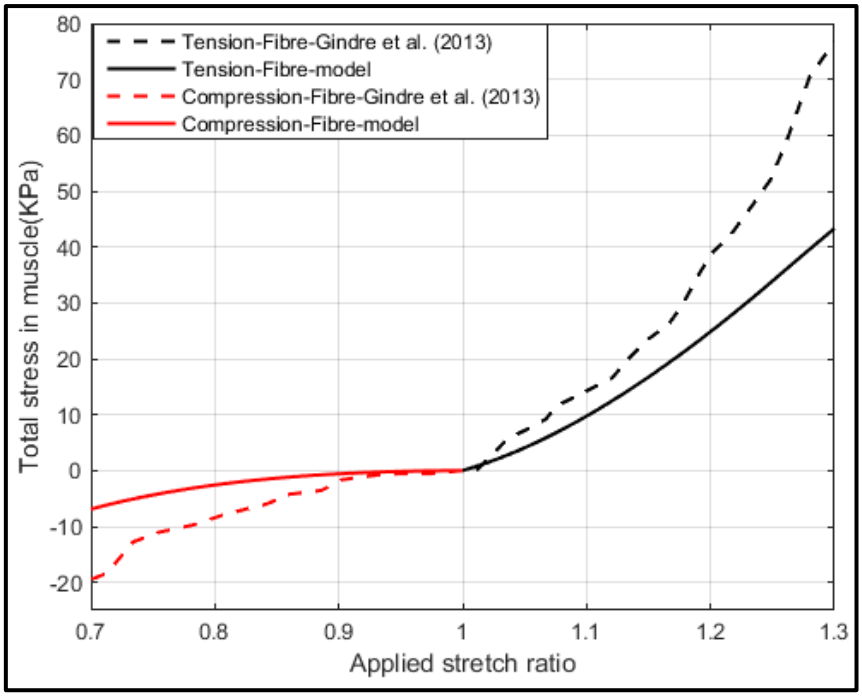

Figure 6. 14- Comparison between Gindre et al. (2013) micromechanical model and the current model predication for the response of chicken muscle in tensile and compressive deformations applied in the muscle fibre direction. The current model parameters were selected as connective tissue percentage of $p_c = 1.75$, Elastic modulus of$E_c = 300\ MPa$, and waviness of $w = 1.25$. Gindre et al. (2013) model parameters are the average values.

6.4.3.Limitations

The microstructural-geometrical model presented in this Chapter is limited in predicting the passive response of the skeletal muscle for reasons outlined below:

- In Compression-Fibre deformation, muscle fibres in the model were supposed to be perfectly cylindrical whereas *in vivo*, they are expected to undergo buckling. Consideration of buckling would cause a more compliant response, which makes the model match the experiments better.
- The perimysium was assumed to enclose one muscle fascicle, but in fact it is a shared structure between fascicles (Purslow, 2010). The real muscle sample is made of several fascicles with more connective tissues, and this requires further investigation.
- The model also does not account for viscoelastic property as an important feature in skeletal muscle (Van Loocke et al., 2008, Van Loocke et al., 2009).
- Although sensitivity studies were conducted here for different input parameter combinations to choose the values giving the best results, a formal optimisation method is required to find one suitable combination of model parameters to capture tension/compression asymmetry better as shown in the literature.

- No endomysium contribution was considered in the current modelling. Although the amount of endomysium is less than perimysium in muscles (Purslow, 2010), this connective tissue should also be added to the model for a closer prediction of the muscle behaviour in passive load bearing.

6.5. Conclusion

The current model presents a microstructural-geometrical model to partially explain the passive behaviour of skeletal muscle in tension and compression applied in both the fibre and cross-fibre directions. This model has improved on a previously published micromechanical model in two aspects: first, it aimed to model the whole muscle including the muscle fibres and connective tissues, and, second, it predicted the tensile and compressive response in two directions, while in the Gindre et al. (2013) model only the deformations applied in the fibre direction were modelled. The model showed more asymmetric response which better agrees with the published experimental data and those data reported in Chapter 3. It also showed that although the perimysium was believed to be a key element in the muscle stress response, the muscle fibres (in Tension-Fibre and Compression-XFibre deformations) also showed their contribution to stress-stretch response since the muscle fibre stress has the same order of magnitude as does the perimysium stress.

There are several limitations to this study. For example, different muscle types in different animals have different percentage of connective tissues as well as different extents of perimysium waviness (Lepetit, 2008, Lepetit, 1991). The reporting of Elastic modulus has also been very sparse in the literature. However, the model attempted to fit the experimental data using the best values for input parameters.

The current model can be extensively improved by adding some missing aspects: the endomysium contribution to stress response, a more realistic arrangement of perimysium around muscle fascicle, the viscoelastic properties of muscle, considering $w3$ as a model parameter to evaluate its effect on the stress response, and a better assessment of the pressure term to account for the accurate stress response in Tension-XFibre deformation. It would also be interesting to know how the distribution of the angle that the collagen fibres within perimysium sheet make with the muscle fibres changes under different deformations, as it may partially be a reason for the observed stress-stretch response.

Chapter 7- General discussion and future work

Science never solves a problem without creating ten more.
GEORGE BERNARD SHAW.

7.1. The main contributions of the thesis

For many years only the force producing capabilities of skeletal muscle was of interest to researchers. However, in recent years, the study of the ECM in skeletal muscle has been extensively expanded because in passive mechanical properties of muscle, the ECM was found to be a key element contributing to stress response in different loadings (Purslow, 2010, Purslow, 1989, Purslow and Trotter, 1994, Takaza et al., 2014, Pietsch et al., 2014, Gillies and Lieber, 2011, Gillies et al., 2011). Therefore this study aimed to add further understanding on skeletal muscle behaviour particularly tension/compression asymmetry which certainly arises from its microstructure. Figure 7.1 schematically summarises the tasks conducted in the current study exploring the reason for the thesis question to investigate whether tension/compression asymmetry is also observed in species other than pigs, and what are the microstructural reasons for this response. In order to achieve this, a combination of mechanical testing and microstructural analysis was carried out which further helped create a microstructural model to predict the passive behaviour observed in the muscle and to observe how capable the model is to explain tension/compression asymmetry. The ultimate goal of the model

is to relate the macro mechanical behaviour of the muscle to its microstructure and further help for a better constitutive representation of muscle for biomechanical applications.

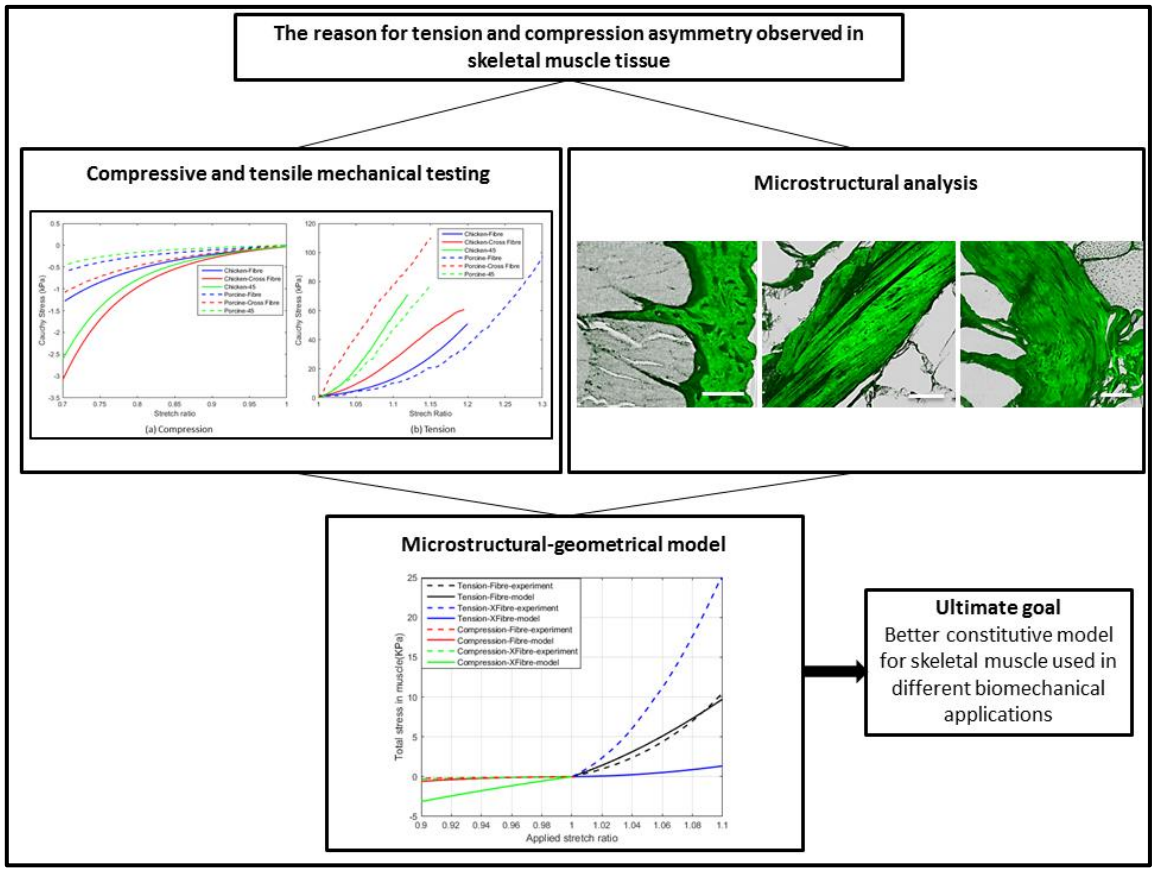

Figure 7. 1-Schematic illustration of the different steps conducted in the current thesis as an effort to explore the microstructural reason for tension /compression asymmetry observed in skeletal muscle of different species.

Previous experimental studies provided well established and important insight into the nonlinear, incompressible, anisotropic, and viscoelastic characteristics of skeletal muscle under compressive and tensile deformation (Van Loocke et al., 2008, Van Loocke et al., 2006, Böl et al., 2014, Böl et al., 2012, Takaza et al., 2013a, Nie et al., 2011, Calvo et al., 2010, Pietsch et al., 2014). However, due to the use of different experimental protocols and different species, large variations are recorded in compressive and tensile published data for skeletal muscle. Thus, in order to make systematic comparisons across species the passive elastic stress-stretch and Poisson's ratio properties of chicken muscle tissue have been presented in the current study for the first time in comparison with those of porcine tissue conducted with the same test protocol (Takaza et al., 2013a, Van Loocke et al., 2006).

When compression is applied, deformation in the cross-fibre direction yields the stiffest response in both tissues. However, the fibre direction is the least stiff tissue in chicken while 45° is the least stiff direction in porcine tissue. In applied tension, the fibre direction is the least stiff response in both species. However, for chicken the stiffest response is when tension is applied at 45° to the fibre

direction while for the porcine tissue the stiffest is when tension is applied in the cross-fibre direction. These results clearly show that while both tensile and compressive behaviours are anisotropic, anisotropy is different in skeletal muscle in different species (see Figure 3.9).

The Poisson's ratio results show broadly transversely isotropic behaviour for compression or tension applied in the fibre direction (υ_{LT} of almost 0.5), but clear anisotropy for compression or tension applied in the cross-fibre direction. For applied cross-fibre compression υ_{TL} = 0.34 and υ_{TL} = 0.36 were observed for chicken and porcine tissue respectively, while for applied cross-fibre tension, $\upsilon_{TL} =$ 0.83 and υ_{TL} = 0.74 were observed for chicken and porcine tissue respectively. However, $\upsilon_{TT'}$ = 0.64 and $\upsilon_{TT'}$ = 0.65 were observed for compression of chicken and porcine tissue respectively, and $\upsilon_{TT'}$ = 0.17 and $\upsilon_{TT'} =$ 0.28 for tension in chicken and porcine tissue respectively (see Table 3.4). The values of Poisson's ratios (υ_{TL} and $\upsilon_{TT'}$) in compression are quite similar for both species. It means that when both species compressed in the cross-fibre direction (T) by a certain amount, the Poisson's ratio values for induced deformation either in T' or L directions are very similar for both species; the strains are accordingly the same. This can explain why the difference in stress-stretch response observed in compression between the two species is smaller compared to the difference observed in tension. In general, Poisson's ratio results were qualitatively similar for chicken and porcine skeletal muscle. This is surprising given the qualitative differences observed in the stress-stretch curves particularly in tension, which highlighted the requirement of microstructural analysis to provide an adequate explanation.

The tension/compression asymmetry previously reported in porcine skeletal muscle is now evident across two very different kinds of skeletal muscle (chicken vs. porcine), with the stress in tension being much higher than in compression for all directions tested. This mechanical response cannot be captured by conventional fibre reinforced composite constitutive models with a single set of material parameters. Therefore, to investigate the different passive mechanical response of skeletal muscle to deformation observed in porcine and chicken, microscopic analysis is required to observe conformational/structural changes in the tissue under different conditions. The first challenge in such analysis is to develop a suitable method to visualise collagen fibres within the muscle in order to examine conformational changes in these important components of load bearing (Takaza et al., 2014, Purslow, 2010).

The collagenous network structure in skeletal muscle tissue in different animals has been mostly investigated through high quality SEM micrographs of endomysium and perimysium structures, which were able to show very detailed structure of collagen fibrils at a very small scale. But this does not permit observation of the connective tissue realignment across whole tissues under different deformations; for this larger scale visualisation is required, which also provides sufficient resolution

and quality of images to show the organisational changes occurred in connective structure in contact with the muscle fibres under load applications. The available SEM micrographs in the literature were mostly obtained through decellularising methods which removed the muscle fibres (Gillies and Lieber, 2011, Passerieux et al., 2006, Purslow and Trotter, 1994, Gillies et al., 2011). The connective tissue has a firm bond to the surrounding muscle fibres so under different applied deformations, it is of importance to know how the connective tissue contributes to load bearing in contact with the muscle fibres. However, decellularising methods would not permit changes in cross sectional shape and reorientation of the muscle fibres to be visualised together with the ECM.

It has also been shown that it is very difficult to unravel different layers of connective tissue, and in particular to distinguish between perimysium and epimysium (Gillies and Lieber, 2011, Nishimura et al., 1994, Passerieux et al., 2006, Purslow, 1989, Purslow and Trotter, 1994, Das et al., 2010). However, the amount of perimysium in muscles varies far more than the amount of endomysium (Purslow, 2010) and as variation in the amount and organisation of perimysium has been shown to play a strong role in the functioning of each muscle, it may also relate to differences observed in mechanical behaviour under tension and compression deformations (Takaza et al., 2014, Purslow, 2010).

Although unfixed tissue can be sectioned following freezing, presenting proteins in their more 'native' form (Renshaw, 2013, Ralton and Murray, 2011, Kumar and Rudbeck, 2009), there are some cases where fixation of tissue is required. In particular tissue samples need to be fixed tissue under applied deformation in order to preserve structure under those conditions. A repeatable uniform compressive or tensile stretch is possible in isolated tissue blocks which can then be fixed and sectioned, whereas the very soft nature of muscle means that applied deformation will not be preserved in unfixed tissue and the effects will be lost as soon as the deformation is removed. Wax embedded sections can give better structural preservation. Therefore, the current study adapts the use of the collagen binding protein CNA35 for detection of all collagen fibres in fixed tissue for the first time; although the use of CNA35 to detect collagen was previously reported in unfixed cells and live tissues (Krahn et al., 2006). Given that the detection of collagen and visualisation of perimysium and endomysium structure is challenging in mature skeletal muscle, given the complexity of the tissue and the fact that it was previously untested, a series of sensitivity studies were carried out to determine suitable conditions and parameters for sensitive and specific detection using CNA35- binding protein fused to EGFP and tdTomato for ease of fluorescent visualisation and the added advantage of using confocal microscopy.

The images shown in Chapter 4 were mostly produced with a standard fluorescent microscope, clearly showing the localisation of collagens within the overall tissue structure. However, analysis of

fluorescent CNA35 probed tissue sections, as produced in Chapter 5, by confocal microscope provided much higher resolution and more detailed description of collagen organisation, and has furthered our understanding of how the microstructure can explain the mechanical behaviour observed in skeletal muscle, reported in Chapter 3.

Although some efforts has been performed to study collagen organisation in response to applied loading and further explain tension/compression asymmetry (Trotter and Purslow, 1992, Lewis and Purslow, 1989, Takaza et al., 2014), the relationship between collagenous network organisation to externally applied deformation is not sufficiently defined. Thus, in the current study, to investigate the structural changes in skeletal muscle and to interpret the passive mechanical response, collagen fibril orientation in perimysium under different loading conditions was viewed in transverse and longitudinal section planes in two different species. First, a three dimensional schematic illustration of perimysium structure and different degrees of waviness/straightness in transverse (w_1) and longitudinal (w_2) planes was established and from this it was proposed for the first time that it could be used to improve our understanding of how perimysium responds to three-dimensional deformations. This helped frame the analysis of observations in chicken and porcine tissues in order find an explanation for tension/compression asymmetry.

For the first time it was shown that perimysium, which is believed to be the main load bearing structure in skeletal muscle behaves differently under different loading conditions in fibre and cross-fibre directions and in both tension and compression through observations of the changes in waviness in the longitudinal and transverse planes, potentially explaining some aspects of the behaviour as follows:

- In undeformed (control) samples, the collagen fibrils in both transverse (w1) and longitudinal planes (w2 for chicken) were wavy, as they bear no load.
- In compression in the fibre direction (Comp-F), the collagen fibrils in longitudinal direction are wavy (w2) and bear no load and this does not additionally inform the species difference, but since the collagen fibrils are straight in the transverse plane (w1) for both chicken and porcine tissues they are assumed to take part in load bearing in this condition.
- In compression in the cross-fibre direction (Comp-XF) there is both wavy and straight perimysium in the transverse plane (w1) for both species. In Comp-XF, where the perimysium is aligned with the deformation direction, the collagen fibrils become wavy, whereas if the deformation direction is perpendicular to the perimysium the fibrils were straight. However, the portion of perimysium which is aligned perpendicular to the applied deformation (straight fibrils) is greater than the proportion that is wavy, indicating that perimysium mostly reorients to bear the load. On the other hand, the collagen fibrils in the

longitudinal direction (w2) under Comp-XF for chicken tissue become straight, also contributing to passive load bearing. Unfortunately these data were missing for porcine tissue. The stiffer response observed in both species in Comp-XF than Comp-F (regardless of small difference between them-reported in Chapter 3) can be due to the fact that in Comp-XF collagen bears load in two perpendicular planes (the less wavy collagen seen in the longitudinal direction induced by the deformation (see Figure 5.7(c), w2) as well as the stretched collagen in the transverse plane caused by direct deformation (see Figure 5.6i(c), w1). However in Comp-F only induced straightness in the transverse plane is responsible for passive load bearing. Furthermore, the collagen fibril waviness in the transverse plane (w1) showed a straighter pattern in chicken than porcine tissue (see Figure 5.6i and iii), so the stiffer mechanical response observed in chicken in Comp-XF reported in Chapter 3 is explained by this pattern.

- In tension in the fibre direction (Ten-F), the collagen fibrils in the transverse plane (w1) are wavy in both species. Collagen fibril orientation in the longitudinal direction (w2) is important in Ten-F deformation as they contribute to stress response by their straightness. The very straight collagen fibrils in the longitudinal direction (w2) mostly bear the load. Lack of data in the longitudinal direction for porcine tissue is acknowledged. At the same time, the reduced waviness observed in the transverse plane (w1) in chicken than porcine tissue (especially compared to those of porcine BF) can partially explain the stiffer tensile response in chicken.
- In tension in the cross-fibre direction (Ten-XF), the stretched perimysium in the transverse plane (w1) plays a key role in resisting the load in both species (see Figure 5.6i(e), Figure 5.6ii(d), or Figure 5.6iii(e)). However, it cannot be stated clearly in which species waviness viewed in the transverse plane (w1) is greater, so it is difficult to address the stiffer tensile response observed for porcine tissue. Stretched perimysium in the transverse plane (w1) observed in Ten-XF and those in the longitudinal direction (w2) observed in Ten-F are both caused by direct deformation in that direction. It seems the straightness is more extreme in Ten-XF (Figure 5.6i(e)) than Ten-F (Figure 5.7(d)) which may explain the stiffer response seen in Ten-XF compared to Ten-F for both animals.

These observations do not show a strong evidence to explain why the stress response in tension is two orders of magnitude higher than in compression as there were no actual load measures in these cases. However, the findings are consistent with load bearing and they generally explain anisotropy observed in stress-strain response of skeletal muscle both in tension and compression. To summarise,

for each deformation condition, collagen straightness in one of the planes, or sometimes in both planes, appears to play a role in resisting externally applied deformations. It should be noted there were some challenges mainly associated with sectioning of longitudinal sections led to having few slides to work with. Therefore, sufficient evidence is missing especially for the porcine tissue, which caused difficulty to make a strong argument for cases that comparison for longitudinal sections between the species was needed.

The validity of three-dimensional models of skeletal muscle proposed in the literature strongly depends on the choice of constitutive models and the material properties employed (Sharafi et al., 2011, Sharafi and Blemker, 2011, Blemker and Delp, 2005, Blemker et al., 2005). Therefore, the compressive and tensile data obtained in the literature and those presented in Chapter 3 literature together with a good understanding of muscle microstructure in response to mechanical loading are valuable to enhance the current constitutive models suitable for FE analysis implementation. The suggested nonlinear and transversely isotropic constitutive model obtained from analysing the experimental data such as Ogden hyperelastic model (Ogden, 1978b, Ogden et al., 2004) may be the most appropriate model for skeletal muscle at the moment. However, Moerman et al. (2016) recently improved the Ogden model through assessment of how the sign of Ogden coefficient (positive or negative values) affecting the tension/compression asymmetry and nonlinearity in their model. They only demonstrated the use of their proposed formulation for nonlinear anisotropic behaviour in compression using Van Loocke et al. (2006) data. However, it was not demonstrated whether their model is able to predict the tensile stress-stretch response. Overall, the Moerman et al. (2016) work was about to assess the influence of the coefficient of Ogden model using different generalised strains measures such as Bazant (Bazant, 1998) or Seth-Hill (Hill, 1968, Seth, 1961) to observe which can better predict the tension/compression asymmetry. However, still, understanding the relationship between the mechanical stress response and the muscle microstructure which can partially explain the tension/compression asymmetry will definitely help suggest a better constitutive model for a wide range of applications, such as impact biomechanics, surgical simulation etc. Therefore, the model presented in Chapter 6 worked towards a microstructural-geometrical model characterising the compressive and tensile behaviour of muscle and relating this with the muscle microstructure. The current model developed the work of Gindre et al. (2013) model which was a simplified structural model to show the direct mechanical interaction between one muscle fibre and its surrounding endomysium, which contributes to muscle stiffness through two resisting mechanisms; a longitudinal force resisiting tension and a pressure force on the muscle fibre resisting compression. Their model was not fully capable of addressing the observed mechanical behaviour in the skeletal muscle because their model generally showed stiffer response compared to the literature and less

tension/compression assymetry was observed by the model. They also only modelled the tension and comparession applied in the fibre direction, thus their model cannot be used to predict the deformations applied in the cross-fibre direction.

Therefore, the model built in Chapter 6 aimed to model the whole muscle including a group of muscle fibres and perimysium, and to predict the tensile and compressive response in two directions. Although the model proposed here was a development on Gindre et al. (2013) model, the Poisson's ratio values obtained in Chapter 3 as well as the findings of Chapter 5 in relation to the straightness of perimysium under deformations also helped create this model. The model was able to show the anisotropic behaviour observed for load applications in different directions. The model also showed that although perimysium was believed to be a key element in the muscle stress response, the muscle fibres (in Tension-Fibre and Compression-XFibre deformations) also showed their contribution to stress-stretch response since the muscle fibres stress has the same order of magnitude similar to perimysium stress. This model also showed more asymmetric response which better agrees with the published data. It should be noted that the result from this study was obtained on an excised muscle, which most likely will behave in a different manner than the whole muscle. The layers of the ECM may act differently in muscle behaviour, particularly the epimysium, which was removed for this study. Therefore, these data should only be applied to describe the muscle behaviour at a local fascicle level when developing computational models.

The model is dependent to the choice of input parameters. Although sensitivity studies were conducted here for different input parameter combinations to choose the values giving the best results, a formal optimisation method is required to find one suitable combination of model parameters to capture tension/compression asymmetry better as shown in the literature. The model presented in Chapter 6 predicted the Tension-Fibre and Compression-Fibre deformations quite well using the optimum model parameters obtained from the sensitivity studies as reported in Chapter 6. However, Tension-XFibre and Compression-XFibre deformations were not predicted agreeably. For Tension-XFibre deformation, the pressure term is influential in stress response contribution so this requires further study to enable the model to predict the mechanical stress behaviour better. In Compression-XFibre the muscle fibres undergo the stretch as in Tension-Fibre, but in Tension-Fibre the stretch observed by the muscle fibres are due to the direct deformation in the longitudinal direction whereas in Compression-XFibre the muscle fibres undergo the induced stretch due to the cross-fibre deformation. Although in Compression-XFibre, for Δz in equation 6.3, the correct stretch ratio induced in the longitudinal direction (using Poisson's ratio effect) was used, the worm like chain model may not be suitable to explain this and a better model should be employed.

The perimysium thickness was assumed to be constant, but the thickness changes differently under different deformations applied in different directions, which changes the results obtained from the model. However, this does not seem to make a large difference.

7.2. Guidelines for future work

The author of this thesis provides some new and useful information on the compressive/tensile macro mechanical and micromechanical behaviour of skeletal muscle for further use in applications where more accurate models of muscle are needed, for example in pressure sore modelling (e.g. (Bosboom et al., 2003)), rehabilitation engineering (e.g. (Linder-Ganz et al., 2007)), surgical simulations (e.g. (Linder-Ganz and Gefen, 2008)), impact biomechanics (e.g. (Ivancic et al., 2007)) and modelling of soft tissue drug transport (e.g. (Wu et al., 2009)). However, in spite of the advances made in this thesis, the knowledge of skeletal muscle properties still remains insufficient. Therefore, several avenues of future work are required to learn more about this complex tissue. Some specific suggestions are provided here for such further research:

1) From an experimental point of view

Experimentally, due to the difficulties of access to human tissue, one of the challenges of future research will be to relate data obtained from muscle of animal models to human muscle. Although the differences observed in the stress-stretch response between species are mostly qualitative, the microstructural analysis here could partially explain the observed mechanical behaviour differences. Therefore improvement on understanding the cross-species stress response differences can explain the quantitative variations between species, and further relate this to human tissue.

In vivo methods for deformation measurement can be a promising tool to observe the skeletal muscle behaviour in a more native condition. This potentially could be combined with improved, live, non-invasive methods of imaging muscle such as Optical Projection Tomography (OPT). However, it is as yet unclear how collagen microstructure could be captured in live muscle non-invasively.

Furthermore, Moerman et al. (2016) suggested that to demonstrate whether a material shows tension/compression asymmetry, multidirectional tests are required. However, for soft tissues, mechanical experiments are often conducted, only in tension (Takaza et al., 2013a), or only in compression (Van Loocke et al., 2006). This certainly needs further investigation.

2) From a microscopic point of view:

Two-photon microscopy (Sahai et al., 2005, Foolen et al., 2008) or stimulated emission depletion (STED) microscopy (Lauterbach et al., 2010, Mishina et al., 2015) can be used in conjunction with the collagen binding fluorescent probes would provide further detail in the visualisation of collagen organisation including imaging of tissues to about one milimetre in depth. However, this would require the development of, on one hand, a custom made mechanical device of suitable size to fit on a microscope stage, and also a method of achieving penetration of the collagen binding protein into mature muscle tissue. This was therefore not possible in the current study. Optical Projection Tomography (OPT) could also be used to scan an intact muscle rather than a section to help visualise the tissue in three dimensions (Summerhurst et al., 2008). The great advantage of this would be to reduce the damaging consequences of mechanical sectioning, which was a challenging issue in the current study. However, penetration of the probes into intact mature muscle tissue was very limited due to the superficial nature of the penetration. Scanning Electron Microscopy (SEM) (Takaza et al., 2014, Lu et al., 2004) and Strong forward scattered Second Harmonic Generation (SHG) (Cox et al., 2003, Williams et al., 2005) can also be used to visualise organisation in collagen rich tissues, however, these approaches do not specifically detect collagen.

3) From a modelling point of view:

The following aspects could be considered to help improve the model presented in Chapter 6:

- Endomysium contribution to stress response: hierarchical structure of skeletal muscle is formed by endomysium, perimysium and epimysium. Distinguishing between epimysium and perimysium is difficult (Gillies and Lieber, 2011) and also epimysium is normally removed through sample preparation prior to mechanical testing. Therefore, at least, it is required to consider endomysium in conjunction with perimysium for future development on the model presented in this work. A better description of muscle behaviour would be then achieved.
- More realistic arrangement of perimysium: perimysium is not a sheath surrounding on muscle fascicle, but instead it is a shared structure between some muscle fascicles (Purslow, 2010). Therefore, this requires to be taken into account in future models.
- Viscoelastic properties of muscle: about 80% of skeletal muscle is made of water which shows that muscle has a high fluid content. This emphasises the importance of viscoelastic properties of muscle in a model descriptive of muscle behaviour, and perhaps a poroelastic

approach is appropriate to consider the role of fluid content within the tissue (Wheatley et al., 2016).

- Inclusion of $w3$ and θ in the model: additional model parameters such as $w3$ (the waviness of individual collagen fibres within perimysium sheet) and distribution of θ (the angle that the collagen fibres within perimysium sheet make with the muscle fibres) could be considered to evaluate their effects on the stress response observed in muscle.
- Better assessment of the pressure term in the model: the pressure inside muscle which results in a longitudinal force along the muscle length in Tension-XFibre and Compression-Fibre deformation conditions was calculated through analogy with the calculations of pressure in a thin-wall pressure vessel. The use of this calculation in the model well predicted the muscle response in Compression-Fibre deformation. However, Tension-XFibre deformation response was underestimated by the model so more investigation on this would help to account for the accurate stress response (Sleboda and Roberts, 2017) particularly for Tension-XFibre deformation condition.
- Perimysium sheet waviness: an influential factor in the microstructural model proposed here is the choice of value for waviness. This parameter is less defined in the literature compared to the other model parameters such as the Elastic modulus and the percentage of connective tissue. This requires more investigation to see whether there is any difference in the waviness of the perimysium sheet observed in different planes of sectioning.

So in summary this work provides a set of mechanical stress-stretch data as well as the microstructural descriptions for tension and compression applied in the fibre and cross-fibre directions in skeletal muscle tissue in order to create a microstructural-geometrical model for prediction of the passive mechanical behaviour observed in the muscle. It lays clear foundations for additional work needed in order to develop better constitutive models for several biomechanical applications in which the accurate response of a muscle to load is required.

Bibliography

ABRAHAM, A. C., KAUFMAN, K. R. & HAUT DONAHUE, T. L. 2013. Phenomenological consequences of sectioning and bathing on passive muscle mechanics of the New Zealand white rabbit tibialis anterior. *Journal of the Mechanical Behavior of Biomedical Materials,* 17**,** 290-295.

ABRAMOWITCH, S. D. & WOO, S. L. Y. 2004. An improved method to analyze the stress relaxation of ligaments following a finite ramp time based on the quasi-linear viscoelastic theory. *Journal of Biomechanical Engineering,* 126**,** 92-97.

AKDENIZ, Z. D., BAYRAMIÇLI, M., ATEŞ, F., ÖZKAN, N., YUCESOY, C. A. & ERCAN, F. 2015. The role of botulinum toxin type a-induced motor endplates after peripheral nerve repair. *Muscle and Nerve,* 52**,** 412-418.

AKIZUKI, S., MOW, V. C., MÜLLER, F., PITA, J. C., HOWELL, D. S. & MANICOURT, D. H. 1986. Tensile properties of human knee joint cartilage: I. Influence of ionic conditions, weight bearing, and fibrillation on the tensile modulus. *Journal of Orthopaedic Research,* 4**,** 379-392.

APER, S. J. A., VAN SPREEUWEL, A. C. C., VAN TURNHOUT, M. C., VAN DER LINDEN, A. J., PIETERS, P. A., VAN DER ZON, N. L. L., DE LA RAMBELJE, S. L., BOUTEN, C. V. C. & MERKX, M. 2014. Colorful protein-based fluorescent probes for collagen imaging. *PLoS ONE,* 9.

ARCHILE-CONTRERAS, A. C., MANDELL, I. B. & PURSLOW, P. P. 2010. Disparity of dietary effects on collagen characteristics and toughness between two beef muscles. *Meat Science,* 86**,** 491-497.

BAILEY, A. & LIGHT, N. 1989. The role of connective tissue in determining the textural quality of meat. *Connective tissue in meat and meat products***,** 170-194.

BAZANT, Z. P. 1998. Easy-to-compute tensors with symmetric inverse approximating Hencky finite strain and its rate. *TRANSACTIONS-AMERICAN SOCIETY OF MECHANICAL ENGINEERS JOURNAL OF ENGINEERING MATERIALS AND TECHNOLOGY,* 120**,** 131-136.

BENNINGHOFF, A. & ROLLHÄUSER, H. 1952. Zur inneren Mechanik des gefiederten Muskels. *Pflügers Archiv für die Gesamte Physiologie des Menschen und der Tiere,* 254**,** 527-548.

BEST, T. M. 1994. Characterization of the passive responses of live skeletal muscle using the quasi-linear theory of viscoelasticity. *Journal of Biomechanics,* 27**,** 413-419.

BIEWENER, A. A., WAKELING, J. M., LEE, S. S. & ARNOLD, A. S. 2014. Validation of hill-type muscle models in relation to neuromuscular recruitment and force–velocity properties: predicting patterns of in vivo muscle force. *Integrative and comparative biology***,** icu070.

BILLIAR, K. L. & SACKS, M. S. 2000. Biaxial mechanical properties of the natural and glutaraldehyde treated aortic valve cusp - Part I: Experimental results. *Journal of Biomechanical Engineering,* 122**,** 23-30.

BLACKBURN, G., KILROY, H., TAKAZA, M. & SIMMS, C. K. The influence of sample size on apparent stress-strain behaviour in passive skeletal muscle. 7th World Congress of Biomechanics (WCB 2014), 6-10 July 2014 2014 Boston, Massachusetts, USA

BLEMKER, S. & DELP, S. 2005. Three-Dimensional Representation of Complex Muscle Architectures and Geometries. *Annals of Biomedical Engineering,* 33**,** 661-673.

BLEMKER, S. S., PINSKY, P. M. & DELP, S. L. 2005. A 3D model of muscle reveals the causes of nonuniform strains in the biceps brachii. *Journal of Biomechanics,* 38**,** 657-665.

BOERBOOM, R. A., KRAHN, K. N., MEGENS, R. T. A., VAN ZANDVOORT, M. A. M. J., MERKX, M. & BOUTEN, C. V. C. 2007. High resolution imaging of collagen organisation and synthesis using a versatile collagen specific probe. *Journal of Structural Biology,* 159**,** 392-399.

BÖL, M., EHRET, A. E., LEICHSENRING, K., WEICHERT, C. & KRUSE, R. 2014. On the anisotropy of skeletal muscle tissue under compression. *Acta Biomaterialia,* 10**,** 3225-3234.

BÖL, M., KRUSE, R., EHRET, A. E., LEICHSENRING, K. & SIEBERT, T. 2012. Compressive properties of passive skeletal muscle—The impact of precise sample geometry on parameter identification in inverse finite element analysis. *Journal of Biomechanics,* 45**,** 2673-2679.

BORG, T. K. & CAULFIELD, J. B. 1980. Morphology of connective tissue in skeletal muscle. *Tissue and Cell,* 12**,** 197-207.

BOSBOOM, E. M. H., BOUTEN, C. V. C., OOMENS, C. W. J., BAAIJENS, F. P. T. & NICOLAY, K. 2003. Quantifying pressure sore-related muscle damage using high-resolution MRI. *Journal of Applied Physiology,* 95**,** 2235-2240.

BOSBOOM, E. M. H., HESSELINK, M. K. C., OOMENS, C. W. J., BOUTEN, C. V. C., DROST, M. R. & BAAIJENS, F. P. T. 2001. Passive transverse mechanical properties of skeletal muscle under in vivo compression. *Journal of Biomechanics,* 34**,** 1365-1368.

BRIGUET, A., COURDIER-FRUH, I., FOSTER, M., MEIER, T. & MAGYAR, J. P. 2004. Histological parameters for the quantitative assessment of muscular dystrophy in the mdx-mouse. *Neuromuscular Disorders,* 14**,** 675-682.

BROWN, I. E., SCOTT, S. H. & LOEB, G. E. 1996. Mechanics of feline soleus: II design and validation of a mathematical model. *Journal of Muscle Research and Cell Motility,* 17**,** 221-233.

BROWN, S. H., CARR, J. A., WARD, S. R. & LIEBER, R. L. 2012. Passive mechanical properties of rat abdominal wall muscles suggest an important role of the extracellular connective tissue matrix. *Journal of Orthopaedic Research,* 30**,** 1321-1326.

CAI, Z., LAN, F. & CHEN, J. 2014. Development and validation of a human biomechanical model for rib fracture and thorax injuries in blunt impact. *Computer Methods in Biomechanics and Biomedical Engineering***,** 1-7.

CALDWELL, G. E. 1995. Tendon elasticity and relative length: effects on the Hill two-component muscle model. *Journal of Applied Biomechanics,* 11**,** 1-24.

CALVO, B., RAMÍREZ, A., ALONSO, A., GRASA, J., SOTERAS, F., OSTA, R. & MUÑOZ, M. J. 2010. Passive nonlinear elastic behaviour of skeletal muscle: Experimental results and model formulation. *Journal of Biomechanics,* 43**,** 318-325.

CAMPBELL, K. S. 2009. Interactions between connected half-sarcomeres produce emergent mechanical behavior in a mathematical model of muscle. *PLoS Comput Biol,* 5**,** e1000560.

ČANDEK-POTOKAR, M., ŽLENDER, B., LEFAUCHEUR, L. & BONNEAU, M. 1998. Effects of age and/or weight at slaughter on longissimus dorsi muscle: Biochemical traits and sensory quality in pigs. *Meat Science,* 48**,** 287-300.

CARBONE, V., VAN DER KROGT, M., KOOPMAN, H. & VERDONSCHOT, N. 2016. Sensitivity of subject-specific models to Hill muscle–tendon model parameters in simulations of gait. *Journal of biomechanics,* 49**,** 1953-1960.

CHAGNON, G., REBOUAH, M. & FAVIER, D. 2015. Hyperelastic energy densities for soft biological tissues: a review. *Journal of Elasticity,* 120**,** 129-160.

CHARROIN, C., ABELIN-GENEVOIS, K., CUNIN, V., BERTHILLER, J., CONSTANT, H., KOHLER, R., AULAGNER, G., SERRIER, H. & ARMOIRY, X. 2014. Direct costs associated with the management of progressive early onset scoliosis: Estimations based on gold standard technique or with magnetically controlled growing rods. *Orthopaedics & Traumatology: Surgery & Research,* 100**,** 469-474.

CHOMENTOWSKI, P., COEN, P. M., RADIKOVÁ, Z., GOODPASTER, B. H. & TOLEDO, F. G. S. 2011. Skeletal Muscle Mitochondria in Insulin Resistance: Differences in Intermyofibrillar Versus Subsarcolemmal Subpopulations and Relationship to Metabolic Flexibility. *The Journal of Clinical Endocrinology & Metabolism,* 96**,** 494-503.

CHUNG, K., WALLACE, J., KIM, S. Y., KALYANASUNDARAM, S., ANDALMAN, A. S., DAVIDSON, T. J., MIRZABEKOV, J. J., ZALOCUSKY, K. A., MATTIS, J., DENISIN, A. K., PAK, S., BERNSTEIN, H., RAMAKRISHNAN, C., GROSENICK, L., GRADINARU, V. & DEISSEROTH, K. 2013. Structural and molecular interrogation of intact biological systems. *Nature,* 497**,** 332-337.

COLE, G. K., VAN DEN BOGERT, A. J., HERZOG, W. & GERRITSEN, K. G. M. 1996. Modelling of force production in skeletal muscle undergoing stretch. *Journal of Biomechanics,* 29**,** 1091-1104.

COONEY, G. M., MOERMAN, K. M., TAKAZA, M., WINTER, D. C. & SIMMS, C. K. 2015. Uniaxial and biaxial mechanical properties of porcine linea alba. *Journal of the Mechanical Behavior of Biomedical Materials,* 41**,** 68-82.

COX, G., KABLE, E., JONES, A., FRASER, I., MANCONI, F. & GORRELL, M. D. 2003. 3-Dimensional imaging of collagen using second harmonic generation. *Journal of Structural Biology,* 141**,** 53-62.

CUSHING, C. A. & PHILLIPS, L. G. 2013. Evidence-Based Medicine: Pressure Sores. *Plastic and Reconstructive Surgery,* 132**,** 1720-1732 10.1097/PRS.0b013e3182a808ba.

DAS, C., ROY, B. C., OSHIMA, I., MIYACHI, H., NISHIMURA, S., IWAMOTO, H. & TABATA, S. 2010. Collagen content and architecture of the pectoralis muscle in male chicks and broilers reared under various nutritional conditions. *Animal Science Journal,* 81**,** 252-263.

DE GROOTE, F., VAN CAMPEN, A., JONKERS, I. & DE SCHUTTER, J. 2010. Sensitivity of dynamic simulations of gait and dynamometer experiments to hill muscle model parameters of knee flexors and extensors. *Journal of biomechanics,* 43**,** 1876-1883.

DE JONGE, N., MUYLAERT, D. E., FIORETTA, E. S., BAAIJENS, F. P., FLEDDERUS, J. O., VERHAAR, M. C. & BOUTEN, C. V. 2013. Matrix production and organization by endothelial colony forming cells in mechanically strained engineered tissue constructs. *PloS one,* 8.

DELP, S. L., ANDERSON, F. C., ARNOLD, A. S., LOAN, P., HABIB, A., JOHN, C. T., GUENDELMAN, E. & THELEN, D. G. 2007. OpenSim: open-source software to create and analyze dynamic simulations of movement. *IEEE transactions on biomedical engineering,* 54**,** 1940-1950.

DILL, E. H. 2007. *Continuum mechanics : elasticity, plasticity, viscoelasticity,* Boca Raton, Fla., London : CRC.

DOEHRING, T. C., CAREW, E. O. & VESELY, I. 2004. The effect of strain rate on the viscoelastic response of aortic valve tissue: A direct-fit approach. *Annals of Biomedical Engineering,* 32**,** 223-232.

DRANSFIELD, E. 1977. Intramuscular composition and texture of beef muscles. *Journal of the Science of Food and Agriculture,* 28**,** 833-842.

DRAPACA, C. S., SIVALOGANATHAN, S. & TENTI, G. 2007. Nonlinear constitutive laws in viscoelasticity. *Mathematics and Mechanics of Solids,* 12**,** 475-501.

DUENWALD, S. E., VANDERBY JR, R. & LAKES, R. S. 2009. Viscoelastic relaxation and recovery of tendon. *Annals of Biomedical Engineering,* 37**,** 1131-1140.

FANG, F., SAWHNEY, A. S. & LAKE, S. P. 2014. Different regions of bovine deep digital flexor tendon exhibit distinct elastic, but not viscous, mechanical properties under both compression and shear loading. *Journal of Biomechanics,* 47**,** 2869-2877.

FANG, S. H., NISHIMURA, T. & TAKAHASHI, K. 1999. Relationship between development of intramuscular connective tissue and toughness of pork during growth of pigs. *Journal of Animal Science,* 77**,** 120-130.

FERGUSON, R. A., BALL, D. & SARGEANT, A. J. 2002. Effect of muscle temperature on rate of oxygen uptake during exercise in humans at different contraction frequencies. *Journal of experimental biology,* 205**,** 981-987.

FILIUS, A., DAMEN, T. H. C., SCHUIJER-MAASKANT, K. P., POLINDER, S., HOVIUS, S. E. R. & WALBEEHM, E. T. 2013. Cost analysis of surgically treated pressure sores stage III and IV. *Journal of Plastic, Reconstructive & Aesthetic Surgery,* 66**,** 1580-1586.

FIORENTINO, N. M., EPSTEIN, F. H. & BLEMKER, S. S. 2012. Activation and aponeurosis morphology affect in vivo muscle tissue strains near the myotendinous junction. *J Biomech,* 45**,** 647-52.

FOOLEN, J., VAN DONKELAAR, C. C., NOWLAN, N., MURPHY, P., HUISKES, R. & ITO, K. 2008. Collagen orientation in periosteum and perichondrium is aligned with preferential directions of tissue growth. *Journal of Orthopaedic Research,* 26**,** 1263-1268.

FUNG, Y. C. 1970. Mathematical representation of the mechanical properties of the heart muscle. *Journal of biomechanics,* 3**,** 381-404.

FUNG, Y. C. 1993. *Biomechanics: mechanical properties of living tissues 2nd ed*, Springer-Verlag.

FUNG, Y. C., FRONEK, K., PATITUCCI, P. 1979. Pseudoelasticity of arteries and the choice of its mathematical expression. Am J Physiol, 237, H6. *Physioloy,* 237**,** 20-31.

GANS, C. & BOCK, W. J. 1965. The functional significance of muscle architecture--a theoretical analysis. *Ergebnisse der Anatomie und Entwicklungsgeschichte,* 38**,** 115-142.

GASSER, T. C., OGDEN, R. W. & HOLZAPFEL, G. A. 2006. Hyperelastic modelling of arterial layers with distributed collagen fibre orientations. *Journal of the royal society interface,* 3**,** 15-35.

GILLIES, A. R., BUSHONG, E. A., DEERINCK, T. J., ELLISMAN, M. H. & LIEBER, R. L. 2014. Three-dimensional reconstruction of skeletal muscle extracellular matrix ultrastructure. *Microscopy and Microanalysis,* 20**,** 1835-1840.

GILLIES, A. R. & LIEBER, R. L. 2011. Structure and function of the skeletal muscle extracellular matrix. *Muscle and Nerve,* 44**,** 318-331.

GILLIES, A. R., SMITH, L. R., LIEBER, R. L. & VARGHESE, S. 2011. Method for decellularizing skeletal muscle without detergents or proteolytic enzymes. *Tissue Engineering - Part C: Methods,* 17**,** 383-389.

GINDRE, J., TAKAZA, M., MOERMAN, K. M. & SIMMS, C. K. 2013. A structural model of passive skeletal muscle shows two reinforcement processes in resisting deformation. *Journal of the Mechanical Behavior of Biomedical Materials,* 22**,** 84-94.

GOULD, P. L. 1994. *Introduction to linear elasticity*, Springer.

GRAS, L.-L., MITTON, D., VIOT, P. & LAPORTE, S. 2012a. Hyper-elastic properties of the human sternocleidomastoideus muscle in tension. *Journal of the Mechanical Behavior of Biomedical Materials,* 15**,** 131-140.

GRAS, L. L., LAPORTE, S., MITTON, D., CREVIER-DENOIX, N. & VIOT, P. Tensile tests on a muscle: Influence of experimental conditions and of velocity on its passive response. 2012 IRCOBI Conference Proceedings - International Research Council on the Biomechanics of Injury, 2012b. 515-523.

GRAS, L. L., MITTON, D., CREVIER-DENOIX, N. & LAPORTE, S. 2012c. The non-linear response of a muscle in transverse compression: Assessment of geometry influence using a finite element model. *Computer Methods in Biomechanics and Biomedical Engineering,* 15**,** 13-21.

GRIEVE, A. P. & ARMSTRONG, C. G. 1988. Compressive properties of soft tissues. *International series on Biomechanics.* Armsterdam: Free University Press.

GROVES, R. B., COULMAN, S., BIRCHALL, J. C. & EVANS, S. L. 2012. Quantifying the mechanical properties of human skin to optimise future microneedle device design. *Computer methods in biomechanics and biomedical engineering,* 15**,** 73-82.

HENAK, C. R., ABRAHAM, C. L., ANDERSON, A. E., MAAS, S. A., ELLIS, B. J., PETERS, C. L. & WEISS, J. A. 2014. Patient-specific analysis of cartilage and labrum mechanics in human hips with acetabular dysplasia. *Osteoarthritis and Cartilage,* 22**,** 210-217.

HERNÁNDEZ, B., PEÑA, E., PASCUAL, G., RODRÍGUEZ, M., CALVO, B., DOBLARÉ, M. & BELLÓN, J. M. 2011. Mechanical and histological characterization of the abdominal muscle. A previous step to modelling hernia surgery. *Journal of the Mechanical Behavior of Biomedical Materials,* 4**,** 392-404.

HERZOG, W. 2001. Book review: Skeletal muscle mechanics: from mechanisms to function. Walter Herzog (Ed.); Wiley, Ltd 1 Oldlands Way, Bognor Regis, West Sussex, PO22 9SA, England, 2000, p. 554 Price $ 165.00 ISBN 0-471-49238-8. *Journal of Biomechanics,* 34**,** 1223.

HILL, A. V. The heat of shortening and dynamic constants of muscle. Proceeding of the Royal Society, 1938 London. 136-195.

HILL, R. 1968. On constitutive inequalities for simple materials—I. *Journal of the Mechanics and Physics of Solids,* 16**,** 229-242.

HODGSON, J. A., CHI, S.-W., YANG, J. P., CHEN, J.-S., EDGERTON, V. R. & SINHA, S. 2012. Finite element modeling of passive material influence on the deformation and force output of skeletal muscle. *Journal of the Mechanical Behavior of Biomedical Materials,* 9**,** 163-183.

HOF, A. L. & VAN DEN BERG, J. 1981. EMG to force processing I: An electrical analogue of the Hill muscle model. *Journal of Biomechanics,* 14**,** 747-758.

HOLZAPFEL, G. A. 2000. *Nonlinear solid mechanics*, Wiley Chichester.

HOLZAPFEL, G. A. 2008. Collagen in arterial walls: biomechanical aspects. *Collagen.* Springer.

HOLZAPFEL, G. A. & GASSER, T. C. 2001. A viscoelastic model for fiber-reinforced composites at finite strains: Continuum basis, computational aspects and applications. *Computer methods in applied mechanics and engineering,* 190**,** 4379-4403.

HOLZAPFEL, G. A., SOMMER, G. & REGITNIG, P. 2004. Anisotropic mechanical properties of tissue components in human atherosclerotic plaques. *Journal of Biomechanical Engineering,* 126**,** 657-665.

HUANG, C. Y., MOW, V. C. & ATESHIAN, G. A. 2001. The role of flow-independent viscoelasticity in the biphasic tensile and compressive responses of articular cartilage. *Journal of Biomechanical Engineering,* 123**,** 410-417.

HUANG, C. Y., SOLTZ, M. A., KOPACZ, M., MOW, V. C. & ATESHIAN, G. A. 2003. Experimental verification of the roles of intrinsic matrix viscoelasticity and tension-compression nonlinearity in the biphasic response of cartilage. *Journal of Biomechanical Engineering,* 125**,** 84-93.

HUIJING, P. A. 1999. Muscular force transmission: a unified, dual or multiple system? A review and some explorative experimental results. *Archives of physiology and biochemistry,* 107**,** 292-311.

HUIJING, P. A. 2009. Epimuscular myofascial force transmission: A historical review and implications for new research. International society of biomechanics Muybridge award lecture, Taipei, 2007. *Journal of Biomechanics,* 42**,** 9-21.

HUIJING, P. A., YAMAN, A., OZTURK, C. & YUCESOY, C. A. 2011. Effects of knee joint angle on global and local strains within human triceps surae muscle: MRI analysis indicating in vivo myofascial force transmission between synergistic muscles. *Surg Radiol Anat,* 33**,** 869-79.

HUMPHREY, J. D., STRUMPF, R. K. & YIN, F. C. P. 1990a. Determination of a constitutive relation for passive myocardium: I. A new functional form. *Journal of Biomechanical Engineering,* 112**,** 333-339.

HUMPHREY, J. D., STRUMPF, R. K. & YIN, F. C. P. 1990b. Determination of a constitutive relation for passive myocardium: II. - Parameter estimation. *Journal of Biomechanical Engineering,* 112**,** 340-346.

HUXLEY, A. F. 1957. Muscle structure and theories of contraction. *Progress in biophysics and biophysical chemistry,* 7**,** 255-318.

HUXLEY, A. F. & SIMMONS, R. M. 1971. Proposed mechanism of force generation in striated muscle. *Nature,* 233**,** 533-538.

HUXLEY, H. & RECONDITI, M. 2012. Modeling the Working Stroke of the Muscle Crossbridges. *Biophysical Journal,* 102**,** 148a.

HUXLEY, H. E. 1977. 6 - Past and Present Studies on the Interaction of Actin and Myosin A2 - KAMINER, BENJAMIN. *Search and Discovery.* Academic Press.

IVANCIC, P. C., ITO, S. & PANJABI, M. M. 2007. Dynamic sagittal flexibility coefficients of the human cervical spine. *Accident Analysis and Prevention,* 39**,** 688-695.

IWAMOTO, H., TABATA, S., SAKAKIBARA, K., NISHIMURA, S., GOTOH, T. & KOGA, Y. 2001. Scanning electron microscopic observation of the architecture of collagen fibres in chicken M. iliotibialis lateralis. *British Poultry Science,* 42**,** 321-326.

IWASAKI, T., TERRILL, J., SHAVLAKADZE, T., GROUNDS, M. D. & ARTHUR, P. G. 2013. Visualizing and quantifying oxidized protein thiols in tissue sections: A comparison of dystrophic mdx and normal skeletal mouse muscles. *Free Radical Biology and Medicine,* 65**,** 1408-1416.

JUNQUEIRA, L. C. U., BIGNOLAS, G. & BRENTANI, R. R. 1979. Picrosirius staining plus polarization microscopy, a specific method for collagen detection in tissue sections. *The Histochemical Journal,* 11**,** 447-455.

KELLERMAYER, M. S., BUSTAMANTE, C. & GRANZIER, H. L. 2003. Mechanics and structure of titin oligomers explored with atomic force microscopy. *Biochimica et Biophysica Acta (BBA)-Bioenergetics,* 1604**,** 105-114.

KJAER, M. 2004. Role of extracellular matrix in adaptation of tendon and skeletal muscle to mechanical loading. *Physiological Reviews,* 84**,** 649-698.

KORTHUIS, R. J. 2011. Skeletal Muscle Circulation.

KOVANEN, V., SUOMINEN, H. & HEIKKINEN, E. 1980. Connective tissue of “fast” and “slow” skeletal muscle in rats… effects of endurance training. *Acta Physiologica Scandinavica,* 108**,** 173-180.

KOVANEN, V., SUOMINEN, H. & HEIKKINEN, E. 1984. Collagen of slow twitch and fast twitch muscle fibres in different types of rat skeletal muscle. *European journal of applied physiology and occupational physiology,* 52**,** 235-242.

KRAHN, K. N., BOUTEN, C. V. C., VAN TUIJL, S., VAN ZANDVOORT, M. A. M. J. & MERKX, M. 2006. Fluorescently labeled collagen binding proteins allow specific visualization of collagen in tissues and live cell culture. *Analytical Biochemistry,* 350**,** 177-185.

KRESS, M., HUXLEY, H. E., FARUQI, A. R. & HENDRIX, J. 1986. Structural changes during activation of frog muscle studied by time-resolved X-ray diffraction. *Journal of Molecular Biology,* 188**,** 325-342.

KUMAR, G. L. & RUDBECK, L. 2009. *Education Guide / Immunohistochemical (IHC) Stainig Methods,* California, Dako North America

LAI, A., SCHACHE, A. G., LIN, Y.-C. & PANDY, M. G. 2014. Tendon elastic strain energy in the human ankle plantar-flexors and its role with increased running speed. *Journal of Experimental Biology,* 217**,** 3159-3168.

LAUTERBACH, M. A., KELLER, J., SCHÖNLE, A., KAMIN, D., WESTPHAL, V., RIZZOLI, S. O. & HELL, S. W. 2010. Comparing video-rate STED nanoscopy and confocal microscopy of living neurons. *Journal of biophotonics,* 3**,** 417-424.

LEAKE, M. C., WILSON, D., GAUTEL, M. & SIMMONS, R. M. 2004. The elasticity of single titin molecules using a two-bead optical tweezers assay. *Biophysical journal,* 87**,** 1112-1135.

LEE, S. S., ARNOLD, A. S., DE BOEF MIARA, M., BIEWENER, A. A. & WAKELING, J. M. 2013. Accuracy of gastrocnemius muscles forces in walking and running goats predicted by one-element and two-element Hill-type models. *Journal of biomechanics,* 46**,** 2288-2295.

LEPETIT, J. 1991. Theoretical strain ranges in raw meat. *Meat science,* 29**,** 271-283.

LEPETIT, J. 2008. Collagen contribution to meat toughness: Theoretical aspects. *Meat Science,* 80**,** 960-967.

LEWIS, G. J. & PURSLOW, P. P. 1989. The strength and stiffness of perimysial connective tissue isolated from cooked beef muscle. *Meat Science,* 26**,** 255-269.

LEWIS, G. J. & PURSLOW, P. P. 1990. Connective tissue differences in the strength of cooked meat across the muscle fibre direction due to test specimen size. *Meat Science,* 28**,** 183-194.

LEWIS, G. J., PURSLOW, P. P. & RICE, A. E. 1991. The effect of conditioning on the strength of perimysial connective tissue dissected from cooked meat. *Meat Science,* 30**,** 1-12.

LI, J., LUO, X. Y. & KUANG, Z. B. 2001. A nonlinear anisotropic model for porcine aortic heart valves. *Journal of Biomechanics,* 34**,** 1279-1289.

LI, L. P., CHEUNG, J. T. M. & HERZOG, W. 2009. Three-dimensional fibril-reinforced finite element model of articular cartilage. *Medical & Biological Engineering & Computing,* 47**,** 607-615.

LIEBER, R. L. & FRIDÉN, J. 2000. Functional and clinical significance of skeletal muscle architecture. *Muscle and Nerve,* 23**,** 1647-1666.

LIGHT, N. & CHAMPION, A. E. 1984. Characterization of muscle epimysium, perimysium and endomysium collagens. *Biochemical Journal,* 219**,** 1017-1026.

LIGHT, N., CHAMPION, A. E., VOYLE, C. & BAILEY, A. J. 1985. The rôle of epimysial, perimysial and endomysial collagen in determining texture in six bovine muscles. *Meat Science,* 13**,** 137-149.

LIMBERT, G. & MIDDLETON, J. 2004. A transversely isotropic viscohyperelastic material Application to the modeling of biological soft connective tissues. *International Journal of Solids and Structures,* 41**,** 4237-4260.

LINDER-GANZ, E. & GEFEN, A. 2008. Stress Analyses Coupled With Damage Laws to Determine Biomechanical Risk Factors for Deep Tissue Injury During Sitting. *Journal of Biomechanical Engineering,* 131**,** 011003-011003.

LINDER-GANZ, E., SHABSHIN, N., ITZCHAK, Y. & GEFEN, A. 2007. Assessment of mechanical conditions in sub-dermal tissues during sitting: A combined experimental-MRI and finite element approach. *Journal of Biomechanics,* 40**,** 1443-1454.

LINDER-GANZ, E., YARNITZKY, G., YIZHAR, Z., SIEV-NER, I. & GEFEN, A. 2009. Real-time finite element monitoring of sub-dermal tissue stresses in individuals with spinal cord injury: Toward prevention of pressure ulcers. *Annals of Biomedical Engineering,* 37**,** 387-400.

LINKE, W. A., IVEMEYER, M., MUNDEL, P., STOCKMEIER, M. R. & KOLMERER, B. 1998. Nature of PEVK-titin elasticity in skeletal muscle. *Proceedings of the National Academy of Sciences,* 95**,** 8052-8057.

LISTRAT, A., PICARD, B. & GEAY, Y. 1999. Age-related changes and location of type I, III, IV, V and VI collagens during development of four foetal skeletal muscles of double-muscled and normal bovine animals. *Tissue and Cell,* 31**,** 17-27.

LIU, A., NISHIMURA, T. & TAKAHASHI, K. 1994. Structural changes in endomysium and perimysium during post-mortem aging of chicken Semitendinosus muscle—Contribution of structural weakening of intramuscular connective tissue to meat tenderization. *Meat Science,* 38**,** 315-328.

LIU, A., NISHIMURA, T. & TAKAHASHI, K. 1996. Relationship between structural properties of intramuscular connective tissue and toughness of various chicken skeletal muscles. *Meat Science,* 43**,** 43-49.

LU, Q., GANESAN, K., SIMIONESCU, D. T. & VYAVAHARE, N. R. 2004. Novel porous aortic elastin and collagen scaffolds for tissue engineering. *Biomaterials,* 25**,** 5227-5237.

MAGID, A. & LAW, D. J. 1985. Myofibrils bear most of the resting tension in frog skeletal muscle. *Science,* 230**,** 1280-1282.

MAK, A. F. T., YU, Y., KWAN, L. P. C., SUN, L. & TAM, E. W. C. 2011. Deformation and reperfusion damages and their accumulation in subcutaneous tissues during loading and unloading: A theoretical modeling of deep tissue injuries. *Journal of Theoretical Biology,* 289**,** 65-73.

MARCKMANN, G. & VERRON, E. 2006. Comparison of hyperelastic models for rubber-like materials. *Rubber chemistry and technology,* 79**,** 835-858.

MARTIN, R. B., BURR, D. B. & SHARKEY, N. A. 1998. *Skeletal tissue mechanics,* New York ; London, Springer.

MARTINI, F. 1989. *Fundamentals of anatomy and physiology*, Prentice-Hall.

MARTINS, J. A. C., PIRES, E. B., SALVADO, R. & DINIS, P. B. 1998. A numerical model of passive and active behavior of skeletal muscles. *Computer Methods in Applied Mechanics and Engineering,* 151**,** 419-433.

MARTINS, P. A. L. S., NATAL JORGE, R. M. & FERREIRA, A. J. M. 2006. A Comparative Study of Several Material Models for Prediction of Hyperelastic Properties: Application to Silicone-Rubber and Soft Tissues. *Strain,* 42**,** 135-147.

MARUYAMA, K. 1994. Connectin, an elastic protein of striated muscle. *Biophysical chemistry,* 50**,** 73-85.

MCCORMICK, R. J. 1994. The flexibility of the collagen compartment of muscle. *Meat Science,* 36**,** 79-91.

MCLELLAND, J. 1990. *A Colour Atlas of Avian Anatomy,* England, Wolfe Publishing Ltd.

MEIJER, R., BROOS, J., ELROFAI, H., DE BRUIJN, E., FORBES, P. & HAPPEE, R. Modelling of bracing in a multi-body active human model. 2013 IRCOBI Conference Proceedings - International Research Council on the Biomechanics of Injury, 2013. 576-587.

MEYER, G. A. & LIEBER, R. L. 2011. Elucidation of extracellular matrix mechanics from muscle fibers and fiber bundles. *Journal of biomechanics,* 44**,** 771-773.

MILLER, K. 1999. Constitutive model of brain tissue suitable for finite element analysis of surgical procedures. *Journal of Biomechanics,* 32**,** 531-537.

MILLER, K. & CHINZEI, K. 1997. Constitutive modelling of brain tissue: Experiment and theory. *Journal of Biomechanics,* 30**,** 1115-1121.

MILLER, K. & CHINZEI, K. 2002. Mechanical properties of brain tissue in tension. *Journal of Biomechanics,* 35**,** 483-490.

MISHINA, N. M., MISHIN, A. S., BELYAEV, Y., BOGDANOVA, E. A., LUKYANOV, S., SCHULTZ, C. & BELOUSOV, V. V. 2015. Live-Cell STED Microscopy with Genetically Encoded Biosensor. *Nano Letters,* 15**,** 2928-2932.

MOERMAN, K. M., NAGEL, T., TAKAZA, M., NEDERVEEN, A. & SIMMS, C. K. 2012. Constitutive modelling of passive skeletal muscle anisotropy in tension and compression. *Journal of Biomechanics,* 45**,** S487.

MOERMAN, K. M., SIMMS, C. K. & NAGEL, T. 2016. Control of tension–compression asymmetry in Ogden hyperelasticity with application to soft tissue modelling. *Journal of the mechanical behavior of biomedical materials,* 56**,** 218-228.

MOO, E. K., HAN, S. K., FEDERICO, S., SIBOLE, S. C., JINHA, A., ABU OSMAN, N. A., PINGGUAN-MURPHY, B. & HERZOG, W. 2014. Extracellular matrix integrity affects the mechanical behaviour of in-situ chondrocytes under compression. *Journal of Biomechanics,* 47**,** 1004-1013.

MOORE, M. 1983. The dual connective tissue system of rat soleus muscle. *Muscle & nerve,* 6**,** 416-422.

MORROW, D. A., DONAHUE, T. H., ODEGARD, G. M. & KAUFMAN, K. R. 2010a. A method for assessing the fit of a constitutive material model to experimental stress-strain data. *Computer Methods in Biomechanics and Biomedical Engineering,* 13**,** 247-256.

MORROW, D. A., HAUT DONAHUE, T. L., ODEGARD, G. M. & KAUFMAN, K. R. 2010b. Transversely isotropic tensile material properties of skeletal muscle tissue. *Journal of the Mechanical Behavior of Biomedical Materials,* 3**,** 124-129.

MOW, V. C., KUEI, S. C., LAI, W. M. & ARMSTRONG, C. G. 1980. Biphasic creep and stress relaxation of articular cartilage in compression: Theory and experiments. *Journal of Biomechanical Engineering,* 102**,** 73-84.

MUKHERJEE, S., CHAWLA, A., KARTHIKEYAN, B. & SONI, A. 2007. Finite element crash simulations of the human body: Passive and active muscle modelling. *Sadhana - Academy Proceedings in Engineering Sciences,* 32**,** 409-426.

NACHMIAS, V. T., HUXLEY, H. E. & KESSLER, D. 1970. Electron microscope observations on actomyosin and actin preparations from Physarum polycephalum, and on their interaction with heavy meromyosin subfragment I from muscle myosin. *Journal of Molecular Biology,* 50**,** 83-IN16.

NAGEL, T., LOERAKKER, S. & OOMENS, C. W. J. 2009. A theoretical model to study the effects of cellular stiffening on the damage evolution in deep tissue injury. *Computer Methods in Biomechanics and Biomedical Engineering,* 12**,** 585-597.

NAKAMURA, Y. N., IWAMOTO, H., TABATA, S., ONO, Y., SHIBA, N. & NISHIMURA, S. 2003. Comparison of collagen content, distribution and architecture among the pectoralis, iliotibialis lateralis and puboischiofemoralis muscles with different myofiber composition in Silky cocks. *Animal Science Journal,* 74**,** 119-128.

NIE, X., CHENG, J. I., CHEN, W. W. & WEERASOORIYA, T. 2011. Dynamic tensile response of porcine muscle. *Journal of Applied Mechanics, Transactions ASME,* 78.

NISHIMURA, T. 2010. The role of intramuscular connective tissue in meat texture. *Animal Science Journal,* 81**,** 21-27.

NISHIMURA, T., FANG, S., ITO, T., WAKAMATSU, J. I. & TAKAHASHI, K. 2008. Structural weakening of intramuscular connective tissue during postmortem aging of pork. *Animal Science Journal,* 79**,** 716-721.

NISHIMURA, T., HATTORI, A. & TAKAHASHI, K. 1994. Ultrastructure of the intramuscular connective tissue in bovine skeletal muscle. *Cells Tissues Organs,* 151**,** 250-257.

NISHIMURA, T., HATTORI, A. & TAKAHASHI, K. 1999. Structural changes in intramuscular connective tissue during the fattening of Japanese Black cattle: Effect of marbling on beef tenderization. *Journal of Animal Science,* 77**,** 93-104.

NISHIMURA, T., LIU, A., HATTORI, A. & TAKAHASHI, K. 1998. Changes in mechanical strength of intramuscular connective tissue during postmortem aging of beef. *Journal of animal science,* 76**,** 528-532.

NISHIMURA, T., OJIMA, K., LIU, A., HATTORI, A. & TAKAHASHI, K. 1996. Structural changes in the intramuscular connective tissue during development of bovine semitendinosus muscle. *Tissue and Cell,* 28**,** 527-536.

NISHIUMI, T., KUNISHIMA, R., NISHIMURA, T. & YOSHIDA, S. 1995. Intramuscular connective tissue components contributing to raw meat toughness in various porcine muscles. *Animal Science and Technology (Japan)*.

NOVAK, V. P. 1994. Regional mechanical properties of passive myocardium. *Journal of Biomechanics,* 27**,** 403-412.

O'MALLEY, B. 2005. *Clinical Anatomy and Physiology of Exotic Species (Structure and function of mammals, birds, reptiles, and amphibians),* Edinburgh, W.B. Saunders.

ODA, T., HIMENO, R., HAY, D. C., KANEHISA, H., FUKUNAGA, T. & KAWAKAMI, Y. 2013. The activation time-course of contractile elements estimated from in vivo fascicle behaviours during twitch contractions. *Journal of Sports Sciences,* 31**,** 1233-1241.

OGDEN, R. 1986. Recent advances in the phenomenological theory of rubber elasticity. *Rubber Chemistry and Technology,* 59**,** 361-383.

OGDEN, R. W. 1978a. Nearly isochoric elastic deformations: Application to rubberlike solids. *Journal of the Mechanics and Physics of Solids,* 26**,** 37-57.

OGDEN, R. W. 1978b. ON PLANE DEFORMATIONS OF INCOMPRESSIBLE ISOTROPIC ELASTIC SOLIDS. *Math Proc Cambridge Phil Soc,* 83**,** 127-136.

OGDEN, R. W., SACCOMANDI, G. & SGURA, I. 2004. Fitting hyperelastic models to experimental data. *Computational Mechanics,* 34**,** 484-502.

OGDEN, R. W. & STERNBERG, E. 1985. Nonlinear Elastic Deformations. *Journal of Applied Mechanics,* 52**,** 740.

OLIVEIRA, L. F. D., PEIXINHO, C. C., SILVA, G. A. & MENEGALDO, L. L. 2016. In vivo passive mechanical properties estimation of Achilles tendon using ultrasound. *Journal of Biomechanics,* 49**,** 507-513.

OOMENS, C. W. J., MAENHOUT, M., VAN OIJEN, C. H., DROST, M. R. & BAAIJENS, F. P. 2003. Finite element modelling of contracting skeletal muscle. *Philosophical Transactions of the Royal Society of London. Series B: Biological Sciences,* 358**,** 1453-1460.

OSHIMA, I., IWAMOTO, H., TABATA, S., ONO, Y., ISHIBASHI, A., SHIBA, N., MIYACHI, H., GOTOH, T. & NISHIMURA, S. 2007a. Comparative observations of the growth changes of the histochemical properties and collagen architecture of the iliotibialis lateralis muscle from Silky, layer and meat type cockerels. *Animal Science Journal,* 78**,** 546-559.

OSHIMA, I., IWAMOTO, H., TABATA, S., ONO, Y., ISHIBASHI, A., SHIBA, N., MIYACHI, H., GOTOH, T. & NISHIMURA, S. 2007b. Comparative observations on the growth changes of the histochemical property and collagen architecture of the Musculus pectoralis from Silky, layer-type and meat-type cockerels. *Animal Science Journal,* 78**,** 619-630.

PALEVSKI, A., GLAICH, I., PORTNOY, S., LINDER-GANZ, E. & GEFEN, A. 2006. Stress relaxation of porcine gluteus muscle subjected to sudden transverse deformation as related to pressure sore modeling. *Journal of Biomechanical Engineering,* 128**,** 782-787.

PAMUK, U. & YUCESOY, C. A. 2015. MRI analyses show that kinesio taping affects much more than just the targeted superficial tissues and causes heterogeneous deformations within the whole limb. *J Biomech,* 48**,** 4262-70.

PASSERIEUX, E., ROSSIGNOL, R., CHOPARD, A., CARNINO, A., MARINI, J. F., LETELLIER, T. & DELAGE, J. P. 2006. Structural organization of the perimysium in bovine skeletal muscle: Junctional plates and associated intracellular subdomains. *Journal of Structural Biology,* 154**,** 206-216.

PATTI, J. M., BREMELL, T., KRAJEWSKA-PIETRASIK, D., ABDELNOUR, A., TARKOWSKI, A., RYDEN, C. & HOOK, M. 1994. The Staphylococcus aureus collagen adhesin is a virulence determinant in experimental septic arthritis. *Infection and Immunity,* 62**,** 152-161.

PIETSCH, R., WHEATLEY, B. B., HAUT DONAHUE, T. L., GILBRECH, R., PRABHU, R., LIAO, J. & WILLIAMS, L. N. 2014. Anisotropic Compressive Properties of Passive Porcine Muscle Tissue. *Journal of Biomechanical Engineering,* 136**,** 111003-111003.

PLOWMAN, S. A. & SMITH, D. L. 2013. *Exercise physiology for health fitness and performance*, Lippincott Williams & Wilkins.

PODOLSKY, R. 1964. The maximum sarcomere length for contraction of isolated myofibrils. *The Journal of physiology,* 170**,** 110.

POWERS, S. K. & HOWLEY, E. T. 2012. *Exercise physiology : theory and application to fitness and performance,* New York, McGraw-Hill.

PRAXL, N., ADAMEC, J., MUGGENTHALER, H. & VON MERTEN, K. 2008. Numerical human models for accident research and safety - potentials and limitations. *Studies in health technology and informatics,* 133**,** 201-207.

PURSLOW, P. P. 1989. Strain-induced reorientation of an intramuscular connective tissue network: Implications for passive muscle elasticity. *Journal of Biomechanics,* 22**,** 21-31.

PURSLOW, P. P. 2002. The structure and functional significance of variations in the connective tissue within muscle. *Comparative Biochemistry and Physiology - A Molecular and Integrative Physiology,* 133**,** 947-966.

PURSLOW, P. P. 2005. Intramuscular connective tissue and its role in meat quality. *Meat Science,* 70**,** 435-447.

PURSLOW, P. P. 2008. The extracellular matrix of skeletal and cardiac muscle. *Collagen: Structure and Mechanics.*

PURSLOW, P. P. 2010. Muscle fascia and force transmission. *Journal of Bodywork and Movement Therapies,* 14**,** 411-417.

PURSLOW, P. P. & TROTTER, J. A. 1994. The morphology and mechanical properties of endomysium in series-fibred muscles: variations with muscle length. *Journal of Muscle Research and Cell Motility,* 15**,** 299-308.

PUSO, M. A. & WEISS, J. A. 1998. Finite element implementation of anisotropic quasi-linear viscoelasticity using a discrete spectrum approximation. *Journal of Biomechanical Engineering,* 120**,** 62-70.

RALTON, L. D. & MURRAY, G. I. 2011. The use of formalin fixed wax embedded tissue for proteomic analysis. *Journal of Clinical Pathology,* 64**,** 297-302.

REHORN, M. R. & BLEMKER, S. S. 2010. The effects of aponeurosis geometry on strain injury susceptibility explored with a 3D muscle model. *Journal of Biomechanics,* 43**,** 2574-2581.

REHORN, M. R., SCHROER, A. K. & BLEMKER, S. S. 2014. The passive properties of muscle fibers are velocity dependent. *Journal of Biomechanics,* 47**,** 687-693.

RENSHAW, S. 2013. Immunohistochemmistry and imunocytochemistry. *In:* WILD, D. (ed.) *The Immunoassay Handbook:Theory and Applications of Ligand Binding, ELISA and Related Techniques.* fourth ed. Great Britain: Elsevier Ltd.

RICH, L. & WHITTAKER, P. 2005. Collagen and picrosirius red staining: a polarized light assessment of fibrillar hue and spatial distribution. *Braz J Morphol Sci,* 22**,** 97-104.

RICH, R. L., DEIVANAYAGAM, C. C., OWENS, R. T., CARSON, M., HÖÖK, A., MOORE, D., YANG, V. W.-C., STHANAM, V. & HÖÖK, M. 1999. Trench-shaped binding sites promote multiple classes of interactions between collagen and the adherence receptors, α1β1 integrin and Staphylococcus aureus Cna MSCRAMM. *Journal of Biological Chemistry,* 274**,** 24906-24913.

RODRIGUES, C. J., RODRIGUES, J. A. J. & BOHM, G. M. 1996. Effects of Aging on Muscle Fibers and Collagen Content of the Diaphragm: A Comparison with the Rectus abdominis Muscle. *Gerontology,* 42**,** 218-228.

ROUSSEAU, E. P. M., SAUREN, A. A. H. J., VAN HOUT, M. C. & VAN STEENHOVEN, A. A. 1983. Elastic and viscoelastic material behaviour of fresh and glutaraldehyde-treated porcine aortic valve tissue. *Journal of Biomechanics,* 16**,** 339-348.

ROWE, R. 1981. Morphology of perimysial and endomysial connective tissue in skeletal muscle. *Tissue and Cell,* 13**,** 681-690.

ROWE, R. W. D. 1974. Collagen fibre arrangement in intramuscular connective tissue. Changes associated with muscle shortening and their possible relevance to raw meat toughness measurements. *International Journal of Food Science & Technology,* 9**,** 501-508.

ROY, B. C., OSHIMA, I., MIYACHI, H., SHIBA, N., NISHIMURA, S., TABATA, S. & IWAMOTO, H. 2006. Effects of nutritional level on muscle development, histochemical properties of myofibre and collagen architecture in the pectoralis muscle of male broilers. *British Poultry Science,* 47**,** 433-442.

SAHAI, E., WYCKOFF, J., PHILIPPAR, U., SEGALL, J. E., GERTLER, F. & CONDEELIS, J. 2005. Simultaneous imaging of GFP, CFP and collagen in tumors in vivo using multiphoton microscopy. *BMC Biotechnology,* 5**,** 1-9.

SAKAKIBARA, K., TABATA, S., SHIBA, N., GOTOH, T., NISHIMURA, S. & IWAMOTO, H. 2000. Myofibre composition and total collagen content in M. iliotibialis lateralis and M. pectoralis of Silkie and White Leghorn chickens. *British Poultry Science,* 41**,** 570-574.

SCARR, G. 2016. Fascial hierarchies and the relevance of crossed-helical arrangements of collagen to changes in the shape of muscles. *Journal of Bodywork and Movement Therapies,* 20**,** 377-387.

SCHMALBRUCH, H. 2012. *Skeletal muscle*, Springer Science & Business Media.

SCOVIL, C. Y. & RONSKY, J. L. 2006. Sensitivity of a Hill-based muscle model to perturbations in model parameters. *Journal of biomechanics,* 39**,** 2055-2063.

SETH, B. R. 1961. *Generelised strain measure with applications to physical problems*, MRC Technical Summary Report #248 (Mathematics Research Centre, United States Army, The University of Wisconsin).

SHARAFI, B., AMES, E. G., HOLMES, J. W. & BLEMKER, S. S. 2011. Strains at the myotendinous junction predicted by a micromechanical model. *Journal of Biomechanics,* 44**,** 2795-2801.

SHARAFI, B. & BLEMKER, S. S. 2010. A micromechanical model of skeletal muscle to explore the effects of fiber and fascicle geometry. *Journal of Biomechanics,* 43**,** 3207-3213.

SHARAFI, B. & BLEMKER, S. S. 2011. A mathematical model of force transmission from intrafascicularly terminating muscle fibers. *Journal of Biomechanics,* 44**,** 2031-2039.

SHEN, Z. L., DODGE, M. R., KAHN, H., BALLARINI, R. & EPPELL, S. J. 2008. Stress-strain experiments on individual collagen fibrils. *Biophysical Journal,* 95**,** 3956-3963.

SIEBERT, T., RODE, C., HERZOG, W., TILL, O. & BLICKHAN, R. 2008. Nonlinearities make a difference: comparison of two common Hill-type models with real muscle. *Biological Cybernetics,* 98**,** 133-143.

SIEBERT, T., TILL, O. & BLICKHAN, R. 2014. Work partitioning of transversally loaded muscle: Experimentation and simulation. *Computer Methods in Biomechanics and Biomedical Engineering,* 17**,** 217-229.

SIMMS, C. K., VAN LOOCKE, M. & LYONS, C. G. 2012. SKELETAL MUSCLE IN COMPRESSION: MODELING APPROACHES FOR THE PASSIVE MUSCLE BULK. *International Journal for Multiscale Computational Engineering,* 10**,** 143-154.

SLEBODA, D. A. & ROBERTS, T. J. 2017. Incompressible fluid plays a mechanical role in the development of passive muscle tension. *Biology Letters,* 13.

SNEDEKER, J. G., NIEDERER, P., SCHMIDLIN, F. R., FARSHAD, M., DEMETROPOULOS, C. K., LEE, J. B. & YANG, K. H. 2005. Strain-rate dependent material properties of the porcine and human kidney capsule. *Journal of Biomechanics,* 38**,** 1011-1021.

SONG, B., CHEN, W., GE, Y. & WEERASOORIYA, T. 2007. Dynamic and quasi-static compressive response of porcine muscle. *Journal of Biomechanics,* 40**,** 2999-3005.

SPENCER, A. J. M. & HASHIN, Z. 1986. Continuum Theory of the Mechanics of Fibre-Reinforced Composites. *Journal of Applied Mechanics,* 53**,** 233.

STÅLHAND, J., KLARBRING, A. & HOLZAPFEL, G. A. 2008. Smooth muscle contraction: mechanochemical formulation for homogeneous finite strains. *Progress in biophysics and molecular biology,* 96**,** 465-481.

STREET, S. F. 1983. Lateral transmission of tension in frog myofibers: A myofibrillar network and transverse cytoskeletal connections are possible transmitters. *Journal of Cellular Physiology,* 114**,** 346-364.

SUMMERHURST, K., STARK, M., SHARPE, J., DAVIDSON, D. & MURPHY, P. 2008. 3D representation of Wnt and Frizzled gene expression patterns in the mouse embryo at embryonic day 11.5 (Ts19). *Gene Expression Patterns,* 8**,** 331-348.

SUSAKI, E. A. & UEDA, H. R. 2016. Whole-body and Whole-Organ Clearing and Imaging Techniques with Single-Cell Resolution: Toward Organism-Level Systems Biology in Mammals. *Cell Chemical Biology,* 23**,** 137-157.

TAKAZA, M., COONEY, G. M., MCMANUS, G., STAFFORD, P. & SIMMS, C. K. 2014. Assessing the microstructural response to applied deformation in porcine passive skeletal muscle. *Journal of the Mechanical Behavior of Biomedical Materials,* 40**,** 115-126.

TAKAZA, M., MOERMAN, K. M., GINDRE, J., LYONS, G. & SIMMS, C. K. 2013a. The anisotropic mechanical behaviour of passive skeletal muscle tissue subjected to large tensile strain. *Journal of the Mechanical Behavior of Biomedical Materials,* 17**,** 209-220.

TAKAZA, M., MOERMAN, K. M. & SIMMS, C. K. 2013b. Passive skeletal muscle response to impact loading: Experimental testing and inverse modelling. *Journal of the Mechanical Behavior of Biomedical Materials,* 27**,** 214-225.

TAKAZA, M. & SIMMS, C. K. The passive response of skeletal muscle to compressive impact loading. 2012 IRCOBI Conference Proceedings - International Research Council on the Biomechanics of Injury, 2012. 503-514.

TAYLOR, C. A. & HUMPHREY, J. 2009. Open problems in computational vascular biomechanics: hemodynamics and arterial wall mechanics. *Computer methods in applied mechanics and engineering,* 198**,** 3514-3523.

TÖZEREN, A. 1985. Constitutive equations of skeletal muscle based on cross-bridge mechanism. *Biophysical journal,* 47**,** 225-236.

TROTTER, J. A. & PURSLOW, P. P. 1992. Functional morphology of the endomysium in series fibered muscles. *Journal of Morphology,* 212**,** 109-122.

TURKOGLU, A. N., HUIJING, P. A. & YUCESOY, C. A. 2014. Mechanical principles of effects of botulinum toxin on muscle length-force characteristics: An assessment by finite element modeling. *Journal of Biomechanics,* 47**,** 1565-1571.

TURRINA, A., MARTÍNEZ-GONZÁLEZ, M. A. & STECCO, C. 2013. The muscular force transmission system: role of the intramuscular connective tissue. *Journal of bodywork and movement therapies,* 17**,** 95-102.

VALDEZ, M. & BALACHANDRAN, B. 2013. Longitudinal nonlinear wave propagation through soft tissue. *Journal of the Mechanical Behavior of Biomedical Materials,* 20**,** 192-208.

VALIC, Z., BUCKWALTER, J. B. & CLIFFORD, P. S. 2005. Muscle blood flow response to contraction: influence of venous pressure. *J Appl Physiol (1985),* 98**,** 72-6.

VAN DER RIJT, J. A., VAN DER WERF, K. O., BENNINK, M. L., DIJKSTRA, P. J. & FEIJEN, J. 2006. Micromechanical testing of individual collagen fibrils. *Macromolecular bioscience,* 6**,** 697-702.

VAN LOOCKE, M. 2007. *Passive mechanical properties of skeletal muscle in compression.* Ph.D., Trinity College Dublin.

VAN LOOCKE, M., LYONS, C. G. & SIMMS, C. K. 2006. A validated model of passive muscle in compression. *Journal of Biomechanics,* 39**,** 2999-3009.

VAN LOOCKE, M., LYONS, C. G. & SIMMS, C. K. 2008. Viscoelastic properties of passive skeletal muscle in compression: Stress-relaxation behaviour and constitutive modelling. *Journal of Biomechanics,* 41**,** 1555-1566.

VAN LOOCKE, M., SIMMS, C. K. & LYONS, C. G. 2009. Viscoelastic properties of passive skeletal muscle in compression—Cyclic behaviour. *Journal of Biomechanics,* 42**,** 1038-1048.

VAN SLIGTENHORST, C., CRONIN, D. S. & WAYNE BRODLAND, G. 2006. High strain rate compressive properties of bovine muscle tissue determined using a split Hopkinson bar apparatus. *Journal of Biomechanics,* 39**,** 1852-1858.

VANPUTTE, C. L. & SEELEY, R. R. 2014. *Seeley's anatomy & physiology,* New York, NY McGraw-Hill.

VELTEN, B. P. & WELCH JR, K. C. 2014. Myosin heavy-chain isoforms in the flight and leg muscles of hummingbirds and zebra finches. *American Journal of Physiology - Regulatory Integrative and Comparative Physiology,* 306**,** R845-R851.

VIDAL, B. D. C., MELLO, M. L. S. & PIMENTEL, E. R. 1982. Polarization microscopy and microspectrophotometry of Sirius Red, Picrosirius and Chlorantine Fast Red aggregates and of their complexes with collagen. *The Histochemical Journal,* 14**,** 857-878.

VOYTIK-HARBIN, S. L., RAJWA, B. & ROBINSON, J. P. 2001. Three-dimensional imaging of extracellular matrix and extracellular matrix - Cell interactions. *Methods in Cell Biology.*

WEISS, J. A., MAKER, B. N. & GOVINDJEE, S. 1996. Finite element implementation of incompressible, transversely isotropic hyperelasticity. *Computer Methods in Applied Mechanics and Engineering,* 135**,** 107-128.

WHEATLEY, B. B., ODEGARD, G. M., KAUFMAN, K. R. & DONAHUE, T. L. H. 2016. A validated model of passive skeletal muscle to predict force and intramuscular pressure. *Biomechanics and Modeling in Mechanobiology***,** 1-12.

WILLIAMS, P. L., BANNISTER, L. H., GRAY, H. A. D. & SURGICAL 1995. *Gray's anatomy : the anatomical basis of medicine and surgery,* New York ; Edinburgh, Churchill Livingstone.

WILLIAMS, R. M., ZIPFEL, W. R. & WEBB, W. W. 2005. Interpreting second-harmonic generation images of collagen I fibrils. *Biophysical Journal,* 88**,** 1377-1386.

WISNES, A. & KIRKEBO, A. 1976. Regional distribution of blood flow in calf muscles of rat during passive stretch and sustained contraction. *Acta Physiol Scand,* 96**,** 256-66.

WOLF, K., MÜLLER, R., BORGMANN, S., BRÖCKER, E.-B. & FRIEDL, P. 2003. Amoeboid shape change and contact guidance: T-lymphocyte crawling through fibrillar collagen is independent of matrix remodeling by MMPs and other proteases. *Blood,* 102**,** 3262-3269.

WOO, S. L. Y., GOMEZ, M. A. & AKESON, W. H. 1981. The time and history-dependent viscoelastic properties of the canine medial collateral ligament. *Journal of Biomechanical Engineering,* 103**,** 293-298.

WU, J. Z., SINSEL, E. W., SHROYER, J. F., WARREN, C. M., WELCOME, D. E., ZHAO, K. D., AN, K.-N. & BUCZEK, F. L. 2014. Analysis of the musculoskeletal loading of the thumb during pipetting – A pilot study. *Journal of Biomechanics,* 47**,** 392-399.

WU, P. I., MINISINI, S. & EDELMAN, E. R. 2009. Intramuscular drug transport under mechanical loading: Resonance between tissue function and uptake. *Journal of Controlled Release,* 136**,** 99-109.

XIAO, D. Z. T., WU, S. Y. Q. & MAK, A. F. T. 2014. Accumulation of loading damage and unloading reperfusion injury — Modeling of the propagation of deep tissue ulcers. *Journal of Biomechanics,* 47**,** 1658-1664.

XU, Y., RIVAS, J. M., BROWN, E. L., LIANG, X. & HÖÖK, M. 2004. Virulence potential of the staphylococcal adhesin CNA in experimental arthritis is determined by its affinity for collagen. *Journal of Infectious Diseases,* 189**,** 2323-2333.

YAMAN, A., OZTURK, C., HUIJING, P. A. & YUCESOY, C. A. 2013. Magnetic resonance imaging assessment of mechanical interactions between human lower leg muscles in vivo. *J Biomech Eng,* 135**,** 91003.

YANG, L., VAN DER WERF, K. O., FITIÉ, C. F., BENNINK, M. L., DIJKSTRA, P. J. & FEIJEN, J. 2008. Mechanical properties of native and cross-linked type I collagen fibrils. *Biophysical journal,* 94**,** 2204-2211.

YUCESOY, C. A. & HUIJING, P. A. 2009. Assessment by finite element modeling indicates that surgical intramuscular aponeurotomy performed closer to the tendon enhances intended acute effects in extramuscularly connected muscle. *Journal of Biomechanical Engineering,* 131.

YUCESOY, C. A., KOOPMAN, B. H. F. J. M., BAAN, G. C., GROOTENBOER, H. J. & HUIJING, P. A. 2003. Effects of inter- and extramuscular myofascial force transmission on adjacent synergistic muscles: assessment by experiments and finite-element modeling. *Journal of Biomechanics,* 36**,** 1797-1811.

YUCESOY, C. A., KOOPMAN, B. H. F. J. M., HUIJING, P. A. & GROOTENBOER, H. J. 2002. Three-dimensional finite element modeling of skeletal muscle using a two-domain approach: linked fiber-matrix mesh model. *Journal of Biomechanics,* 35**,** 1253-1262.

YUCESOY, C. A., TURKOĞLU, A. N., UMUR, S. & ATEŞ, F. 2015. Intact muscle compartment exposed to botulinum toxin type a shows compromised intermuscular mechanical interaction. *Muscle and Nerve,* 51**,** 106-116.

ZONG, Y., XU, Y., LIANG, X., KEENE, D. R., HÖÖK, A., GURUSIDDAPPA, S., HÖÖK, M. & NARAYANA, S. V. L. 2005. A 'Collagen Hug' Model for Staphylococcus aureus CNA binding to collagen. *EMBO Journal,* 24**,** 4224-4236.

ZURLO, F., LARSON, K., BOGARDUS, C. & RAVUSSIN, E. 1990. Skeletal muscle metabolism is a major determinant of resting energy expenditure. *The Journal of Clinical Investigation,* 86**,** 1423-1427.

Appendix A-The Poisson’s ratio versus stretch ratio in tension and compression deformations for chicken pectoralis muscle

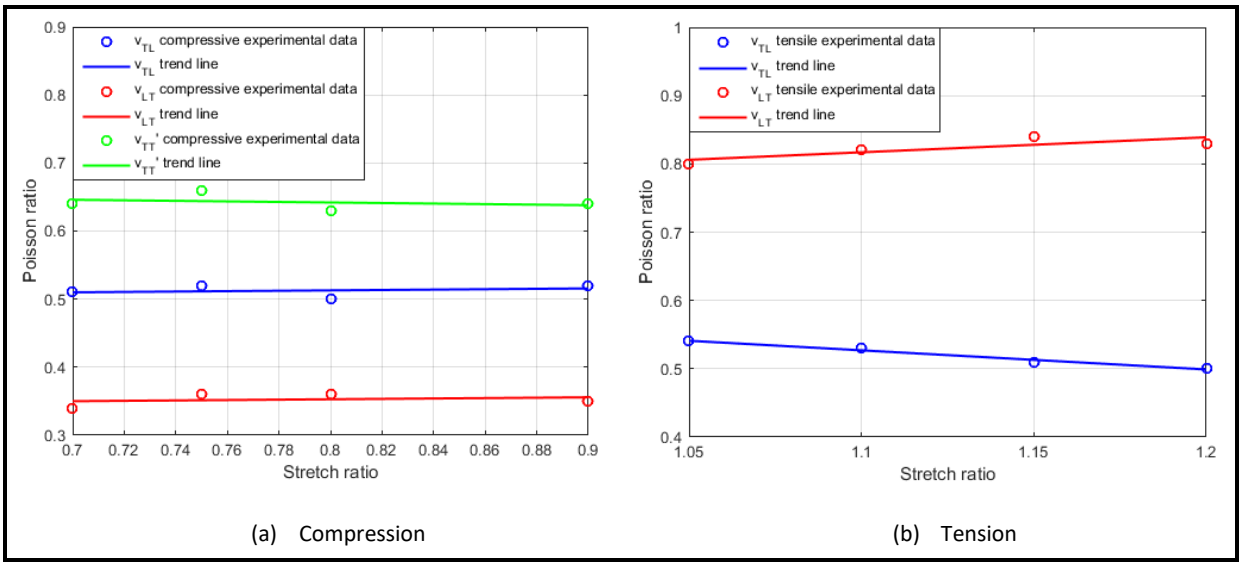

(a) Compression (b) Tension

Figure 1- The change in Poisson’s ratio by changing stretch ratio in (a) compression and (b) tension deformations for chicken pectoralis muscle.

Appendix B-Purification of fusion protein from bacteria

Materials for growing bacteria and bacteria transformation:

- LB agar (the instruction for making LB agar is attached in Appendix C).
- Antibiotic (Kanamycin)-stock concentration: 10 mg/ml in H_2O, working concentration: 30 µg/ml.
- Competent cells (E.coli BL21 (DE3))
- Plasmid DNA
- Water bath 42 °C
- SOC broth or LB broth
- Sterile flasks

Bacteria Transformation

Aseptic technique should be used throughout the process; use sterile tips, tubes etc. and work close to Bunsen flame

1. Keep plasmid DNA samples and kanamycin on ice.
2. Take 1 aliquot of bacteria cells (BL21 competent cells) from -80 °C and let thaw slowly on ice.
3. Prepare water bath by pouring distilled water and adjust the temperature to 42 °C.
4. Melt sterile LB-agar (the bacteria food) in the microwave.
5. Cool LB-agar to 60 °C (the temperature that hand can bear otherwise it inactivates the antibiotic).
6. Pour LB-agar plus 30 µg/ml of kanamycin in the 9 cm plate; prepare 50 ml of agar for each plasmid. (Stock concentration for kanamycin is 10 mg/ml in H_2O, so dilution factor for 30 µg/ml working concentration of kanamycin is 10/. 03=333; therefore 50000/333=154 µl of kanamycin is required to be added to 50 ml of LB agar and then make 3 plates; a plate for each plasmid DNA)- make sure to label on the base of plate not the lid as the lid can be detached.

   LB-kanamycin is LB containing the antibiotic kanamycin. Because LB is a rich medium for growing bacteria, adding kanamycin provides a means of selecting transformants that have taken up plasmid DNA containing a gene, which encodes resistance to kanamycin. Consequently, only bacteria that have been successfully transformed with such a plasmid will survive in LB-Kan plate.
7. Remove cells from -80 degrees and let thaw on ice.

8. Gently mix cells by flicking tubes.
9. Add 1 µl of each plasmid DNA (25ng/ µl-CNA35) to 50-100 µl of cell suspension and gently swirl tubes for a few seconds to mix- each plasmid DNA in a separate eppendorf tube as well as a control tube)- don't forget to label tubes.

   The control insures that the cells have not been killed by the manipulations. This control uses a sample of the same competent cells used for the rest of the experiment. The cells are treated the same as the experimental cells through the heat shock, recovery, and plating steps. However, they do not have a plasmid added to them.
10. Incubate on ice for 30 minutes to make a close connection between DNA and cells.
11. Then place the tubes in water bath for 45 seconds without shaking to give a heat shock. This opens the channels and forces the cell to take up DNA.
12. Replace tubes on ice for 2 minutes.
13. Dilute transformation reaction by adding of 950 µl of SOC (SOC is used as a recovery medium during the final stage of transformation of E.coli. the use of SOC improves transformation efficiency)
14. Shake tubes in an incubator at 37 °C, @ 200 rpm for 60 min (it can be more but less than 2 hours). Now we have "cell transformation mixture-CTM"
15. Plate by spreading 5-200 µl of CTM on LB-agar plates containing appropriate antibiotics and incubate with base up/lid down over night not more than 16 hours- make 2 different plates (100 µl of CTM and the other 10 µl of CTM diluted with 90 µl LB broth) for each plasmid since we want single colonies.
16. Store the plates, which are wrapped with Para film in the fridge with base up/lid down position.
17. Count the number of colonies on each plate.

Protein expression and purification

At this stage, the plasmid encoding for the CNA35 proteins were transformed into E.coli BL21 competent bacteria.

1. Single colonies are picked and used to inoculate 8 ml of LB broth supplemented with 30 µg/ml kanamycin into 15 ml falcon tubes.
2. The bacteria are grown over night at 37 °C and 200 rpm in incubator.
3. Next day, the cells in the mini cultures are transferred to the flasks containing 200ml of LB supplemented with 3o µg/ml kanamycin.
4. The bacteria are grown at 37 °C and 200 rpm.

5. Measure OD every 15 min; bear in mind that it is not fast, and roughly it takes 2.5 hours when OD gets 0.6 at 600 nm- don't leave the flasks in the room after filling each cuvette but also put back the flask to the incubator, then measure the OD). You will set the OD at 0 i.e. use the control cuvette to "blank" the machine.
6. To preserve a frozen stock of living transformed bacteria, add 4ml Glycerol (80%) into 8ml of the bacterial culture; pipette up and down gently to mix, and put them in bacterial stock boxes at -80 °C.
7. Expression is induced when OD at 600nm is 0.6 by adding 0.5 mM IPTG.
8. So, add 0.5 mM IPTG and then leave into incubator for 20 hours at 37 °C and 200 rpm (IPTG stimulates the promoter).
9. Then transfer the grown bacteria into tubes. Make 4 tubes of 45 ml for each culture (EGFP, µTurquoise and so on).
10. Bacteria are harvested by centrifugation for 10 min at 10000 xg (the speed is 8000 rpm). Make sure to make a balance while using centrifuge. Be careful that we cannot pour the grown bacteria directly to the sink as they are contaminated so we have to kill bacteria by disinfectant tablets. Bear in mind for the tubes containing bacteria plus bugbuster we do not need to use killer tablets as bugbuster has killed the bacteria.
11. After centrifugation, decant the supernatant and then add 4ml bugbuster (1 ml each tube) to the pellet. While adding bugbuster, swirl in order not to have lumps. Keep bugbuster into ice, as it is not stable
12. Then keep the tubes in the room temperature for 40 min in a dark place, as they are sensitive to light.
13. The bugbuster suspension must be centrifuged for 20 min @ 16000 xg (10000 rpm is the maximum speed that the centrifuge in the lab can work).
14. The resulting soluble fraction (supernatant) containing the protein is further purified via Ni^{2+} affinity chromatography (Use Nicole columns for each protein).
15. Now make one tube for one supernatant containing each protein (EGFP, µTurquoise…), and add 5ml of binding buffer.
16. Cut off the bottom tip and remove the top cap of columns, pour off excess liquid.
17. Equilibrate the columns with 10 ml binding buffer
18. Add sample
19. Wash with 10 ml binding buffer
20. Apply 3 ml elution buffer and collect the eluate. Buffer preparation for "His GraviTrap" column:

Buffer	Phosphate buffer stock solution (ml)	Imidazole 2M (ml)	Dest water	Imidazole final cons (mM)
Binding	3.75	0.3	To 30 mL	20
Elution	1.0	2.0	To 8 ml	500

21. At this stage we cannot freeze protein as it contains imidazole which can lead to protein aggregation, so the buffer in which the protein is dissolved needs to be changed-Change of buffer using Amicon-Ultra-4-centrifugal filter.
22. Prepare the protein storage buffer. For 1 L of storage buffer (50mM Tris-HCl, ph. 8.0 + 100 mM NaCl, add 1 L non-DEPC sterilized H_2O). For 50 ml (2.5 ml of 1M Tris, 1ml of 5M NaCl, and 46.5 ml H_2O
23. Load the protein sample in the centrifugal filter (max vol=4 ml)
24. Centrifuge for 15 min@7500 rpm @4 °C (fixed angle) or longer if the volume of sample in the filter has not been reduced to 1:10 of start volume. Discard the flow-through.
25. Add storage buffer to the sample in the filter till the volume is again 4 ml. mix the sample with the fresh buffer by pipetting up and down (never vortex protein samples).
26. Centrifuge and repeat the procedure of buffer loading, mixing and centrifugation another 3x.
27. After the last washing add just 2 ml of buffer and pipette 100 µl of the protein sample out of the filter into eppendorf tubes (overall 20 eppendorf tubes). Mix well and make sure no protein sticks to the membrane of the filter and keep them in -80 °C.

Appendix C-Making LB broth/agar

1. Weigh out: 5 g Tryptone (or Peptone), 2.5 g Yeast Extract, 5 g NaCl
2. Add 475 ml dH_2O and shake
3. Check pH is 7- use NaOH adjust pH if necessary
4. Bring volume to 500mls
5. This step is optional. Add 7.5 g of agar for LB agar.
6. Autoclave the solution
7. Remove from autoclave and swirl gently. Allow to cool down to 60 degrees before adding antibiotic.

Appendix D-The capability of the microstructural-geometrical model in predicting the porcine compressive and tensile stress response reported in Takaza et al. (2013) and Van Loocke et al. (2006)

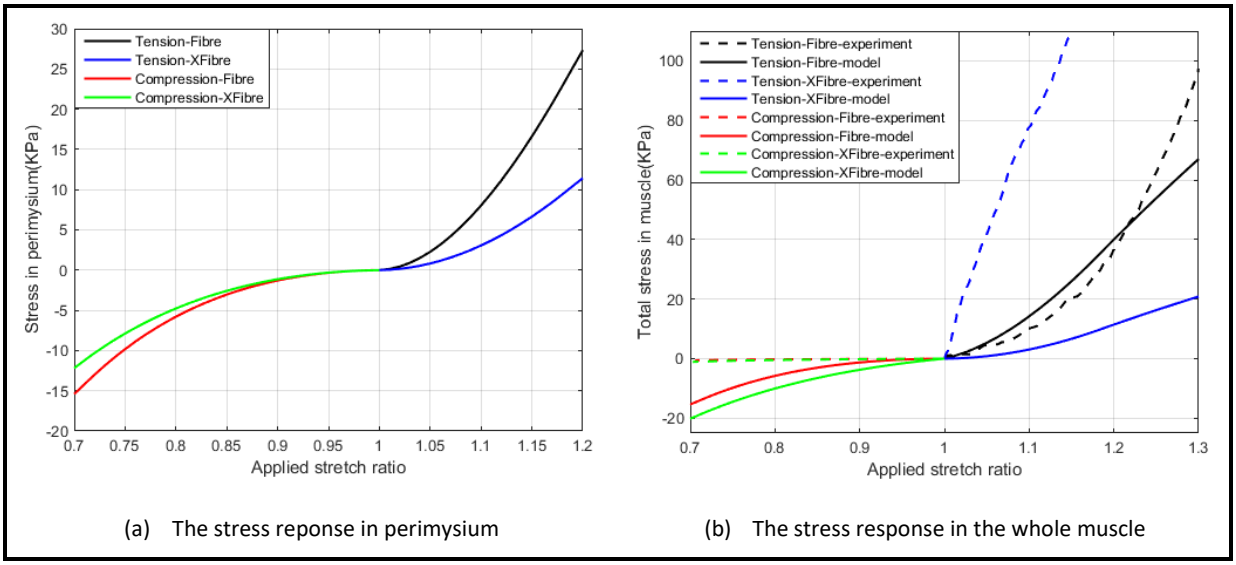

(a) The stress reponse in perimysium (b) The stress response in the whole muscle

Figure 1- Model-predicted stress response in tension and compression in both the fibre and cross-fibre directions for the whole muscle as well as perimysium; (a) The stress-stretch response in perimysium, (b) The stress-stretch response in the whole muscle (fascicle+perimysium) in comparison with the porcine experimental data. This base model is based on the middle values for the variables ($w = 1.18$, $E_{sheet} = 500\ MPa$ and $pc = 1.75\%$).

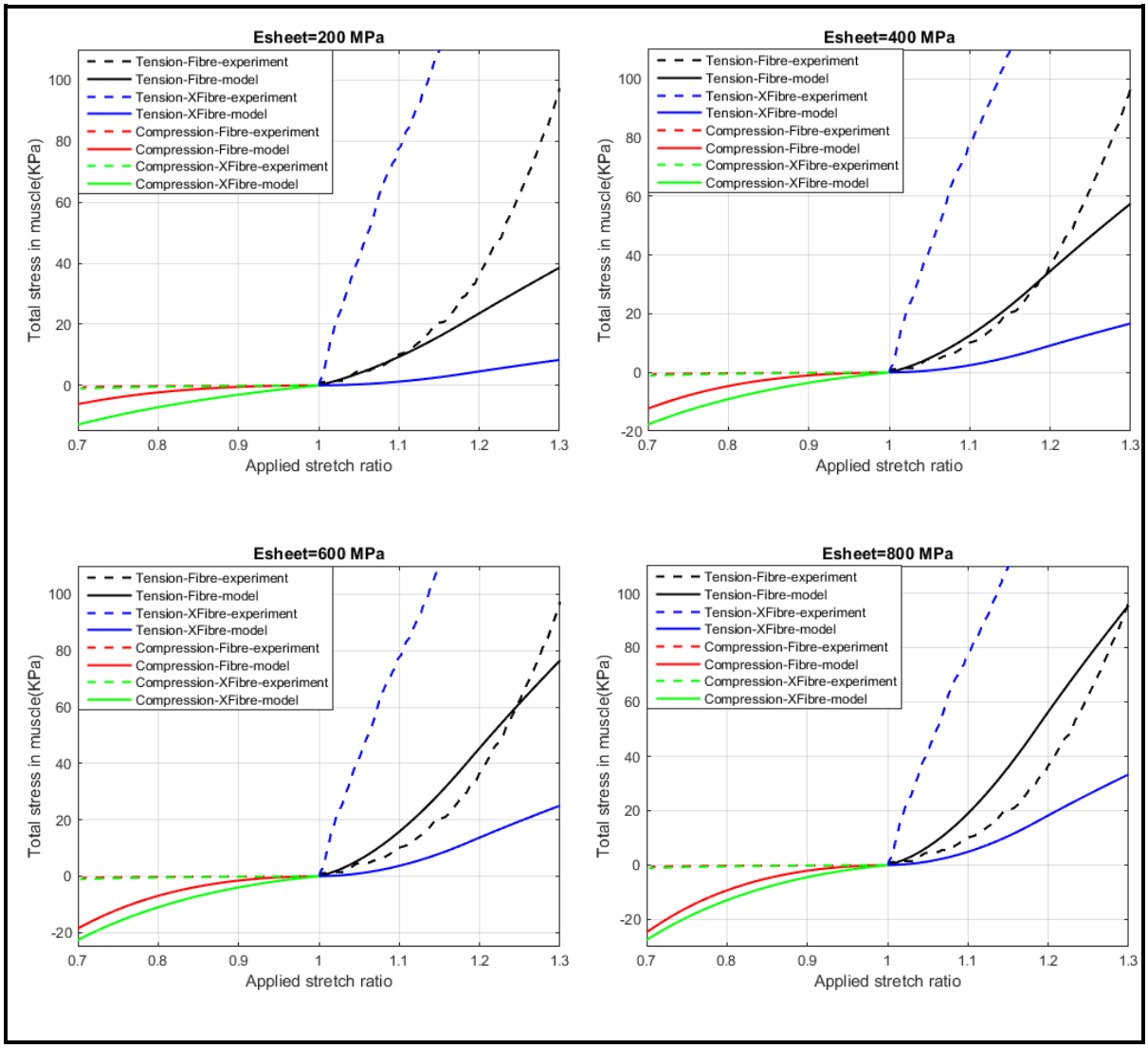

Figure 2-The comparison between the stress-stretch response of the whole muscle predicted by the model and the experimental results for porcine tissue at fixed waviness of 1.18 and 1.75% connective tissue for different Elastic modulus ranging from 200-800 MPa.

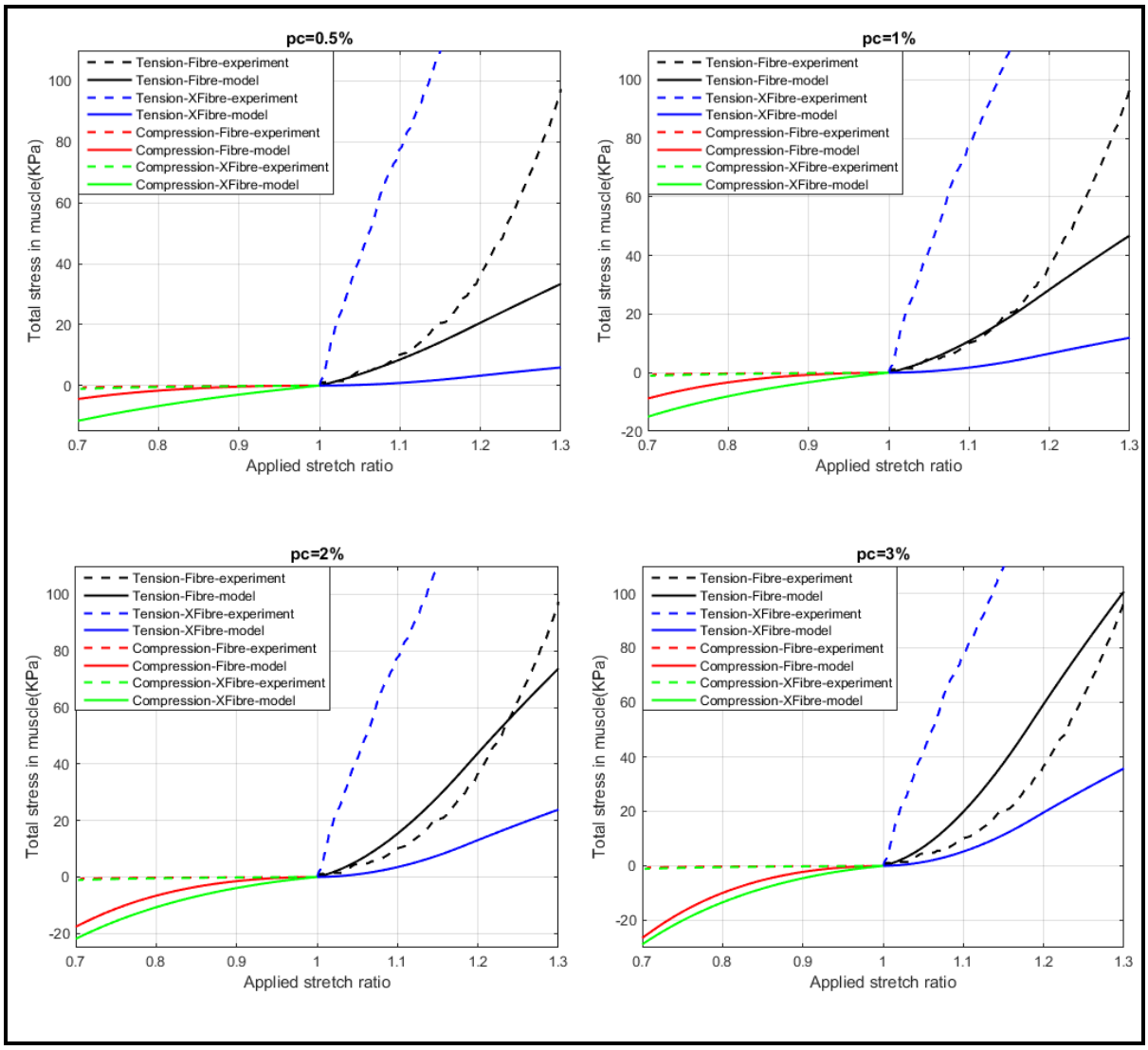

Figure 3-The comparison between stress-stretch response of the whole muscle predicted by the model and the experimental results for porcine tissue at fixed waviness of 1.18 and Elastic modulus of 500 MPa for different percentage of connective tissue existed in the muscle ranging from 0.5-3%.

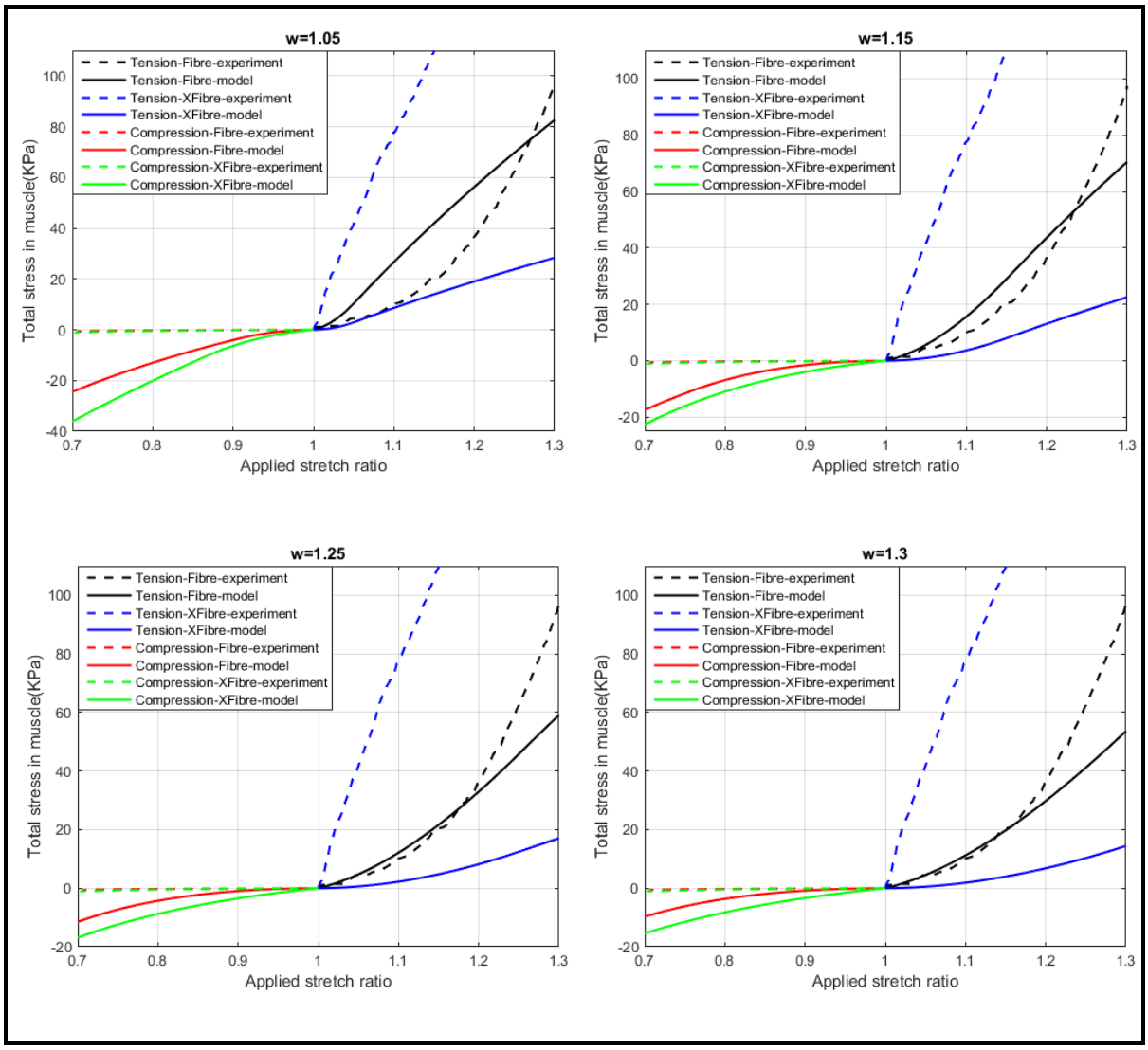

Figure 4-The comparison between stress-stretch response of the whole muscle predicted by the model and the experimental results for porcine tissue at fixed 1.75% of connective tissue and Elastic modulus of 500 MPa for different waviness ranging from 1.05-1.3.

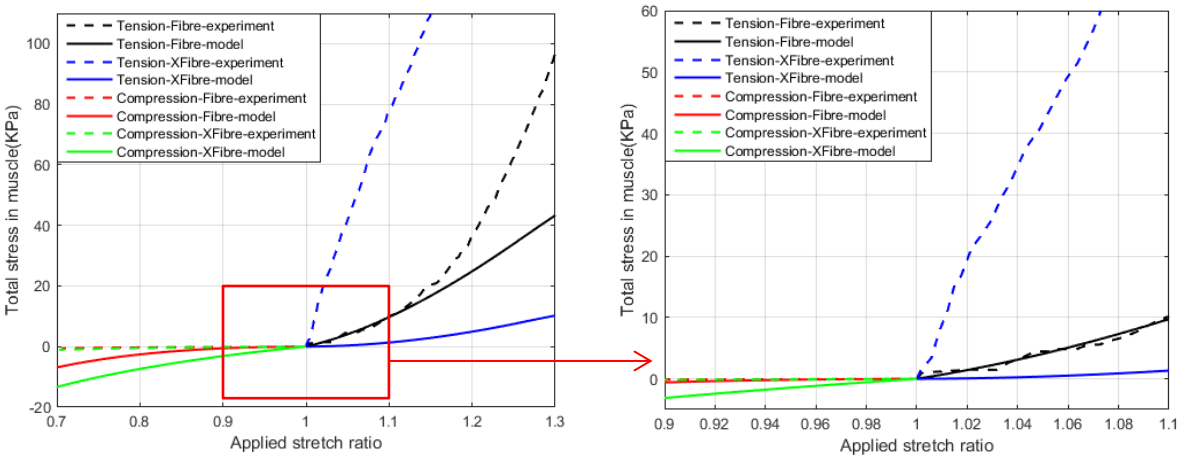

(a)The stress reponse in the muscle using the optimum parameters

(b)The stress response in the muscle from the stretch ratio of 0.9-1.1

Figure 5- The best predication of the model for tensile and compressive response of porcine muscle tissue. (a) The stress-stretch response of the muscle predicted by the model using the optimum model parameters; connective tissue percentage of $p_c = 1.75$, Elast modulus of $E_c = 300\ MPa$, and waviness of $w = 1.25$. (b) The stress response of the muscle in limited range of stretch ratios (from 0.9-1.1) to show the capability of the model to predict the experimental data.

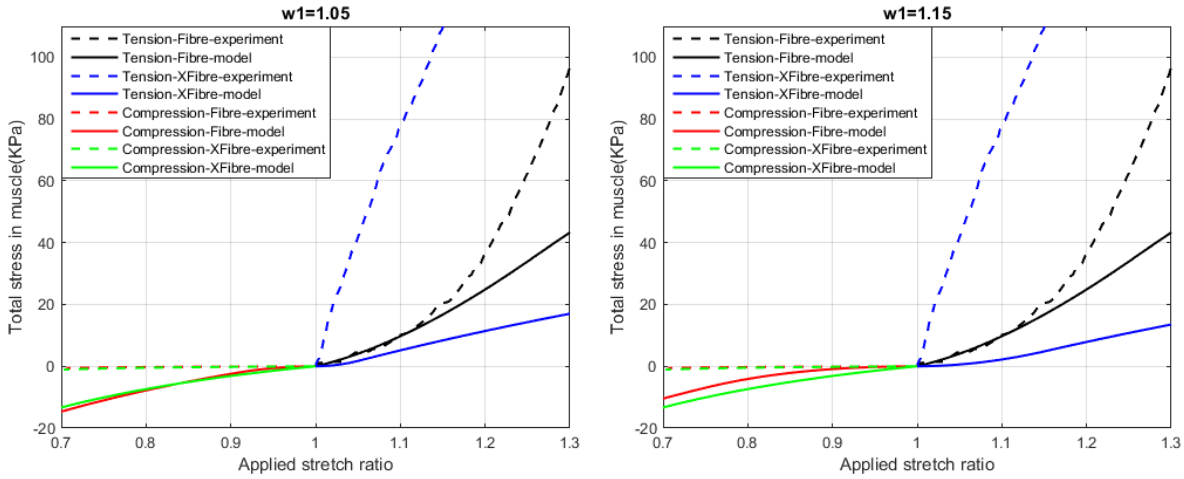

(a)The stress reponse in the muscle using the optimum parameters, but $w1 = 1.05$

(b) The stress reponse in the muscle using the optimum parameters, but $w1 = 1.15$

Figure 6- The model predication for tensile and compressive response of porcine muscle tissue by changing the waviness observed in the transverse direction(w_1)using the optimum model parameters; connective tissue percentage of $p_c = 1.75$, Elast modulus of $E_c = 300\ MPa$, and waviness of $w2 = 1.25$. (a) The stress-stretch response of the muscle predicted by the model using $w1 = 1.05$. (b) The stress-stretch response of the muscle predicted by the model using $w1 = 1.15$.